Characterisation of cardiac mitochondrial dysregulation in a model of Maturity Onset diabetes in the Young (MODY2) and impact of diet

A thesis submitted to the University of Manchester for the degree of Doctor of Philosophy in the Faculty of Biology, Medicine and Health

2020

Bodour S Rajab

School of Medical sciences/Division of Cardiovascular

Table of Contents

LIST OF FIGURES

LIST OF TABLES

Word Count: 68018

ABBREVIATIONS

ATP	Adenosine Triphosphate
Akt	Protein kinase B
BSA	Bovine Serum Albumin
CD	Cervical Dislocation
CD3+	Cluster of Differentiation 3+
CD4+	Cluster of Differentiation 4+
CD8a	Cluster of Differentiation 8a
db/db	Diabetic mouse
dIVS	Diastolic interventricular septum
dLVD	Diastolic left ventricular diameter
DNA	Deoxy-ribose Nucleic Acid
DPPI	Dipeptidyl Peptidase I
dPW	Diastolic posterior wall
EDTA	Ethylenediaminetetraacetic acid
ENU	N-Ethyl-Nitrosourea
fa/fa	Zucker Rat
FAO	Fatty acid β-oxidation
FFA	Free Fatty Acids
Gck	Glucokinase
HF	Heart Failure
HFD	High fat diet

HFpEF	Heart Failure with Preserved Ejection Fraction
HFrEF	Heart Failure with Reduced Ejection Fraction
Hk3	Hexokinase 3
HNF	Hepatocyte nuclear factor
HW	Heart weight
IFM	Interfibrillar mitochondria
IL-6	Interleukin 6
IMT	Intima-media thickness
iNOS	inducible nitric oxide synthase
IPF	Insulin Promoter Factor
ISP	Inflammatory Serine Proteases
KIF51	Kinesin Family Member 1B
KIF5B	Kinesin Family Member 5B
LV	Left Ventricular
Mfn1	Mitofusin1
Mfn2	Mitofusin2
MIRO1	Mitochondrial Rho GTPase 1
MODY	Maturity Onset Diabetes of the Young
MODY 2	Maturity Onset Diabetes of the Young Type 2
OD	Optical Density
ob/ob	Obese mouse
PCR	Polymerase Chain Reaction

PGC-1α	Peroxisome proliferator-activated receptor gamma coactivator1-α
PINK1	PTEN-induced kinase 1
P/O Ratio	Phosphate/Oxygen Ratio
PNDM	Permanent Neonatal Diabetes Mellitus
PNM	Perinuclear mitochondria
PTMs	Post-Translational Modifications
RIPA Buffer	Radioimmunoprecipitation assay buffer
ROS	Reactive Oxygen Species
SD	Standard deviation
SDS	Sodium dodecyl sulphate
SDS	Special Diet Service
SIRT1	Sirtuin 1
SSM	Subsarcolemma mitochondria
STZ	Streptozotocin
sIVS	Systolic interventricular septum
sLVD	Systolic left ventricular diameter
SNP	Single Nucleotide Polymorphism
T-cell	Thymus Cell
TFAM	Mitochondrial transcription factor A
TMB Substrate	Tetramethylbenzidine Substrate
TNF-α	Tumour Necrosis Factor A
TRAK1-2	Trafficking Kinesin Protein 1-2

TRAK2	Trafficking Kinesin Protein 2
ZDF	Zucker Diabetic Fatty

Abstract

Maturity Onset of Diabetes in the Young (MODY2) is a genetic form of diabetes with a mutation in the *Gck* gene. MODY affects 1-2% of people diagnosed with diabetes mellitus with the majority of MODY2 cases undiagnosed due to the absence of diabetes-like clinical symptoms. Diabetes suffers are at a higher risk of developing cardiovascular dysfunction. Despite this, treatment for cardiovascular dysfunction, particularly for MODY2 patients, is limited as the molecular mechanisms leading to dysfunction are complex and poorly understood. Molecular and cellular mechanisms are yet to be defined or examined within the heart. Here we employed a clinically relevant genetic mouse model of *Gck*-MODY2, GENA348, to investigate mitochondrial structural and molecular remodelling that may contribute to reduced contractile function and development of diabetic cardiomyopathy.

Employing a combination of physiological measurements, biochemical and mitochondrial functional assays coupled with proteomics we characterised the cardiac phenotype of the GENA348 mouse (Chapter 2). Our results revealed that the GENA348 mice develop early LV dysfunction at 6 months of age (in agreement with previous work from the Cartwright group) and demonstrated for the first time that mitochondrial dysfunction is a feature of the GENA348 myocardium. Specifically, we determined a down-regulation of several cardiac mitochondrial protein subunits that regulate oxidative phosphorylation (OXPHOS) with impaired Complex I, II and Complex IV activity and altered rates of oxygen consumption. Further, at the molecular level we determined that proteins regulating mitochondrial fission and fusion and mitophagy were perturbed. Chapter 3 revealed that in keeping with the molecular data that the GENA348 mitochondria were enlarged compared to control, in particular the mitochondria in contact with the sarcolemma were most affected. Together, this data reveals that the GENA348 mice develop cardiovascular complications, with impaired mitochondrial function that will likely contribute to aberrant metabolic function. We further showed in Chapter 4 that obesity exacerbates mitochondrial dysfunction in the GENA348 mice through introducing a high fat (60%) feeding (HFD) regimen for 12 weeks. Here, we noted a common pathological development in the GENA348-chow mice compared to wild-type mice fed either chow or a HFD, suggesting a similar pathophysiology in obesity and MODY2 diabetes. We also recorded further decreases to mitochondrial complex activity and OXPHOS in the GENA348 HFD mice, suggesting that obesity adds a further stress impacting upon mitochondrial function.

Through both biochemical and quantitative mass spectrometry analysis of isolated mitochondria from the GENA348 mouse myocardium we determined that there was a 0.2-fold decrease in Miro1 expression compared to WT control mice; a protein important for regulating mitochondrial movement and turnover. Therefore in Chapter 5 we investigated the effects of Miro1 knockdown in a cardiomyocyte cell line (H9c2). While depletion of Miro1 had no effect upon the expression of proteins mediating mitochondrial motility there was a significant increase in the fusion protein Opa1 and regulator of mitophagy PINK1 expression in si-Miro1 lines, suggesting an important role in regulating mitochondrial quality control through fission/fusion pathways and mitophagy. We also determined that levels of the inflammatory molecules IL-1β, IL-6 and TNF-α were elevated in the GENA348 heart; therefore, we developed cell-based studies to investigate how these cytokines may influence mitochondrial function and dynamics. We determined that each cytokine had differential effects upon Miro1 expression as well as proteins influencing mitochondrial fission and fusion; indicating a link between inflammation and mitochondrial function but through a diverse number of complex pathways.

In conclusion, this thesis work has yielded novel data with potential translational impact in the longer term for the management of MODY2 patients. Importantly, we have determined that mitochondrial dysfunction is a feature of MODY2, a mild form of type 2 diabetes and thus represents an early pathophysiological manifestation. The identification of altered mitochondrial proteins and pathways reported here therefore provide novel information that may be exploited in future studies for developing therapeutic intervention in the treatment of cardiac mitochondrial dysfunction. Additionally, our studies of the effect of a high fat Western diet upon cardiac and mitochondrial function also indicate that lifestyle management is important for MODY2 patients. Further given the overlapping pathways we identified in wild-type mice and GENA348 mice in response to a HFD the outputs from this thesis may have relevance to not just MODY2 diabetes. Finally, we have investigated a putative mechanistic link between inflammation (a feature of both obesity and diabetes) and altered mitochondrial dynamics generating new insights into the regulation and dysregulation of mitochondrial quality control.

Declaration

I, Bodour Rajab, confirm that the work presented in this thesis is my own. Where information has been derived from other sources, I confirm that this has been indicated in the thesis.

Copyright Statement

Acknowledgements

Firstly, I would like to express my gratitude to my supervisor Dr Ashraf Kitmitto for the continual mentoring, guidance and support granted to me over the past few years throughout my PhD. Many thanks to my secondary supervisor, Dr Elly cartwright, for the provision and advice during my studies. In addition, I would like to extend my thanks to my friends, colleagues, and present members of the Kitmitto group, especially to the great Postdoc Dr Sarah Kassab. Thanks to Florence Baudoin for assisting me with lab techniques; thanks to Sukpal Prehar for looking after my mice and for kindly carrying out the physiological measurements. Amongst many things, you have all provided me with a wealth of knowledge that I will value for the rest of my life. A special thanks goes to Mass spectrometry and Electron microscopy facilities for their services and support.

Most importantly, I would like to acknowledge my family who unconditionally supported me from a distance. Thank you to my late father, Saeed Rajab, who would have been proud of my achievements. He always wished for me to be a doctor and so this achievement and success is for him, first and foremost. Thank you also to my mother, Dr Jehan Al Sabban, my brother Dr Badr Rajab and my sister Dr Aeshah Rajab. With your moral support, I have been able to preserve through the challenging times and have managed to stay calm through our laughs and conversation. Also, I would like to extend my thank to my best friends Dr. Halah Al- Bar and Dr. Nadyh Al Awfi for their help and support throughout all years.

Conference Proceedings

Poster presentations

Title: Defect of mitochondrial dynamics and fusion in maturity onset of diabetes in the young (MODY). Presented at the Division of Cardiovascular Sciences Postgraduate showcase; Manchester, UK; 30th April 2016.

Title: An imbalance of mitochondrial fission and fusion is a feature of maturity onset of diabetes in the young (MODY). Presented at the World Mitochondria Society; Berlin, Germany 2017. 6th World Congress on Targeting Mitochondria.

Title: An imbalance of mitochondrial fission and fusion is a feature of maturity onset of diabetes in the young (MODY). Presented at the 26th Northern Cardiovascular Research Group conference; Newcastle, UK; 24th April 2018.

Publications

Daghistani, H. M., Rajab, B. S. & Kitmitto, A. (2019). 'Three‐dimensional electron microscopy techniques for unravelling mitochondrial dysfunction in heart failure and identification of new pharmacological targets', British Journal of Pharmacology, 176(22), pp. 4340-4359.

Chapter 1 Introduction

1.1 Diabetes Mellitus

Diabetes mellitus is a chronic metabolic disease, characterised by hyperglycaemia (Guthrie and Guthrie, 2004). According to the World Health Organization (WHO), an estimated 550 million people globally are likely to develop diabetes by 2030 (WHO, 2016). Long-term complications of diabetes include loss of vision, renal failure, cardiovascular dysfunction, amputations and Charcot joints, a progressive degenerative joint disorder (Association, 2014).

Diabetes mellitus can be categorised into two broad etiopathogenetic groups; Type 1 diabetes (T1DM) and Type 2 diabetes (T2DM). In T1DM, the pancreas of the affected individual produces little or no insulin resulting in insulin secretion deficiency (Association, 2014). Thus, an individual with T1DM is administered exogenous insulin at regular intervals to regulate blood sugar levels (Atkinson et al., 2014). In this form of diabetes, cellular-mediated autoimmune destruction of the β-cells of the pancreas occurs, although the rate of β-cell destruction varies. T1DM is generally hereditary and sufferers are known to be prone to other autoimmune disorders such as Graves' disease, Hashimoto's thyroiditis, vitiligo, autoimmune hepatitis, and pernicious anaemia (Barker, 2006). There are also rare forms of T1DM that are idiopathic, whereby ketoacidosis and insulin deficiency present at varying degrees (Piñero-Piloña and Raskin, 2001). T2DM is more prevalent, accounting for approximately 90% of diabetes cases (Zaccardi et al., 2016). The disease is typically diagnosed later in life, associated with obesity and unlike T1DM, is often preventable (Leroith et al., 2015). The Who (2016) identified an unhealthy lifestyle and diet as the predominant cause of T2DM cases. In T2DM, a resistance to insulin action and inadequate glucose compensation, results in eventual hyperglycaemia. In T2DM, autoimmune destruction of β-cells does not occur, rather, hyperglycaemia develops over time as a result of an increased percentage of body fat in the abdominal region, leading to insulin resistance.

Insulin resistance and prediabetes are considered precursors to diabetes. During insulin resistance, insulin is sufficiently produced by the body, however it cannot be used efficiently. Here, cells are unable to utilise glucose, resulting in its accumulation in the bloodstream. This high blood glucose triggers pancreatic cells to release more insulin, in order to maintain normal blood glucose levels. Eventually the pancreatic cells are unable to maintain the insulin requirement, resulting in high glucose levels (Greene et al., 2018). This results in insulin resistance when in fasting conditions and an increase in blood glucose levels (hyperglycaemia) and excessive insulin in the blood (hyperinsulinemia). Pre-diabetes, heart ailments, and T2DM occurs in people who are insulin resistant. A diagnosis of prediabetes indicates an elevated risk of developing T2DM (Skyler et al., 2015).

There are also other specific types of diabetes including, genetic defects of the β-cell, genetic defects in insulin action, endocrinopathies, drug or chemical-induced diabetes, infections and gestational diabetes mellitus (Association, 2014).

1.1.1 Maturity-Onset Diabetes of the Young (MODY)

Maturity-onset diabetes of the young (MODY) is a monogenic form of diabetes mellitus, encompassing a small group of heterogeneous disorders associated with β-cell dysfunction (Miller et al., 1999; Thanabalasingham and Owen, 2011). MODY is an autosomal dominant disorder, believed to account for 1% of T2DM cases and is characterised by impaired insulin secretion with minimal or no defects in insulin action (Ledermann, 1995). Although MODY is often compared to T2DM due to similarities in symptoms, its rare form has resulted in difficulty with diagnosis and a lack of research compared to other types of diabetes. Consequently, it is often misdiagnosed with limited treatments and management strategies. Abnormalities at fourteen genetic loci on different chromosomes have been identified to date as leading to the MODY phenotype (Anık et al., 2015; Prudente et al., 2015). The most common of these are glucokinase (*Gck*) (MODY2), hepatocyte nuclear factor 1α (HNF1α) (MODY 3) and hepatocyte nuclear factor 4α (HNF4α) (MODY 1) (Table 1.1) (Thanabalasingham and Owen, 2011).

Gck mutations result in mild, asymptomatic, stable fasting hyperglycaemia, usually requiring no specific treatment. On the other hand, HNF1α and HNF4α mutations cause progressive pancreatic β-cell dysfunction and hyperglycaemia that can result in micro- and macrovascular complications (Table 1.1) (Anık et al., 2015).

Table 1.1 Genetic and clinical characteristics of MODY subgroups

	MODY 1	MODY 2	MODY 3	MODY 4	MODY 5
Genetics	HNF-4α (20q13)	Glucokinase (7p15)	HNF-1α (12q24)	IPF-1 (13q12)	HNF-1β (17cen-q21)
Prevalence	5%	15%	70%	<1%	2%
Severity	Progressive IGT	Mild, stable hyperglycemia	Progressive IGT	Progressive IGT	Progressive IGT
Onset	12-35 years	Birth	12-28 years	14-40 years	12-28 years
Microvascular complications	Yes	Rare	Yes	Yes	Yes (renal)
Treatment	Progressive need	Pregnancy	Progressive need	Progressive need	Progressive need

IGT= Impaired glucose tolerance

As mentioned above, accurate clinical diagnosis of MODY presents as a challenge due to overlapping clinical features. Previously, Mcdonald et al. (2011) and Owen et al. (2010) demonstrated that C-reactive protein (hsCRP) is significantly lower in MODY3 patients than in those with T2DM. Furthermore, MODY2 patients were shown to present with a small

increase in glucose levels, when recorded through an oral glucose tolerance test (Mcdonald and Ellard, 2013). In a recent study of Chinese MODY2 and MODY3 patients, Fu et al. (2019) further investigated the feasibility of such clinical biomarkers for distinguishing phenotypical diabetes sub-types. The authors measured fasting C-peptide, hsCRP, and lipid levels between T1DM, MODY2 and MODY3 patients (Fu et al., 2019). The study did not yield a single marker to differentiate between MODY types and between T1DM, highlighting the need for a combination of indicators was apparent. For example, C-peptide, hsCRP, total cholesterol and LDL-C levels were shown to discriminate between MODY2 and T1DM; however, only hsCRP and triglyceride levels were suitable for discriminating MODY2 from MODY3 (Fu et al., 2019). Discrimination is important to accurately diagnose the disease and select the appropriate treatment (Fu et al., 2019). It should be noted that this study was based on Chinese patients, meaning extrapolation to other ethnicities requires investigation. Thus, clinical features appear to be progressively used as diagnostic markers.

Recent studies have investigated the aetiology of MODY across varying ethnic populations. There are discrepancies in the prevalence of the disease in Asian and Caucasian populations, including identification of the disease-causing locus in MODY patients (Jang, 2020). As mentioned, MODY2 and MODY3 account for the majority of MODY cases. Recently, MODY mutations were screened in North African Tunisian patients with MODY clinical profiles (Khelifa et al., 2018). The authors reported no mutations in the common MODY genes, unlike Caucasian populations, suggesting the presence of unidentified genes contributing to MODY in Tunisian patients. In another study, genetic variants of MODY were investigated in Chinese patients using whole-exome sequencing (Xu et al., 2020). In the majority of patients (20 out of 24), the *Gck* mutation was identified, with four novel *Gck* mutations reported. The other four mutations were in the ABCC8 gene, HNF4α gene, INS gene and a 17q12 microdeletion (Xu et al., 2020). The *Gck* prominence is similar to that reported in Polish (Fendler et al., 2012) and Italian (Delvecchio et al., 2017) studies. In contrast, a minority of MODY cases were *Gck*-MODY in a Korean (Hwang et al., 2006) and different Chinese study (Xu et al., 2005). In addition, a study reported a similar prevalence of HNF1α amongst Croatian MODY patients

as that previously measured in other European countries (Pavić et al., 2018). It is possible that differences in ages of MODY participants within these studies is a causative factor in the variation between reported data. Overall, these studies suggest that MODY mutations may differ between ethnicities, emphasising the need for accurate genetic testing to enable proper disease management.

1.1.2 MODY2 (Gck-MODY)

The focus in this thesis is the *Gck*-MODY mutation, also known as MODY2. MODY2 is a result of mutations in the Glucokinase (*Gck*) gene. *Gck* is a key regulating enzyme in the pancreatic β-cell, important for insulin secretion and glucose sensing (Osbak et al., 2009). *Gck* acts by phosphorylating glucose on carbon 6 using MgATP as a second substrate to form glucose-6-phosphate (G6P). *Gck* catalyses the first reaction of the glycolytic pathway, regulating phosphorylation over a range of glucose concentrations (Figure. 1.1). At the protein level the *Gck* mutation causes the replacement of an isoleucine with a phenylalanine (I366F) amino acid, leading to an inability of Gck to phosphorylate glucose to glucose-6-phosphate (Toye et al., 2004).

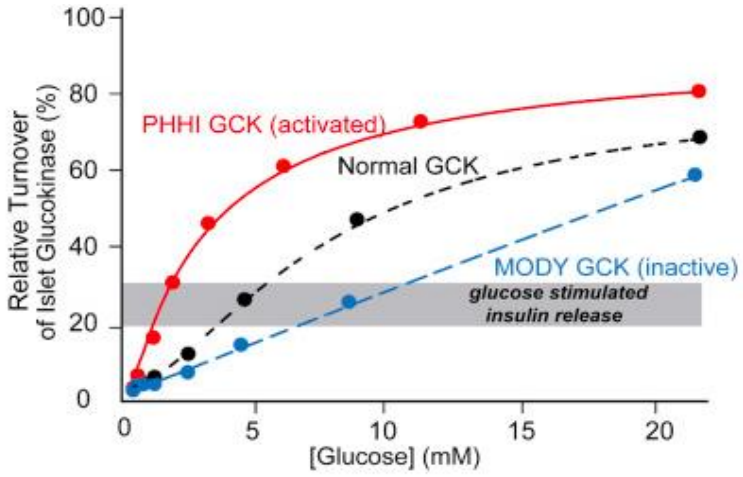

Figure 1.1 Precise control of Gck activity is required for glucose homeostasis.

Activating Gck mutations produce persistent hyperinsulinemia hypoglycaemia of infancy (PHHI) (red), where lower glucose is required for insulin secretion compared to MODY2 variants (blue) (Sternisha and Miller, 2019)

In animal models of global homozygous *Gck* knockout, mice developed severe diabetes leading to death (Sternisha and Miller, 2019). In contrast, heterozygous *Gck* knockout mice developed early mild-onset diabetes, similar to that of the MODY phenotype (Postic et al., 1999). The *Gck* mutation was the first MODY gene to be identified (Hattersley et al., 1992). Since then, over 600 *Gck* gene mutations have been reported (Osbak et al., 2009), with more mutations reported recently in Chinese MODY genetic screening (Liu et al., 2018). Patients with MODY2 display mild hyperglycaemia and an absence of acute symptoms, resulting in missed or misdiagnosis. Consequently, there is limited information regarding the Gck-MODY2 phenotype and the long-term effects on cardiac function.

1.1.3 Diabetic Cardiomyopathy

Cardiovascular diseases are a common cause of death among diabetic patients. High blood pressure and myocardial infarction are common among people with T1DM, T2DM and obesity (Brocheriou et al., 2000). There are several controversies surrounding whether diabetic cardiomyopathy (DCM) is distinct from other forms of cardiomyopathy. First described by (Rubler et al., 1972), DCM describes a distinct primary heart disease, that progresses independently of coronary heart diseases and ends in heart failure (Asghar et al., 2009). Despite the controversy surrounding the definition of DCM, there is evidence that the structural and functional damage of cardiac tissue occurs in diabetic patients in the absence of any other cardiovascular risk factors (Lee et al., 2004). Whilst high risk for cardiomyopathies and heart failure in patients with poor glycaemic control has been reported, studies also identified that intensive glycaemic control did not reduce risk of heart failure (Asghar et al., 2009) indicating that the remodelling observed in diabetic cardiomyopathy is likely to be highly complex. Thus, it has been proposed that ‘diabetic cardiomyopathy’ should be defined as ‘cardiac abnormalities not wholly explained by other cardiovascular or non-cardiovascular causes and likely to be due to diabetes’ (Lee et al., 2019).

In terms of pathophysiology, DCM has been described as a disease with abnormal cardiac structure and performance, particularly a decrease in systolic and diastolic function of the left ventricle (Lorenzo-Almoros et al., 2017; Voulgari et al., 2010). Again, this definition is contested, as questions remain to be answered regarding the clinical abnormalities that reveal DCM during diagnosis. Four progressive stages of DCM have been reported as characteristic of diabetic heart disease (Maisch et al., 2011). Patients with stage 1 DCM (early/middle) display no symptoms and only diastolic dysfunction. Abnormalities in diastolic and systolic function are described as typical of stages 2 (middle) and 3 (middle/late). Finally, in stage 4 (late), patients appear with symptomatic heart failure and dilated hearts characterised by fibrosis and coronary artery disease (Maisch et al., 2011). Although defined in four stages, it is apparent that individuals can present differently, making it difficult to distinctly characterise and diagnose an individual with DCM. Undoubtedly, the impact upon cardiac metabolism due to mitochondrial dysfunction in DCM affects cardiac function. However, the distinct characteristics and clinical pathophysiology of DCM requires elucidating.

1.1.4 Diabetic Cardiomyopathy in MODY2 (Gck-MODY)

In this thesis, DCM in MODY2 will be investigated due to the scarcity of studies that analyse the cardiac macrovascular complications in patients, distinct from T2DM. One observational patient study suggested that *Gck*-MODY does not lead to microvascular diabetes-related complications (Steele et al., 2014); although there is a lack of a concise characterisation of the diabetic cardiac phenotype and limited number of patients included in the study (n=99). Another study that compared *Gck* mutation carriers with controls reported no difference in carotid intima-media thickness, myocardial infarction or ischemic stroke (Pruhova et al., 2013). A few reports that have linked *Gck*-MODY with cardiac dysfunction have been on patients with co-morbidities and were of an older age (Page et al., 1995; Velho et al., 1997). As mentioned, there is a lack of research on long-term macrovascular complication in patients with MODY, compared to diabetes sufferers. It is important to clarify their distinct profiles for a better understanding of the cardiac landscape for effective treatment and management. Therefore,

one of the goals of this thesis work has been characterise the cardiac phenotype of a mouse model of *Gck*-MODY2.

1.1.5 Obesity and diabetes

Obesity is identified as a risk factor for cardiovascular complications. Obesity was identified as the single major contributor for the alarming rise in diabetes incidence and is quickly becoming the leading cause of death (Mokdad et al., 2003). Obesity has the potential to affect the clinical course of diabetes (Gorman et al., 2008). There is evidence to indicate that diet may also play an important role in the prognosis of *Gck*-MODY patients with a short-term high carbohydrate diet shown to be detrimental, leading to increased hyperglycaemic events (Klupa et al., 2011). It has been shown that a high fat diet induced a greater effect on insulin levels than on glucose, repressing gluconeogenesis enzymes and up-regulating genes involved in fatty acids oxidation, adipogenesis and transport (Gorman et al., 2008) Therefore, given the high incidence of obesity in the Western world, a second focus of this project has involved investigating the impact of a high fat diet (HFD) upon cardiac function using the GENA348 diabetes mouse model of *Gck*-MODY2. The onset of obesity correlates with lifestyle features and the causes of T2DM are varied, including nutritional routine, physical action, drinking of alcohol and smoking. Obesity occurs through the lower expenditure of energy compared to consumption for a continued period. However, the predominant cause of obesity is considered to be the high consumption of high calorie nutrition over years. In T2DM, it has been revealed that energy constraints, without a decrease in weight, can increase insulin sensitivity. Thus, it is expected that an increase in calorie consumption and not essentially obesity is a threat for diabetes (Franz et al., 2015).

1.1.6 Animal Models of Diabetes (The GENA348 Mouse)

Animal models are invaluable for acquiring knowledge about diabetes through experimentation. A mouse model of *Gck*-MODY2 has been developed, the GENA348 mouse.

In GENA348, the underlying gene was mapped to MODY2 homology region of mouse chromosome 11. Positional gene analyses revealed an A to T transversion mutation in exon 9 of the glucokinase gene, causing an isoleucine to phenylalanine change at amino acid 366 (Toye et al., 2004). The GENA348 mouse is therefore generated through a missense I366F mutation of the *Gck* protein. The I366F GENA348 allele is a unique mutation as it is located in the corresponding amino acid position (Toye et al., 2004). Thus, this locality provides a good model for investigating *Gck* protein function. Other animal models for diabetes and obesity will be discussed in more detail in Chapter 4.

A previous PhD study in the Cartwright group has shown using *in vivo,* hemodynamic and histology studies that at 3 months of age cardiac function appears normal. By 6 months, these animals developed cardiac hypertrophy, fibrosis and diastolic dysfunction (Gibbons et al., 2011). Cardiac function was found to progressively worsen at 12 months, indicating that impaired cardiac function could be an unidentified feature of *Gck*-MODY. However, little is known about the exact mechanics underlying the disease at the cellular level. To this aim, in this project, GENA348 will be used to examine the development of diabetic cardiomyopathy and characterise the molecular changes that occur during this process.

1.1.7 Mitochondria and the development of diabetic cardiomyopathy

The heart relies on mitochondria for the supply of ATP, enabling cardiac heart cells to function normally. The heart is an energetically demanding organ, requiring a high and constant supply of energy (Bugger and Abel, 2010). Thus, failure of mitochondria to produce sufficient ATP is known to lead to cardiac cell death and eventual heart failure (Bugger and Abel, 2010). Mitochondrial dysfunction is apparent during the early stages of heart failure, marked by excess ROS production, ion homeostasis and changes to substrate utilisation (Facundo et al., 2017). Changes in mitochondrial size and structure are common features of mitochondrial morphology modifications associated with diabetes and heart failure pathologies (Daghistani

et al., 2018). Mitochondrial dysfunction and its role in the development of diabetic cardiomyopathy will be discussed in the following sections and in later chapters.

Mitochondria are important for the homeostasis of critical cellular pathways, including its primary function of energy production, generation of reactive oxidative species (ROS) and apoptosis. Due to its importance, mitochondrial damage is associated with the pathophysiology of diabetic heart disease (Schilling, 2015). Dysfunctional mitochondria fail to regulate ROS production, resulting in the increased release of apoptosis-inducing factors (Frustaci et al., 2000). Although successful in animal models, ROS scavengers have been reported as unsuccessful in diabetic patients (Lonn et al., 2005), suggesting the need to enhance healthy mitochondrial capacity and quality.

The mechanism of mitochondrial dysfunction in the diabetic heart is attributed to; (1) altered energy metabolism, (2) oxidative stress, (3) microRNA regulation involved in genetic cardiac remodelling (Schilling, 2015). Due to higher energy demands, the cardiomyocyte heart cells consist of a greater number of mitochondria compared to other cells in the body. Due to insulin resistance in Type 2 diabetes, the diabetic heart has increased rate of fatty acid oxidation. The combination of increased fatty acid oxidation and reduced cardiac efficiency has been shown to lead to contractile dysfunction (Buchanan et al., 2005). In heart failure, the electron transport chain complexes are supressed, thus, increasing ROS levels and oxidative DNA damage (Ide et al., 2001)This provides strong evidence to suggest that mitochondrial function is imperative to healthy cardiac function.

Mitochondrial fission and fusion are important process that enable the mitochondria to uphold its functions, including control of cellular calcium handling, ROS production, and energetic output (Chen and Chan, 2005). Mitofusin-2 (MFN2), a protein that regulates mitochondrial fusion, has been shown to be reduced in obesity and diabetes, correlating with insulin resistance (Bach et al., 2003). It would be interesting to investigate this further in the GENA348 model, to elucidate if fusion and fusion-regulating proteins are impacted in obesity. The

relationship between obesity, diabetes and mitochondrial damage has been further explored through electron microscopy, whereby diminished mitochondrial size was observed in diabetic patients, paired with a significant reduction in OXPHOS activity (Petersen et al., 2004). There is a plethora of studies that show the increased tissue lipid load in obesity experimentally links to impaired mitochondrial function and metabolism.

Changes in the levels of OXPHOS occur in response to metabolic needs, ensuring that genetic products are assembled into their functional complexes. In addition to impacting fission and fusion, it has been reported that obesity has an impact on mitochondrial biogenesis proteins, such as PGC-1α. In fact, obesity and saturated fatty acids decrease PGC-1α transcriptor activity, OXPHOS expression and O^2 consumption (Crunkhorn et al., 2007). This suggests that stress placed upon the mitochondria due to diabetes results in the modulation of translation factors that play a role in mitochondrial biogenesis. This balance is carefully maintained; however, obesity causes mitochondrial failure and thus, a mismatch in mitochondrial homeostasis.

1.2 Mitochondria

1.2.1 Mitochondria structure and function

Mitochondria structurally consist of an outer membrane, inner membrane and matrix (Palade, 1952). The space between the outer membrane and the inner membrane is called the intermembrane space, resembling the cytosol and containing a number of small biomolecules essential for its function (Palade, 1952). The inner mitochondrial membrane is made of a phospholipid cardiolipin. The inner membrane carries many proteins that serve important functions in the electron transport chain, ATP synthesis, membrane transport, mitochondrial fission and fusion. The inner membrane is folded to form structures termed cristae. It is thought that cristae can vary from simple tubular structures to more complex lamellar structures merging with the inner boundary membrane through tubular structures (Frey and Mannella, 2000). Through this precise structural organisation, the mitochondria produce ATP. It serves

other functions including storing calcium (Rizzuto et al., 2012), heat production in brown adipose tissue and is involved in programmed cell death (Bratic and Larsson, 2013). Mitochondria replicate through binary fission, correlating with the cell cycle. Mitochondria are also able to divide in response to energy needs of the cell. Thus, energy intensive cells have a greater number of mitochondria. It is estimated that approximately 30% of the volume of a cardiomyocyte is occupied by mitochondria (Sivitz and Yorek, 2010).

ATP is generated through oxidative phosphorylation (OXPHOS) in mitochondria (Figure. 1.2). The electrons generated through glycolysis, citric acid cycle and fatty acid oxidation are fed into the electron transport chain (ETC) of the mitochondria, to produce ATP. The ETC is composed of five complexes (CI-CV) that contain different electron carriers. For every electron reduced by the ETC, the mitochondria convert one oxygen molecule to superoxide anions. Superoxide anions are converted into other forms of reactive oxygen species (ROS) that can harm the cell. The generation of ROS is a product of the OXPHOS process. Complexes I, II and III contribute to the production of ROS in the matrix and intermembrane space (Turrens, 2003). Mitochondria are therefore also the main site for production of superoxide anions in the cell (Sivitz and Yorek, 2010). In heart failure, it has been shown that the ETC complexes display impaired activity. Scheubel et al. (2002) measured the activity of complex I in explanted failing hearts and found a 28% decrease in citrate synthase activity and a reduction in maximal respiratory capacity, compared to non-failing donor hearts. No change was reported in the other complexes. Thus, it is evident that healthy functioning of mitochondrial complexes is important for cardiac energy provision.

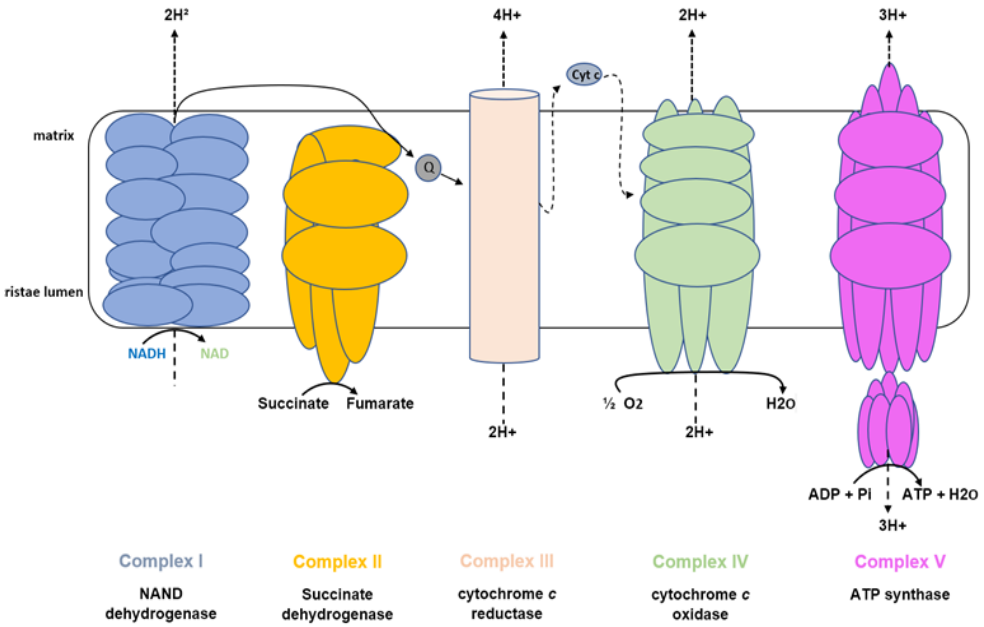

Figure 1.2 Mitochondrial respiratory chain complexes.

Electron transport complexes I, II, III, IV and ATP synthase (complex V) work together during oxidative phosphorylation. Electron transport complexes I, III and IV pump protons across the cristae membrane, creating a proton gradient, driving ATP synthesis. Figure adapted from Alston et al. (2017).

1.2.2 Mitochondrial organisation within cardiac cells

Cardiac mitochondria are spatially arranged into three distinct populations; subsarcolemmal (SSM), lying beneath the sarcolemma, interfibrillar (IFM) sandwiched between the myofilaments and perinuclear (PNM) surrounding the nucleus (Figure. 1.3). The interior of biochemically-defined mitochondria were examined by high-resolution SEM (Riva et al., 2005). SSM have been shown to have roles in insulin signalling, fatty acid oxidation and glucose transport as well as provide a first line of defence against oxidative stress (Riva et al., 2005). Respiratory activity and capacity is reported to be greater in IFM which are thought to optimise energy production for contraction (Joseph et al., 2011; Ruiz-Meana et al., 2010). It is unclear whether these populations are differentially affected in diabetes and obesity. Studies have identified a lower number and smaller size of mitochondria in human skeletal muscle in individuals both obese and diabetic, compared to lean people (Kelley et al., 2002). There is a

direct correlation between mitochondrial size and insulin sensitivity due to many factors, including glucose disorders and lipid metabolism. Furthermore, mutations in mtDNA contribute to the production of smaller and more fragile mitochondria (Morino et al., 2005). Data indicates that the size and number of mitochondria in the skeletal muscle and cardiomyocytes are important determinants of mitochondrial activity (Morino et al., 2005).

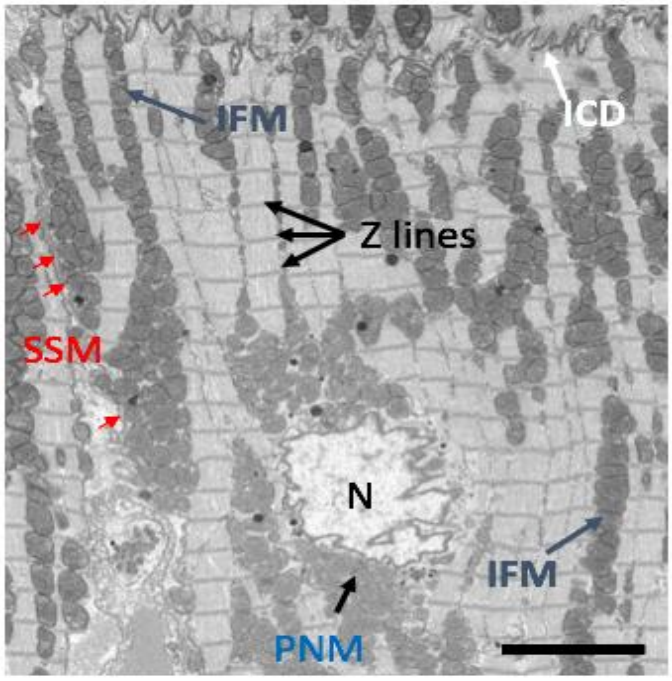

Figure 1.3 Mitochondrial ultrastructure and subpopulation.

Portion of a serial image from SBF-SEM illustrating the spatially distinct subtypes of mitochondria. SSM= subsarcolemma mitochondria; IFM = interfibrillar mitochondria; PNM = perinuclear mitochondria; ICD = intercalated disc; N=nucleus. Scale bar = 5 µm

The Akita mouse is a T1DM model developed from a spontaneous mutation in the insulin 2 gene, resulting in incorrect proinsulin processing (Al-Awar et al., 2016). This mutation results in misfolded protein aggregation and subsequently, *β*-cell death (Al-Awar et al., 2016). An electron-microscopy study done in Akita mice with T1DM revealed that mitochondria in the cardiomyocytes of the mice have reduced crista density and are smaller in size, compared to mice that did not have diabetes (Bugger and Abel, 2010). The number of mitochondria was similar in both diabetic and non-diabetic mice. Though similar observations were made by

other groups regarding the size of the mitochondria in the cardiomyocyte, there are inconsistencies regarding the number of mitochondria. These discrepancies may be due to a difference between disease progression and also the limitations of 2D electron microscopy techniques. Our group pioneered the use of serial block face scanning electron microscopy (SBF-SEM) to investigate cardiac myocyte ultrastructure (Pinali and Kitmitto, 2014). This technique allows reconstruction of organelles, such as mitochondria allowing details of the surface area and volume to be calculated for each mitochondrion as well as investigation into the mitochondrial distribution. This technique is applied in Chapter 3. Mitochondria shape and size are influenced by dynamic processes, fission (mitochondria dividing) and fusion (mitochondria combining).

Such volume scanning electron microscopy technique have been utilised for mitochondrial structural observations using blocks of tissue, a modification of traditional SEM. This technique has been of particular use for the investigation of the structural architecture of inter-mitochondrial junctions (IMJ). Colca et al. (2004) identified the protein mitoNEET (mNT) as required for IMJ formation via a dimerisation process whereby mNT of neighbouring mitochondria tether to form an IMJ. These tethering arms are thought to be flexible, enabling changes in orientation, such as that conformational changes can be made in response to oxidative stress within heart tissue (Landry et al., 2015). mNT knock out studies also shown a reduction of IMJs, whilst an increase in IMJs resulted in mitochondrial clustering (Vernay et al., 2017). Interestingly, ablated mNT in cardiac mitochondria were shown to have reduced oxidative capacity, compared to wild type, further supporting a strong role of mNT for mitochondrial cardiac function (Wiley et al., 2007).

1.2.3 Mitochondrial Dynamics

1.2.3.1 Mitochondrial Fusion

Both mitochondrial fission and fusion are required to maintain the function of mitochondria (Figure. 1.4). Fusion is the process whereby adjacent mitochondria fuse together mix contents

to complement each other. This mechanism enables protein complementation, repair of mtDNA and distribution of metabolites. In comparison, fission is important for mitochondrial segregation and for the distribution of mitochondria across the cell. Fission also helps to remove damaged portions of the mitochondria. Mitochondria fission has a role in cell protection and when the protective mechanism fails, it can initiate apoptosis (Sheridan and Martin, 2010). While GTP is required for both processes, the fusion of outer membrane and inner membrane (inner membrane fusion) requires the presence of an inner membrane potential (Hoppins and Nunnari, 2009). The mitochondrial membrane potential is generated by proton pumps (complex I, II, III) and works together with the proton gradient to form the transmembrane potential of hydrogen ions to make ATP (Zorova et al., 2018). The mitochondria depends on this membrane potential for the transport of proteins into the mitochondria; it has been postulated that the functional state of mitochondria can be assessed by the membrane potential magnitude (Popkov et al., 2015). *In vitro* work has shown that outer membrane fusion requires an inner membrane proton gradient (Meeusen et al., 2004) .On the other hand, inner membrane fusion requires the electrical component of the inner membrane. It is thought that this membrane potential results in the remodelling of fusion protein complexes, functionally linking outer and inner membrane fusion events (Hoppins and Nunnari, 2009).

Different sets of dynamin proteins govern outer and inner membrane fusion through three large GTPases; mitofusin 1 (Mfn1) and mitofusin 2 (Mfn2) in the outer membrane which form homo- and hetero-dimers and the optic atrophy protein 1 (Opa1) which facilitates fusion of the inner membranes (Liesa et al., 2009). The expression of Mfn proteins vary dependent upon tissue type; high levels of Mfn1 and Mfn2 are present in the heart, where Mfn2 is thought to be present at a higher concentration to Mfn1 (Santel et al., 2003). In the first step of outer mitochondrial membrane fusion, the heptad-repeat domain (HR2) of Mfn1 or Mfn2 on one mitochondrion forms dimers or complexes with Mfn1 or Mfn2 on adjacent mitochondria through assembly of a dimeric, antiparallel coiled coil (Koshiba et al., 2004). This structural process allows two adjacent mitochondria to tether together (Figure. 1.4).

In addition to Mfn1 and Mfn2, Opa1, an inner mitochondrial membrane protein, acts to promote mitochondrial fusion through the anchoring of its hydrophobic segments to the mitochondrial membranes (Olichon et al., 2007). In order for mitochondrial fusion to occur, Opa1 requires the presence of Mfn1 (Cipolat et al., 2004). Cipolat et al. (2004) tested the ability of overexpressed Opa1 in the absence of Mfn1 and Mfn2 to ascertain whether Opa1 fusion depended on other mitochondrial dynamics proteins. A functional difference was observed between Mfn1 and Mfn2; in Mfn1 null cells, mitochondria appeared globular, whereas in Mfn2 null cells, mitochondria ranged from round dots to short rods (Cipolat et al., 2004). These rods formations are important for the tubulation of mitochondria. Interestingly, the reintroduction of Mfn1 corrected Opa1-induced mitochondrial elongation, further confirming the interdependence between Mfn1 and Opa1. Overall, fusion is a two-step process, requiring the fusing of two outer membrane mitochondrion followed by fusion of the inner membrane; these steps require Mfn1/2 and Opa1.

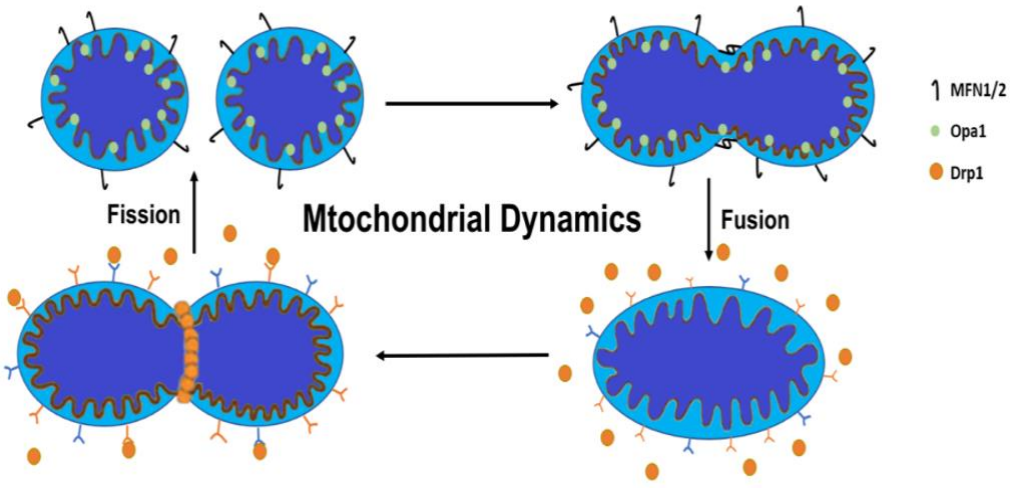

Figure 1.4 The fusion and fission reaction of mitochondria regulated by several key proteins, members of the dynamin family.

Mitofusins (Mfn) mediate the fusion of mitochondrial outer membrane, Opa1 mediates the fusion of mitochondrial inner membrane and Drp1 mediates mitochondrial fission. Figure taken from Tieu and Imm (2014).

1.2.3.2 Mitochondrial Fission

Fission is a division process whereby one or more daughter mitochondria are produced (Wada and Nakatsuka, 2016) (Figure. 1.4). Fission is under the control of a group of mitochondrial fission proteins, dynamin-related peptide 1 (Drp1), and mitochondrial fission protein 1 (Fis1) (Ong et al., 2013). The process of mitochondrial fission is complex and can be divided into five stages; the initial constriction of the mitochondria, the recruitment of cytosolic Drp1 to mitochondria, the assembly of a scission complex on the outer mitochondrial membrane, the actual scission event, and finally the disassembly of the scission complex (Ong et al., 2013). Drp1 was first identified as a protein that induces mitochondrial division (Smirnova et al., 1998). Upon activation, Drp1 oligomerises and constricts the mitochondrial scission site, through the use of GTPase. Fis1 is a small protein that promotes mitochondrial fission through inserting into the outer mitochondrial membrane via its COOH-terminal part, encouraging protein-protein interaction (Jofuku et al., 2005). It is thought that although Fis1 is required for fission, it is not a limiting factor and Drp1 is able to be recruited through other factors (Lee et al., 2004). In addition, to Drp1 and Fis1, mitochondrial dynamics proteins of 49 kDa (MiD49) and 51 kDa (MiD51) were identified as regulators of mitochondrial dynamics in fission/fusion. These proteins were found to form foci and rings around mitochondria and have the ability to directly recruit Drp1 to the mitochondria (Palmer et al., 2011).

Fission proteins are also recruited for the interplay of processes leading up to apoptosis. Upon apoptosis induction, the OMM is fragmented by the translocation of Drp1 from the cytosol to the mitochondria (Frank et al., 2001). During mitochondrial fragmentation, Drp1 phosphorylation is reduced, leading to an enhanced interaction between Drp1 and mitochondrial fission factor (MFF), and a decreased interaction between Drp1 and MiD51 (Zhang et al., 2016). The functional regulation of Drp1 through post-translation modifications is an important status to be considered (Chang and blackstone, 2007). Thus, Drp1 appears to play a number of important roles acting to orchestrate mitochondrial dynamics.

1.2.3.3 Mitochondrial Mitophagy

In instances of mitochondrial damage or dysfunction, mitochondria are either complemented with an undamaged part of the mitochondrial network by fusion or prepared for mitophagy (Twig and Shirihai, 2011). Mitophagy is an organelle-specific process whereby damaged mitochondria and mitochondria with reduced membrane potential are removed through ubiquitination and the fusion of autophagosomes with lysosomes, ensuring quality control of cellular mitochondria (Ashrafi and Schwarz, 2013). Fission can cause the production of daughter mitochondria with reduced membrane potential as a result of uneven fission (Joseph et al., 2011). This reduced membrane potential is thought to stimulate the activity of PINK1 (PTEN-induced putative kinase protein 1), a serine/threonine kinase (Chen and Dorn, 2013). PINK1 and Parkin, an E3 ubiquitin ligase, interact to form the PINK1-Parkin signalling pathway, important for regulation of the mitochondrial mitophagy pathway. It is thought that the initial sensing of damaged mitochondria is regulated by PINK1, leading on to the induction of mitophagy through the expression of Parkin (Narendra et al., 2008).

Upon membrane depolarisation, PINK1 accumulates on the OMM, as a result of restricted cleavage that normally enables proteasomal degradation (Narendra et al., 2010). Once identified by PINK1, PINK1 phosphorylates OMM proteins and recruits Parkin (Chen and Dorn, 2013). Parkin can translocate to depolarised mitochondria (Narendra et al., 2008), ubiquitinating OMM proteins, including Mfn1 and Mfn2, activating mitophagy (Sarraf et al., 2013). This process is important for mitochondrial maintenance and quality control, ensuring that damaged or dysfunctional mitochondria are efficiently removed. As one of the interests of this research project, it has been shown that mitochondrial integrity is compromised in diabetes, suggesting a possible link with the failure of mitochondrial quality control due to the inhibition of mitochondrial dynamics proteins in diabetes.

1.2.3.4 Mitochondrial Motility

Mitochondrial motility is important for the regulation of calcium signalling and for energy supply around the cell. The regulation of these processes is dependent upon the motility of mitochondria up and down microtubules in a calcium-sensitive manner (Ong et al., 2013). The proteins that control mitochondrial motility are Miro, Milton and motor proteins, dynein or kinesin. In addition to controlling motility, these proteins have been shown to influence mitochondrial morphology. In H9c2 cells that overexpress Miro1 and Miro2, mitochondrial elongation was induced, whereas ablating Miro resulted in Drp1-mediated mitochondrial fragmentation (Saotome et al., 2008).

1.3 Miro proteins and mitochondrial motility

Miro GTPases are members of the Ras superfamily and are important mediators of mitochondrial dynamics (Boureux et al., 2007). Miro1 is a protein that promotes mitochondrial transport by binding the mitochondria to kinesin and dynein motors. Mitochondrial Rho (Miro) is a small GTPase known to be involved in mitochondrial transport and homeostasis (Tang, 2016). Miro proteins are composed of two GTPase domains, in comparison to the one GTPase domain found in other small GTPases. In mammals, two Miro proteins exist, Miro1 and Miro2 sharing approximately 60% sequence identity (Figure 1.5) (Fransson et al., 2003). *D. melanogaster* Miro is known to regulate the movement of mitochondria by recruiting the motor proteins kinesin and dynein based on the microtubule network, forming a protein complex with the kinesin adaptor Milton (Glater et al., 2006). On the other hand, in humans, Miro proteins interact with motor proteins by the formation of a protein complex with the TRAK1/2 cargo adaptor proteins (Macaskill et al., 2009a).

1.3.1 Miro structure

Miro1 and Miro2 are 618 amino acids in length and are 60% identical to each other (Fransson et al., 2003). Both proteins consist of two EF motifs linking the GTP-binding domains and a C-terminal transmembrane domain that binds proteins to the OMM (Figure. 1.5). The EF-hand

motif functions as a binding site for the Milton modifier protein and kinesin heavy chain. These domains can also bind calcium ions and this binding causes conformational changes that separate the mitochondrial surface from kinases (Wang and Schwarz, 2009). The EF-hands bind calcium (Macaskill et al., 2009b) allowing it to act as a calcium sensor. Structurally, Miro GTPases are the only known human protein that contain two different GTPase domains in the same polypeptide chain (Kay et al., 2018).

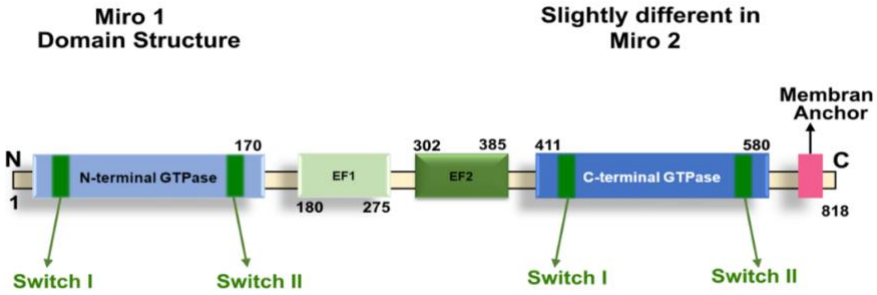

Figure 1.5 Domain architecture of human Miro GTPase.

The structure consists of an amino terminal and carboxy terminal GTPase domain (light and dark blue, respectively); two calcium-binding EF-hand domains, flanked by the catalytic domains; and the C-terminal transmembrane domain anchors mitochondria to the outer membrane (pink rectangle). Figure taken from (Eberhardt et al.,2020)

There are slight differences in the switch regions between Miro1 and Miro2. Miro GTPases are atypical in their structure, varying in their Switch I/II regions compared to other Ras superfamily members (Eberhardt et al., 2020). In Miro proteins the Switch I/II regions are located at both the N- and C-terminals, with a slight regional difference at the C-terminal domain in Miro2, compared to in Miro1 (Figure 1.5). Typically, Switch I regions are involved in nucleotide stabilisation and Switch II regions are involved in the regulation of nucleotide hydrolysis (Peters et al., 2018). In Miro2, the C-terminal Switch regions differ slightly from Miro1 with Switch I corresponding to residues 446-455 and Switch II comprising residues 472-489 (Peters et al., 2018). The presence of two GTPase domains suggest a dual potential of

Miro regulation. A number of studies have employed point mutations at N- or C-terminal GTPase positions, with the aim to stabilise the GTP/GDP Miro forms (Fransson et al., 2003; Fransson et al., 2006; Macaskill et al., 2009b). Here, the behaviours of these mutants were observed to further elucidate the functions of Miro in different states. Miro GTPases are found anchored to the outer mitochondrial membrane, bound by their C-terminal domain (Figure 1.6) and play a key role in the intracellular mitochondrial movement in the majority of neurons studied (Tang, 2018).

The majority of studies of Miro1 have been in neuronal cells. In order to maintain the health of neurones, mitochondria are required to be transported along the neuronal body and positioned for efficient energy production. Poor neuronal health has been implicated in Parkinson's Disease, where it has been hypothesised that Miro1 is upregulated on damaged mitochondria, resulting in increased mitochondrial motility (Hsieh et al., 2016). Thus, this increased mitochondrial motility causes delayed mitophagy and ultimately, neurodegeneration. For this reason, the majority of studies investigating Miro proteins are investigating the neuronal impact and function of these proteins.

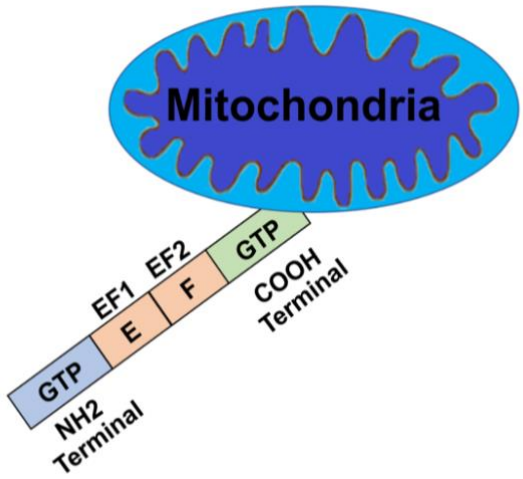

Figure 1.6 Miro1 anchors to the outer mitochondrial membrane (OMM).
Miro1 tethers to the OMM via its C-terminal domain.

1.3.2 Miro function

Functionally, Miro is responsible for a number of different mitochondrial processes. Miro is known to facilitate mitochondrial transport, calcium-dependent mitochondrial transport, mitochondrial morphology, fission and fusion, neuronal health and has reported effects on ATP homeostasis (Kay et al., 2018). Miro is known to aid mitochondrial transport through intracellular microtubules (Chen et al., 2017). Although Miro1 has been studied primarily in neurons, this protein has also been found to be involved in mitochondrial transport and lymphocyte adhesion during inflammation to activated endothelium (Morlino et al., 2014). At high concentrations, calcium ions inhibit mitochondrial transport by binding to Miro1, thereby removing the complex from the organelles (Nemani et al., 2018). Miro1 degradation inhibited mitochondrial removal and degradation preventing the fusing with healthy mitochondria, thereby promoting clearance by their own phagosomes. Although the exact mechanism remains to be clarified, Miro1 is involved in promoting caspase-dependent apoptosis (Kay et al., 2018). Ectopic expression of a Miro1 mutant has been associated with an increase of M30, an apoptotic marker that recognises caspase cleavage (Fransson et al., 2003). Further evidence of this caspase-dependent apoptosis process was shown by the use of caspase inhibitors reducing the presence of the M30 marker, supporting the role of Miro1 in apoptosis (Fransson et al., 2003).

Miro1 has been shown to have a number of interacting partners (Figure 1.7). These proteins include: TRAK1 and TRAK2 (microtubule-based mitochondrial transport) (Macaskill et al., 2009a); KIF5 (microtubule-based transport (anterograde) (Wang and Schwarz, 2009); mitofusin 1 and 2 (mitochondrial fusion) (Misko et al., 2010); PINK1 (regulator of mitochondrial stress response and mitophagy) (Weihofen et al., 2009); and Parkin (component of the ubiquitin-proteasome system of protein degradation) (Birsa et al., 2014). This wide array of Miro1 binding partners suggests that it has a pivotal role in mitochondrial dynamics, quality control and transport.

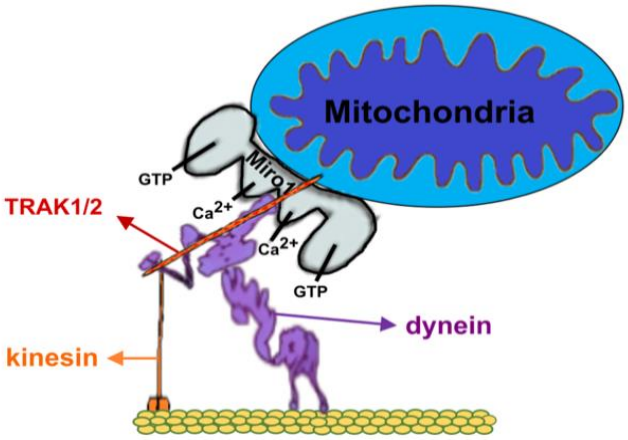

Figure 1.7 Miro1 interacting partners

Docking of motor complexes (dynein, kinesin and TRAK1/2) onto mitochondria and microtubules. Figure adapted from (Eberhardt et al.,2020)

As a C-terminal anchored outer mitochondrial membrane protein, Miro1 acts as a receptor on which motor proteins assemble, forming a link between the mitochondria and microtubule (Guo et al., 2005). As mentioned above, Miro1 interacts with the adaptor TRAK proteins (mammals) or Milton (*Drosophila*) to recruit kinesin and dynein, driving anterograde (towards the (+)-end) and retrograde (towards the (-)-end) mitochondrial transport, respectively (Figure 1.8) (Fransson et al., 2003; Fransson et al., 2006). Mouse studies have eluded to functional differences between Miro1 and Miro2 López‐Doménech et al. (2018). To characterise these differences, López‐Doménech et al. (2018) generated Miro1/2 single and double-knockouts in mice and analysed the localisation of the motor proteins TRAK1/2. The authors showed that TRAK proteins were still able to localise to the mitochondria in the complete absence of Miro proteins, with mitochondria still found aligned to microtubule filaments. When investigated separately, Miro2-KO cells exhibited unaltered fast tubulin-dependent mitochondrial transport events, whereas in Miro1-KO there was a significant reduction in the number of such events (López-Doménech et al., 2018). Secondly, López-Doménech et al. (2018) showed that overexpression of TRAK2 in Miro1-KO cells resulted in the inability of cells to redistribute mitochondria, as observed in WT and Miro2-KD cells. Thus, Miro1 may facilitates the TRAK2-dependent redistribution of mitochondria. Together, this data suggests that Miro1 and Miro2

differentially regulate mitochondrial transport. In this chapter, Miro1 will be investigated as it was identified as downregulated in our previous data (Chapter 2).

Mitochondrial transport by Miro1/2 is facilitated by kinesin and dynein proteins (Macaskill et al., 2009). Miro forms a protein complex with the kinesin-associated protein, Milton, trafficking kinesin-binding protein 1 (TRAK1) and TRAK2 (Macaskill et al., 2009b). It is thought that Miro anchors to the mitochondrial outer membrane, Milton aids with linking the kinesin/dynein motor protein to Miro1, facilitating the movement of mitochondria along the microtubules (Figure 1.8).

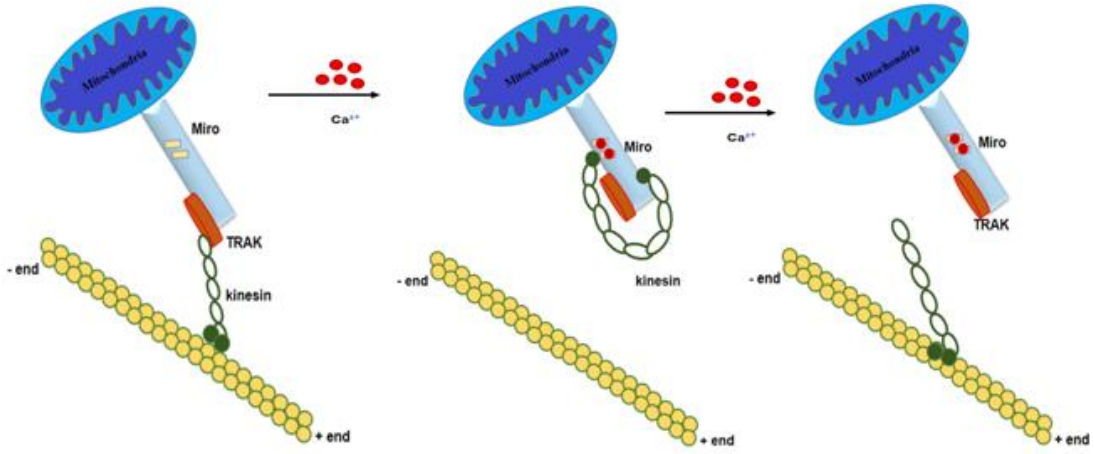

Figure 1.8 Miro is involved in the movement of mitochondria in cooperation with TRAK1/2 across microtubules.

TRAK1, predominantly localised in axons, binds both kinesin and dynein, whilst TRAK2, localised in the dendrites, binds dynein. Miro's binding to both TRAK proteins enables the bi-directional movement of mitochondria. Figure taken from (Kay et al.,2018)

In *Drosophila*, Russo et al. (2009) investigated the mechanism regulating the opposing movements facilitated by kinesin and dynein motors, to promote microtubule-based transport of mitochondria. dMiro was genetically manipulated and mitochondrial transport in Drosophila motor axons was measured. Dysfunctional dMiro resulted in the impairment of both anterograde and retrograde mitochondrial movement (Russo et al., 2009), further evidencing the importance of Miro in mitochondrial transport. The role of cytosolic calcium in this process has been disputed. Studies show that the EF-hands are involved in binding calcium and

sensing calcium influx when activated, leading to conformational changes in Miro that directly impact mitochondrial mobilisation (Wang and Schwarz, 2009). It has also been argued whether Miro binds directly to kinesin, without the need for Milton (Macaskill et al., 2009b), or if increased cytosolic calcium concentrations cause the dissociation of the kinesin motor and the subsequent interaction of Miro with the mitochondria (Kay et al., 2018). Wang and Schwarz (2009) proposed a model of how calcium and Miro1 control mitochondrial trafikking. Their results showed that Miro1 requires the presence of Milton as an adaptor to enable binding to KIF, however, a low level of Miro-KIF association was measured without Milton present (Wang and Schwarz, 2009), suggesting that Milton may not be a necessary binding factor. The other model suggests that increased cytosolic calcium may arrest movement by dissociating the Miro-Milton complex, releasing mitochondria from the motor. The authors showed that calcium works through Miro's EF-hands to cause kinesin heavy chain dissociation from microtubules (Wang and Schwarz, 2009). Thus, these results show that there is an association between mitochondrial motor machinery, movement of the mitochondria and calcium concentration.

In H9c2 cells, Miro1 expression at the OMM has been shown to affect calcium concentration in the mitochondrial matrix, acting as a calcium-sensitive switch (Saotome et al., 2008). Saotome et al. (2008) investigated the association of Miro1 and Miro2 with regards to mitochondrial dynamics and calcium oscillations. At resting calcium concentrations, Miro1 overexpression caused an elevation in mitochondrial movement and calcium. This calcium-switch is representative of Miro's role as regulating both motility and fusion-fission mitochondria dynamics (Saotome et al., 2008). It has also been suggested that Miro has a role in mitochondrial morphology. Overexpression of Miro in *Drosophila* resulted in the aggregation of mitochondria in neurones (Liu et al., 2012), whilst elongated mitochondria were observed in a similar study (Russo et al., 2009). This research suggests that Miro proteins impact mitochondrial appearance potentially through its binding partners. As mentioned previously, Miro mediates the balance between mitochondrial fission and fusion. As mentioned above, fission and fusion processes enable mitochondrial morphology changes with the availability of Miro1 shown to be directly proportional to mitochondrial length.

1.3.3 Calcium dependency

The EF-hands of Miro1 enable the binding of Ca^{2+} through the helix-loop-helix motif (Chazin, 2011). This binding enables Miro's EF-hands to act as a calcium-dependent switch, regulating mitochondrial transport. Live-cell imaging studies have shown that the influx of cytoplasmic Ca^{2+} results in the blockage of mitochondrial transport (Wang and Schwarz, 2009). This regulatory mechanism causes mitochondria to position themselves near Ca^{2+} sources, enhancing ATP production during high demand (Yi et al., 2004). In order to address how Ca^{2+} regulates motor proteins in mitochondrial motility, Wang and Schwarz (2009) examined mitochondrial movement in transfected neurones. The authors showed that the EF-hands of Miro1 are essential for the Ca^{2+} dependent arrest of axonal mitochondria and that the Miro1-Ca^{2+} interaction results in kinesin heavy chain to lose association with microtubules (Wang and Schwarz, 2009). Genetic deletion of Miro1 has also shown to be lethal, suggesting a non-redundant role of Miro1 (Nguyen et al., 2014). Thus, mitochondrial transport via Miro1 is dependent on Ca^{2+}.

1.4 Conclusion

Diabetes sufferers are at greater risk for developing cardiovascular complications and have poorer outcomes. Work from our group indicate that GENA348 mice develop cardiac dysfunction and thus may indicate that MODY2 patients may also be at risk. Currently, there are limited treatments for diabetics and in particular for MODY patients. Mitochondria dysfunction has been identified as a driver of cardiovascular disease in both obese and diabetic patients. However, the pathological effectors and mechanisms that lead to mitochondrial dysfunction are incompletely understood. A common feature of mitochondrial dysfunction is changes to the structure and distribution, characteristics influenced by the processes of fission and fusion. Previous work in our group has revealed that in a T1DM model of diabetes, the fusion protein Mfn2 is dysregulated but Drp1 and Opa1 are unchanged, which leads to an imbalance in the fission-fusion axis and thus, mitochondrial morphology and

function. It is evident that proteins such as Miro, Mfn1/2 and Opa1 are key to the regulation of mitochondrial processes and for quality control. This project investigates whether impaired mitochondrial dynamics is a feature of MODY2 and if a high fat diet exacerbates the phenotype. Delineating the pathways underlying changes to mitochondrial dynamics in the diabetic and obese myocardium may reveal novel therapeutic targets and also provide new insights into management of MODY.

1.5 Project aims & Objectives

Research into the MODY2 cardiac phenotype is limited, with a lack of understanding into how the mitochondria are impacted and the molecular players that are implicated in the disease. The specific aims of this study are:

1) Characterisation of the cardiac and mitochondrial phenotype of MODY2 in GENA348 mice using quantitative mass spectrometry for global protein profiling (Chapter 2)

2) Characterisation of cardiac mitochondrial subpopulation ultrastructure in the GENA348 mice using serial block face scanning electron microscopy (Chapter 3)

3) Investigation of the effect of a high fat diet on GENA348 cardiac phenotype and how the pathology compares to wild type (WT) animals fed a high fat diet (Chapter 4)

4) Investigation of the role of Miro1 in mitochondrial structure-function and fission-fusion (Chapter 5).

Chapter 2 Characterisation of the cardiac and mitochondrial phenotype of a mouse model of MODY2 (GENA348)

2.1 Introduction

As described in the introduction to this thesis (Section 1.1.2), Maturity Onset of Diabetes in the Young (MODY2) is a genetic form of diabetes with a mutation in the *Gck* gene (Carmody et al., 2016). Although less prevalent in comparison to T1DM or T2DM, it is thought that MODY affects 1-2% of people diagnosed with diabetes mellitus (Kleinberger and Pollin, 2015).

Clinical diagnosis of MODY can be recognised and diagnosed through a number of clinical characteristics including; parental history of neonatal diabetes, early onset of diabetes, low insulin required for treatment (insulin independence) and lack of significant obesity (Urbanova et al., 2018). Historically, MODY has proven challenging to identify due to the clinical heterogeneity of the disease. Genetic sequencing methods are used for diagnosis (Kleinberger and Pollin, 2015) although a limitation with this method is the lack of research characteristics in African or Latino populations, leading to gaps in correct diagnosis (Kleinberger and Pollin, 2015). To manage the disease, patients are categorised dependent on their disease type and genetic cause (Thanabalasingham and Owen, 2011). Treatment includes a change in diet, insulin administration and oral antidiabetic agents. For example, ABCC8-type MODY is characterised by a dysfunction of ATP-sensitive potassium channels. For treatment, patients are given sulfonylureas, an oral antidiabetic agent (Bowman et al., 2012).

Because of the absence of clinical symptoms, MODY may go undiagnosed (Velho et al., 1997). Children and adults may be symptom-free, merely experiencing mild fasting hyperglycaemia (6–7mM); therefore, many MODY patients are only identified by chance through routine or prenatal check-ups (Velho and Robert, 2002). There is a broad spectrum of clinical features presented by patients with MODY. These extend from the mild, such as fasting hyperglycaemia and limited complications to severe, with progressive hyperglycaemia

and chronic vascular problems (Aigner et al., 2008). However, some patients may present with marked hyperglycaemia that becomes more severe with age and go on to develop diabetic complications similar to those exhibited by patients with T2DM (Velho et al., 1996). Distinguishing between advanced MODY and T2DM is a challenge for clinicians, leading to the claim that many MODY patients may have been misdiagnosed and that its prevalence is greater than expected (Ehtisham et al., 2004). Ledermann places an estimate of 2–5% of patients that have been diagnosed as T2DM as being MODY patients (Ledermann, 1995). Further, the number of cases of MODY is likely to be underestimated due to lack of large population screening programmes. For example, the introduction and development of monogenic diabetes testing methods in one region of the UK ,which had only identified 50 MODY patients in 1996, was able to diagnose 5000 by 2016 (Hattersley and Patel, 2017). Kleinberger and Pollin (2015) reported that MODY cases are missed due to a lack of awareness amongst people. As a result, further complications occur, resulting in increased complexity.

As previously mentioned, (Section 1.1.2, Table 1.1) the *Gck* (MODY2) and hepatocyte nuclear factor 1A (HNF1α, MODY3) mutations are the most frequently diagnosed MODY types (Szopa et al., 2015). In order to investigate the cardiovascular complications in both MODY types, Szopa et al. (2015) examined carotid artery intima-media thickness (IMT) and endothelial function in human subjects diagnosed with MODY. Results showed that both MODY types were associated with arterial wall dysfunction and abnormalities in endothelial function (Szopa et al., 2015). HNF1α-MODY patients were more likely to have higher IMT values than *Gck* MODY types. Similarly, Pruhova et al. (2013) used IMT measurements as an indicator of macrovascular complications; they reported that *Gck* MODY patients were not at risk of IMT increase. Furthermore, an impairment in maximum microvascular hyperaemia was reported in HNF1α-MODY patients (Lee et al., 1999). Jaap et al. (1994) reported the importance of microvascular function as a key change that can be associated as a cardiac phenotype in diabetes.

More recently, the spectrum of genetic variants of monogenic diabetes were investigated (Glotov et al., 2019). Using whole-exome sequencing, Glotov et al. (2019) screened 35 genes causative of MODY and transient or permanent neonatal diabetes in a cohort of Russian children. These genes included 13 genes causative of MODY, amongst them *Gck* (MODY2). Their results revealed a high rate of genetic variants causative of monogenic diabetes. Interestingly, the authors confirm ethnic differences (Glotov et al., 2019).

Interestingly, there is a reported increased prevalence of HNF1α-MODY frequency in Northern Europe and *Gck*-MODY is more prevalent in Southern Europe (Glotov et al., 2019). In fact, the majority of patients in this study had genetic variants in *Gck* (MODY2) (Glotov et al., 2019). This is further corroborated by a recent study investigating the molecular basis of MODY in Chinese patients (Xu et al., 2020). Similarly, the authors report that most MODY patients were due to *Gck* mutations, further suggesting region-dependent differences in the prevalence of MODY types.

2.1.1 Gck-MODY (MODY2)

Glucokinase-maturity-onset diabetes of the young (*Gck*-MODY), also known as MODY Type 2 is one of the common types of MODY diabetes (Table 1.1). This mild disease type is caused by a heterozygous mutation on the glucokinase gene on chromosome 7 (Vionnet et al., 1992). In contrast, homozygous mutations cause a complete loss of glucokinase and results in permanent neonatal diabetes necessitating insulin treatment in the first few days of life. Glucokinase acts as a blood glucose sensor for the pancreas, thereby controlling insulin release. Normal function of glucokinase ensures blood glucose is kept at normal levels. As a result of this mutation, the insulin threshold is impaired causing persistent hyperglycaemia (Byrne et al., 1994). This may go unnoticed due to a lack of long-term complications and only noticed during routine checks, such as during pregnancy. *Gck* MODY patients do not usually require treatment and are non-obese, differentiating this type from T1DM and T2DM.

Glucokinase mutations in MODY patients have been shown to affect the catalytic properties of the enzyme. With facilitated diffusion, glucose is taken into the β-cell, leading to its phosphorylation by *Gck*. This rate-limiting step is followed by glycolysis in the tricarboxylic acid (TCA) cycle, resulting in a rise in the ATP/ADP ratio (Figure. 2.1). Eventually, insulin is secreted, and cellular homeostasis can occur. Hence, glycolytic metabolism is tightly coupled to mitochondrial metabolism (Fex et al., 2018). The impairment of this process as a result of the point mutation, such as in MODY2 patients, causes an impact on mitochondrial and metabolic mechanisms.

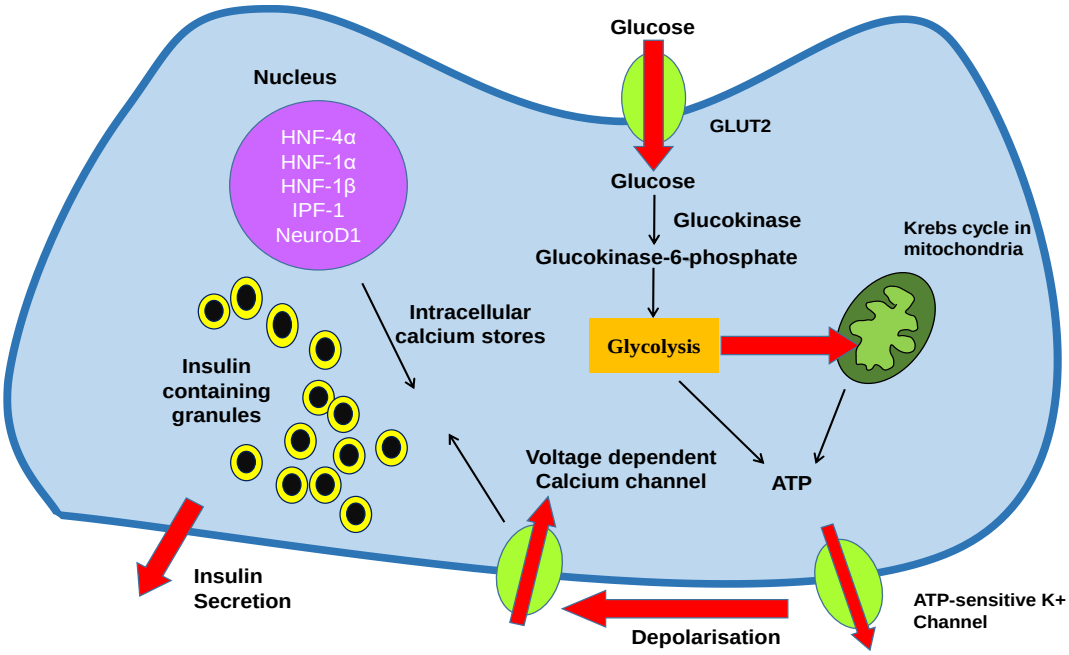

Figure 2.1 The pancreatic β cell response to glucose.

Glucose is transported into β cells of the pancreas via GLUT-2 transporters. Once in the cell, the glucokinase enzyme, which is the β cell's glucose sensor, catalyses its conversion to glucose-6-phosphate. ATP, generated through the Krebs cycle, binds to ATP-sensitive potassium channels, causing them to close and the membrane to depolarise. The change in membrane potential causes the voltage-dependent calcium channels to open and calcium influx; this stimulates further calcium to be released from intracellular stores. In response to the elevated intracellular calcium concentration, granules containing insulin fuse with the plasma membrane, leading to exocytosis of the insulin. The mechanism for insulin secretion is disrupted by mutations in the glucokinase enzyme.

2.1.2 GENA348 Mouse Model

Thus, the development of the GENA348 mouse model provides an ideal system for investigating disease development. The GENA348 mouse model contains an A to T transversion mutation in the glucokinase gene, resulting in an isoleucine to phenylalanine change at amino acid 366 (Toye et al., 2004).

As first reported by Toye et al. (2004), the GENA348 *Gck* gene mutation is located in exon 9 of the gene, resulting in a missense amino acid change in amino acid 366 from isoleucine to phenylalanine (I366F). In humans, it has been shown that a missense mutation in an adjacent amino acid, V367M, results in diabetes (Toye et al., 2004). This demonstrates the functional significance of this gene region in protein function, further reflecting on the use of GENA348 as a mouse model. Fabiano et al. (2016) reported the major advantage of the GENA348 mouse model as being analogous and clinically relevant to the MODY2 model, which helps in determining the different mutation factors and genes that could affect the functioning. The study of Postic et al. (2001) outlined that insulin secretion, as well as impaired glucose levels, are increased due to the *Gck* gene just as in humans, therefore, the mouse model is an effective clinical model. Traditionally, animal models have not reflected the human genetic condition of diabetes, limiting their use. As mentioned in the introduction, Toye et al. (2004) introduced the GENA348 mouse model of diabetes, exhibiting similar impaired glucokinase function and decreased insulin secretion in humans with MODY2. The GENA348 mouse model was studied for its expression of a cardiac phenotype (Mamas et al. (2009) to determine its applicability for studies of diabetes-associated heart failure. Using echocardiography, authors reported significant cardiac hypertrophy observed in the homozygote mutants in comparison to the WT mice, making this model a good option for use in MODY2 research. In addition, Akt phosphorylation levels were measured by Western blot analysis. Akt phosphorylation increases the insulin-dependent transport of glucose into the cell (Mackenzie and Elliott, 2014). GENA348 demonstrated increased Akt phosphorylation, involved in cardiac hypertrophy (Jin et al., 2019). It was observed that mice had exhibited progressive cardiac

phenotype with the development of hypertrophy as well as diastolic dysfunction (Mamas et al., 2009).

2.1.3 Mitochondrial Dysfunction in GENA348

While Mammas et al. (2009) has demonstrated that the GENA348 mouse develops LV diastolic dysfunction, there has since been very little information pertaining to the cardiac phenotype especially at the cellular level. Given that mitochondrial dysfunction is an early development in the progression of diabetic cardiomyopathy e.g. (Sivitz and Yorek, 2010) (Section 1.1.8), a focus of this component of the thesis was to investigate mitochondrial function in the GENA348 mouse. In addition, investigations of proteins regulating mitochondrial size and shape i.e fission, fusion and motility were undertaken (Section 1.2.3)

Zhong et al. (2017) have linked diabetes with cardiac dysfunction as a result of inflammation. Increasing evidence has shown that diabetes can be classified as in inflammatory disease as a result of the auto-immune destruction of pancreatic B-cells (Zhong et al., 2017) (Marques-Vidal et al., 2012). To our knowledge, there have been no published studies of inflammation and MODY2. Therefore, another aim to this study was to investigate cytokine levels in GENA348 mice. This data will advance understanding of the characteristics of GENA348 and effect of glucokinase malfunction with potential translational value for MODY2 patients.

2.1.4 Miro1 and mitochondrial function

PINK1 and Parkin play a central role for regulating mitochondrial quality control, marking damaged mitochondria through ubiquitination for mitophagy (Eiyama and Okamoto, 2015). Mitophagy is the process by which damaged mitochondria are cleared through autophagy machinery. As previously mentioned, Miro is reported to interact with PINK and Parkin, suggesting a role for Miro in mitochondrial turnover and destruction. The PINK1/Parkin pathway is known to target Miro1 for phosphorylation and degradation, leading to the arrest

of mitochondrial movement (Wang et al., 2011). It is thought that PINK1 phosphorylates Miro1, activating the degradation of Miro1 in a Parkin-dependent process. As mentioned earlier, Miro1 is an important protein involved in anchoring the mitochondria to motor proteins and the microtubules enabling mitochondrial movement. Thus, removal of Miro1 in this PINK1/Parkin pathway, is thought to detach kinesins from the mitochondria, preventing mitochondrial movement.

2.1.5 Miro1 in the heart

Although there is a lack of mitochondrial motility in adult cardiomyocytes, Miro, TRAK and motor protein kinesins are abundantly present in heart and skeletal muscles (Cao et al., 2019). This could suggest an important role for Miro1 in regulating communication between mitochondria and microtubules. Drp1 inhibition, an important fission-fusion protein, has been shown to cause mitochondrial condensation and elongation, suggesting a change in Miro-mediated fission-fusion activity (Varadi et al., 2004). Saotome et al.,(2008) further investigated this by overexpressing a dominant-negative form of Drp1 and showed that this inhibited the Miro-induced mitochondrial fragmentation in H9c2 cells, suggesting that fission is required for Miro-induced mitochondrial changes. Overall, while there are only a few studies of Miro1 in the heart, current evidence supports a similar role as that identified in neuronal cells (Hsieh et al., 2016) and that it is important for the modulation of mitochondrial dynamics and cell function.

2.1.6 Primary cardiomyocytes vs H9c2

Primary cardiomyocytes can be difficult to isolate, requiring animal sacrifice for each stage of study. The H9c2 line of embryonic rat cardiomyocytes are considered a sub-clonal line of the original clonal cell line, derived from the embryonic rat tissues of BD1X. As an animal free alternative, rat ventricular H9c2 cells are a validated line that closely mimic the response of adult cardiomyocytes in conditions of cardiac hypoxia, ischaemia reperfusion, myocardial infarction and hypertrophic response, making then a suitable substitute for studying

cardiomyocyte function. When compared to primary rat neonatal cardiomyocytes, H9c2 cells showed an almost identical response to hypertrophic factors angiotensin II and endothelin-1 (Watkins et al., 2011). Furthermore, in conditions of myocardial infarction they are more energetically similar to primary cardiomyocytes than other cell lines, such as mouse atrial HL-1 cells (Kuznetsov et al., 2015). In addition to energetics, Kuznetsov et al. (2015) measured the levels of the cytoskeletal protein β-tubulin II, important for regulating cardiac energy metabolism. They showed that in H9c2 cells, β-tubulin II was present, suggesting a similar mode of regulation for mitochondrial functions as adult primary cardiomyocytes (Kuznetsov et al., 2015). Importantly, H9c2 cells were also highly sensitive to hypoxia and oxidative stress (Kuznetsov et al., 2015), further supporting the use of H9c2 cells due to the similarity of their mitochondrial function and bioenergetics to adult primary cardiomyocytes.

Another alternative model is the use of neonatal rat cardiomyocytes. Neonatal rat cardiomyocytes offer the ability to study adaptive mechanisms, due to their homogeneous population of cardiac cells (Kuznetsov et al., 2015). However, they lack mitochondrial creatine kinase and have increased levels/activity of membrane-bound hexokinase, suggesting a greater dependence on glucose, in comparison to adult cardiomyocytes (Kuznetsov et al., 2015). Adult hearts are aerobic, whereas new-born hearts rely more on glycolysis. Thus, substrate use would differ to that of adult cardiomyocytes, making neonatal rat cardiomyocytes a less attractive option for use in this study. In addition, to generate the neonatal rat cardiomyocytes requires regular animal sacrifice. Therefore, in this chapter, H9c2 cells were employed to study cardiomyocyte function and Miro1. Here, we employed functional studies and morphological assessment to further investigate the role of Miro1 in mitochondrial function.

2.1.7 Aim of study

A previous study by Stephen Gibbons identified that at 6 months of age, GENA348 mice exhibit impaired cardiac function. The aims of this chapter are:

1) Functional studies to determine if oxygen consumption and OXPHOS is impaired in the GENA348 cardiac mitochondria.

2) Employ proteomics to investigate global changes to mitochondrial protein expression, with ingenuity pathway analysis (IPA) to map the pathways that have been impacted.

3) To determine if proteins associated with mitochondrial dynamics are altered in the GENA348 mouse LV compared to controls.

4) To determine if there is evidence of inflammation in the GENA348 mouse heart compared to WT.

5) To establish and characterise the role of Miro1, the following parameters were investigated after Miro1 knockdown (KD) in a cardiomyoblast cell line. Specifically: i) The expression and regulation of fission-fusion proteins

ii) Mitochondrial function, including oxygen consumption

iii) Changes to mitochondrial morphology

2.2 Methods

2.2.1 GENA348 mouse model of Gck-MODY

All experiments were performed according to current UK Home Office regulations and under approval of the relevant University of Manchester local ethics committee. The GENA348 mice were cloned after mapping the glucokinase gene and introducing a Transversion mutation (A to T) in exon 9 of the gene. The resultant mice were used as a model for MODY2 diabetes, and the process of single nucleotide polymorphism (SNP) was established to genotype the mice. As the Cartwright group had previously shown that GENA348 mice develop cardiac dysfunction at 6 months, the animals were treated with the following regimen: at 3 months the aged-matched wild type and GENA348 mice were randomly divided into two groups; one chow-fed and the other on a high fat diet (60% kcal from fat) - a custom made diet (Special Diet Services) containing 24% fat. This led to 4 groups; wild type normal chow; wild type on HFD, GENA348 on normal chow; GENA348 on HFD.

An Acuson Sequoia 256 cardiac ultrasound system with 15L8 transducer probe set to 14MHz was used to obtain transthoracic echocardiograms of the mice (performed by Dr Min Zi) after removal of the chest hair using a depilatory cream. The probe was covered with warm transmission gel (Henleys Medical) prior to positioning on the thorax. M-Mod was used to measure the following chamber parameters: diastolic left ventricular diameter (dLVD), systolic left ventricular diameter (sLVD), diastolic interventricular septum (dIVS), systolic interventricular septum (sIVS) and diastolic posterior wall (dPW) thickness.

Animals were sacrificed by cervical dislocation (CD) at 6 months of age (Peformed by Sukhpal Prehar). Blood was collected from the tail vein and terminal blood glucose analysed using the Accu-Check (Aviva) blood glucose meter. For each mouse three measurements were obtained and the average recorded. The heart, body weight, lung weight, and the tibia length were measured. The atria were discarded, and the ventricles immediately frozen in liquid nitrogen and stored at -80°C for further analysis.

2.2.2 Insulin assay

Serum was collected via the Jugular, Femoral or Carotid; under Isoflurane anaesthesia. Placed in Eppendorf's for a minimum of 2-4 hours, in order to allow clotting, then centrifuged at 4°C, spin it at 2000 rpm for 5-10 mins. The top Serum layer was used and freeze at -80°C. Collected serum was used to determine the insulin levels through the ALPCO Mouse Insulin ELISA Kit (80-INSMS-E01, E10). Firstly, 75 µL of Working Strength Conjugate in addition to a further 10 µL of standards, controls and samples were added to each microplate wells. Secondly, the microplate was left on a microplate shaker at 700-900 rpm for 2 hr at room temperature. Following on from the incubation period, each well was cleaned 6 times using 350 µL of Working Strength Wash Buffer. The wells then had TMB Substrate added to the microplate well and the microplate well then had a secondary incubation period using a microplate shaker at 700 – 900 rpm for 15 min. Upon completion of the secondary incubation period, each well had 100 µL of Stop Solution added and a reading of their optical density (OD) was taken by a spectrophotometer at 450 nm. This was taken using the Thermo Labsystem microplate reader.

2.2.3 Tissue lysis for Western blotting

Hearts were lysed for Western blotting using a fastPrep -54 5G instrument (MP Biomedicals Inc). The tissue was homogenised in RIPA Buffer (one protein inhibitor tablet (Sigma) per 10 ml volume of RIPA Buffer). Samples were placed in an MP Biomedical lysis tube and lysed using 4 x shaking for 15 secs, with 300 secs on ice between each shaking. The lysate was then centrifuged for 10 mins at 8,000 x g to remove cell debris.

2.2.4 Bradford Assay

The protein concentration of sample lysates was determined using the Bradford Assay. The protein bovine serum albumin (BSA) was used as a standard to construct a standard curve

(concentration range; 0 mg/ml, 0.125 mg/ml, 0.25 mg/ml and 0.4 mg/ml). In brief, the Bradford reagent binds to the proteins leading to a shift in absorbance to 595 nm. Aliquots of lysates (5-10 μl) were diluted in ddH_2O (1:10). 10 μl from each BSA was added to 990 μl of Bradford reagent, (Bio-Rad) to generate a standard curve. 10 μl of diluted lysate was added to 990 μl of Bradford reagent. A Jenway 6305 spectrophotometer was used to measure the absorbance at 595nm. The BSA standard curve was used to convert the absorbance to a protein concentration (mg/ml). This value was then corrected for the dilution factor. The lysate was then frozen at -80°C until further analysis.

2.2.5 Stain-free SDS-PAGE

Aliquots of the lysate corresponding to between 10-20 μg of protein were mixed with 5x sodium dodecyl sulphate (SDS) loading buffer. The samples were heated for 10mins at 90 ˚C. The samples were loaded to a gel that is stain-free (Bio-Rad) along with a Pre-Scission Plus (Bio-Rad) ladder. Gels were run at 45mA for 25 mins in the SDS Running Buffer (25 mM Tris, 192 mM glycine, 0.1% SDS). Images of the gel were captured using ChemiDoc™ MP (Bio-Rad).

2.2.6 Western Blot

Transfer of the proteins to the PVDF membranes was done using the Trans-Blot® Turbo™ transfer system (Bio-Rad). The blocking of the membranes was achieved using milk 5% w/v in TBS/Tween (10mM Tris Base pH 8, 500mM NaCl, 2ml Tween) for 60 mins. The dilution of the primary antibodies (Table 2.1) was prepared by adding 5 μl of the primary antibodies to 10mls of 1% (w/v) of milk in TBS/Tween and incubated at 4°C for overnight or at room temperature for 60 mins depending on the type of the antibody. Membranes were washed 3x with TBS/Tween for 3 x 10 mins prior to addition of the secondary antibody at the appropriate dilution (Table 1) and incubated for 1h. The membranes were rinsed again with TBS/Tween. Subsequently, the chemiluminescence process was conducted by adding the Clarity™ Western ECL Substrate (Bio-Rad) in the ratio of 1:1 onto the membrane in the dark for 5 mins.

The ChemiDoc™ MP (Bio-Rad) was used to image the membrane. The protein quantity was calculated via the measurements of the band density normalized against the total loading of the proteins. A method of total protein was used rather than a housekeeping protein as previous studies from our group and others have determined that there is an often change to these proteins in disease models. A schematic and table of analysis is shown in (Figure. 2.2).

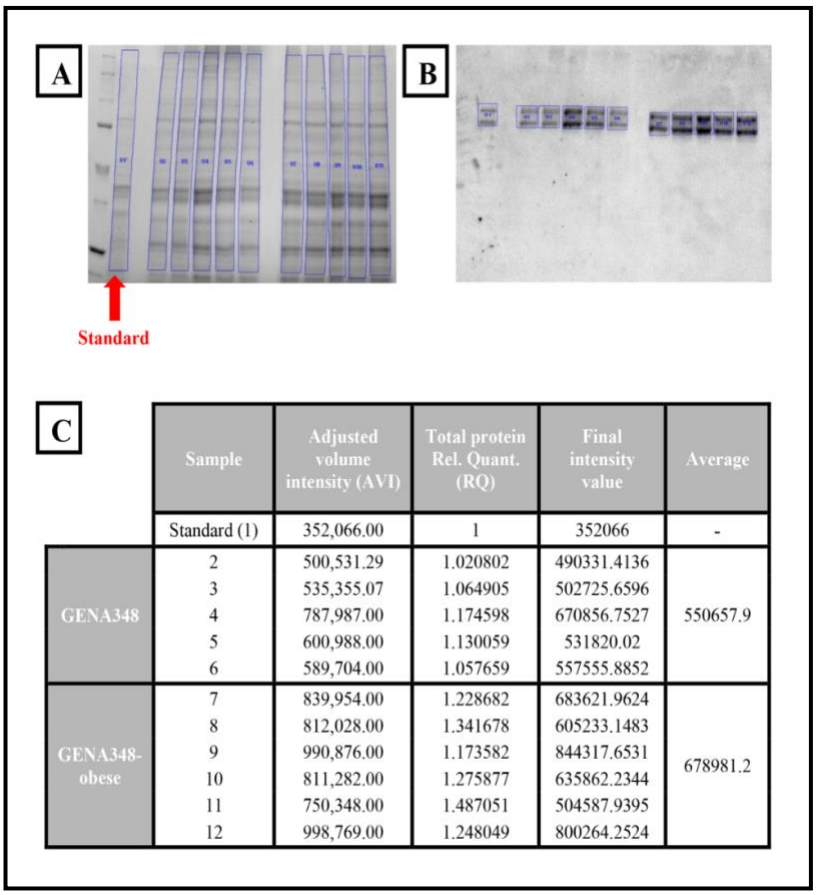

	Sample	Adjusted volume intensity (AVI)	Total protein Rel. Quant. (RQ)	Final intensity value	Average
	Standard (1)	352,066.00	1	352066	-
GENA348	2	500,531.29	1.020802	490331.4136	550657.9
	3	535,355.07	1.064905	502725.6596	
	4	787,987.00	1.174598	670856.7527	
	5	600,988.00	1.130059	531820.02	
	6	589,704.00	1.057659	557555.8852	
GENA348-obese	7	839,954.00	1.228682	683621.9624	678981.2
	8	812,028.00	1.341678	605233.1483	
	9	990,876.00	1.173582	844317.6531	
	10	811,282.00	1.275877	635862.2344	
	11	750,348.00	1.487051	504587.9395	
	12	998,769.00	1.248049	800264.2524	

Figure 2.2 Western Blot Analysis using total protein.

(A) The total protein loaded into each lane (using the same box size used for each lane) was normalised to the loading control standard on the stain free gel (Figure. 2.2A: lane 2). The ImageLab (Bio-Rad) software was used to calculate the total protein relative quantification (C; RQ). (B) Exemplar blot for Opa1, the final intensity values were calculated for each protein band (in this case a doublet). (C) Using the BioRad Software ImageLab the table quantifying protein loading and image intensity were calculated. The final intensity values and the adjusted volume intensities (C; AVI) for the protein bands on the Western blot (B) were corrected using the values for the normalized total protein loading (AVI divided by RQ). The average of these final intensity values for the Western blot was calculated.

Table 2.1 Antibodies for Western Blot

Protein	Primary Antibody	Dilution	Secondary Antibody	Dilution
Mfn_1	Mouse monoclonal IgG (abcam ab57602)	1:2000	Goat anti-mouse IgG (Bio-Rad 170-6516)	1:2000
Mfn_2	Rabbit polyclonal IgG (abcam ab56889)	1.2000	Goat anti-rabbit IgG (Bio-Rad 170-6515)	1:2000
Opa1	Goat polyclonal IgG (Santa Cruz SC-30572)	1:2000	Goat anti-mouse IgG (Santa Cruz SC-2020)	1:2000
Drp1	Rabbit polyclonal IgG (Santa Cruz SC-32898)	1:2000	Goat anti-rabbit IgG (Bio-Rad 170-6515)	1:2000
PINK1	Rabbit polyclonal IgG (Santa Cruz SC-33796)	1:2000	Goat anti-rabbit IgG (Bio-Rad 170-6515)	1:2000
Parkin	Mouse Monoclonal IgG (abcam ab77924)	1:2000	Goat anti-mouse IgG (Bio-Rad 170-6516)	1:2000
Miro1	Mouse monoclonal IgG (abcam ab188029)	1:2000	Goat anti-mouse IgG (Bio-Rad 170-6516)	1:2000
Miro1	Rabbit polyclonal IgG (abcam ab56889)	1:2000	Goat anti-rabbit IgG (Bio-Rad 170-6515)	1:1000
Miro2	Rabbit monoclonal IgG (abcam ab57602)	1:2000	Goat anti-mouse IgG (Bio-Rad 170-6516)	1:1000

2.2.7 RNA extraction

The frozen heart tissue was placed in a tube with 500 µl Trizol. Using an electrical tissue grinder (IKA RW 16 basic) the tissue was homogenised, and the resulting homogenate was incubated for 15 min at room temperature. Homogenates were then treated with 200 µl chloroform and the tubes were shaken for 15 seconds then incubated at room temperature for 2 min. Then the mixture was centrifuged for 15 min at 9184 x g at 4°C. A fresh Eppendorf tube was prepared with 250 µl isopropanol then the supernatant aqueous phase was drawn off and added to the fresh tube. The tubes were inverted 30 times then left to settle at room temperature for 10 min before being centrifuged for 10 min at 15,521 x g at 4°C. The pellets were washed with 1ml of 75% ethanol and centrifuged for 10 min at 15,521 x g for at 4°C. The resultant pellet was re-suspended in 60 µl RNase-free water. To quantify the concentration of RNA, the Nanodrop 1000 spectrophotometer (Thermo Scientific) was used to measure the absorbance at 260 nm wavelength. The purity of the RNA product was determined by the A260/A280 ratio of absorbance. Samples were stored at −80ºC until required.

2.2.8 DNase treatment

To enable RNA purification, DNA was degraded using DNase I, Amplification Grade (Invitrogen™). A mixture was prepared using 1 µg RNA, 1 µl DNase I and 1 µl 10X DNase I reaction buffer. RNase free water was added to a final volume of 10 µl then incubated for 15 min at room temperature. Then 1 µl 25mM EDTA was added to stop the reaction. The mixture was then incubated at 70°C for 10 min. A High-Capacity cDNA Reverse Transcription Kit (Applied Biosystems) was used to synthesise cDNA. Reverse transcription master mix was prepared as described in (Table 2.2). To create a negative reverse transcription control, reverse transcription enzyme was replaced with RNase-free water.

2.2.9 Reverse transcription

Table 2.2 Reverse transcription master mix

Component	Volume per reaction
10X RT buffer	2
10X Random primers	2
RNase free water	4.2
25X dNTP Mix	0.8
MultiScribe Reverse Transcriptase	1
Total per reaction	10

A 1 µg sample of RNA and 10 µl of master mix were added to a PCR tubes and loaded on the PCR thermal cycler (MJ Research PTC-200). Details the elements of the single cycle programme shown in (Table 2.3).

Table 2.3 Thermal Cycler set up

Step	Time (minutes)	Temperature (°C)
1	10	25
2	120	37
3	5	85
4	∞	4

Dilution 1 in 5 was done on the cDNA, then stored at –20°C until required.

2.2.10 Quantitative Polymerase chain Reaction (qPCR)

To establish the changes in transcript expression, qPCR was used. Specific primers were used to amplify targeted genes; these are presented in (Table 2.4).

Table 2.4 List of primers

Target gene	Catalogue number	Primar assay	Supplier
Opa1	Qiagen	Mm_Opa1_1_SG	Qiagen
Drp1	Qiagen	Mm_Dnm1L_2_SG	Qiagen
Mfn1	Qiagen	Mm_Mfn1_1_SG	Qiagen
Mfn2	Qiagen	Mm_Mfn2_1_SG	Qiagen
Gapdh	Qiagen	Mm_Gapdh_3_SG	Qiagen

Brilliant III Ultra-Fast SYBR Green qPCR Master Mix (Agilent Technologies) was used to prepare qPCR reactions as described in (Table 2.5).

Table 2.5 Composition of qPCR mix

Ingredients - Composition	volume
2× Brilliant III Ultra-Fast SYBR Green QPCR Master Mix	5
RNase free water	2.85
Primers	1
Reference Dye 1mM (diluted 1:500)	0.15
Total	9

For each reaction, 9 µl qPCR reaction mix 1 µl cDNA was added. Triplicates of samples, negative RT controls and RNase-free water were loaded onto a 96-well plate. The inclusion of the water control was to exclude primer-dimer amplification. Negative RT controls were assayed to establish DNA contamination. To evaluate between-run variations, plates were assessed twice using a 7500 Fast Real-Time PCR system. The amplification cycles used are presented in (Table 2.6). Relative gene expression analysis was performed using the Livak method.

Table 2.6 Cycling Conditions

Stage	Number of cycles	Temperature(°C)	Time
Holding	1	95	3 minutes
Cycling	40	95	5 seconds
		60	25 seconds
Melt curve	1	95	15 seconds
		60	1 minutes
		95	15 seconds
		60	15 seconds
Holding		4	∞

2.2.11 Mitochondrial Isolation

Mitochondria were isolated using the abcam kit (Abcam, ab110168). 50 mg of heart tissue was taken from each mouse and rinsed twice with Washing Buffer. The heart tissue was placed in 2 ml of Dounce homogeniser, and homogenised with 500 µl of Isolation Buffer using 40 strokes, and centrifuged at 1,000 x g for 10 mins at 4°C. The supernatant was divided into

two micro-centrifuge tubes, 500 µl of Isolation Buffer was added to each tube, and tubes were centrifuged at 12,000 x g for 15 mins at 4°C. Pellets were then rinsed with mixture of 250 µl of Isolation Buffer and 2.5 µl of protease inhibitor stock, centrifuged at 12,000 x g for 15 mins at 4°C, and washed again with the mixture of Isolation Buffer and protease inhibitor. The two pellets were combined, added to a mixture of 125 µl of Isolation Buffer and 2.5 µl of protease inhibitor stock, and stored at -80°C.

2.2.12 Mitochondrial enzymatic assays

Mitochondrial function was assayed using ABCAM kits, according to the manufacturer's instructions. The assessment of mitochondrial function was via immune capture of the protein complexes of the OXPHOS pathway from the mitochondria. After the isolation of target complexes, measurement of activity was observed as a change in absorbance due to conversion of substrate to product (Figure. 2.3).

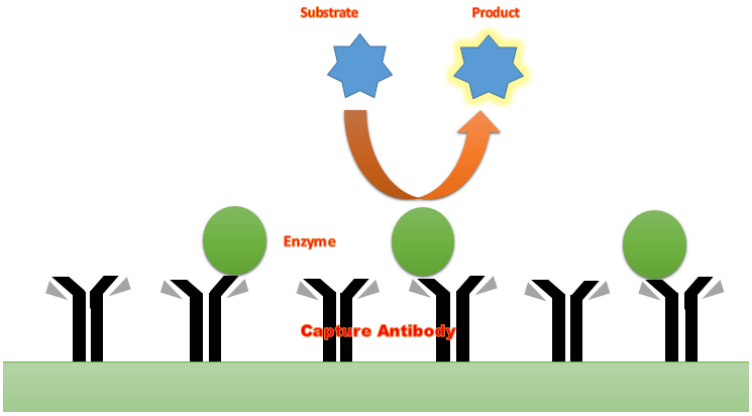

Figure 2.3 Mitochondrial enzymatic assay.

The binding of protein complexes of OXPHOS to microplate through their interaction with the capture antibody. Measurement of complex activity as an absorbance change resulted as a substrate conversion into product.

2.2.13 Analysis of Complex I activity

To determine Complex I activity, the oxidation of NADH to NAD+ was measured, followed by the simultaneous reduction of a dye which leads to increased absorbance at OD=450 nm. Isolated mitochondrial samples were adjusted to 1mg/ml, 20µl was taken and then detergent added (1:10 dilution of a 10x detergent stock). The samples were incubated on ice for 30 mins, centrifuged at 14,000 x g for 30 mins at 4°C, and then, diluted to 0.1mg/ml. 200 µl of each diluted sample was loaded into each well of the microplate. 200 µl of Blocking Buffer was used as a control. The samples were incubated for 3 hours at room temperature. The microplate was inverted in order to empty the wells and rinsed twice with 300 µl of Wash Buffer. 200 µl of an Assay Buffer was added to each well to measure the enzyme activity. The Thermo Labsystem microplate reader was utilized to read the changes in absorbance of samples at 450 nm for 30 mins at room temperature.

2.2.14 Analysis of Complex II activity

To determine Complex II activity, production of ubiquinol by the enzyme is coupled to the reduction of the dye DCPIP (2,6-diclorophenolindophenol) and a decrease in absorbance, resulting in the recycling of substrate ubiquinone. The isolated mitochondria were solubilised as described for complex I, followed by dilution to 0.1 mg/ml and loading on the microplate (50 µl per well). After 2 h incubation at room temperature, the samples were extracted by inversion, washed two times with wash buffer (300 µl) and incubated with lipid solution (40 µl) for 30 mins at room temperature. The activity solution (200 µl) was then added and the Thermo Labsystem microplate reader was used to monitor the absorbance change at 600 nm for 1 h at room temperature. A negative control assay was run using the buffer alone, while a background control was run using the sample in the absence of assay buffer.

2.2.15 Analysis of Complex IV activity

To determine Complex IV activity, cytochrome c oxidase activity was measured and determined calorimetrically by following the oxidation of reduced cytochrome c by the absorbance change at 550 nm. The solubilised mitochondria were diluted to 0.1 mg/ml, loaded onto the microplate (200 µl per well) and incubated for 3 h at room temperature. The samples were then extracted by inversion and washed twice with Solution 1 (300 µl). Following addition of the assay solution (200 µl), the Thermo Labsystem microplate reader was used to monitor the absorbance change at 550 nm for 120 min at 30 °C. A negative control assay was run using the buffer alone, and a background control using the sample in the absence of the assay buffer.

2.2.16 Analysis of Complex V activity

To determine Complex V activity, the direct inhibitory effect of compounds on Complex V activity was measured. The solubilised mitochondria were diluted to 0.1 mg/ml, loaded onto the microplate (50 µl per well) and incubated for 3 h at room temperature. The samples were then extracted by inversion, washed twice with Solution 1 (300 µl) and incubated with lipid solution (40 µl) for 45 min at room temperature. The reagent mix (200 µl) was then added and the activity was measured using the Thermo Labsystem microplate reader to monitor the absorbance change at 340 nm for 120 min at 30 °C. A negative control assay was run using the buffer alone, while a background control was run using the sample in the absence of assay buffer.

2.2.17 Citrate synthase activity assay

According to Larsen et al. (2012), mitochondrial content is frequently evaluated by measuring the citrate synthase activity. In the present work, a MitoCheck® Citrate Synthase Activity Assay Kit (Cayman Chemical Company) was used to measure the citrate synthase activity

based on the reaction of SH-CoA with DTNB to generate 5-thio-2-nitrobenzoic acid (TNB). In a 96-well plate, a 1:200 dilution of the isolated mitochondria (30 µl) was mixed with 50 µl of Tube A, which contained acetyl-CoA reagent (20 µl), developing reagent (20 µl) and assay buffer (960 µl). This was followed by addition of 20 µl of Tube B, containing oxaloacetate reagent (20 µl) and assay buffer (480 µl) and a the Thermo Labsystem microplate reader was used to monitor the absorbance change at 412 nm at 25 °C for 30 min.

2.2.18 Oxygen consumption rate

The isolated mitochondria (100 µl) were added to the chamber after being diluted with OCR buffer (pH 7.4) containing mannitol (210 mM), sucrose (70 mM), KH_2PO_4 (5 mM), BSA (0.5 mg/ml) and MOPS (10 mM) to a final concentration 0.25 mg/ml. To this was added 5 µl of each substrate, namely: pyruvate (2,000 mM), malate (400 mM), glutamate (2,000 mM), ADP (500 mM) and succinate (1,000 mM)(Eigentler et al., 2012). A fibre optic oxygen monitoring system (Instech) was then calibrated and used to record the oxygen consumption rate (OCR) until 0% oxygen (or plateau) was reached. Technical readings were obtained in triplicate.

2.2.19 Mass spectrometry of isolated mitochondria

Isolated mitochondria (50 µg) from each group were analysed using quantitative mass spectrometry in the University of Manchester Mass spectrometry Facility. In brief, isolated mitochondria were treated with 0.2 mM EDTA and 4 mM 25 mM Tris-HCl pH 8, 5 mM dithiothreitol, DTT, and n-Dodecyl β-D-maltoside (DDM), all Sigma Aldrich) was added to a final concentration of 0.03%. The sample was placed in a Covaris tube and sonicated in an S2 machine for 60 secs at 4°C. The samples were allowed to stand for 20 mins on ice. The protein concentration was determined using a Direct Detect spectrometer (Millipore), where the average concentration was determined to be 0.5 mg ml^{-1}. Iodoacetamide (IAM) was added to the samples to a final concentration of 15 mM for 20 minutes at room temperature. Trypsin was added to the samples at a ratio of 50:1 (protein: enzyme) to digest the proteins and left

overnight at 37°C. To stop the digestion, formic acid was added to a final concentration of 0.1%. The samples were desalted using reversed phase beads (POROS R3 Bulk Media, 1-339-03, Applied Biosystems), in a 96 -well format. Samples were analysed by LC-MS/MS coupled to an Orbitrap Elite MS.

The MS data was analysed using Progenesis LC-MS (v4.1 Non-linear Dynamics). The retention times in each sample were aligned using one LC-MS run as a reference, then the "Automatic Alignment" algorithim was used to create maximal overlay of the two-dimensional feature maps. The resulting peaklists were searched against the Uniprot mouse database (version 2013 -5) using Mascot v2.4.1, and the results imported into Progenesis LC-MS for annotation of peptide peaks. The identification of three unique peptides was used as an inclusion criterion and $P<0.05$ (ANOVA) as a measure of significance to changes in protein abundance.

2.2.20 Cell culture

All cell culture was prepared under aseptic conditions in a class II biological safety cabinet. The H9c2 myoblasts were cultured at 37^{o}C in a humidified atmosphere of 5% CO_2 using Dulbecco's Modified Eagle Medium (DMEM; Gibco) containing Pen/Strep (5 ml), FBS (50 ml) and (5 ml) MEM 100X with non-essential amino acids. The media was replaced every second day until cells were 70% confluent, after which they were prepared using standard procedures. siRNA transfection protocol to knockdown Miro1 (Rhot1).

The H9c2 cells (2 x 10^5) were added to a 6-well plate and incubated for 24 h before washing two times with PBS (Sigma, D8537-500ml). 10 µl of 5 nmol Rhot1 siRNA (Dharmacon L-085139-02-0005) and (190 µl) (Thermo fischer scientific, 311986) was added to tube A and 4 µl of Dharmafect transfection reagent (Dharmacon T-2001-01) and (196 µl) optiMEM was added to tube B. Tubes A and B were vortexed and incubated for 20 min. The transfection mixture was then added to maintenance media (1.6 ml) and incubated for 24 hours. As a

control parallel experiments were undertaken using 5 nmol Control Non- targeting siRNA (Dharmacon D-001810-10-05).

2.2.21 Cell MTT assay (thiazolyl blue tetrazolium bromide)

To determine if cell viability was influenced by treatment with inflammatory molecules, an MTT assay was performed. H9c2 cells were added to a 24-well plate (3 x 10^4 cells/well) and grown at 37^{o}C under a humidified atmosphere of 5% CO_2 with culture media for 24h. Cells were treated with si-NTC and si-MIiro1 to evaluate cell viability MTT solution (25 µl) was added to each well, followed by a further 1 h incubation under the same conditions. Then, after removing 250 µl of media from each well, the solubilisation solution (100 µl) was added to each well and mixed to dissolve the crystals. The Thermo lab system microplate reader was used to measure absorbance at 570 nm.

2.2.22 SDS-PAGE and Western blot analysis

Samples were separated based on molecular weight stain-free SDS-PAGE and protein expression assessed using Western blot as described previously in section 2.2.5.

Table 2.7 Antibodies used for Western blot

Protein	**Praimary Antibody**	**Dilution**	**Secondary Antibody**	**Dilution**
Miro1	Rabbit polyclonal IgG (abcam ab56889)	1:2000	Goat anti-rabbit IgG (Bio-Rad 170-6515)	1:1000
Miro2	Rabbit monoclonal IgG (abcam ab57602)	1:2000	Goat anti-mouse IgG (Bio-Rad 170-6516)	1:1000

2.2.23 RNA Extraction from H9c2 cells

1 ml of Trizol was added was added to each well and a cell scraper was used to lyse cells. Well mixtures were pipetted up and down several times before being drawn up and transferred to 1.5 ml sterile, RNAse-free Eppendorf tubes. Tubes were then incubated for 5 min at room temperature. 200 µl chloroform was then added to the tubes, and tubes vortexed for 15 s, followed by 2 min incubation at room temperature. The suspension was then centrifuged at 12000 rpm for 15 min at 4°C. Fresh Eppendorf tubes were prepared to contain 500 µl isopropanol, into which the supernatant aqueous phase was drawn from the mixture was added. The tubes were inverted 30 times then left to settle at room temperature for 10 min before being centrifuged at 12000 rpm for 10 min at 4°C. The pellets were washed with 1 ml 75% ethanol and were once more centrifuged at 1000 rpm for 10 min at 4^{o}C. The resultant pellet was re-suspended in 50 µl RNase-free water. To quantify the concentration of RNA, the Nanodrop 1000 spectrophotometer (Thermo Scientific) was used at 260 nm wavelengths. The purity of the RNA product was determined by the A260/A280 ratio of absorbance. Samples were stored at −80^{o}C until required. DNase treatment and Reverse transcription master mix were completed as described in Chapter 2 (section 2.2.8).

2.2.24 Quantitative Polymerase Chain Reaction (qPCR)

Changes to transcript expression levels were analysed using qPCR as described in section 2.2.10. Miro1 gene transcript expression levels were investigated using Qiagen QuantiTect® primer assay primers highlighted in (Table 5.2).

Table 2.8 List of primers

Target gene	Catalogue number	Primar assay	Supplier
Opa1	Qiagen	Mm_Opa1_1_SG	Qiagen
Drp1	Qiagen	Mm_Dnm1L_2_SG	Qiagen
Mfn1	Qiagen	Mm_Mfn1_1_SG	Qiagen
Mfn2	Qiagen	Mm_Mfn2_1_SG	Qiagen
Gapdh	Qiagen	Mm_Gapdh_3_SG	Qiagen

2.2.25 Citrate synthase activity for H9C2 cells

The citrate synthase activity was determined using a CS0720-1KT kit (Sigma), based on spectrophotometric monitoring (405 nm, omega star) of the reaction of SH-CoA with DTNB to generate 5-thio-2-nitrobenzoic acid (TNB). In brief, 10^6 cells were placed in a petri dish and washed two times with PBS prior to addition of cellLytic™ reagent (1.5 mL). Cells were detached using a cell scraper and incubated for 15 min on a shaker. The lysed cells were then collected and centrifuged at 20,000 g for 15 min. The supernatant was transferred to a chilled test tube to measure the protein concentration. 30 µg of protein was mixed with the assay buffer, acetyl Co-A reagent (2 µl) and DNTB solution (2 µl). The mixture was added to a 96 well plate and the baseline reaction measured for 1.5 min, followed by addition of oxaloacetate with monitoring of the change in absorbance at 412 nm for a further 1.5 min.

2.2.26 Mitochondrial isolation from H9c2 cells

Differential centrifugation was used to isolate the mitochondria from the H9c2 cells (3 x 10^5 cells per well). A mixture of the homogenisation buffer (HB) containing HEPES-KOH (20 mM, pH 7.4), mannitol (220 mM) and sucrose (70 mM) with a protease inhibitor mixture (Sigma-

Aldrich) was used to harvest the cells from culture dishes. The harvested cells were centrifuged for 5 min at 2,300 g to obtain a pellet which was then resuspended in HB and incubated for 5 min on ice. All processes were performed at 4^{o}C. Cells were ruptured using a 27-gauge needle (10 strokes) and the homogenate was centrifuged two times at 5,800 g for 5 minutes each. The isolated mitochondria were re-suspended in 1 ml of HB for use in evaluating the rate of oxygen consumption (see Methods section 2.2.18). The quantity of isolated mitochondria was stated as protein concentration.

2.2.27 Specimen preparation for SBF-SEM

A (2 x 10^{6}) H9c2 cells were added to a Petri dish and incubated for 24 before washing two times with PBS (Sigma, D8537-500Ml). Primary fixative, 2.5% glutaraldehyde with 2% formaldehyde in 0.1M HEPES pH7.4 buffer was added to the cells. Cells kept in the fixative overnight in the fridge and centrifuged to form a pellet. The pellet was resuspended with secondary fixative following the same methods as described in the Methods section 3.2.2.

2.2.28 Statistical analysis

All data are reported as the mean ± the standard error of the mean (SEM). Statistical analyses employed a Student t-test or one-way ANOVA as appropriate. Outcomes were considered as significant when $p<0.05$. GraphPad Prism 8 was used in order to perform the statistical analysis. *$p \leq 0.05$, **$p \leq 0.01$, ***$p \leq 0.001$ and ****$p \leq 0.0001$.

2.3 Results

2.3.1 Physiological Assessments of GENA348 Mouse Model

At 6 months of age the GENA348 mice demonstrated a significant increase to both heart weight 174.5 mg ± 4.248 (*P*<0.0001) (Figure. 2.4A) and body weight 45.23 g ± 0.681 (*P*=0.0069) (Figure. 2.4B) compared to WT 41.71mg ± 0.9834, 146.8g ± 2.055 respectively. Additionally, the GENA348 mice showed a significant increase in the heart weight (HW): tibia length (TL) ratio 7.365 mg/mm ± 0.169 *(P*=0.0022*)* compared to control 6.562 mg/mm ± 0.1733, which indicates cardiac hypertrophy (Figure. 2.4C), although there was no change in lung weight (Figure. 2.4D) which is indicative of pulmonary congestion. In keeping with MODY2 patient observations, blood glucose levels were significantly increased in GENA348 mice 9.583 mmol/L ± 0.3833 (*P*=0052) compared to control 7.56 mmol/L ± 0.3906 (Figure. 2.4E) but with no change to insulin levels (Figure. 2.4F).

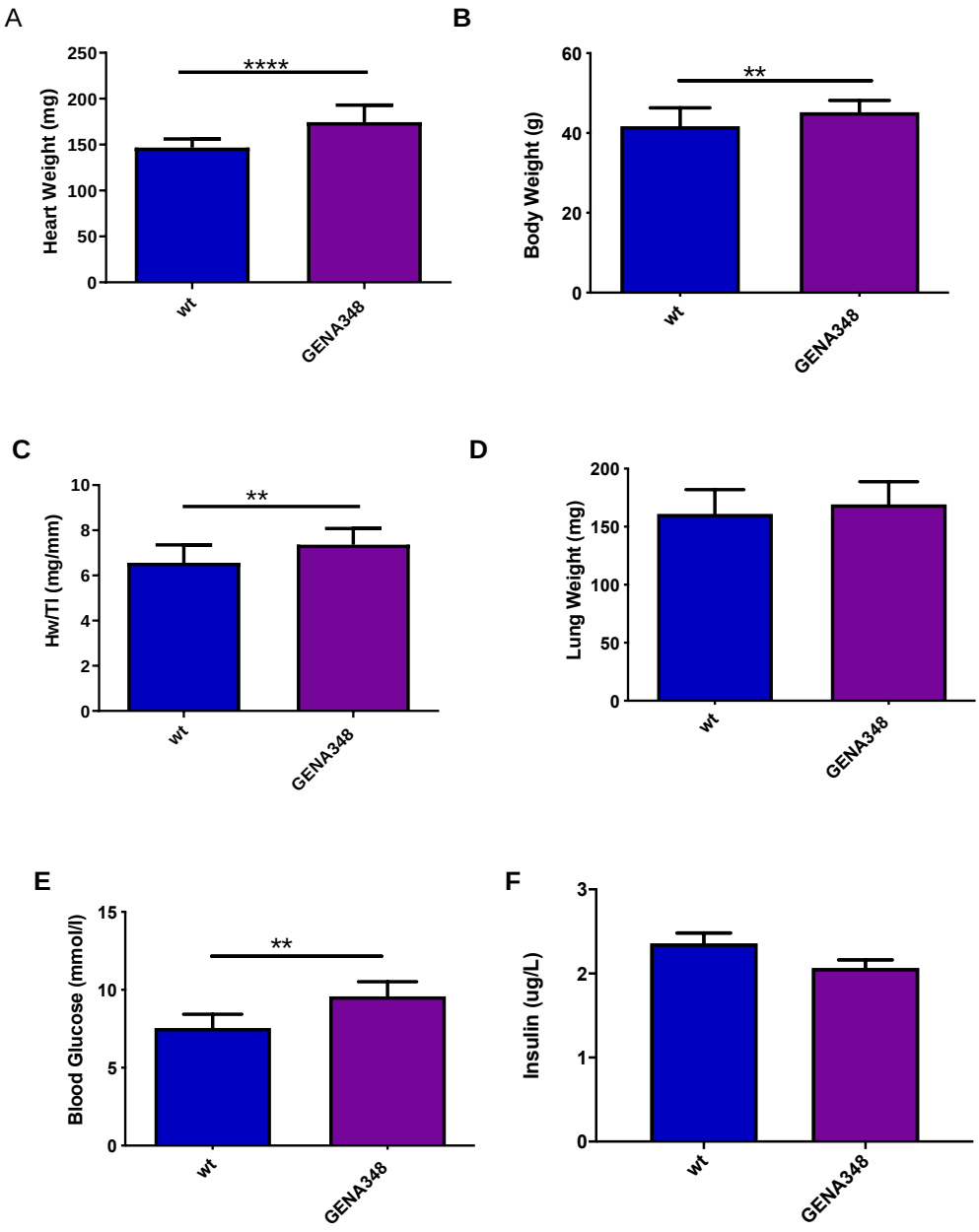

Figure 2.4 Effect of GENA348 on the blood glucose level, heart weight and body weight on control and 19 GENA348 mice.

(A) Significant increase in the heart weight of GENA348 (n=19) mouse compared to control (n=21) groups. (B) There was slight increase in the body weight of GENA348 (n=19) compared to control (n=22). (C) The ratio of HW: TL ratio showed significant increase in GENA348 (n=18) compared to control (n=21). (D) There was no change in the lung weight of GENA348 (n=18) compared to control (n=21). (E) There was an increase in the blood glucose level of GENA348 (n=7) in comparison to control (n=6) group. (F) There was no significant difference in the expression profiles of insulin between the control (n=5) and GENA348 mice (n=6). Data represented as mean +/- SEM $^{**}p \leq 0.01$ and $^{****}p \leq 0.0001$.

2.3.2 Echocardiographic parameters

Transthoracic echocardiography on GENA348 mice (6 months old) and age-matched controls was carried out by Dr Stephen Gibbons (Gibbons, 2011). The dimensions of left ventricle (sPW, dPW, sIVS, dIVS, sLVD, and dLVD) were measured using M-Mode tracings (Figure. 2.5) and the derived indices (FS, EF, RWT and LV mass) were calculated through standard formulas [(dVol - sVol)/dVol] x100, [(dLVD-sLVD)/dLVD] x 100, (dIVS+dPW)/dLVD, 1.055 x [$(dLVD+dPW+dIVS)^3$ – $dLVD^3$]. Data are summarised below with parameters showing a significant change highlighted in grey (Table 2.7).

Table 2.9 Parameters of Echocardiography in 6-month-old GENA348 mice

Parameter	WT (n=15)	GENA348 (n=8)	*P* value
dLVD (mm)	4.57±0.06	4.43±0.09	0.24
sLVD (mm)	3.47±0.08	3.27±0.09	0.15
dIVS (mm)	0.98±0.03	1.03±0.03	0.37
sIVS (mm)	1.41±0.03	1.42±0.06	0.82
dPW (mm)	1.06±0.03	1.28±0.06	0.002
sPW (mm)	1.31±0.03	1.54±0.07	0.0006
HR (b/min)	469±8	456±456	0.34
LV mass/ (mg)	194±7.0	222±11	0.05
RWT	0.45±0.01	0.53±0.02	0.02
EF%	55±1.9	59.5±2.1	0.22
FS%	24.2±1.2	26. 3±1.3	0.28
E:A	2.65±0.20	1.84±0.19	0.03
IVRT	15.2±1.13	20.5±0.37	0.004

dLVD: diastolic diameter, sLVD: systolic diameter, dIVS: diastolic intraventricular septum, sIVS: systolic intraventricular septum, dPW: diastolic posterior wall, sPW: systolic posterior wall, HR: heart rate, EF: ejection fraction. FS: fractional shortening, LV mass: left ventricular mass, RWT: relative wall thickness, E: A: early to late ventricular filling ratio, IVRT: isovolumetric relaxation time. Data are presented as the mean +/- SEM ($p<0.05$ considered as a significant change).

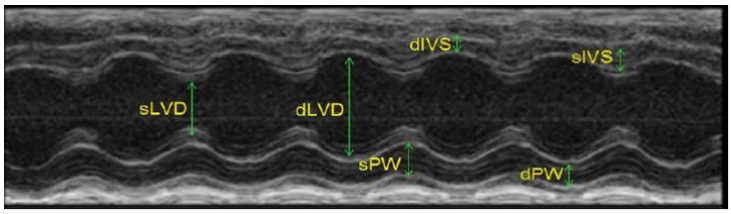

Figure 2.5 Echocardiography image of a WT mouse.

The M Mod view shows how the parameter obtained (Adapted Gibbon, 2011). sLVD: systolic diameter, dLVD: diastolic diameter, dIVS: diastolic intraventricular septum, sPW: systolic posterior wall, sIVS: systolic intraventricular septum, dPW.

There was a significant increase in several measured parameters (Table 2.7). Hypertrophic markers, such as heart-weight-to-tibia length (HW/TL) ratios are generally used to assess and evaluate cardiac hypertrophy. GENA348 mice have significantly higher HW, BW and HW/TL compared to the control groups (Figure. 2.5). An increase in RWT ($p=0.02$) and LV mass ($p=0.05$) may also suggest the establishment of cardiac hypertrophy in the GENA348 mice. Furthermore, the echocardiography data suggests concentric hypertrophy due to the increased left ventricular wall thickness.

2.3.3 Characterisation of the mitochondrial phenotype in the GENA348 mouse heart

In order to compare biochemical characteristics between the GENA348 and WT group citrate synthase activity was first measured as an indicator of overall mitochondrial content and activity. Citrate synthase regulates the condensation of acetyl-CoA with oxaloacetate, to produce citrate. Thus, it plays a crucial role in ensuring the TCA cycle progresses as expected

and to screen for mitochondrial function (Kelley et al., 2002) and so is commonly employed as a measure of mitochondrial content and as a means to compare data between different experimental group. Mitochondria were isolated from the GENA348 and WT hearts and citrate synthase activity described in Methods 2.2.16. Citrate synthase action was found to be increased by ~1.9-fold in the GENA348 mitochondrial fraction compared to WT, implying an increase in mitochondrial content (p= 0.0476; Figure. 2.6). Therefore, functional measurements such as the O_2 consumption rate (OCR) and Complex activities were corrected for citrate synthase activity.

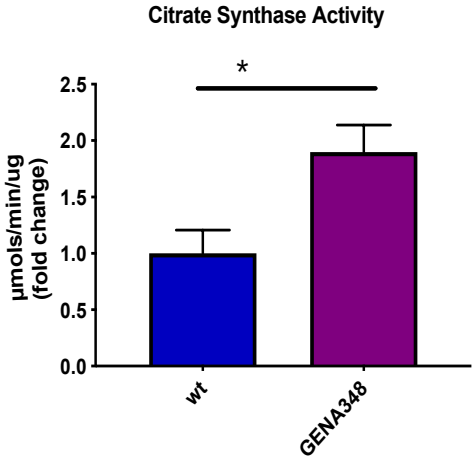

Figure 2.6 Increased citrate synthase activity in GENA348.

Isolated mitochondria from GENA348 myocardium (n=3) revealed a significant increase of citrate synthase action compared to control (n=3). Data represented as mean +/- SEM *$p \leq 0.05$.

2.3.4 Measurement of O_2 consumption

Mitochondria require oxygen for ATP production, in order to complete energy-dependent reactions (Li and Graham, 2012). Oxygen is predominantly consumed during the last enzyme step of the electron transport chain, involving cytochrome oxidase, driving ATP production (Wittenberg and Wittenberg, 2007). There are several different techniques that can be employed to measure O_2 consumption rate. Here a fibre optics system from Instech was employed for measuring of O_2 consumption rate (OCR) using isolated mitochondria from each experimental group.

Mitochondria from WT mouse ventricle show a linear profile (taking typically 40 minutes to plateau). In contrast the mitochondria from the GENA348 hearts showed a rapid consumption of O_2 plateauing after 12 minutes. For comparison purposes the initial gradient between 13-9% O2 consumption was calculated for each group (Figure. 2.7A). The rate of O_2 consumption values which were then corrected to citrate synthase levels (Spinazzi et al., 2012).

The oxygen profile change in GENA348 mice shows that GENA348 mice consume more oxygen as compare to the wild type (Figure. 2.7B). The oxygen percentage of GENA348 mice was not significant after corrected to citrate synthase activity.

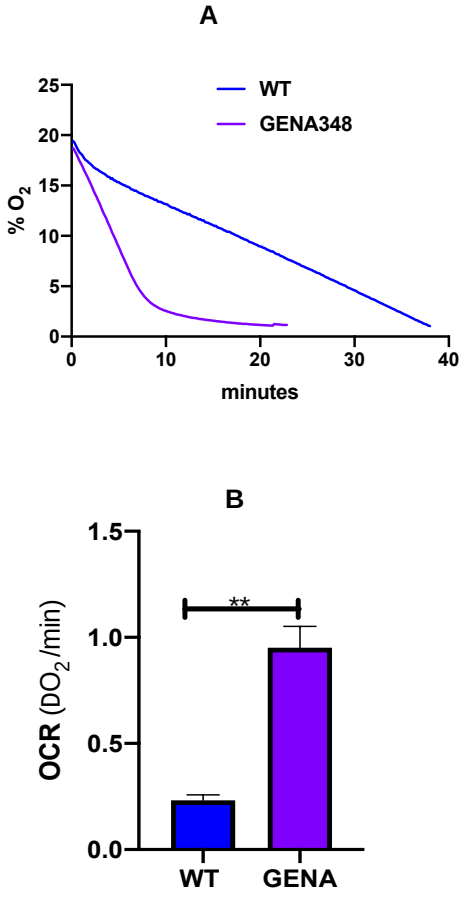

Figure 2.7 Increase in the oxygen consumption rate in the GENA348 myocardium.

(A) Representative image of an OCR plot comparing the GENA348 (n=4) compared to wild type (n=4). (B) Representative plot showing the OCR in GENA348 and WT mice after correction for citrate synthase. Data represented as mean +/- SEM ** *P=0*.0023

2.3.5 Investigation of OXPHOS

In a complementary approach to measuring OCR we next investigated whether there was a change to the activity of the Complexes regulating OXPHOS. As shown in Figure 2.8, the activities of Complex I, IV and V were found to be significantly decreased by 0.6, 0.5, 0.4-fold (mean of GENA348/ mean of WT), espectively. Complex II activity was less affected but was still reduced in GENA348 compared to control group (*P*=0.030) (Figure. 2.8). Therefore, the biochemical and functional data analyses converge to indicate that the Gck-mutation resulted in OXPHOS impairment, subsequently impacting ATP production.

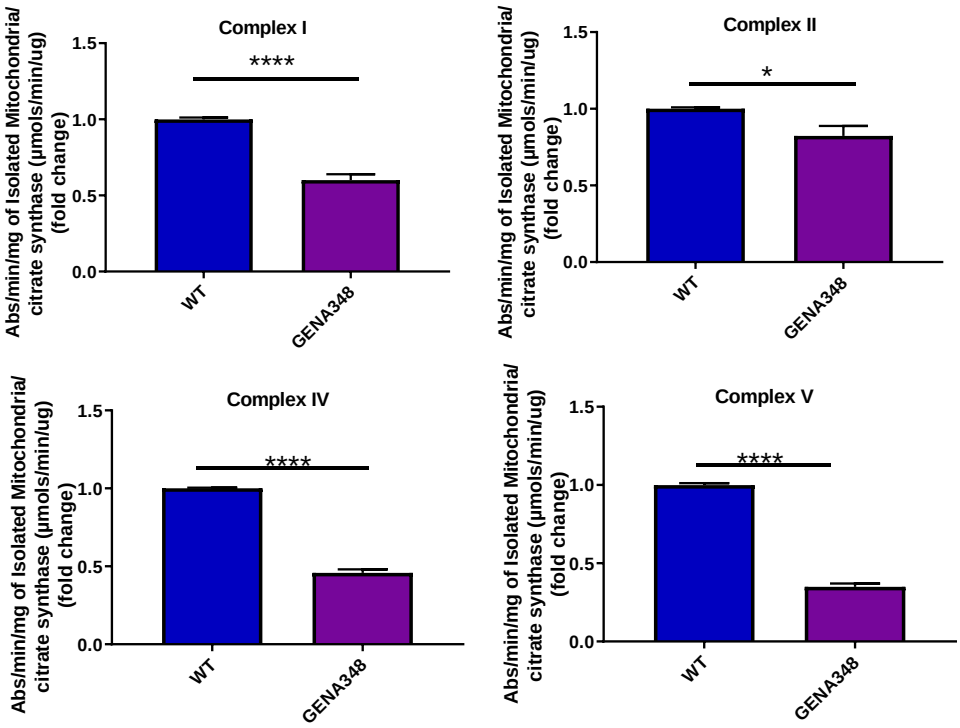

Figure 2.8 Impaired activity of mitochondrial complexes in OXPHOS regulation in the GENA348 myocardium.

Enzymatic assay revealed that the Complex activity of isolated mitochondria was decrease from GENA348 (n=5) in comparison to control (n=5) group. Data represented as mean +/- SEM *$p \leq 0.05$ and ****$p \leq 0.0001$.

2.3.6 Quantitative Mass Spectrometry Analysis of isolated mitochondria

To develop a broader understanding of how mitochondria are dysregulated in the GENA348 mouse compared to WT we next undertook quantitative proteomics of isolated mitochondria (prepared according to Methods 2.2.11; GENA348 (n=5) and WT (n=5). 1136 proteins were identified in each group with a total of 179 proteins that were either up- or down-regulated in the GENA348 mitochondria compared to WT. As depicted in (Figure. 2.9A). Most proteins were downregulated (153 proteins; 14%); with 26 proteins (2%) upregulated (Figure. 2.9A). Ingenuity Pathway Analysis revealed an overall increase of proteins in GENA348 compared to WT, suggesting widespread changes to several pathways regulating mitochondrial function. We noted a significant decrease in protein levels of subunits involved in formation of the mitochondrial complexes (Table 2.9). Examples of such proteins include NADH dehydrogenase proteins (NDUFs) that encode complex I subunits and SDHA/SDHB proteins, two of the four proteins that encode complex II (Table 2.9), Changes to the protein subunit levels in each of the complexes maybe responsible from the decreased complex activity seen in the enzymatic assay (Figure. 2.8). Interestingly, the protein subunit in Sirtuin signalling pathway (Figure. 2.9C) was also found to be downregulated; it plays an important role in different cellular processes such as apoptosis, mitochondrial biosynthesis (Weng et al., 2020), lipid metabolism, fatty acid oxidation (Carafa et al., 2016). In keeping with a decrease of complex activities and change to O2 consumption rates, our proteomics revealed widespread changes to the pathways linked to OXPHOS (Figure.2.9C). For example, we noted a significant decrease in the protein expression of prohibitin-2, involved in mitochondrial scaffolding (Ande et al., 2017). Interestingly, the loss of prohibitin-2 has been reported to lead to diabetes as a result of metabolic disruption and disruption of glucose homeostasis (Supale et al., 2013).

Quantitative MS additionally identified a significant decrease in the carnitine palmitoyltransferase protein subunit (CPT1B) included in the mitochondrial l-carnitine shuttle pathway (Figure. 2.9C) that regulates pools of coenzyme A derivatives leading to decreased

transport of fatty acids into the lumen for energy production via β-oxidation (Figure 14) (Table 2.9). Furthermore, with GENA348 being a model of diabetes, there was a significant decrease in T2DM signalling pathways (Figure. 2.9C). An example of one of these downregulated proteins signalling pathways was heat shock protein family A (Hsp70) member 5 (HsPA5). Altered production of HsPA5 has been reported to result in endoplasmic reticulum stress and has been shown as present in T2DM, through β cell failure (Laybutt et al., 2007). Thus, proteins such as these are involved in T2DM and were predominantly downregulated in the GENA348, compared to WT. Quantitative MS revealed a significant decrease in Miro1 expression which plays a key role in mitochondria homeostasis and transportation that leads to decrease in regulation of actin-based motility by Rho pathway (Figure. 2.9C).

Wild type vs GENA348

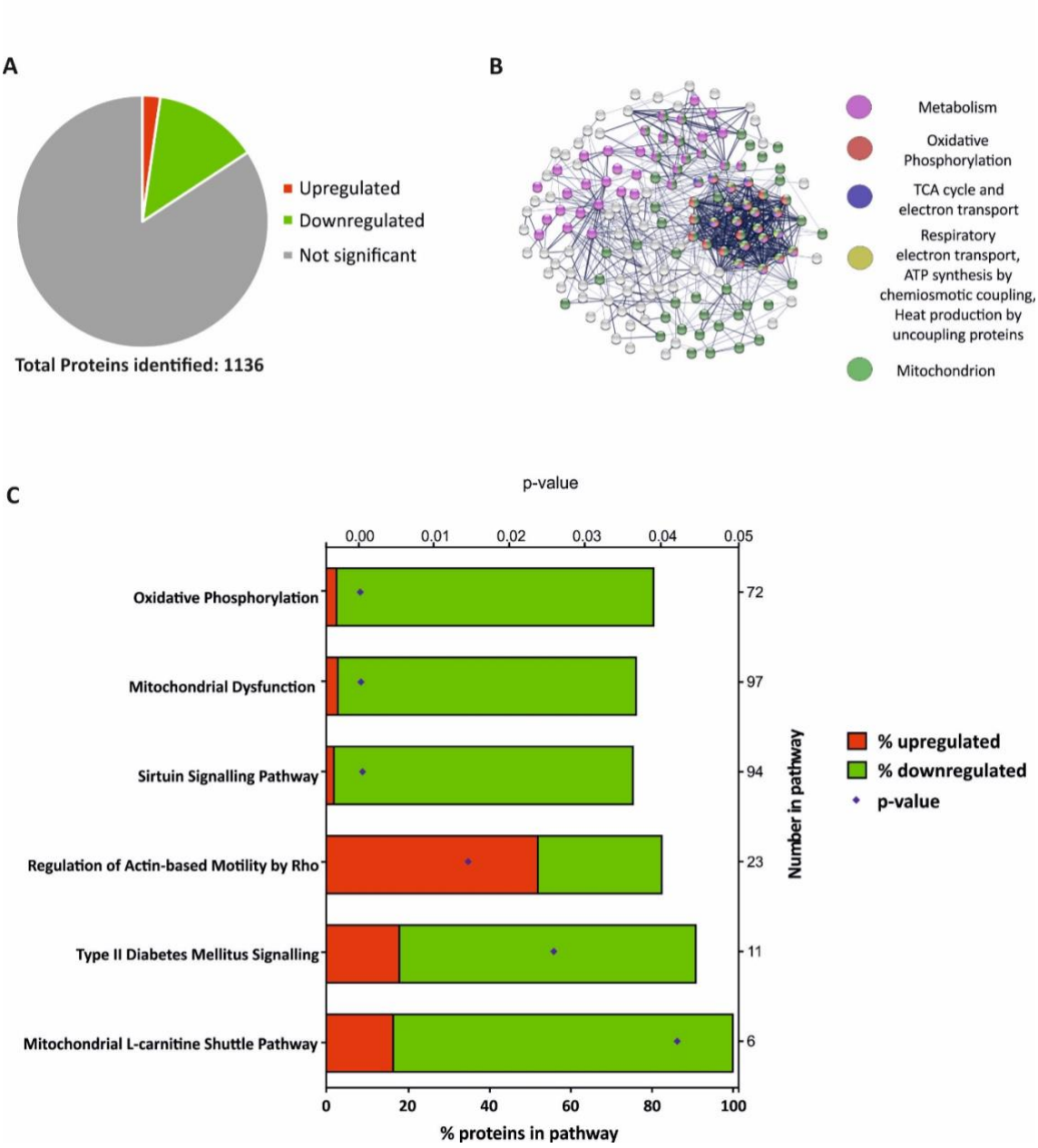

Figure 2.9 Mass spectrometry analysis of GENA348 protein compared to wild type.

(A) Pie chart illustrating that of the 1136 proteins identified, approximately 1/6th of the mitochondrial proteome is altered, with the majority of proteins down-regulated. (B) STRING Network analysis highlights significantly altered proteins networks (p<0.05). C. Ingenuity Pathway Analysis reveals 6 significantly changed protein pathways organised by *P* value (shown on top x-axis); the bars show percentage of proteins in each pathway (bottom x-axis) that are up-regulated (red) or down-regulated (green), total number of proteins within each named pathway is shown on the right-hand Y axis.

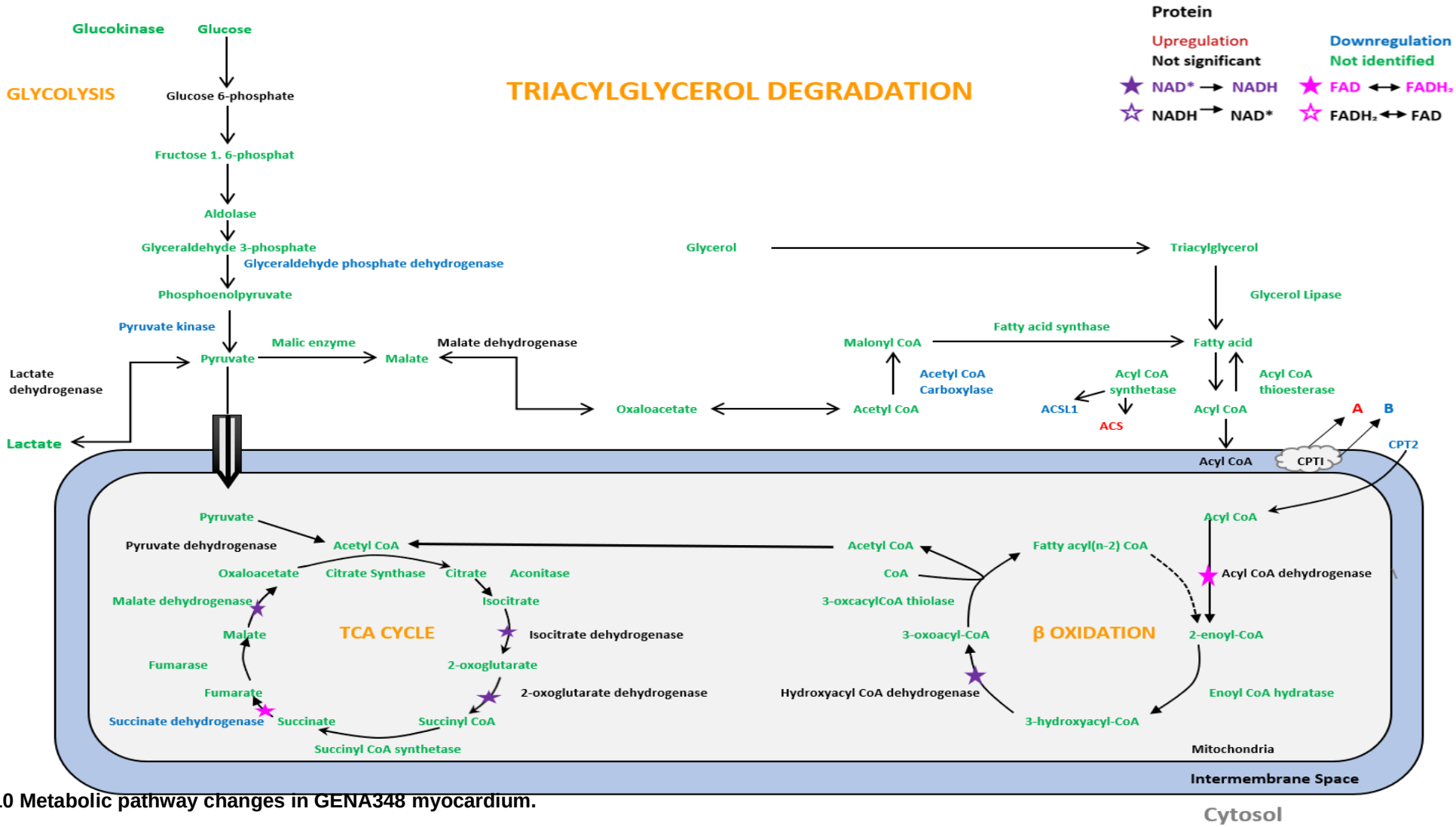

Figure 2.10 Metabolic pathway changes in GENA348 myocardium.

GENA348 proteomics (proteins and metabolites) present substantial alterations to various metabolic pathways. Upregulation shown in red, downregulation in blue, no changes shown in black and unidentified in green. Electron donor, NADH and FADH2, pathways are dedicated by a star.

Table 2.10 Mitochondrial dysfunction pathway protein expression changes from quantitative MS in wild-type vs GENA348 mice

Role	Protein	Accession Number	Peptide count	Unique peptide	P Value	Fold Change
Complex I	**NDUFA4**	NDUA4_MOUSE	9	9	0.0292	1.6
	NDUFA7	NDUA7_MOUSE	12	10	0.0145	1.7
	NDUFS1	A0A087WSU3_ MOUSE	5	2	0.0252	2.7
	NDUFS4	E9QPX3_MOUSE	12	10	0.0054	1.7
	NDUFS6	NDUS6_MOUSE	7	7	0.0411	1.4
	NDUFS7	NDUS7_MOUSE	11	5	0.0428	1.5
Complex II	**SDHA**	SDHA_MOUSE	42	35	0.0327	1.4
	SDHB	SDHB_MOUSE	26	20	0.0178	1.5
Complex IV	**COX15**	COX15_MOUSE	6	5	0.0300	1.8
	COX20	COX20_MOUSE	3	3	0.0299	1.6
	COX4I1	A2RSV8_MOUSE	16	11	0.0407	1.5
	COX5B	COX5B_MOUSE	11	7	0.0260	1.7
	COX7A2L	Q99KD6_MOUSE	5	5	0.0366	1.4
	UQCRB	QCR7_MOUSE	15	14	0.0152	1.6
	UQCRC2	QCR7_MOUSE	28	23	0.0089	1.6
Complex V	**ATP5F1**	AT5F1_MOUSE	23	18	0.0219	1.82
	ATP5L	ATP5L_MOUSE	7	6	0.0245	1.4
	ATP5I	ATP5I_MOUSE	10	9	0.0483	1.6

Oxidative Stress	**catalase**	Q3TVZ1_MOUSE	17	6	0.0500	2
	SOD1	SODC_MOUSE	4	4	0.0020	1.8
	SOD2	SODM_MOUSE	5	5	0.0008	1.8
	ALDH3A2	B1ATI0_MOUSE	6	4	0.0222	1.4
	prohibitin-2	PHB2_MOUSE	17	14	0.0240	1.6
	CAT	CATB_MOUSE	4	4	0.0379	1.4
Fatty Acid Metabolism	**ACSL1**	ACSL1_MOUSE	54	36	0.0475	1.5
	ACSL5	ACSL5_MOUSE	6	2	0.0029	2.8
	CAT	CATB_MOUSE	4	4	0.0379	1.4
	CPT1A	CPT1A_MOUSE	15	9	0.0451	1.6
	CPT1B	CPT1B_MOUSE	47	28	0.0245	1.5
Motility	**MIRO1**	MIRO1_MOUSE	9	3	0.0251	1.8

Note. Fold change in red- increase, fold change in blue- decrease

In terms of mitochondrial proteins regulating dynamics, there was no change to levels of Mfn1 (13 unique peptides, *p*=0.070), Mfn2 (5 unique peptides, *p*=0.141), Opa1 (14 unique peptides, *p*=0.116) or the receptors for Drp1, Fis1 (2 unique peptides, p=0.196). Drp1 was not detected but since it is a soluble, cytosolic protein the mitochondrial isolation process may have led to loss of the non-bound Drp1. The, proteins involved in Mfn turnover PINK1 and Parkin were not detected. Interestingly, Miro1 (Rhot1) involved in mitochondrial transport was significantly downregulated in the GENA348 mouse mitochondria 1.8-fold (*p*=0.0251). Miro1 is located on the outer membrane of mitochondria and through complex formation with Trak1/2 and KIFA/B regulated the movement of mitochondria along the microtubule cytoskeleton. Further analysis of the MS data revealed no change to the abundance of Trak1 (Trak2 was not detected). KIF5B and dynein light chain 2 showed no significant difference in abundance while KIF5A

was not detected. These data indicate that there is a change in the expression of proteins mediating mitochondrial morphology and movement within the cardiomyocyte, Therefore, we next undertook molecular investigations using Western blotting and RT-qPCR to determine if these changes were at the protein level only or are due to changes in transcript levels.

2.3.7 Increased expression of proteins involved in mitochondrial fusion in the GENA348 myocardium

To investigate changes in expression levels of involved in mitochondrial fusion in the GENA348 myocardium, ventricular tissue was divided, part lysed for Western Blotting and probed for proteins regulating mitochondrial fission and fusion. As summarised in (Figure. 2.10), a 3-fold increase in the expression of Mfn1 (P=0.0019) and a 5-fold increase in Mfn2 (P=0.0003) was recorded in the GENA348 myocardium compared to controls (Figure. 2.10). Mfn1 and Mfn2 mediate fusion of the mitochondrial OMM, for complete fusion of two mitochondria the IMM also fuses, under the control of Opa1. Significantly, there is a 1.5-fold increase in expression of the inner fusion protein Opa1 (P=0.0400; Figure. 2.10). There was no change in the expression levels of fission protein Drp1. As previously stated, MS results differed with Western blotting protein expression levels in GENA348 mice; MS data revealed no change in Mfn1, Mfn2, Opa1, and Drp1 was not detected (Figure. 2.10).

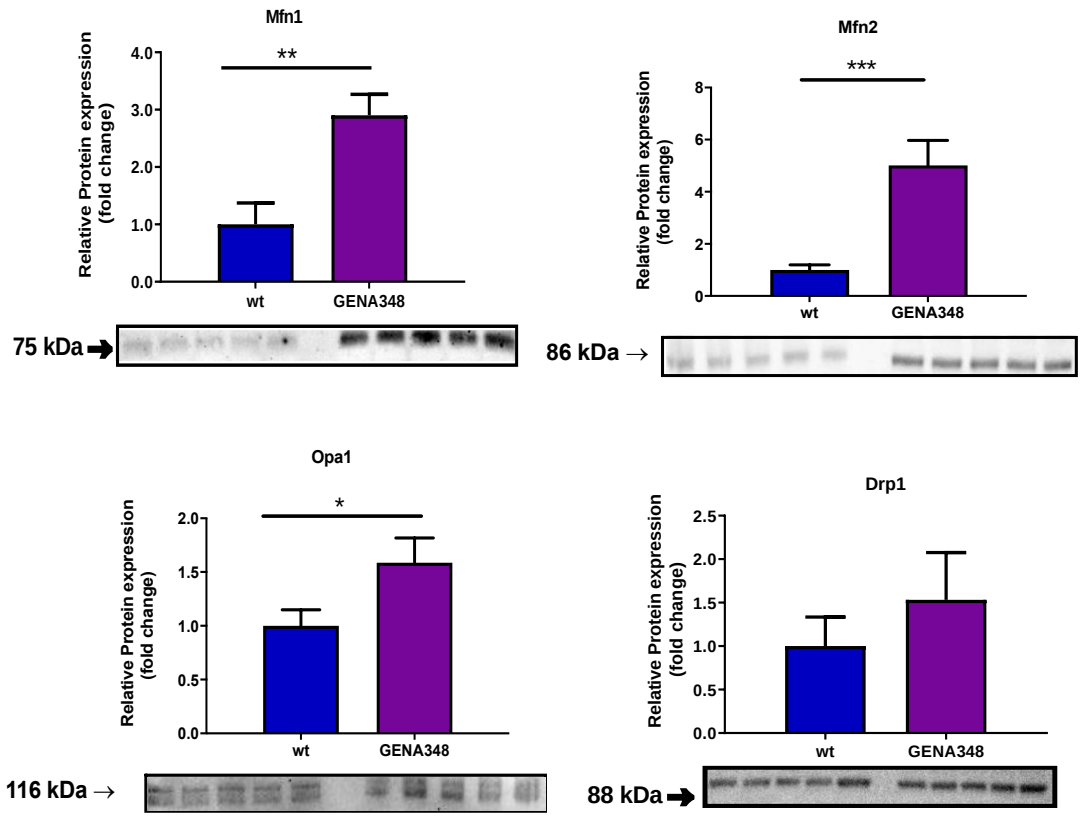

Figure 2.11 GENA348 myocardium exhibits significant upregulation of fusion protein.

Western blot analysis of LV from control (n=5) and GENA348 (n=5) revealed an increase in the expression of protein of Mfn1, Mfn2 and Opa1 in the GENA348 myocardium in comparison to control while no change in Drp1 level. Data represented as mean +/- SEM *$p \leq 0.05$, **$p \leq 0.01$, ***$p \leq 0.001$.

In agreement with the MS data, Miro1 expression was shown to be decreased in the GENA348 myocardium by 0.6-fold (P=0.0141; Figure. 2.11).

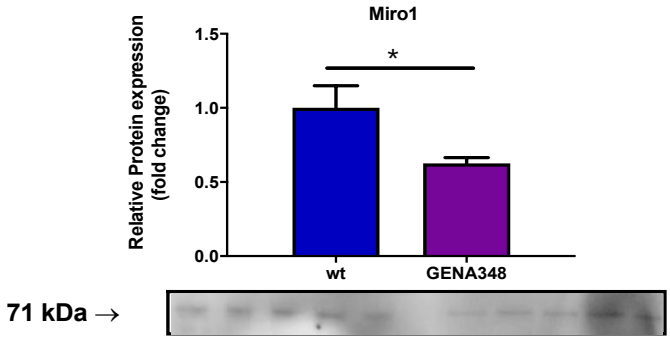

Figure 2.12 Downregulation of Miro1 exhibited by GENA348 myocardium

Western blot analysis of LV from control (n=5) and GENA348 (n=5) revealed a significant decreased in Miro1 expression in GENA348 mice compared to WT. Data represented as mean +/- SEM *$p \leq 0.05$.

PINK1 expression levels showed no change in expression; however, there was a significant decrease in Parkin by 0.4-fold (P<0.0001) in GENA348 compared to WT (Figure. 2.12).

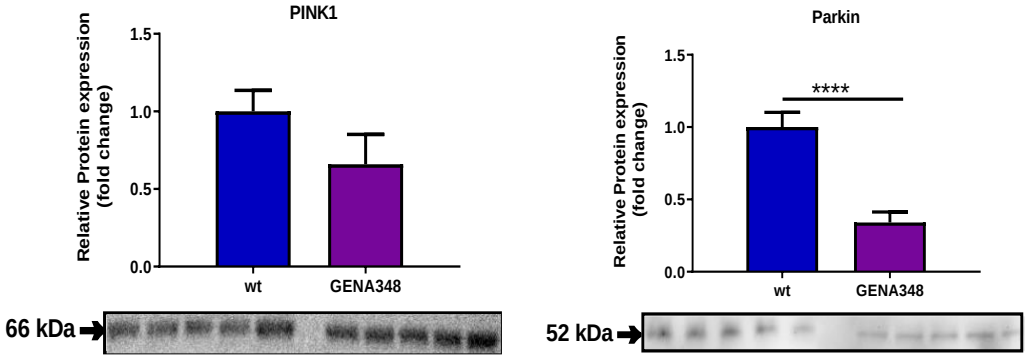

Figure 2.13 GENA348 myocardium exhibit downregulation of parkin protein.

Western blot analysis of LV from GENA348 (n=10) compared to control (n=10) revealed a significant decrease in Parkin with no change in PINK. Data represented as mean +/- SEM ****$p \leq 0.0001$.

2.3.8 Analysis of transcript levels of proteins regulating mitochondrial dynamics

Next, qPCR was carried out in order to determine if the changes to the protein expression of Mfn1, Mfn2 and Opa1 is correlated to increased transcript levels. As shown in (Figure. 2.13) a significant increase in the mRNA of Mfn1, Mfn2, Opa1 was identified (3.2-fold, 2.3-fold, 4.2-fold, P=0.0033, P=0.0022 and P<0.0001 respectively) with no change to levels of Drp1 observed. These data are consistent with the Western blotting data.

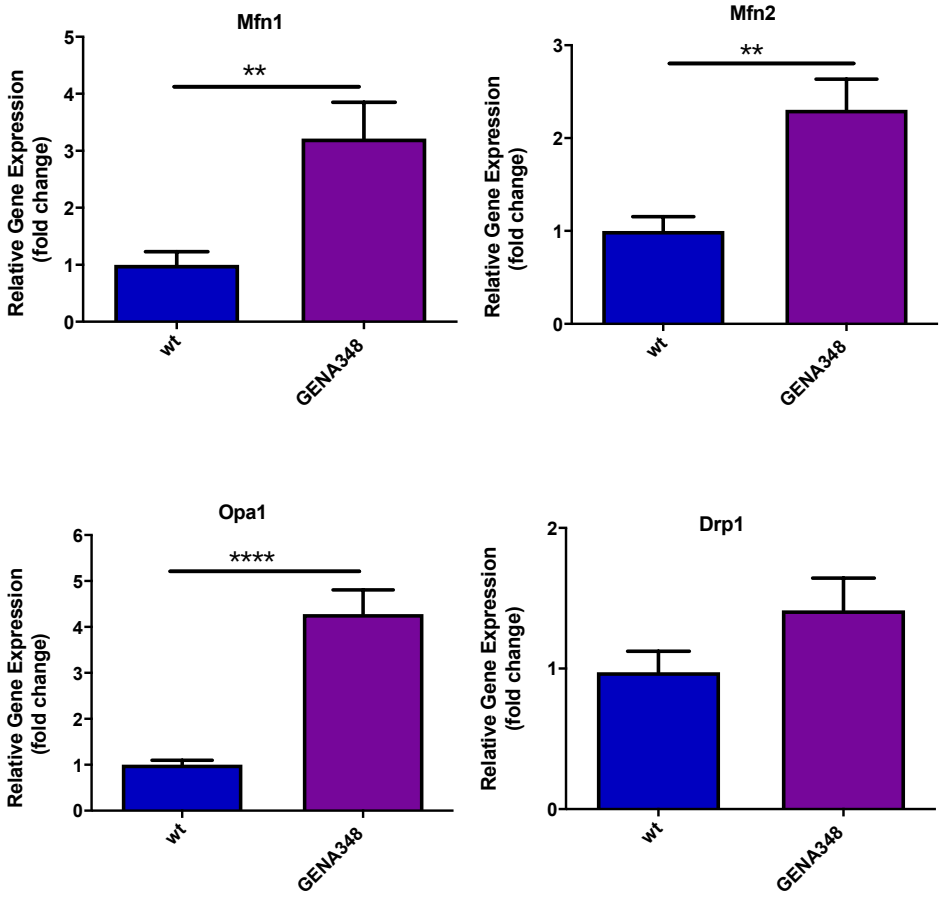

Figure 2.14 Upregulation in fusion transcript expression in GENA348 myocardium.

Mfn1, Mfn2 and Opa1 transcript level were assessed using qPCR and revealed a significant increase in GENA348 (n=6) compared to control (n=6) with no significant difference in transcript level of Drp1. Data represented as mean +/- SEM **p ≤ 0.01 and ****p ≤ 0.0001.

PINK1 and Parkin mRNA was decreased by 0.3-fold (*P*=0.0177) and 0.4-fold (*P*=0.0026) respectively (Figure. 2.14).

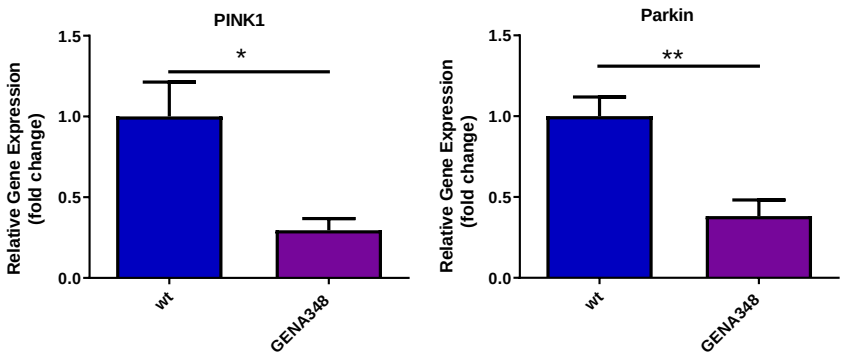

Figure 2.15 Downregulation in the gene transcript of PINK1 and Parkin in GENA348 myocardium.

PINK1 and Parkin transcript levels were decreased in GENA348 (n=6) compared to control (n=6). Data represented as mean +/- SEM *$p \leq 0.05$ and **$p \leq 0.01$.

2.3.9 Upregulation of mitochondrial biogenesis marker transcripts in the GENA348 myocardium

Levels of PGC-1α and TFAM transcripts were increased in the GENA348 group in comparison to control group with a 2-and 3.7-fold increase (*P*=0.0108 and *P*<0.0001*)*, respectively (Figure. 2.15).

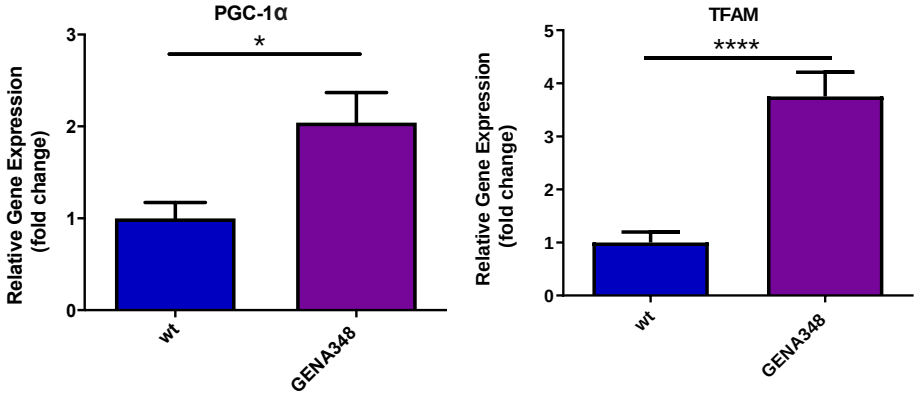

Figure 2.16 GENA348 myocardium exhibit upregulation in the gene expression of PGC-1α and TFAM.

PGC-1α and TFAM transcript level were assed using qPCR and revealed a significant increase in GENA348 (n=6) compared to control (n=6). Data represented as mean +/- SEM *$p \leq 0.05$ and ****$p \leq 0.0001$.

In agreement with the Western blotting and proteomics data there was also a decrease in Miro1 transcript levels in GENA348 compared to control with 0.2-fold (*P*=0.0115). Similarly, in agreement with the MS data there was no change to the mRNA levels of TRAK1, KIF5A and KIF5B in GENA348 compared to WT mice (Figure. 2.16).

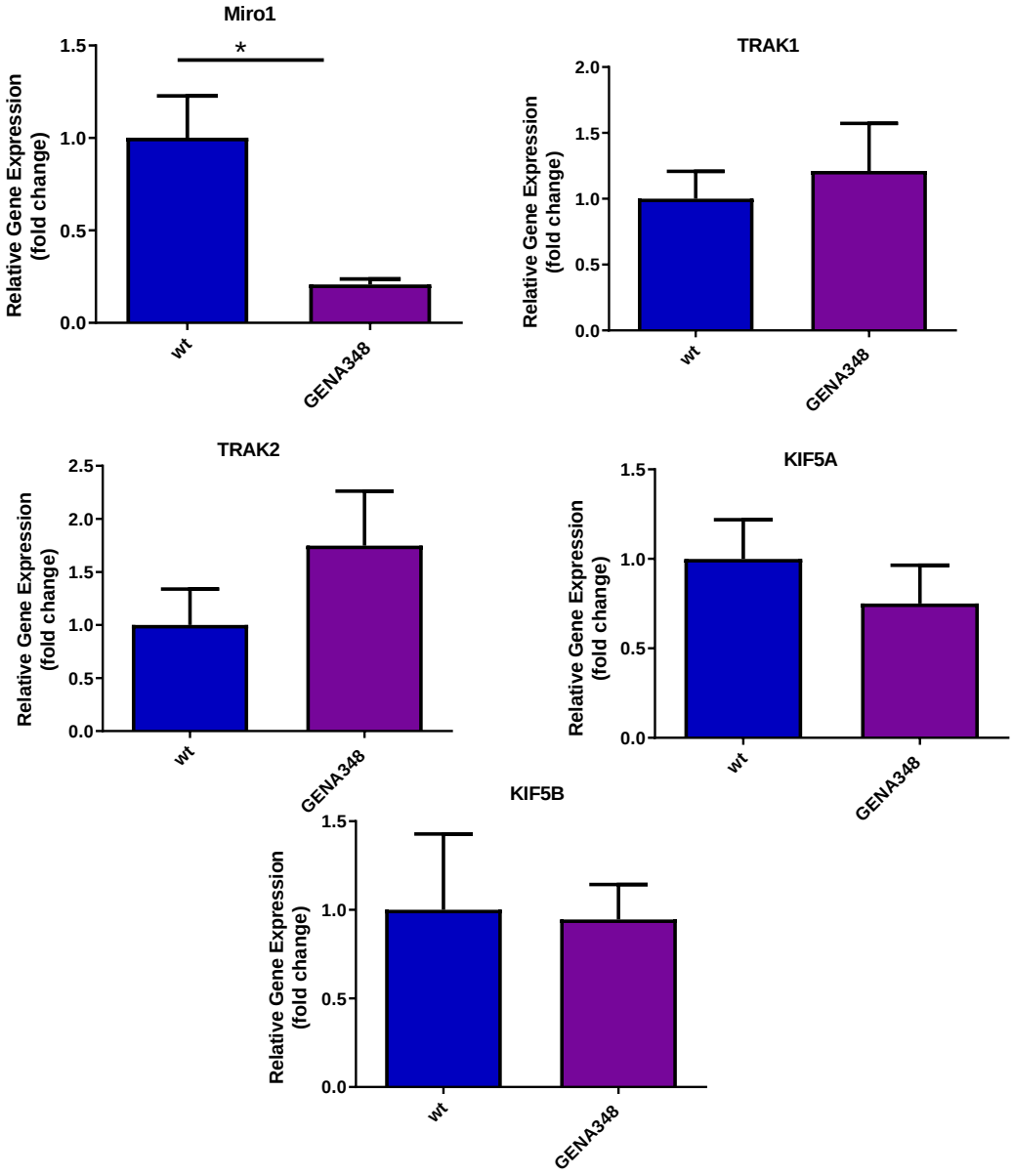

Figure 2.17 GENA348 myocardium exhibit downregulation of Miro1 expression.

Miro1, TRAK1, TRAK2, KIF5A and KIF5B transcript level were assed using qPCR and revealed a significant decrease in Miro1 in GENA348 (n=6) compared to control (n=6). Data represented as mean +/- SEM *p ≤ 0.05.

2.3.10 Impact of Miro1 knockdown on H9c2 cell mitochondria

2.3.10.1 Knock-down of Miro1 has no effect on cell viability or response to oxidative stress

To next investigate the role of Miro1 in H9c2 cells, siRNA silencing was used to knockdown (KD) Miro1 and generate Miro1si-H9c2 lines. To determine Miro1 expression levels in these cells, Western blots were used to measure Miro1 protein expression. Miro1 expression showed an approximate 70% decrease in the si-Miro1 treated H9c2 cells compared to si-NTC transfected cells (*P*= 0.0013) (Figure 2.18).

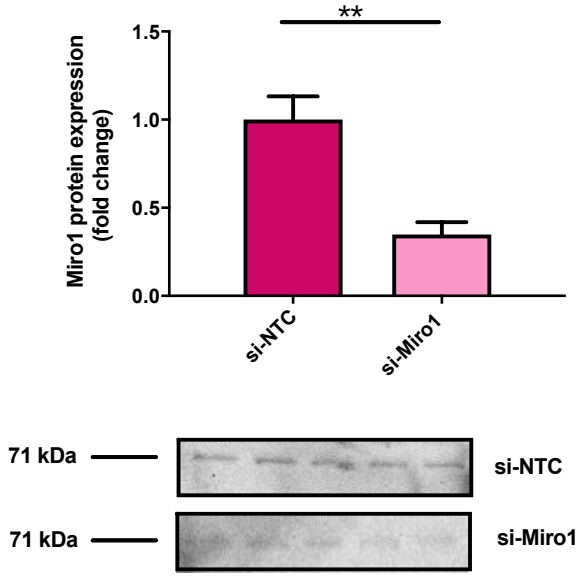

Figure 2.18 si-Miro1 transfected cells exhibit downregulation in Miro1 protein expression.
Western blot analysis revealed a significant decrease in Miro1 protein in si-Miro1 as compared to the si-NTC transfected cells. Data represented as mean +/- SEM $^{**}p \leq 0.01$ (n=5 lanes of the same passage).

Since Miro1 and Miro2 share 60% sequence identity we next checked levels of Miro2 to investigate whether the si-Miro1 treatment had also led to a knockdown or conversely whether the loss of Miro1 was compensated by Miro2. However as can be seen from the Western blot below Miro2 protein expression showed no change in si-Miro1 as compared to the si-NTC transfected cells (Figure 2.19).

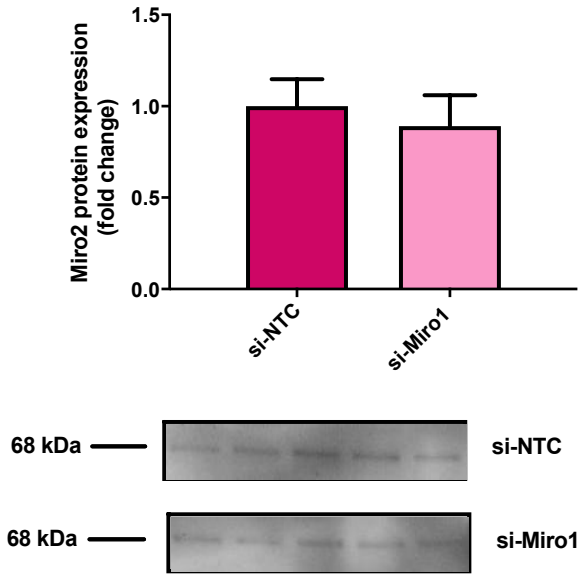

Figure 2.19 Miro2 protein expression in si-Miro1 and si-NTC transfected cells is unchanged.
Western blot analysis revealed no significant difference in the Miro2 protein level in si-Miro1 compared to si-NTC transfected cells. Data represented as mean +/- SEM (n=5 lanes of the same passage).

Before each experiment Miro1 knockdown cells we first checked whether the siRNA treatment had worked. The MTT cell viability assay showed no change in si-NTC and si-Miro1 compared to negative control. All cells transfected and non-transfected where then treated with H_2O_2 Figure 2.20). Both controls, si-NTC and si-Miro1 cells showed 0.1-fold decrease in cell viability after treatment with H_2O_2 (P<0.0001; Figure 2.20) thereby showing H_2O_2 induce apoptosis. This lack of a difference between negative controls, si-NTC and si-Miro1 gave confidence in H9c2 knockdown cells being viable and enabled their continued use in this study.

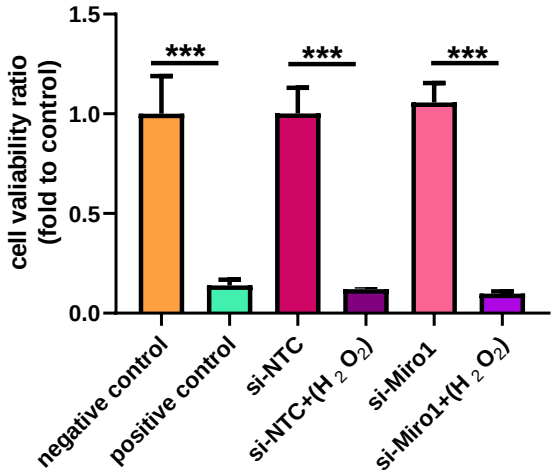

Figure 2.20 Cells treated with H_2O_2 exhibit decrease in cell viability.
The cell viability assay revealed no significant difference in viability between non-transfected and transfected cells compared to negative control, while the H_2O_2 treatment showed an equally significant decrease to the cell viability between all 3 groups. Data represented as mean +/- SEM (n=3 lane from 3 different passage) ***$p \leq 0.001$.

2.3.10.2 Miro1 knockdown causes change in mitochondrial dynamics via Opa1 and PINK1

As mentioned above, the primary regulators of mitochondrial fusion are dynamin related GTPases termed mitofusins (Mfn1 and Mfn2) and optic atrophy protein 1 (Opa1). Mitochondrial fusion involves the process of physical merging of the outer and then the inner mitochondrial membranes of two originally distinct mitochondria. In contrast, fission, mediated by Drp1, leads to the pinching of the mitochondrial membrane, forming daughter mitochondria. By employing RT-qPCR it was determined that at the transcript level Mfn1 and Mfn2 expression wasn't altered in the si- Miro1 transfected cells compared to the si-NTC cells. However, there was a 2-fold increase in Opa1 levels in si-Miro1 compared to the control cells (P= 0.0086; Figure 2.21). The fission protein Drp1 also showed no significant change in transcript levels between si-NTC and si-Miro1 transfected cells.

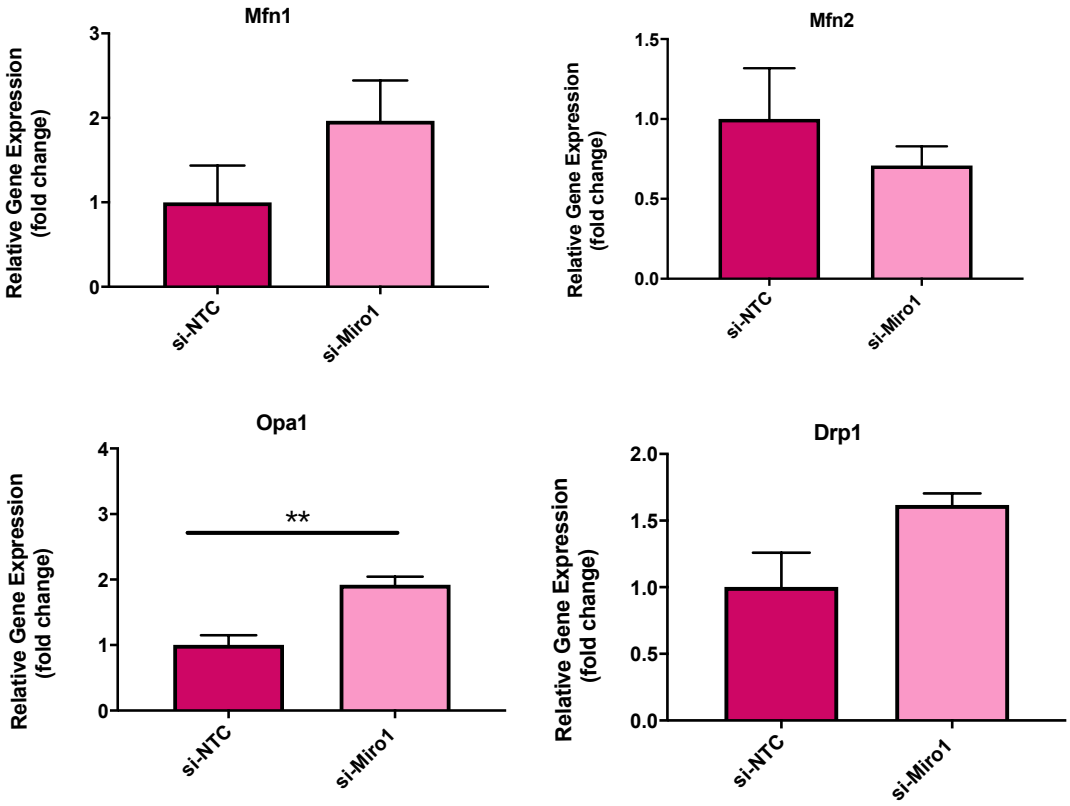

Figure 2.21 si-Miro1 transfected cells exhibit change in mitochondrial dynamics. Mfn1, Mfn2, Opa1 and Drp1 transcript level were assessed using qPCR and revealed a significant increase in Opa1 in si-Miro1 as compare to the si-NTC H9c2 cells. Data represented as mean +/- SEM (n=3 lane from 3 different passage) $^{**}p \leq 0.01$.

The process of mitochondrial maintenance is carried through mitophagy. PINK1 phosphorylation via Mfn2 leads to the conscription of Parkin, resulting in mitochondrial degradation via ubiquitination and lysosomes. Our data revealed a significant increase in gene expression of PINK1 in si-Miro1, compared to si-NTC transfected cells (1.4-fold, P=0.0317; Figure **2.22**). However, gene expression of Parkin remained unchanged. These data suggest that Miro1 knockdown has led to a change in the expression of proteins involved in mitophagy.

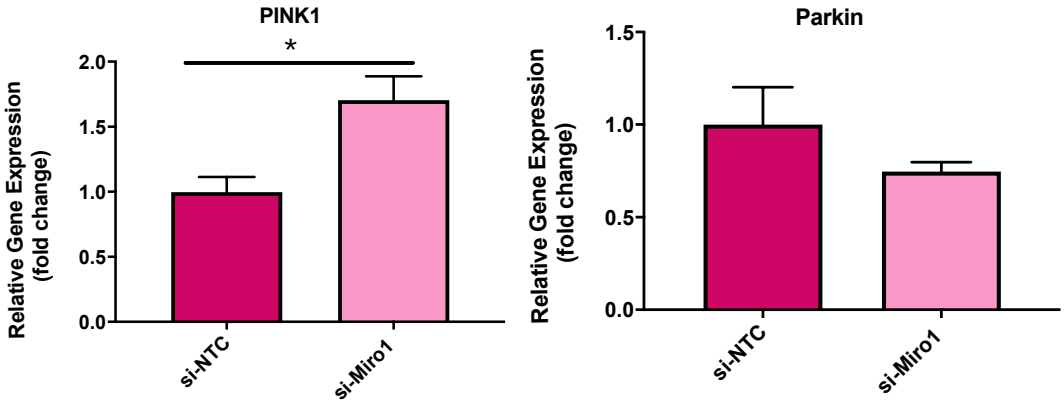

Figure 2.22 si-Miro1 transfected cells exhibit upregulation in PINK1 gene expression. PINK1 and Parkin transcript level were assessed using qPCR and revealed a significant increase in PINK1 gene expression in si-Miro1 compared to si-NTC H9c2 cells. Data represented as mean +/- SEM (n=3 lane from 3 different passage) *$p \leq 0.05$.

2.3.10.3 Knockdown of Miro1 impacts mitochondrial biogenesis

To further understand mitochondrial biogenesis and the role of Miro1 in mediating mitochondrial homeostasis, changes in expression of the biogenesis markers, TFAM and PGC1-α were measured. The Miro1 knock down cells showed a decrease in the gene expression of PGC-1α compared to si-NTC cells (0.2-fold change, *P*=0.0110; Figure 2.23). In contrast, gene expression of TFAM increased in si-Miro1 cells compared to si-NTC cells (2.2-fold change, *P*=0.0288; Figure 2.23). Interestingly, in Chapter 2, we reported that there were increased levels of PGC-1αα and TFAM in the GENA348 mouse myocardium. Reduced levels of PGC-1αα would suggest that the reduction in Miro1 levels has led to fewer mitochondria. Citrate synthase also indicates an increased mitochondrial content in GENA348, suggesting other mechanisms that may be involved.

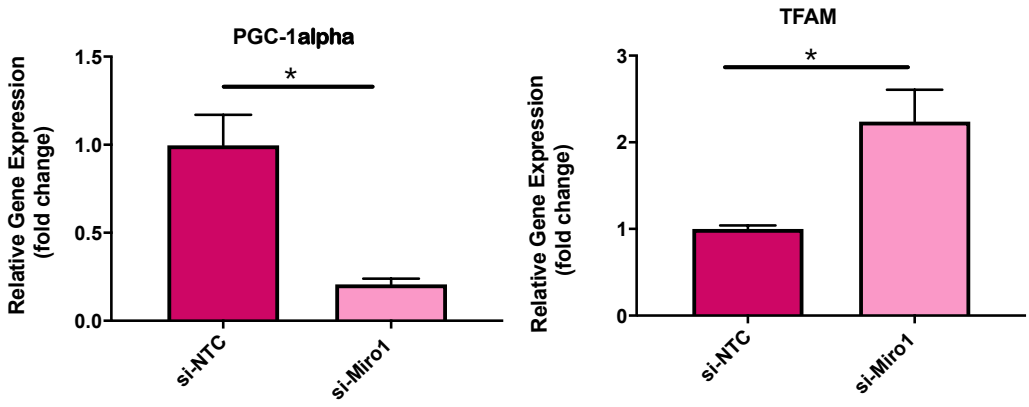

Figure 2.23 Changes in mitochondrial biogenesis markers in si-Miro1 transfected cells. PGC-1α and TFAM transcript levels were assessed using qPCR and revealed a significant decrease in PGC-1α and significant increase in TFAM in si-Miro1 as compared to the si-NTC H9c2 cells. Data represented as mean +/- SEM (n=3 lane from 3 different passage)*$p \leq 0.05$.

2.3.10.4 Downregulation of mitochondrial trafficking proteins in si-Miro1 knockdown cells

It has been reported that kinesin superfamily proteins (KIFs) form a complex with Milton (TRAK1 and TRAK2) and Miro1 (Schwarz, 2013). These have been identified as binding specifically to KIF5A (Randall et al., 2013). In order to investigate the impact of the removal of Miro1 from the complex, gene expression of the interacting proteins was measured. Levels of Miro1 were verified for each new set of experiments, here the level of expression of Miro1 transcript was 0.4-fold compared to si-NTC control (P=0.010; Figure 2.24), again there was no change in transcript levels of Miro2. Further, there was no change to mRNA levels of KIF5A, KIF5B, TRAK1 and TRAK2.

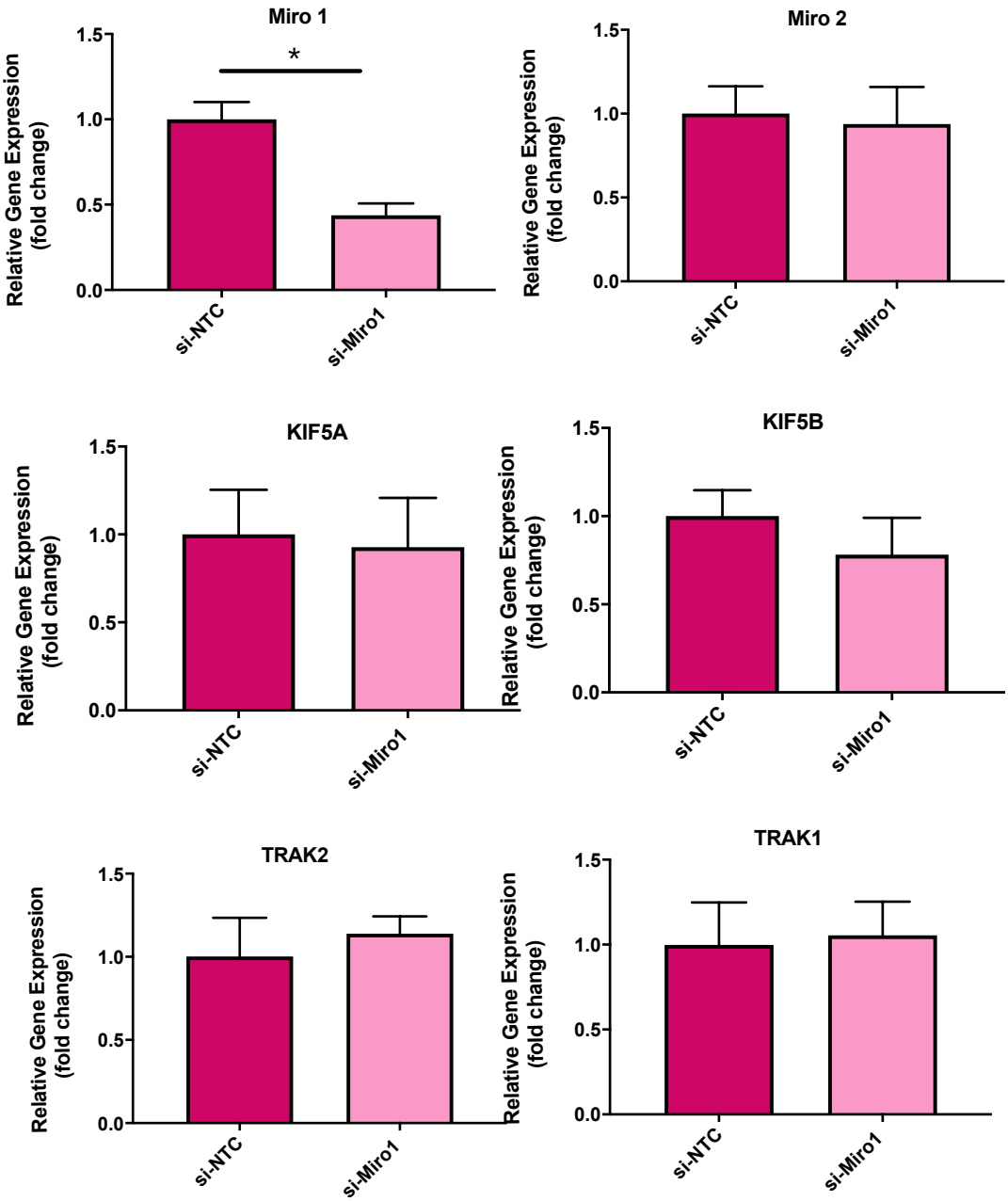

Figure 2.24 si-Miro1 downregulation has no effect upon the expression of proteins associated with mitochondrial trafficking.
Miro1, TRAK1, TRAK2, KIF5A and KIF5B transcript level were assessed using qPCR and revealed a significant decrease in Miro1 in si-Miro1 compared to si-NTC. Data represented as mean +/- SEM (n=3 lane from 3 different passage) *$p \leq 0.05$.

Citrate synthase activity was measured to investigate the impact of Miro1-knock down upon mitochondrial content. However, no change in citrate synthase activity was measured in si-Miro1 compared to si-NTC transfected cells (P= 0.0011; Figure 2.25). This appears inconsistent with the suggestion that down-regulation of PGC-1α and TFAM leads to less mitochondria.

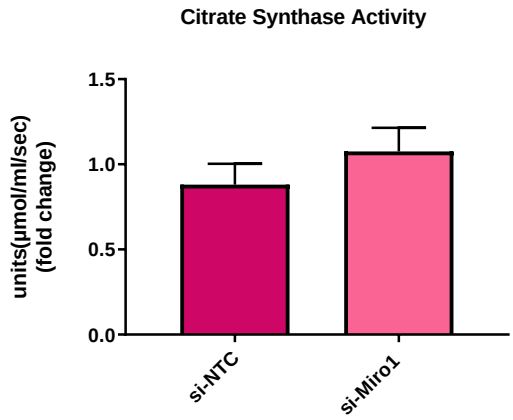

Figure 2.25 Citrate synthase activity in si-Miro1 H9c2 cells.
Citrate synthase activity was measured as the marker of mitochondrial content revealing no difference in si-Miro1 compared to si-NTC H9c2 cells. Data represented as mean +/- SEM (n=3).

2.3.10.5 Miro1 knockdown has no impact on mitochondrial oxygen consumption

Using the fibre-optic Instech respirometer described in Chapter 2, isolated mitochondria were prepared from si-Miro1 and si-NTC transfected cells. As shown in (Figure **2.26**) a linear profile took typically five minutes to plateau. The gradient between (20-140) sec was calculated (Figure **2.26**A) for each group. The oxygen profile in si-Miro1 shows no difference in oxygen consumption compared to si-NTC ((Figure **2.26**B). Overall oxygen percentage of isolate mitochondria in si-Miro1 was found to be the same compared to si-NTC (Figure **2.26**B).

A

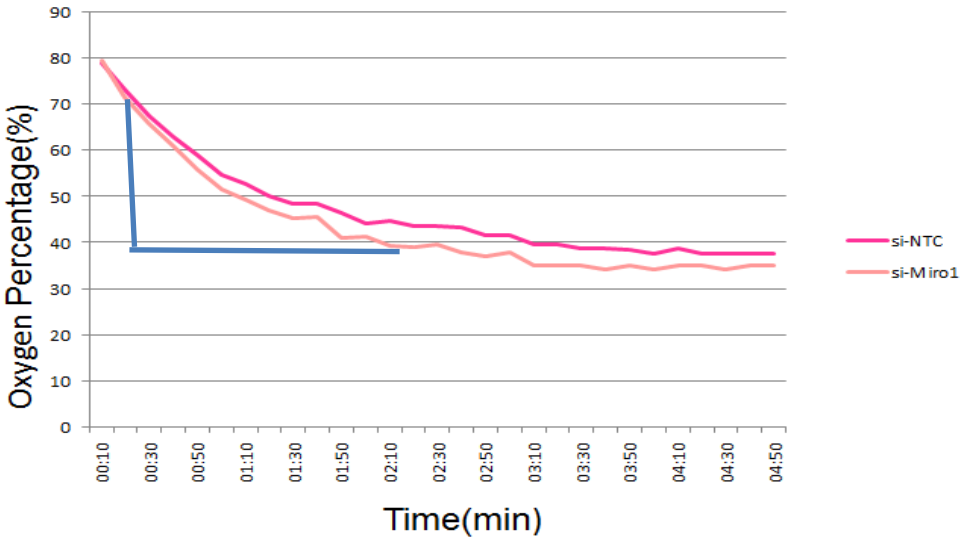

B

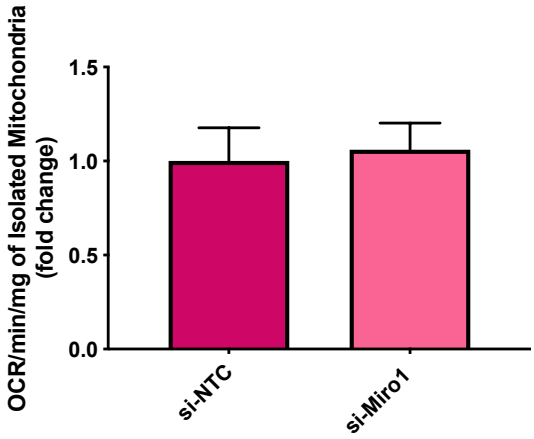

Figure 2.26 No change in oxygen consumption rate in si-NTC H9c2 cells.
(A) There was no change in oxygen consumption rate in si-Miro1 compared to si-NTC H9c2 cells. (B) Representative plot indicating oxygen percentage varying with time in si-Miro1 and si-NTC H9c2 cells. Data represented as mean +/- SEM (n=3 lane from 3 different passage).

2.3.10.6 Miro1 knockdown alters mitochondrial morphology and density as seen by SBF-SEM

Prior to fixing the cells for EM qPCR was carried out to assess Miro1 transcript levels. As shown in (Figure 2.27), si-Miro1 transfected cells showed a significant 0.3- fold decrease in Miro1 protein expression compared to si-NTC (*P*= 0.0013). There was also a significant 0.4-fold decrease in gene expression of Miro1 in si-Miro1 compared to si-NTC transfected cells

(*P*=0.010; Figure 2.27). This result confirmed that the EM samples were of cells with Miro1 knocked down. As described in Chapter 3 3D electron microscopy (SBF-SEM) was carried out to observe mitochondrial structure in si-Miro1 and si-NTC transfected cells. Due to time constraints, datasets were only collected for n=1 per group. 100 mitochondria were segmented from a single passage of each group to investigate mitochondrial structure and size (Figure 2.27).

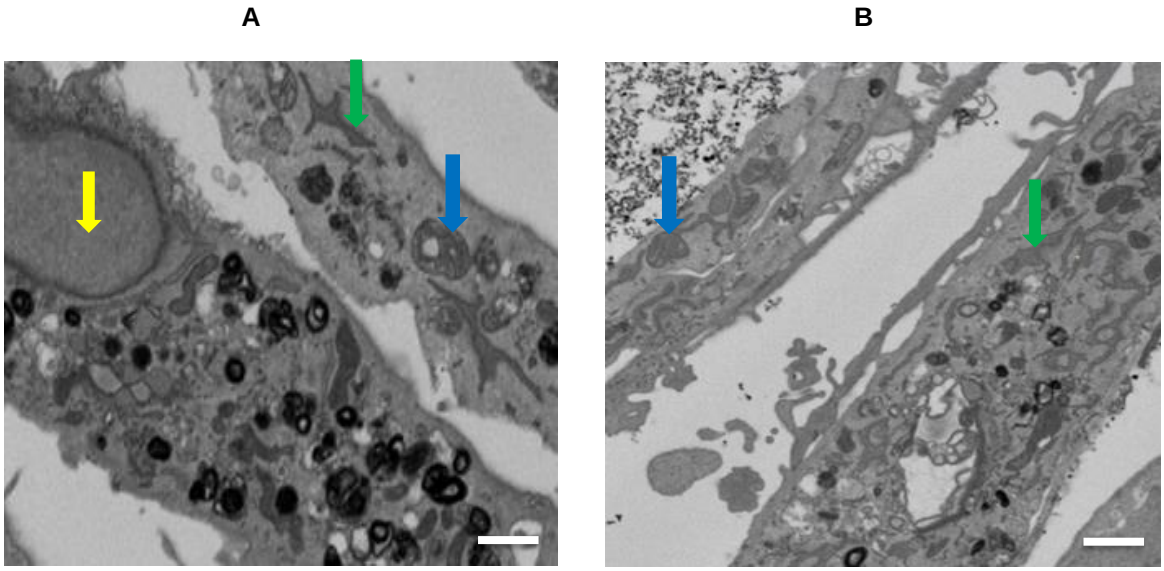

Figure 2.27 Identification of mitochondria using SBF-SEM.
Identification of mitochondria in H9c2 cells is complicated and more complicated in si-Miro1 than si-NTC H9c2 cells. 100 mitochondria were randomly selected for segmentation. (A) Mitochondrial morphology in si-NTC H9c2 cells. (B) Mitochondrial morphology in si-Miro1 H9c2 cells. In both images, blue arrows indicate mitochondria, the green arrow indicates endoplasmic reticulum and the yellow arrow indicates the nucleus. Scale bar: 1µm.

To measure changes in mitochondrial volume and mesh surface area, individual mitochondria were segmented. The surface area and volume of the segmented mitochondria were calculated using a function in the IMOD software as described in Chapter 3. Results indicate that there is a significant decrease in both mitochondrial volume and surface area in si-Miro1 mitochondria (Figure 2.28). Interestingly, this decrease in mitochondrial size is not reflected in the oxygen consumption rate.

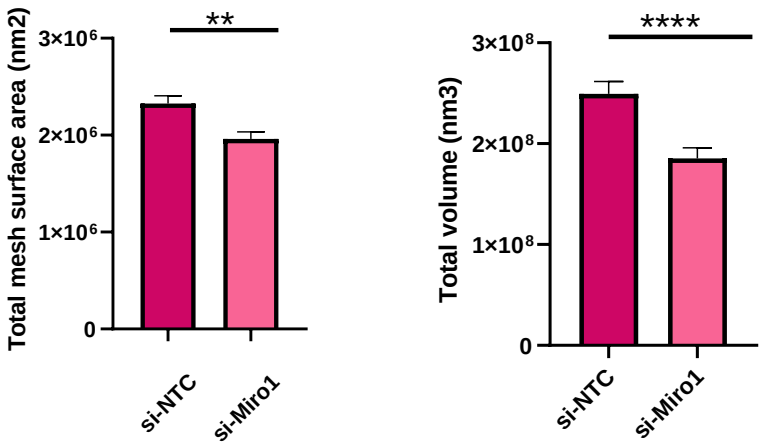

Figure 2.28 Mitochondria size is significantly smaller in si-Miro1 compared to si-NTC H9c2 cells.
si-NTC and si-Miro1 H9c2 cells were imaged using serial block facing SEM. Mitochondria were manually segmented using IMOD. There was a significant decrease in volume and mesh surface area in si-Miro1 compared to si-NTC. Data represented as mean ± SEM (mitochondria n=100, 1 cell) $^{**}p \leq 0.01$ and $^{****}p \leq 0.0001$.

2.4 Discussion

The aim of this study was to investigate cardiac and mitochondrial function in the GENA348 mouse model. To this aim, we began by investigating physiological parameters such as body weight, heart weight and echocardiographic measurement changes. Proteomics was employed to investigate global changes to expression levels of mitochondrial proteins, complemented by functional studies to determine if the early LV dysfunction previously identified in our group in the GENA348 heart involved changes to mitochondrial activity e.g. oxygen consumption and OXPHOS.

The key findings from this chapter are: (1) GENA348 had a significantly larger heart/body weight and there was evidence of cardiac hypertrophy, similar to that observed in patients with MODY2; (2) GENA348 mice have dysfunctional mitochondria with reduced oxidative phosphorylation, at the cellular level; (3) at the molecular level, there was an imbalance between protein expression levels of mitochondrial dynamic regulation; (4) si-Miro1 led to an increase in Opa1 transcript expression (but with no change to the other fission-fusion proteins) with an increase in mitochondrial biogenesis markers. However, although a decrease in mitochondrial volume and surface area was measured there was no change to the mitochondrial oxygen consumption rate.

2.4.1 GENA348 mice have impaired cardiac function

GENA348 mice were larger than the WT controls despite being fed the same diet (Figure. 2.4), with a significant increase recorded in the HW/TL ratio in GENA348 mice, suggesting the development of cardiac hypertrophy. It is known that neuronal *Gck* is involved in regulation of dietary glucose intake (Hussain et al., 2015), thus, controlling appetite. Echocardiography data corroborated these physiological measurements, with 6-month old GENA348 mice presenting an increase in both diastolic and systolic posterior wall thickness (Table 2.7). These data indicate the development of left ventricular hypertrophy (LVH) and abnormal function of the left ventricle is generally connected with left ventricular hypertrophy. The GENA348 mouse displayed a lower early to late ventricular filling ratio in comparison to controls (Table 2.7).

However, no change was observed in ejection fraction between control and GENA348 mouse. This could suggest diastolic dysfunction, defined as impairment in the left ventricle relaxation. Lung weight remained the same in both conditions, indicating that there was no pulmonary congestion, suggesting that the mice are in the early stages of diastolic dysfunction or heart failure. Pulmonary congestion is usually associated with advanced stages of heart failure and is the predominant cause of hospital admission among heart failure patients (Miglioranza et al., 2017). This physiological data may indicate that MODY2 patients are at risk of developing cardiac complications. Diastolic dysfunction is reported to be a feature of T2DM, particularly in early manifestation (Lalande et al., 2010). Significantly, (Wilson et al., 2017) investigated whether impaired left ventricular filing was responsible for the attenuated cardiac reserve in people with T2DM. The authors measured left ventricular volume, along with other parameters, in diabetic individuals during an elevated heart rate in exercise. Their results showed that adults with T2DM were unable to maintain and increase left ventricular filling volumes (Wilson et al., 2017), confirming the presence of diastolic dysfunction as a result of impaired left ventricle function. In a similar MODY2 mouse model, an increase in the left ventricular wall thickness was reported, further suggesting that MODY2 patients are at risk of heart failure.

In addition, echocardiography data showed a further link between heart failure and preserved ejection fraction, HFpEF (Table 2.7). Early diastolic dysfunction suggests that the GENA348 mice had a preserved ejection fraction, which may indicate the development of HFpEF. HFpEF accounts for up to 50% of heart failure cases (Nanayakkara et al., 2018). At present, medication used for HFrEF is less effective for HFpEF, thus, MODY2 patients may be presented with fewer therapeutic options for long-term treatment.

Biochemical studies further suggest the development of impaired cardiac function through the downregulation in the sirtuin signalling pathway (Figure. 2.9) It is thought that sirtuin 1 (SIRT1), is a pivotal protein in cellular metabolism, suggesting its importance in regulating mitochondrial dynamics (Blander and Guarente, 2004). In diabetic cardiomyopathy mice, Blander and Guarente (2004) investigated the possible protective effect of SIRT1 against the development

of diabetic cardiomyopathy mice through mitochondrial regulation. They reported a significant decrease in the expression of SIRT1 diabetic cardiomyopathy mice hearts, suggesting that SIRT1 has a protective role on the mitochondria and a possible target for therapy (Blander and Guarente, 2004). Overall, the decrease in the sirtuin signalling pathway that identified by Quantitative MS in (Figure. 2.9) accompanied with downregulation of mitochondrial dysfunction proteins in GENA348 presents a possible link between sirtuin in diabetic cardiomyopathy and an area for further research.

The reduction in expression levels of NDUFA4 proteins, associated with mitochondrial complex I structure and hence OXPHOS were modified in the GENA348 mitochondria compared to the controls which may be a contributory factor to the decrease in activity that was also identified here. Importantly, functional analysis of the complex activities revealed a decrease in activity, consistent with the MS data. Additionally, the Complexes are known to interact with each other, forming higher order structures, called super complexes (Wittig and Schägger, 2008). Complexes IV and V can form dimers and oligomers. These complexes play an important role in assembly, regulation and stability of the mitochondrial membrane (Signes and Fernandez-Vizarra, 2018); the down-regulation of several of the protein subunits in each of the complexes may also be a contributory factor leading to instability of the super-complexes.

The oxygen profile change in GENA348 mice shows that GENA348 mice consume more oxygen compared to the wild type (Figure. 2.7B). The oxygen percentage of GENA348 mice was not significant after corrected to citrate synthase activity. The enhanced mitochondrial activity observed by increased citrate synthase levels may be due to increased mitochondrial content. The enhanced glycolytic reserve and respiratory capacity observed could reflect a higher metabolic plasticity to maintain intracellular ATP content. Future work should be aimed at increasing sample size of (n=4) for these experiments. Increasing this number was challenging due to difficulties with the technique and acquiring repeated readings. Future work would aim to iterate this methodology to ensure that a greater sample number is included. It would also be interesting to investigate glycolytic genes, such as Aldoart1, a gene encoding a

glycolytic enzyme, as another important energy source for OXPHOS is glycolysis. In our proteomics investigation, Aldoart1 (aldolase 1) expression was increased in GENA348, suggesting some change in its function. We also reported a decrease in hexokinase 3 (Hk3) in GENA348; Hk3 is involved in the first step of the glucose metabolism pathway, phosphorylating glucose to produce glucose-6-phosphate (Wyatt et al., 2010). Again, a change in its expression may suggest an impact on its catalytic role in glucose metabolism.

These data may indicate that GENA348 mice have more efficient mitochondria, although after this rapid burst of activity, the mitochondria are unable to sustain this capacity. However, measuring oxygen consumption alone is argued to be an insufficient marker of energy metabolism, particularly in the mitochondria, due to the variability in oxidation and phosphorylation rates (Salin et al., 2015). The amount of ATP generated per molecule of oxygen consumed by mitochondria is known as the P/O ratio. The P/O ratio can vary in response to environmental causes, such as temperature and food intake (Salin et al., 2015). Thus, this variability may impact animal performance, including growth rate, suggesting that energy function requires to be studied alongside mitochondrial function to study energy metabolism. Thus, measuring both levels of energetic processes, ATP generation and oxygen consumption, may give a better insight into energy metabolism.

In the diabetic state, excess fatty acids are present inside the cell leading to excessive mitochondrial FAO. Increased oxidative stress is another common theme in models of diabetic cardiomyopathy. Studies have shown that oxidative stress correlates with excess lipid delivery and elevated mitochondrial FAO rates, suggesting that mitochondria are a crucial source of free radicals in the diabetic heart (Van De Weijer et al., 2011). It is also a possibility that dysfunctional ROS scavenging mechanisms cause increased oxidative stress in the diabetic heart. Therefore, future work could focus upon measuring levels of ROS to investigate whether increased ROS is a feature of the GENA348 myocardium. In our proteomics analysis, we noted a significant downregulation of several proteins involved in the balance of oxidative stress conditions in the mitochondria (Table 2.9). Catalase is an antioxidant enzyme that mitigates oxidative stress through catabolising hydrogen peroxide (Cong et al., 2015).

Interestingly, Cong et al. (2015) reported that overexpression of catalase in diabetic mice heart led to a reduction of ROS and prevented cardiac structural abnormalities. The authors hypothesise that catalase protects mouse hearts against diabetic cardiomyopathy, through the suppression of inflammatory responses (Cong et al., 2015).

For future work, ATP production could be measured. Luptak et al. (2018) investigated the link between ATP production and heart disease in mice on a high fat, high sucrose (HFHS) diet. To determine the relationship between myocardial energetics and function, myocardial ATP and ADP concentrations were measured, with energy deficit quantified by calculating free energy of ATP hydrolysis (Luptak et al., 2018). Luptak et al. (2018) showed that impaired energy production may contribute to diastolic dysfunction in patients with metabolic heart disease. Interestingly, ATP concentration was reported not to have changed in HFHS hearts, although ADP concentration did increase. This may suggest that ADP concentration contributes to diastolic dysfunction in heart failure. For our study, it may be worthwhile to measure ATP/ADP concentrations, to assess a cause for the oxygen profile change and mitochondrial dysfunction in the GENA348 myocardium.

2.4.2 Insulin sensitivity in GENA348 mice

Quantitative mass spectrometry of isolated mitochondria revealed that the proteins that form the GENA348 mitochondrial proteome were modified. IPA analysis identified and quantified a total of 179 proteins that were either up- or down-regulated in the GENA348 mitochondria compared to WT. As mentioned previously, there was a significant decrease in proteins that are involved in T2DM signalling pathways (Table 2.9).

A significant increase was recorded in the blood glucose level of GENA348 mice compared to controls, with no change in insulin resistance. While it is commonly thought that MODY2 patients do not develop insulin resistance, a recent study has reported that 31% of MODY2 patients show signs of insulin resistance (Liu et al. (2018). Specifically, IR was linked to five novel MODY mutations to the *Gck* gene; however, no differences in MODY2 phenotypes were observed. Although relevant, reported mutations differ from that studied in this report. This

study may indicate that different *Gck* mutations can elicit varied phenotypes through altered *Gck* activity (Liu et al. (2018). In a small follow-up study of 33 MODY2 patients, 13 *Gck* mutations were confirmed with direct sequencing, with the aim to investigate the natural history of MODY2 and factors associated with hyperglycaemia (Martin et al., 2008). This 11-year follow-up study showed that in some cases, glucose tolerance remains stable due to the relative stability of the GCK-related B-cell defect. However, tolerance can deteriorate over several years with the development of insulin resistance (Martin et al., 2008).

2.4.3 GENA348 associated with an imbalance in mitochondrial dynamics

We determined that fusion proteins were upregulated at both the protein and transcript level, with no change in Drp1 (Figure. 2.10 and 2.13). Studies by Martin et al. (2014) showed that the gene expression of Mfn2 is driven by PGC-1α, involved in mediation of increased gene expression of oxidative phosphorylation and is associated with mediation of alternations in structure and function of mitochondria (Cartoni et al., 2005). We further determined that levels of PGC-1α are increased in the GENA348 myocardium. At the protein level PINK1/Parkin regulates levels of Mfn1 and Mfn2 ubiquitination, which in turn marks them for mitophagy. It should be noted that our proteomics data did not correlate with the Western or RT-qpcr investigation regarding a change in Mfn1/2 and Opa1. It is possible that differences in sensitivity between these methods could account for the difference. In top-down proteomics, as in this study, only the most abundant proteins are usually detected (Heck and Van Den Heuvel, 2004). Detection of a protein can also depend on its concentration. For future experiments, strategies to improve sample production and length of the proteomics analysis may be important factors to consider.

Human studies have reported a decrease of Mfn2 in skeletal muscle associated with T2DM and obesity (Bach et al., 2005). Variations of insulin concentration did not impact Mfn2 mRNA levels in healthy, obese or diabetic patients, suggesting Mfn2 reduction is independent of insulin (Bach et al., 2005). In contrast, Pawlikowska et al. (2007) reported an increase in Mfn2

protein expression with prolonged insulin exposure, promoting the formation of tubular mitochondrial networks.

In our study, mice are not insulin resistant, possibly explaining some difference in results to other diabetes mouse models. Furthermore, a link between insulin and the regulation of mitochondrial dynamics, particularly mitochondrial fusion has been reported (Parra et al., 2014). Studies specifically addressing the relationship between fission and fusion of cardiac mitochondrial and insulin sensitivity and diabetes are limited.

Opa1 is upregulated in GENA348 mice and mediates fusion of the mitochondrial inner membrane. Increased expression of Opa1 is therefore consistent with the over-expression of Mfn1/2 and the formation of a new mitochondrion. Miro1 is an important protein that, when inhibited, disturbs pancreatic β-cell function and interferes with insulin releases (Chen et al., 2017). Both Western blot data and qPCR show a decrease in Miro1 expression. Miro1 knockdown in H9c2 cells have been shown to cause defects in mitochondrial morphology, including mitochondrial fragmentation (Saotome et al., 2008). In H9c2 cells, Miro1 co-localised with the mitochondria, inducing mitochondrial thread formation (Saotome et al., 2008). Furthermore, down-regulation of Miro1 may impede the movement of mitochondria through the cardiomyocyte, contributing to disorganisation of the mitochondria within cardiomyocytes, further impairing function. Furthermore, in Miro2 transgenic mice, improved cardiac function and enhanced mitochondrial function was reported after induced cardiac dysfunction (Cao et al., 2019).

More specifically, during cardiac hypertrophy, Miro2 was degraded through Parkin-mediated ubiquitination, with disrupted inter-mitochondrial communication. This was restored by overexpression of Miro2. Miro2 and Miro1 share 60% sequence homology, which may suggest some similarity in function (Reis et al., 2009). Our proteomics data suggest that this mouse model contributes to the inhibition of Miro1 through the *Gck* pathway disruption. Therefore, given that there is no change to proteins regulating fission these data would indicate that in the GENA348 cardiomyocytes there is a shift towards fusion leading to larger mitochondria, potentially impaired mitophagy due to a reduction in PINK1/Parkin and that due to impaired

levels of Miro1 mitochondrial motility is compromised. The accumulation of dysfunctional mitochondria may therefore be a consequence of the molecular remodelling, with this concept supported by the functional data. Our data also showed no changes in levels of TRAK1, TRAK2, KIF5A or KIF5B (Figure. 2.16), in agreement with the proteomics.

The biogenesis of mitochondria was also influenced by PINK1 through regulation of Mfn2 and Drp1 phosphorylation (Peng et al., 2019). The regulation of mitochondrial biogenesis marker transcripts was investigated in the GENA348 myocardium (Figure. 2.15). Our data indicates that in the GENA348 heart mitochondria, an increase in fusion-processing proteins is supported by an increase in markers of biogenesis and citrate synthase activity. However, functional data suggests that there is a population of dysfunctional mitochondria resultant of impaired mitophagy. This change in cellular dynamics and equilibrium could be an explanation for the disease pathway.

2.4.4 No change in Miro2 protein expression in si-Miro1 H9c2 cells

Miro1 is primarily localised at the mitochondrial outer membrane, forming a protein complex with TRAK1 and TRAK2 to support motor movement of mitochondria along the microtubule cytoskeleton. In order to study the impact of Miro1 depletion, we used the siRNA silencing method in H9c2 cells. Western blotting and qPCR analysis confirmed the successful knock down of Miro1 in cells (Figure 2.18Figure 2.19) and confirmed that Miro2 expression was unaltered (Figure 2.19). This was important since similar to Miro1, Miro2 enables intracellular mitochondrial transport through the use of microtubule networks (Tang, 2016). In cardiomyocytes, adenovirus was used to facilitates Miro2 expression through overexpression, which accelerates mitochondrial communication, enhances mitochondrial channelling and enhances mitochondrial osculating of adjacent mitochondrial sets (Tang, 2016). Although our data indicate that there has been no compensatory change to the expression of Miro2 after si-Miro1 knockdown for future investigations, it would be interesting to characterise mitochondrial dynamics in double knockout conditions.

2.4.5 H9c2 cell viability in si-Miro1

To assess H9c2 cell viability after silencing, we utilised the MTT assay. si-Miro1 and si-NTC cells were viable; there was no difference in the cell viability ratio between the negative control and si-Miro1 (Figure 2.18). This provided confidence in the overall viability of cells for use in this chapter. Following this, we tested cell viability in si-Miro1 and si-NTC supplemented with H_2O_2. As expected, cells were unviable with the addition of H_2O_2; both si-Miro1 and si-NTC results a significantly lower cell viability ratio compared to the negative control. It has been reported that in H9c2 cardiac muscle cells, oxidative stress causes an imbalance in the rate of oxidant production and degradation (Mojarrab et al., 2013). The promotion of cell death is caused by the increased formation of ROS and has been identified in the pathophysiology of cardiovascular disease (Schnabel and Blankenberg, 2007). Thus, the cell viability results in this chapter is as expected. Overall, these results show that Miro1 depletion alone does not make the cells unviable and that they behave as control cells under stress conditions.

2.4.6 Change in protein expression regulating mitochondrial dynamics

While there was no change to expression levels of Mfn1, Mfn2 or Drp1 in after knockdown of Miro1, there was an increase in Opa1 gene expression levels in si-Miro1 cells (Figure 2.18). In addition to playing a key role in fusion of the inner membrane Opa1 has been shown to have a protective role through stabilising the cristae morphology (Frezza et al., 2006). Therefore, the increase in Opa1 may indicate that the mitochondria are under stress with upregulation of Opa1 stabilising the inner membrane. However, there are two forms of Opa1, a higher molecular weight long form (Opa1-L) and a lower molecular weight short form (Opa1-S). In fact, mitochondrial fragmentation, after Opa1 ablation, could be rescued by Opa1-L, but not with Opa1-S (Cogliati et al., 2013). Cristae stabilisation as a result of Opa1-L cleavage to Opa1-S has resulted in therapeutic solutions to block the formation of Opa1-S. Having said that, a complementary balance between the two Opa1 isoforms is crucial for the maintenance of mitochondrial bioenergetics (Song et al., 2007). Therefore, to develop our work, if time had allowed, a Western blot could complement the RT-qPCR analysis to measure a change of Opa-L and Opa-S ratio in Miro1 knockdown cells.

However, in support of the concept that depletion of Miro1 may impact upon mitochondrial dynamics levels of PINK1 were increased compared to controls. PINK1 and Parkin are known to work synchronously to govern mitochondrial quality control, through a signalling pathway that marks damaged mitochondria to trigger selective mitophagy (Pickrell and Youle, 2015). No change was measured in Parkin expression levels. Miro1 is involved in this mitophagy pathway; upon mitochondrial damage, Miro1 is rapidly ubiquitinated and depleted to block the microtubule-dependent transport of damaged mitochondria (Birsa et al., 2014); this arrest of mitochondria ensures that quality control is maintained in the cell. The increased PINK1 expression in si-Miro1 cells could suggest that the loss of Miro1 disrupts the PINK1-Parkin pathway and mitochondria are less able to regulate the transportation pathway. Since PINK1 recruits Parkin and there were no changes to Parkin it seems unlikely that there would be increased ubiquitination. PINK1 recruits Parkin, leading to the ubiquitination of Mfn1/2, targeting them for degradation. Although there is more PINK1, this isn't correlated with an increase in Parkin, suggesting no change in ubiquitination of Mfn1/2. This is consistent with our data showing no change to Mfn1/2. In future work, the need for further phosphorylation between PINK1 and Parkin can be investigated; there may be another molecule interaction that is a point of regulation.

2.4.7 Altered expression of mitochondrial biogenesis markers in si-Miro1 cells

Mitochondrial biogenesis is positively controlled through direct activation of PGC-1α, through mTOR, a serine/threonine kinase. In addition to activation of biogenesis and mitophagy, repressors of biogenesis are important for controlling mitochondrial turnover. In the GENA348 mouse myocardium, PGC-1α and TFAM expression were upregulated (Chapter2, Figure 2.14). In this chapter, knockdown of Miro1 in H9c2 cells led to a decrease in PGC-1α whilst TFAM expression was significantly increased (Figure 2.23). PGC-1α plays an important role in the positive regulation of mitochondrial biogenesis (Kiriyama and Nochi, 2018). The downregulation of PGC-1α has been implicated in mitochondrial dysfunction and oxidative stress, possibly suggesting metabolic abnormality in diabetes (Choi et al., 2014).

There is a clear difference between the results of PGC-1α and TFAM, requiring discussion. TFAM mediates the transcription, replication, and packaging of mtDNA. Therefore, an increase in TFAM expression may also indicate that the mitochondria in the knockdown cells are under stress or damaged so that the cell is trying to generate the building blocks to make new mitochondria. It is surprising that PGC-1α is down-regulated, given that it is highly inducible by stress conditions. This may suggest a difference in pathway between the two biogenesis markers. Dysregulation of mitochondrial biogenesis results in impaired ATP production and increased ROS generation (Cheng and Ristow, 2013), impacting cardiovascular health. A signalling mechanism using adenosine monophosphate (AMP)–activated protein kinase (AMPK), control processes involved in energy homeostasis (Marin et al., 2017). AMPK phosphorylates PGC-1α, leading to the increased expression of TFAM. Thus, it may be useful to measure levels of AMPK or ROS to assess possible changes to the activation pathways as a result of Miro1 depletion. It is not clear why citrate synthase activity was unchanged, suggesting no change in mitochondrial content; although in agreement the rate of oxygen consumption was unaltered after Miro1 knockdown. Given that PGC1-α is a regulator of mitochondrial respiration through mediating mitochondria density and altering the respiratory capacity of individual mitochondria (Austin and St-Pierre, 2012), these results from qPCR require further investigation.

2.4.8 Miro1 and mitochondrial trafficking apparatus (KIF/TRAK)

As detailed in the introduction (section 1.3, Figure 1.7; Figure 1.8), Miro1 forms a complex with mitochondrial trafficking proteins. Miro proteins regulate mitochondrial trafficking by acting as essential receptors for mitochondrial recruitment of the TRAK adaptors, driving kinesin and dynein-mediated movement (Sheng, 2014). Miro1 forms a protein complex with TRAK1 and TRAK2, including the motor proteins kinesin and dynein. As mentioned in the introduction (section 1.3.2), this complex aids in mitochondrial movement along the microtubule cytoskeleton, functioning as a multi-subunit complex for the transportation of intracellular organelles. It is hypothesised that without Miro1, TRAK may not be able to localise to the mitochondria to regulate mitochondrial trafficking (López-Doménech et al., 2018). Our data show that depletion of Miro1 does not impact upon the transcript levels of KIF5A, KIF5B,

TRAK1 or TRAK2 (Figure 2.24); this data is in agreement with the analysis of our mouse GENA348 model (Chapter 2, section 2.3.9; Figure 2.17). Similarly, in Miro1/2 double and single mouse knockouts, (López-Doménech et al., 2018) showed TRAK1 and TRAK2 still localise to the OMM, driving mitochondrial motility. In the absence of Miro, TRAK motor proteins formed functional anterograde mitochondrial transport complexes, suggesting that Miro may not be the exclusive acceptor sites on the OMM for TRAK proteins (López-Doménech et al., 2018), as previously reported (Mishra and Chan, 2014). However, it is clear that loss of Miro1 will limit the ability of mitochondria to be transported through the cardiomyocyte (López-Doménech et al., 2018). Mitochondria in Miro1 knockdown cells were unable to migrate to distal regions, instead, accumulated around the nucleus (López-Doménech et al., 2018). Furthermore, TRAK2 mediated retrograde transport is primarily controlled by Miro1 (López-Doménech et al., 2018). Collectively, this shows that Miro1 depletion disrupts mitochondrial transport and may result in eventual cardiac contractile dysfunction.

We determined that knockdown of Miro1 was not compensated for by Miro2 (Figure 2.19). However, there was also no change to the expression of KIF5A/B or TRAK1/2 (Figure 2.24). In cardiomyocytes, it is not clear if the loss of Miro1 leads to mitochondrial arrest. In mouse embryonic fibroblasts, TRAK1/2 can recruit more KIF to the mitochondria, even in the absence of Miro proteins (López-Doménech et al., 2018). .

López-Doménech et al. (2018) suggested that Miro proteins were not critical in regulating respiration rate or the overall energetic metabolic state of the cell. Similarly, in our study, we show no significant changes in citrate synthase activity (Figure 2.25) and no change in oxygen consumption rate in si-Miro1 cells (Figure 2.26A/B), compared to NTC controls. According to Alhindi et al. (2019), citrate synthase is measured as a substantial enzyme of mitochondria. As mentioned above, this suggests that Miro1 is not a necessary protein in the regulation of the mitochondrial metabolic pathways, as a lack of impact was observed in si-Miro1 cells.

2.4.9 Decrease in mitochondrial volume and surface area in si-Miro1

It was previously reported that Miro1 knock down cells showed impacted mitochondrial mobility, leading to their accumulation near the nucleus (López-Doménech et al., 2018). This could indicate a role for Miro1 in regulating mitochondrial distribution within the network. Here, for the first time, we have employed 3D electron microscopy to investigate changes in mitochondrial morphology in si-Miro1 cells compared to control H9c2 cells (Figure 2.27). 3D segmented data was utilised to measure mitochondrial volume and surface area. We determined that there was a decrease in both mitochondrial volume and surface area in si-Miro1 mitochondria. Changes in mitochondrial size may not be indicative of changes to its internal structure. Since Opa1 is upregulated, this may indicate an adaptation to preserve cristae morphology. However, it is important to note that due to time constraints, the sample size for this analysis was n=100 mitochondria but only n=1 cell passage. Therefore, before any firm conclusions can be drawn, further analysis needs to be undertaken. Additionally, examination of the EM images found little evidence of sarcomere structures, although previous group members have shown a developed cytoskeleton. Therefore, another key consideration in developing this aspect of the research would be to consider the passage number. The extensive passage of H9c2 can cause differentiate into myotubes and changes in their phenotype (Witek et al., 2016).

Mitochondria are dynamic organelles that undergo frequent morphological changes, fission and fusion (Chan, 2012). In yeast, Frederick et al. (2004) showed that cells lacking Miro1 (Gem1p) exhibited distorted mitochondrial morphology, with a collapsed, globular and grape-like structure. This supports a potential role for Miro proteins as important for signalling events that determine mitochondrial shape and as well as activity. In addition to mitochondrial transport, Ca^{2+} also regulates mitochondrial shape. It has been reported that Miro1-Ca^{2+} binding determined mitochondrial shape, forming long networks that are able to rapidly produce energy, and short, round mitochondria, associated with disease states (Nemani et al., 2018). In addition, the authors generated MEFs with point mutations in each EF-hand in Miro1 and Miro2, to disrupt Ca^{2+} binding and investigate mitochondrial shape transition with disabled

EF-Ca^{2+} binding. The Miro1 EF-hand 1 mutant did not undergo mitochondrial shape transition, and the process did not require Miro1's GTPase activity. Whereas, the dysfunction of Miro2 EF-hands did not appear to have any impact on shape (Nemani et al., 2018), suggesting a non-redundant role of Miro1 in calcium sensing and mitochondrial morphology phenotypes.

Furthermore, overexpression of Miro1 and Miro2 in H9c2 cells was shown to increase mitochondrial length (Saotome et al., 2008), thought to be a result of Miro's Ca^{2+} binding capacity, heightened by the structurally atypical EF arms of Miro. In dominant-negative Miro constructs, Saotome et al. (2008) showed that Miro knockdown (Miro1/2) caused mitochondrial fragmentation and condensation, suggesting that the length of mitochondria correlates with the availability of Miro. Furthermore, in resting neurons, Miro was also implicated in increased mitochodrial connectivity, with the mean length of mitochondria in Miro1 or Miro2 overexpressed neurones 20% higher than control groups (Saotome et al., 2008), with Miro1EF and Miro2EF overexpression exaggerating this difference. Collevtively, this shows that Miro1 supports the formation of elongated mitochondria, regulated by EF-Ca^{2+} binding and the activity of fusion-fission proteins.

2.5 Conclusion

The main aim of this chapter was to characterise the cardiac and mitochondrial phenotype of the MODY2 mouse model (GENA348). MODY2 patients are thought to be asymptomatic and require little treatment; however, we have now shown that the GENA348 mice develop cardiac complications at the age of 6 months equivalent to 30 years in humans (Dutta and Sengupta, 2016). Therefore, the data here indicates that as well as the need for introducing improved screening for MODY2, monitoring of cardiac function may be important since the mouse model incorporating the *Gck* mutation develops diastolic dysfunction. Thus, these patients are at a greater risk of developing cardiac complications. We further showed that there is down-regulation of Miro1 in the GENA348 myocardium. Subsequently, *in-vitro* experiments showed that Miro1 knockdown leads to an increase in Opa1 expression, to possibly compensate and stabilise the mitochondria but no change to the other fission-fusion protein levels.

Most studies showing a correlation between mitochondrial dysfunction and heart failure have employed models of either T1DM or obesity induced T2DM. Here we show that cardiac mitochondrial dysfunction is a characteristic of the GENA348 mouse mitochondrial dysfunction can be described as the failure of mitochondria to function within 'normal' parameters as compared to those of WT. More specifically, we have determined an imbalance between fission and fusion potentially resulting in larger mitochondria, impaired mitophagy and compromised motility. Interestingly, smaller fragmented mitochondria are generally associated with pathological phenotypes (Ong et al., 2010) , but here it also appears that increased fusion also is associated with dysfunctional mitochondria. Impaired OXPHOS in GENA348 mice suggest defects in cardiomyocyte contractility and metabolism, with physiological assessments indicating the development of cardiac hypertrophy. Given the putative shift towards fusion we next investigated mitochondrial morphology using serial block face scanning electron microscopy (SBF-SEM).

There is evidence that Miro1 expression has a role maintaining the balance between mitochondrial fission and fusion. Knockdown of Miro1 had no effect upon the expression of proteins mediating mitochondrial motility; however, further work is required to investigate if the microtubule network and movement of mitochondria has changed since other factors such as protein post-translational modifications and cellular localisation maybe affected. Additionally, more information may be forthcoming by knocking out Miro1 completely e.g. using CRISPR/Cas9. Overall, the data showed a significant increase in Opa1 and PINK1 expression in si-Miro1 lines. These proteins are both important in regulating mitochondrial quality control through mitophagy and fission/fusion pathways. While the data suggests that Miro1 has an impact in mitochondrial homeostasis, further work is required to fully understand its relationship with Miro2 and with other regulating proteins.

Chapter 3 Characterisation of cardiac mitochondrial subpopulation morphology in the GENA348 myocardium using serial block face scanning electron microscopy

3.1 Introduction

In Chapter 2, the cardiac and mitochondrial phenotype of MODY2 (GENA348) was characterised, through measurements of cardiac function and physiological parameters, which indicated the development of early LV dysfunction. At the molecular level proteins mediating mitochondrial dynamics and biogenesis were perturbed along which changes in OXPHOS, Thus, this chapter will further investigate whether the changes to mitochondrial function translate to ultrastructural changes to the mitochondrial structure.

3.1.1 Mitochondrial morphology and organisation in the heart

The mitochondrial cardiac cytoarchitecture has been well documented using electron microscopy. Since pioneering mitochondrial isolation methods developed by Hoppel et al. (1982), the differences in mitochondrial populations have been revealed. As described in the main introduction (section 1.2.2), there are three distinct mitochondrial populations have been described (Figure. 1.3); the subsarcolemmal (SSM), located directly beneath the sarcolemma; the interfibrillar (IFM), located between the myofibrils; and the perinuclear mitochondria (PNM), located adjacent to the nucleus (Hoppel et al., 1982; Palmer et al., 1977). It is proposed that the mitochondrial subtypes have differing functions. The IFM function as the main producer of ATP, in active contact with the myofibrils and sarcoplasmic reticulum (SR) (Kuznetsov et al., 2009). It is thought that the SSM are involved in ion homeostasis or signalling pathways (Riva et al., 2005) Lastly, due to a close proximity to the nucleus, the PNM is thought to participate in nuclear transcription and translocation (Palmer et al., 1986), although exacts role have yet to be described. This suggests that the location of the mitochondrial population strongly determines its role in supplying ATP for the cardiomyocyte, and thus the impact on structural damage would vary. This tight arrangement allows adult cardiomyocytes to finely regulate contraction.

The concept of separate mitochondrial populations has recently been challenged with 3-D electron microscopy methods revealing that mitochondria form a continuous network throughout the cardiomyocyte; although this does not necessarily negate the idea that different spatially organised mitochondria play differing roles within the cell (Hendgen-Cotta et al., 2018). Interestingly, these structural and localised differences dictate differences between the function of the mitochondrial subpopulations (Kuznetsov et al., 2009).

In monkey myocardial cells, PNM were found to be predominantly spherical in shape with lengths ranging from 0.8 to 1.4 μm (Shimada et al., 1984), containing well-developed cristae and little matrix area. Additionally, in the cat myocardium, the IFM have been identified as elongated in shape, occupying space between the Z-lines (Fawcett and Mcnutt, 1969). In their study, Fawcett and Mcnutt (1969) showed one mitochondrion per sarcomere, at a length of 1.5-2.0 μm, featuring similar curved cristae as the IFM type. Lastly, SSM have a more variable length (0.4–3.0 μm) with tightly-packed cristae (Shimada et al., 1984). It is thought that this network allows the mitochondria to dynamically communicate across the cell, synchronising behaviour and crosstalk between SSM and IFM populations (Zhou and O'rourke, 2012).

3.1.2 Mitochondrial dysmorphology is a feature of heart failure

Mechanical dysfunction of the myocardium in heart failure (HF) results in the inability to sufficiently supply oxygenated blood to the body. In HF, there are multiple studies showing that the mitochondrial network is compromised. Due to the integral role of mitochondria for supplying the hearts' continuous energy demands, preserving mitochondrial function is integral to protecting cardiac function, as reviewed in (Daghistani et al., 2019). For example, (Rosca and Hoppel, 2010) reported that the inner membrane appeared disordered and ATP production impaired. Additionally, mmall fragmented mitochondria have been shown to be a hallmark feature of HF and the diabetic myocardium (Chen et al., 2011).

Additionally, there is evidence to indicate that the mitochondrial subtypes are differentially affected in T2DM. For example, Ritov et al. (2005) firstly demonstrated mitochondrial dysfunction in the skeletal muscle of diabetic volunteers compared to healthy controls. In

particular, the SSM electron transport chain activity was significantly lower than the IFM fractions. Furthermore, there was a depletion in the number of SSM, further corroborating the importance of SSM in signal transduction and substrate transport. Studies of a *db/db* heart mouse model revealed mitochondrial damage, including changes in size, decreased respiration rates, changes in electron transport chain activity, impaired ATP synthase function and changes in membrane potential in the SSM subpopulation (Dabkowski et al., 2009). Interestingly, T1DM and T2DM diabetes influence mitochondrial subpopulations differently, with the IFM more impacted in T1DM (Dabkowski et al., 2009). In another study of the diabetic heart, (Dabkowski et al., 2010) mitochondrial dysfunction was identified as a feature linked to the spatially distinct subsets of mitochondria. The authors measured oxidative damage, mitochondrial morphology and proteomic composition in *db/db* mouse hearts (Dabkowski et al., 2009). Results showed that SSM from diabetic hearts displayed greater dysfunctional profiles compared to IFM, due to altered structure, function and proteomic composition. Furthermore, the SSM appeared to display decreased ETC Complex I, III, IV activity, accompanied by a decrease in ATP synthase activity (Dabkowski et al., 2009). Overall, these results suggest that SSM are more sensitive to glucose homeostasis and are impacted more in T2DM.

However, an important factor to consider is that in the structural studies mentioned above, transmission electron microscopy of thin sections, of 200-300 nm thick, were imaged. This inevitably results in a small fraction of mitochondrion captured for imaging, since mitochondria feature a 1µm thick diameter. Thus, the mitochondrial structure and dimensions will be influenced by this orientation.

3.1.3 Mitochondrial ultrastructural Analysis using electron microscopy

First used approximately 75 years ago, transmission electron microscopy (TEM) provided novel insights into mitochondrial morphology and function (Claude and Fullam, 1945). In TEM, a high energy bean of electrons is focussed through the specimen, and the interaction between electron and atom forms a two-dimensional image, enabling the observation of mitochondrial

features such as shape and size as well as cristae organisation and protein organisation within the mitochondria.

Although TEM has provided valuable visual information for advancing the understanding of mitochondria structure, it has been realised that it is important to understand the three-dimensional (3D) properties of mitochondria and other biological features. Consequently, a number of 3D EM techniques have been developed to study the 3-D ultrastructure of biological specimens. Here we employed serial block face (SBF-SEM) to investigate the 3D structure of the mitochondria in the wild-type and GENA348 myocardium.

SBF-SEM is a relatively novel technique developed by Denk and Horstmann (2004). Denk and Horstmann (2004) required a method to reconstruct 3D tissue at a resolution for studies of neuronal networks. Modifying a scanning electron microscope, they built in a custom-designed microtome. In brief, the sample is chemically fixed and mounted on a pin within the microscope, the top surface of the block is scanned/imaged and then the microtome removes a thin slice (e.g. 50 nm thick), the slice is discarded, and the newly exposed block face is scanned. This is an iterative procedure leading to the collection of serial images that are in register (i.e. there is no need to align the images) – for a summary figure see Figure 3.1. Our group have used this method to reconstruct the t-tubular network of ovine cardiac tissue (Pinali and Kitmitto, 2014) as well as the intercalated disc (Pinali et al., 2015). In addition, SBF-SEM has been used to segment myofibrils, mitochondria and nuclei within single adult cardiac cells (Hussain et al., 2018). Here, the authors used automatic segmentation, providing information about mitochondrial clustering and volumes (Hussain et al., 2018).

However, while TEM generates 2D images with attainable resolutions at < 1 nm that are much higher than SBF-SEM, SBF-SEM is able to generate 3-D data. For an overview of different EM modalities and application to mitochondrial ultrastructure see the recent review by (Daghistani et al., 2019).

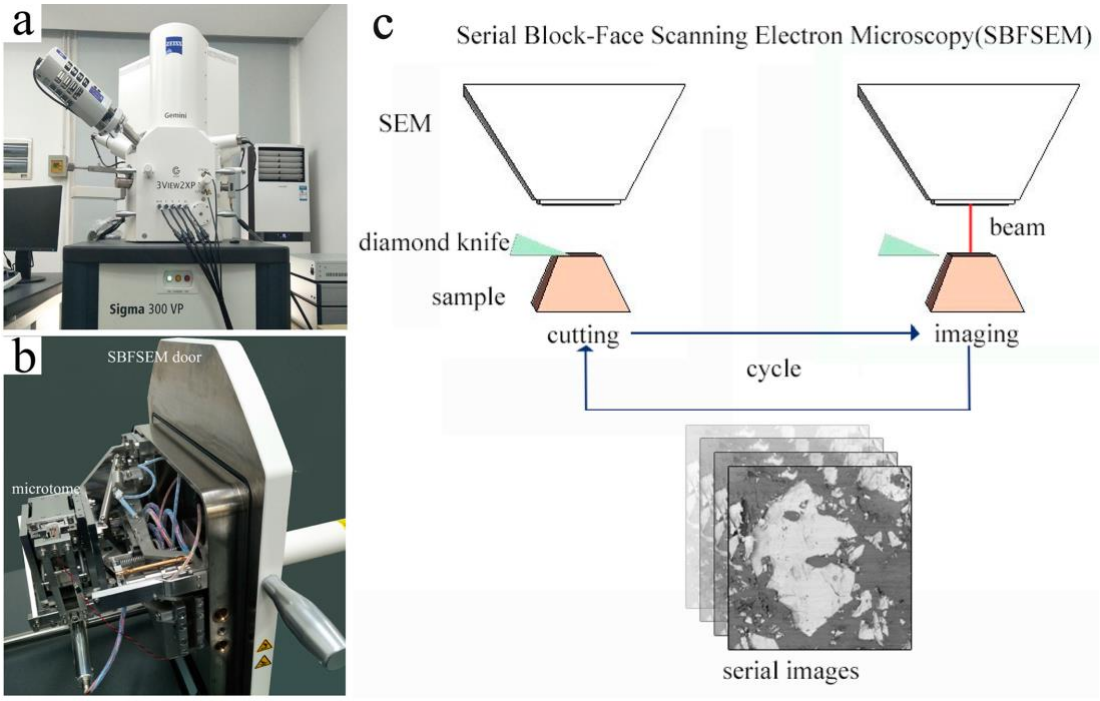

Figure 3.1 Illustration of an SBF-SEM (Yang et al., 2018).

(a) and (b) illustrate a commercially available SBF-SEM. (c) Illustrates the principle of the technique for the collection of serial images through a sample that are in register.

3.1.4 Aim of study

To investigate putative remodelling of the GENA348 cardiac mitochondria compared to WT, we will use SBF-SEM to collect serial images and process the data. The study aims are:

1) Manually segment mitochondrial populations (SSM, IFM, PNM) using IMOD to determine the volume and surface area of individual mitochondria.

2) Determine differences between morphological parameters of SSM, IFM and PNM in WT cells.

3) Investigate mitochondrial volume and surface area changes of each mitochondrial population in GENA348 compared to controls.

4) Investigate changes to cardiac mitochondrial density and distribution in GENA348 mice compared to WT.

3.2 Methods

3.2.1 Specimen preparation for 3-view electron microscopy

At the conclusion of the 24 weeks, three GENA348 mice and three control mice were given a lethal injection of isoflurane and then decapitated. After immediate removal of the heart, 1 − 2 mm^3 of LV was immersed in 4% formaldehyde, 2.5% glutaraldehyde and 0.1 M HEPES and incubated for 24 hours at 4°C. The specimens were washed five times (3 min per wash) with diluted HEPES (20 ml HEPES + 20 ml water) prior to post-fixing at room temperature for 1 h with 4% osmium tetroxide and 3% potassium ferrocyanide in 0.2 M cacodylate and 4 mM calcium chloride buffer. This was followed by five 3-min washes with ddH_2O before 20 mins incubation in filtered thiocarbohydrazide solution at room temperature. An additional cycle of five ddH_2O washes was then followed by incubation at room temperature in 2% osmium tetroxide in ddH_2O for 30 min. The buffer was then removed, and the specimens were washed five times prior to incubation in 1% w/v uranyl acetate at 4°C overnight. The next day, a lead aspartate solution was prepared by adding lead nitrate (0.066 g) to 0.03 M aspartic acid solutions (0.3 to 10 ml) and adjusting the pH to 5.5 with 1 N potassium hydroxide and was placed in an oven for 30 min at 60°C. The specimens were subjected to five further washes with ddH_2O, followed by incubation at 60°C for 30 mins in the lead aspartate solution. The samples were washed five times with ddH_2O prior to dehydration by 10 min in ice-cold 20%, 50%, 70%, 90% and 100% ethanol before final 10 min incubation at room temperature in acetone. This procedure was repeated once prior to 2 h incubation in 25% resin/acetone followed by 2 h incubation in 50% resin/acetone and 24 h incubation in 75% resin/acetone. On the next day, the specimens were placed in 100% resin for 2 hours, during which time the resin was changed three times. The specimens were then embedded in resin and incubated for 48 h at 60°C. A glass knife was then used to trim the blocks to ~1mm^3 and expose tissue on four sides prior to mounting on a metal pin and coating with a thin layer of gold for imaging.

3.2.2 Serial block face scanning SEM

SBF-SEM was used as previously described (Daghistani et al., 2019). Tissue blocks from the peri-infarct, remote, and control myocardium were prepared and three-dimensional (3D) data stacks were collected using FEI Quanta 250 FEG SEM fitted with a Gatan 3View system. FEI Quanta 250 FEG SEM equipped with a Gatan 3View ultramicrotome was used at 3.8 kV operating voltage under a 0.3-0.5 torr vacuum to image the samples. Serial images were collected at different magnifications, leading to voxel sizes ranging from 5.4 to 13.5 nm per pixel in the X-Y plane with the cutting depth along the *Z*-axis fixed at 50 nm. Images were obtained via an automated procedure in which 50 nm sections were sequentially cut *in situ* by a diamond knife and the freshly exposed face was imaged to generate an image stack with X-, Y- and Z-plane voxel sizes of 15, 15 and 50 nm/pixel, respectively.

3.2.3 Image analysis and mitochondrial segmentation

Image processing (IMOD) (Kremer et al., 1996) was applied to a sample of 1000 images (equivalent to 5 µm in the Z-direction) in order to segment the mitochondrial network. Firstly, the 3 different populations of mitochondria, SSM, IFM and PNM, were defined, as described in section 3.1.1. Then, individual mitochondria were segmented using closed contours. Approximately 90 mitochondria of each type i.e. SSM, IFM and PNM in a minimum of 3 different cardiomyocytes per dataset were sampled.

3.2.4 Mitochondrial density

A stereological approach was used to allow sampling of three portions through each dataset (images 10-950 from a stack of 1000 images) using the stereological tool function in ImageJ. The Cavalieri method of point-counting (Roberts et al., 1993) was used to estimate the volume of the serial images occupied by cardiomyocytes and the mitochondria within the cardiomyocytes. Two grids were overlaid onto the datasets for counting features as shown in Figure 3.2.

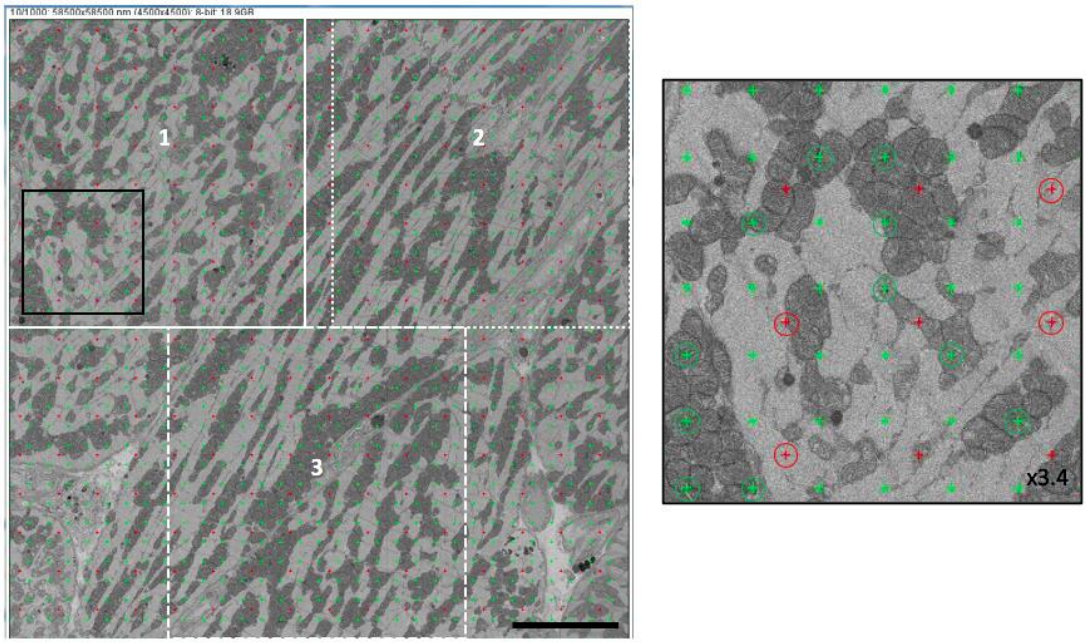

Figure 3.2 Calculation of the mitochondrial density.

The three areas in (Left image) sampled through the stack are indicated by the dashed white boxes numbered 1, 2 and 3. The green and red crosses are the two overlaid grid matrices. Image J generates area information between points on each grid: red 13.368 x 10^6 and green: 2.674 x 10^6 nm^2. Scale bar = 10 μm. The area in the black box has been magnified 3.4 times to show a clearer image of the grids. The points falling within a cardiomyocyte but not mitochondria within the red mesh are circled (these would be counted for calculating the volume occupied by cardiomyocytes within the tissue) and the points in the green matrix falling on mitochondria are circled; these would be counted as mitochondria within cardiomyocytes).

As shown in Figure 3.2, portions of the serial images were sampled in the X-Y plane firstly from the upper left-hand side (through images 10-310), upper right-hand side (330-630 images) and lower middle portion (650 – 950) as shown in Figure 3.2 (areas labelled 1, 2 and 3). To avoid sampling the same mitochondria points in both meshes were only recorded every 20 slices (Z-cut depth 50 nm). The number of points in each area that fell on a mitochondrion from the grid shown in green were counted every 20th image. Similarly, points in the red grid falling on any part of a cardiomyocyte (other than mitochondria) were counted. Points falling outside the boundaries of a cardiomyocytes e.g. extracellular matrix, fibroblasts, blood vessels were not counted.

For each portion, the number of points counted for each grid was tallied and the following equation used to calculate the percentage of the cardiomyocytes volume occupied by mitochondria:

$$\frac{\text{total no. of points (mitochondria) x green grid area x (no. of slices x 50 nm)}}{\text{total no. of points (cardiomyocyte) x red grid area x (no. of slices x 50 nm)}} \text{ x } 100$$

Therefore, for each dataset three density values were calculated, the mean ± SD was then calculated for each dataset. The overall mean for each experimental group was then calculated and an unpaired student's t-test (two-tailed) was used to determine a difference between mitochondrial density in the WT myocardium compared to the GENA348.

3.2.5 Data and statistical analysis

After defining the different subtypes of mitochondria according to their spatial location, SSM, IFM, PNM approximately 90 of each subtype, SSM, IFM and PNM (objects) were segmented using the IMOD software (Kremer et al., 1996) from each dataset (WT n=3 and GENA348 n=3 animals). A minimum of 3 cells per dataset was sampled. To avoid selection bias mitochondrial clusters were selected for each subtype Volume and surface area parameters were extracted from the segmented (3-D) mitochondria. Within each experimental group each subtype of mitochondria was tested for inter-animal variance using a one-way ANOVA; datasets exhibiting no significant difference were then combined to calculate a mean value ± SEM (n=3 per experimental group) for each mitochondrial subtype (SSM, IFM and PNM). A similar approach was taken for analysing the surface area: volume ratio (SA/Vol) for each mitochondrial subtype. Due to the inter-animal variability in the GENA348 datasets we employed a two-way ANOVA with Sidak's multiple comparisons across rows and columns to compare the mitochondrial subtype morphometric parameters. All data were analyzed using GraphPad Prism software (version 8.0; GraphPad Software Inc., La Jolla, CA).

3.3 Results

3.3.1 Three spatial populations of mitochondria were defined in WT

DCM is associated with mitochondrial dysfunction; to understand how changes to the mitochondrial ultrastructure impact diabetes, SBF-SEM was used to examine the differing populations. Firstly, examination of healthy mitochondrial morphology in control tissue from the heart apex was completed. The definition of each mitochondrial subpopulation is described in section 3.1.1. SSM are mitochondria in direct contact with the sarcolemma; PNM mitochondria are in direct contact with the nucleus while IFM are surrounded by myofibrils.

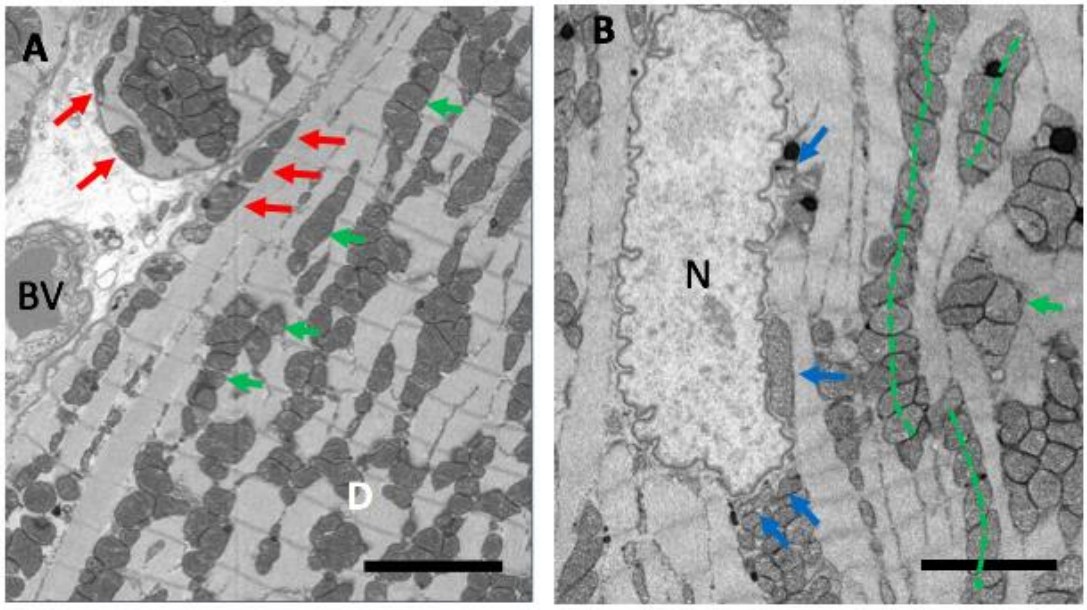

Figure 3.3 Selection and segmentation of different WT spatial populations of mitochondria with SBF-SEM.
Taken from tissue in apex of the heart (WT mouse). (A) Portion of a serial image taken from an SBF-SEM data stack; red arrows highlight SSM, green arrows indicate IFM. BV=blood vessel. (B) Area of a serial image showing a cardiomyocyte nucleus (N) with blue arrows highlighting PNM. The dashed green lines indicate how IFM form rows of mitochondria. Scale bar = 5 µm

Using a general qualitative assessment of the mitochondria in control myocardium, we identified ordered IFM organised into elongated strands amongst myofibrils (Figure 3.3, green lines). These strands of IFM generally appeared to have a thickness of 1 or 2 mitochondria. Furthermore, the PNM appeared smaller and rounder and formed clusters around the poles

of the nuclei (Figure 3.3, blue arrows). Lastly, the SSM appeared as morphologically variable in both size and shape (Figure 3.3, red arrows).

To further illustrate the differing mitochondrial populations, 3D reconstructions were produced from manual segmentation of cardiac tissue in control mice. This highlights the polar nature of the PNM clusters (Figure 3.4A) and clustering of SSM seen at the edge of the sarcolemma (Figure 3.4B). This further shows how IFM strands organise into discrete, parallel strands (Figure 3.4C).

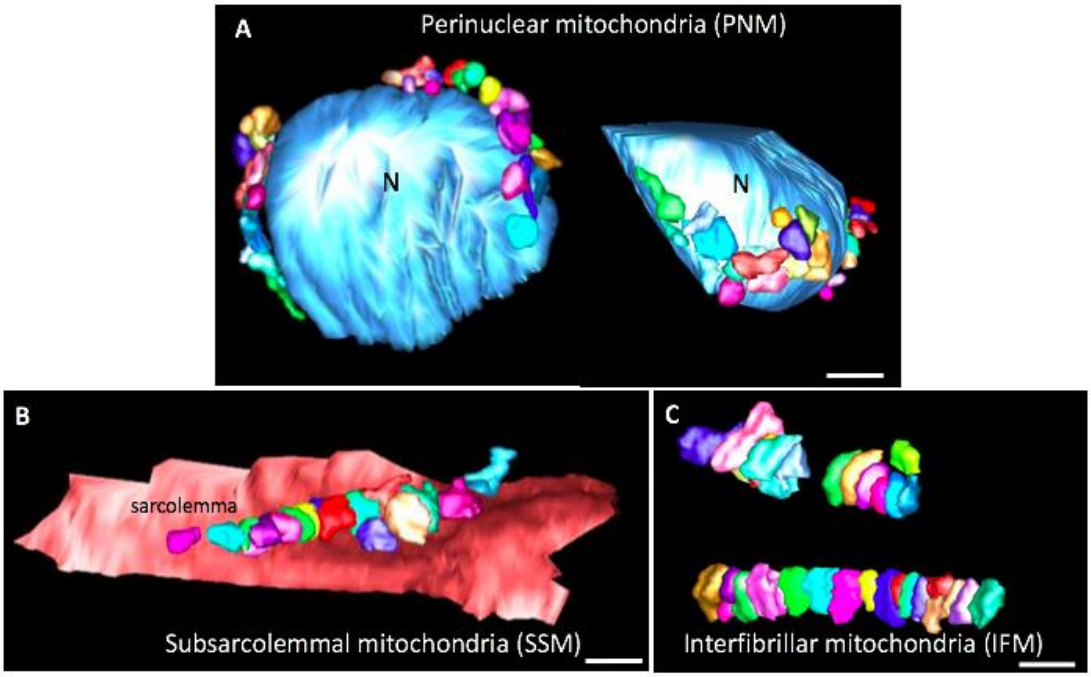

Figure 3.4 3D reconstruction selection and segmentation of different spatial populations of mitochondria.

Taken from tissue in apex of the heart (WT mouse). (A) 3-D Segmentation of part of a nucleus (light blue isosurafce) and PNMs from two-viewpoints either directly in contact with the nuclear envelope of directly juxtaposed (mitochondria are displayed in a range of colours). (B) A cluster of segmented SSM directly adjacent or touching the sarcolemma (pink isosurface) (C) Examples of segmented rows IFMs. Scale bar = 2 µm

3.3.2 WT mice have smaller cardiac PNM compared to SSM and IFM

To measure volume changes of mitochondrial special populations between control animals, a one-way ANOVA analysis was used (section 3.2.5). There were no inter-animal differences for each mitochondrial subtype (SSM, IFM, PNM) volume in each of the control animals

(*P* values, 0.6276, 0.1167, 0.1878, respectively) or surface area (SA). The raw data for each mitochondrial subset is shown in Figure 3.5.

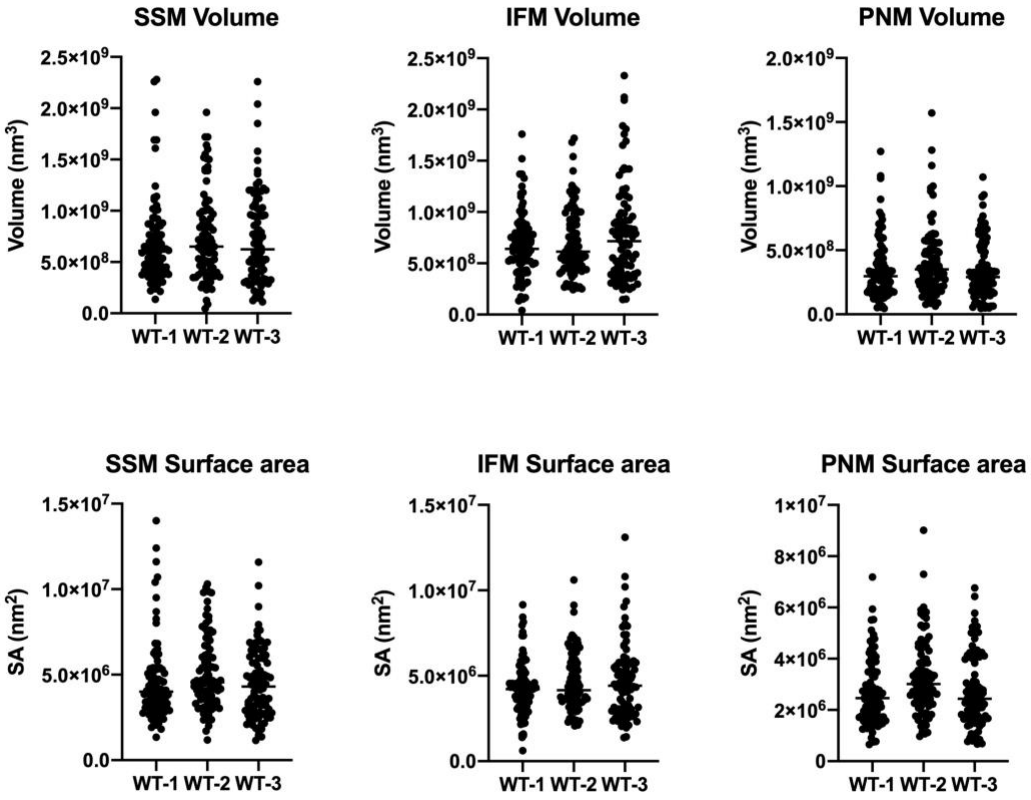

Figure 3.5 Raw data for morphological parameters of each subtype of WT mitochondria
Data from tissue taken from the apex of 6-month-old WT mice. There is no significant difference in the mitochondrial subtype volume (mm^2) and surface area between animals.

Therefore, a mean value for both the volume and surface area of SSM, IFM and PNM was calculated for WT mice as 7.23 ± 0.31 x10^8 (SSM); 7.29 ± 0.59 x10^8 (IFM) and 3.70 ± 0.34 x10^8 (PNM) nm^3. As shown in Figure 3.7A and Figure 3.7B, a comparison of the volume and SA between the three mitochondrial subtypes revealed that there is no difference in either parameter between SSM and IFM, whereas the PNM are smaller than both SSM and IFM. A similar profile was observed for the surface area of each subtype (Figure 3.7); 4.72 ± 0.31 x10^7 (SSM); 4.54 ± 0.23 x10^7 (IFM); 2.92 ± 0.31 x10^7 (PNM) nm^2.

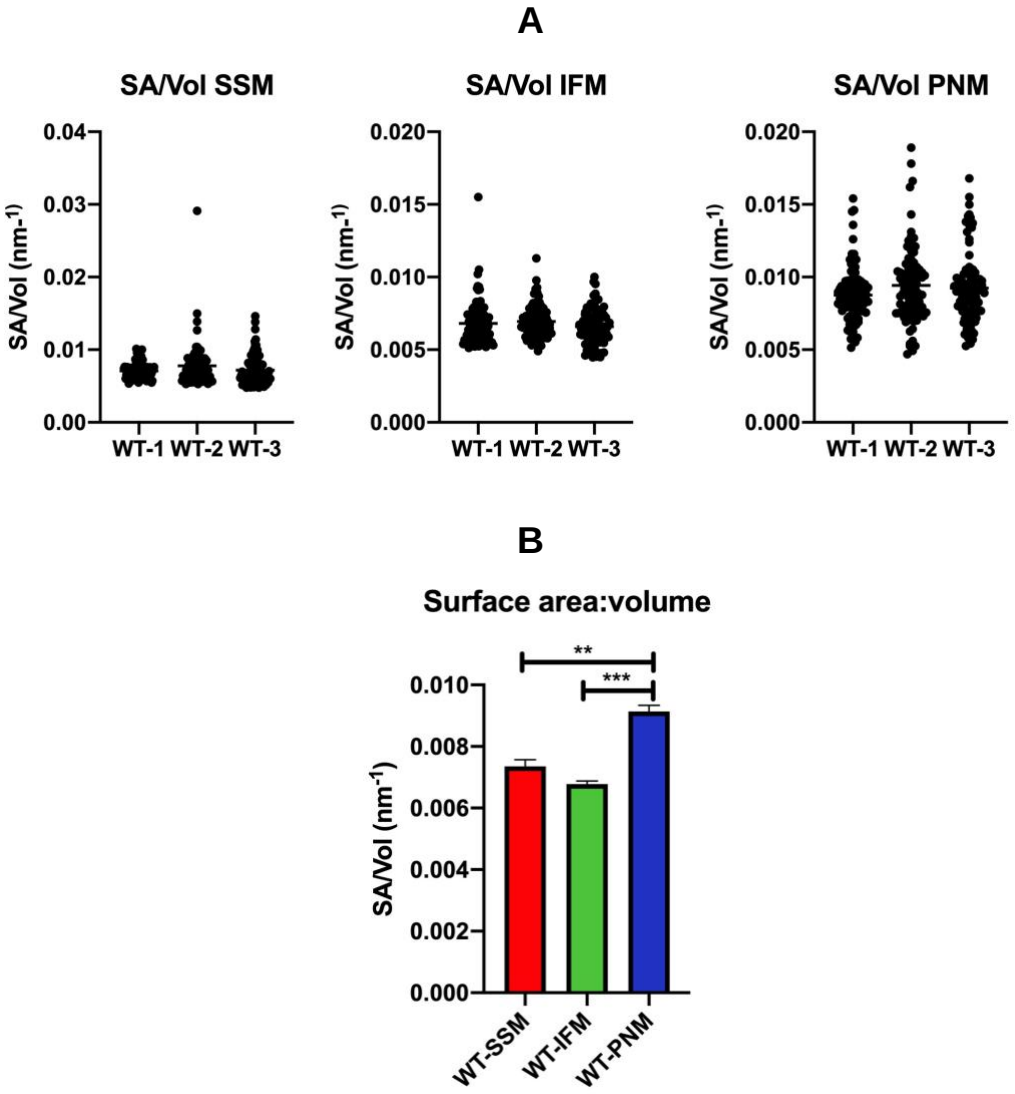

Figure 3.6 PNM have a larger surface area: volume ratio than IFM or SSM in WT mice

(A) Raw data showing spread of data for each sample. (B) SA/Vol properties for each mitochondrial subtype. Mean data ± SEM presented. Data were analysed using a one-way ANOVA (with Tukey's multiple comparison test) for each mitochondrial subtype from n=3 animals. ** P<0.001; *** P<0.0001.

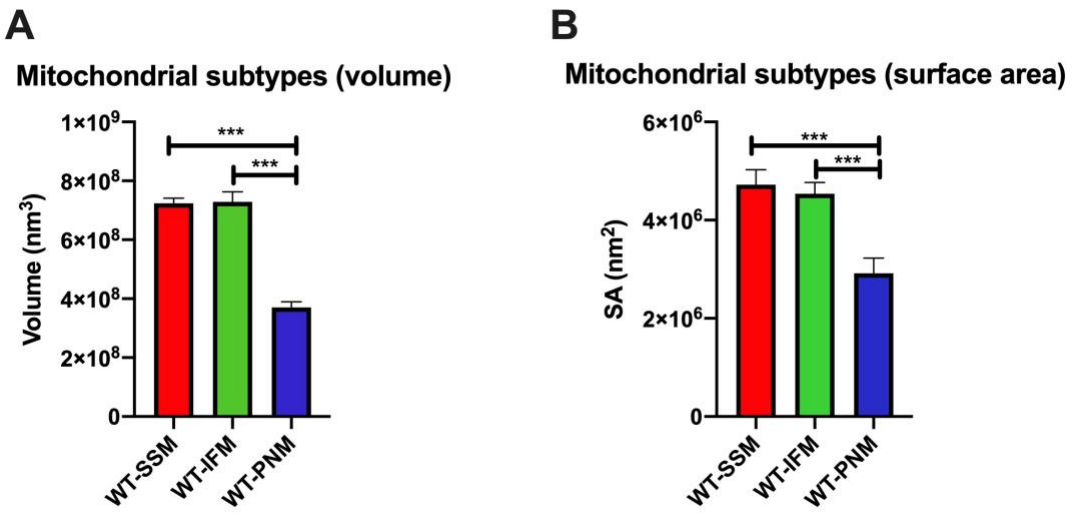

Figure 3.7 Comparison of cardiac mitochondria morphometric parameters in WT mice

(A) Comparison of the volumes indicate that PNM are smaller than that of SSM or IFM. SSM and IFM have a similar volume (B) The surface area of the PNM is smaller than SSM or IFM. The surface area of SSM and IFM are similar. Mean data ± SEM presented. Data were analysed using a one-way ANOVA (with Tukey's multiple comparison test) for each mitochondrial subtype from n=3 animals *** P<0.0001.

Interestingly, a comparison of the SA/volume ratio for each mitochondrial subtype revealed that PNM had a larger ratio (Figure 3.7; Figure 3.7), which we suggest may be linked to the spatial relationship with the nucleus. A comparison of the mean values for SA/Vol for each subtype indicates that the SA/Vol for PNM is 1.24 x greater than SSM and 1.35 x greater than IFM.

3.3.3 GENA348 mice exhibit more variability in mitochondrial size

Using the same approach, we segmented similar numbers of SSM, IFM and PNM in the SBF-SEM datasets from the aged-matched GENA348 mice from tissue also sampled from the apex. However, a comparison within subtypes found a significant variation between each animal (Figure 3.8). Therefore, for each animal we separately compared the surface area and volume of the SSM, IFM and PNM. As shown in Figure 3.8, unlike for WT cardiac mitochondria, the GENA348 showed a progressive decrease in size SSM > IFM > PNM, a pattern that was consistent for all three animals studied.

A similar analyses for the surface area: volume ratio showed a similar profile to the WT with PNM being larger; however, if the data is pooled then there is no longer a difference between the subgroups although there is a trend for SSM<PNM and IFM<PNM (*P*=0.0832 and *P*=0.0976, respectively).

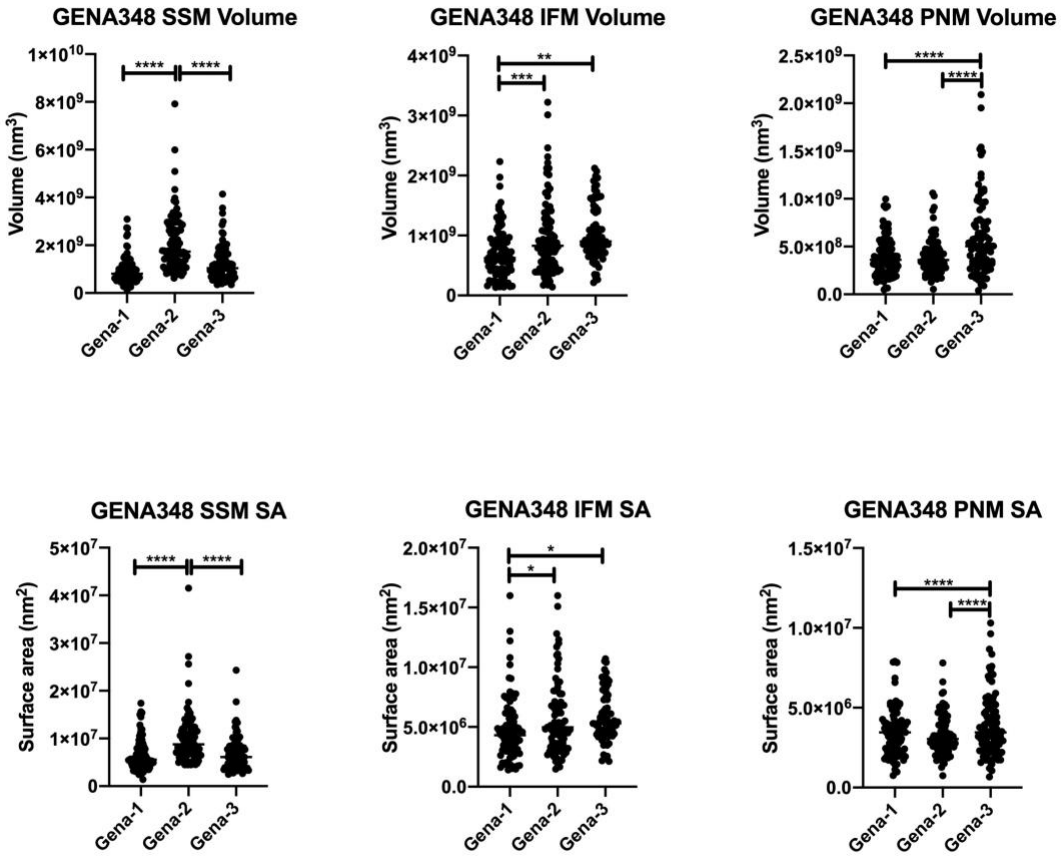

Figure 3.8 Morphological parameters of each subset of mitochondria in tissue taken from the apex of 6-month-old GENA348 mice. A one-way anova (with comparisons of the means) showed a variability between each of the mitochondrial subtypes for each animal. * P< 0.05; ** *P*< 0.01*** *P*<0.001; **** *P*<0.0001.

3.3.4 SSM are larger in the GENA348 compared to WT mitochondria

Upon inspection of the SSM they appeared to be larger and more irregularly shaped compared to the WT SSM (Figure 3.12A/B). As shown in Figure 3.9, the GENA348 SSM are approximately up to 2x larger than WT SSM larger; mean WT volume 7.23 ± 0.31 x 10^8 nm^3 compared to GENA348 volume 14.23 ± 0.60 x 10^8 nm^3; n=3 per experimental group. In keeping with a larger volume, a comparison of the mean surface area for each experimental

group showed an increase of 1.7 in the GENA348 SSM. However, there was no change to the overall surface area: volume ratio (Figure 3.10).

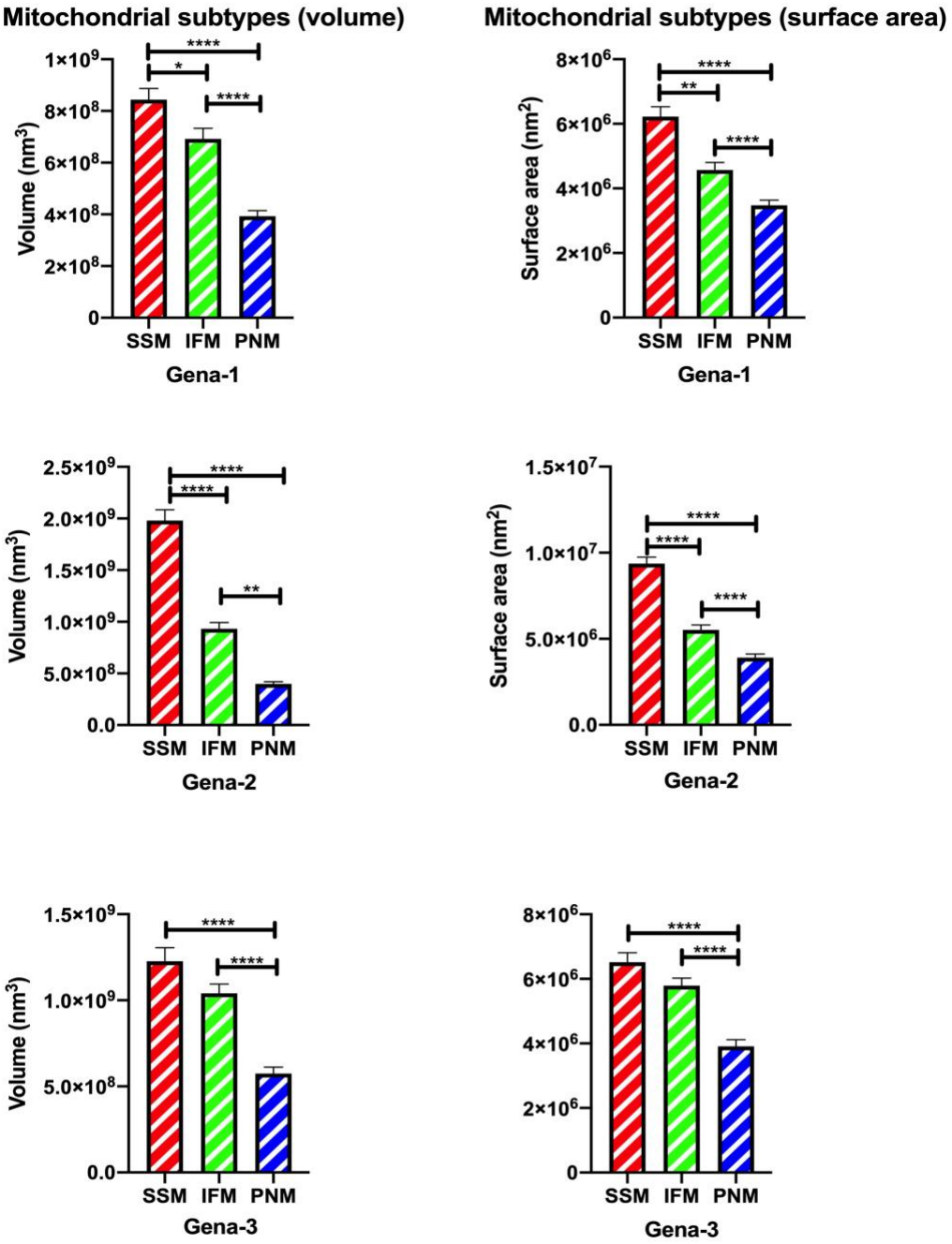

Figure 3.9 Comparison of the morphometric parameters of each subtype of cardiac mitochondria in each GENA348 mice.

There is a general trend in mitochondrial size SSM>IFM>PNM Mean data ± SEM presented. Data were analysed using a one-way ANOVA (with Tukey's multiple comparison test) for each mitochondrial subtype. Due to the intra-animal variation each mitochondrial subtype has been analysed for each animal. * P<0.05; ** P<0.01; *** P<0.001; **** P<0.0001. *Note* for Gena-3 there was not a significant difference between the SSM and IFM but the IFM volume was smaller P = 0.0797.

There is also an increase to the sizes of the IFM and PNM although not to the same extent as the SSM (Figure 3.10). Observations of the SBF-SEM datasets found that IFM were still organised in rows within the cardiomyocytes although there appeared to be more clustering.

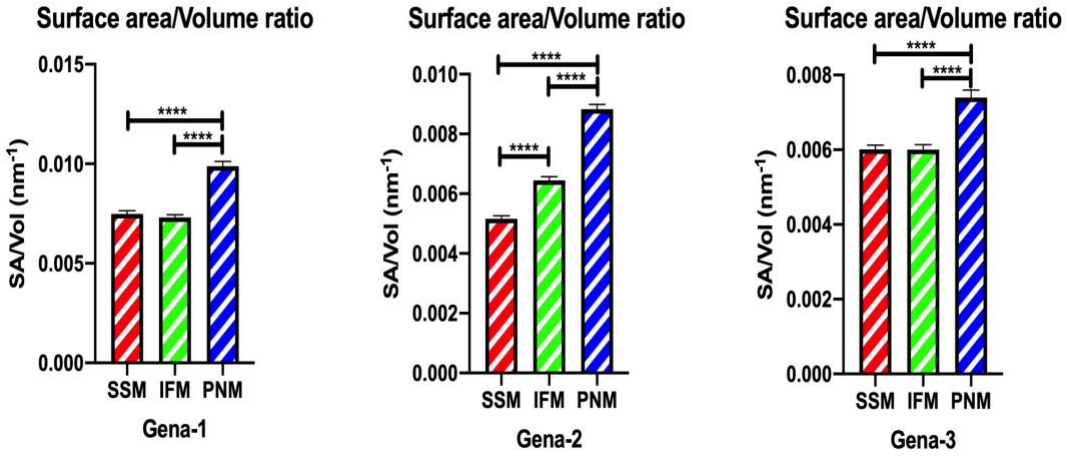

Figure 3.10 A comparison of the surface area: volume of the subtypes of cardiac mitochondria in tissue taken for the apex of GENA348 mice at 6 months of age.

Data analysed using a one-way ANOVA (with Tukey's multiple comparison test) for each mitochondrial subtype from n=3 animals. (*** $P<0.001$; **** $P<0.0001$). Increased mitochondrial density in the GENA348 myocardium

Citrate synthase activity was increased in the GENA348 hearts compared to the WT counterparts (Chapter 2, Figure. 2.6), which is indicative of increased mitochondrial content. Qualitative assessment of the EM datasets indicated that there were often large areas of mitochondrial clustering in the GENA348 myocardium compared to WT (Figure 3.12A). Further, the number of mitochondria at the poles of the nuclei also appeared large in the GENA348 samples compared to WT. Therefore, we next investigated the mitochondrial density. We therefore next applied a stereological method (as described in section 3.2.4) to the SBF-SEM datasets, to quantify the mitochondrial density in each dataset.

Employing this approach, we determined that WT mitochondria occupy 36.8 $\pm$ 2.7% relative to the cardiomyocyte volume. In comparison, a larger percentage of the cardiomyocyte is occupied by mitochondria in the GENA348 left ventricle, 57.6 $\pm$ 7.5% of a cell (Figure 3.12B); P=0.0298.

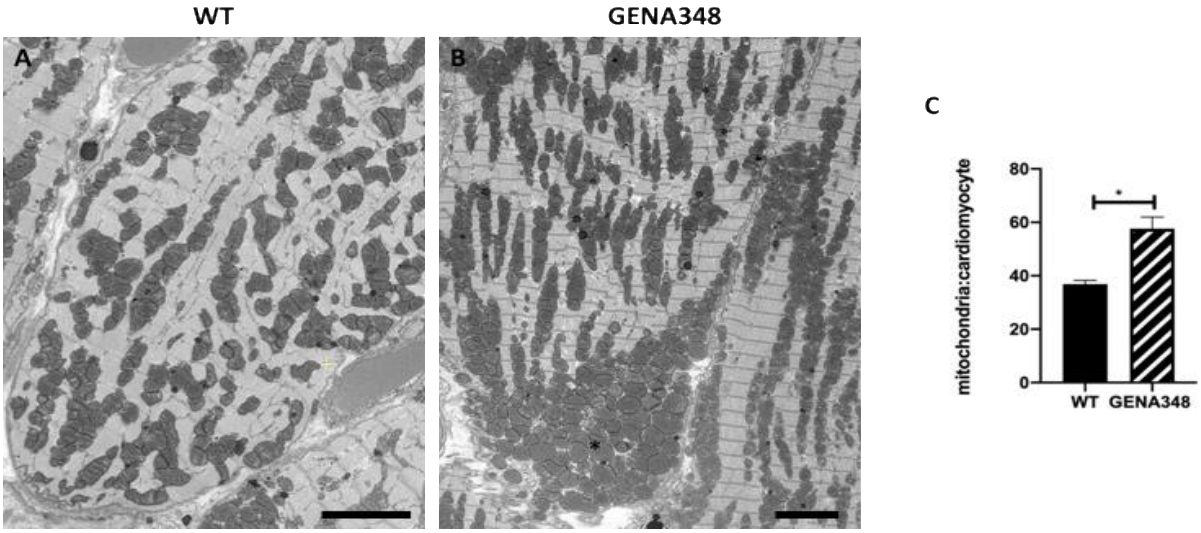

Figure 3.11 (A) Increased mitochondrial density in GENA348 myocardium compared to WT Portion of a serial image from a WT SBF-SEM showing a typical organisation of the mitochondrai (B) Serial image from a GENA348 SBF-SEM dataset showing large clusters of mitochondria (indicated by *). Scale bar = 5 µm (C) Qualitative analysis of mitochondrial density using a stereological approach sampling 1-999 images per SBF-SEM data set (n=3 per group) using a two-tailed unpaired student t-test (* $P < 0.05$)

3.3.5 GENA348 SSM are more irregular in shape and larger than WT SSM

A comparison of each of the mitochondrial subtypes between control and GENA348 revealed a significant increase in the mean mitochondrial volume (Figure 3.12C) and mean mitochondrial surface area (Figure 3.12D) of the SSM in the GENA348 myocardium, compared to controls as shown in Figure 3.12 (see Table 1).

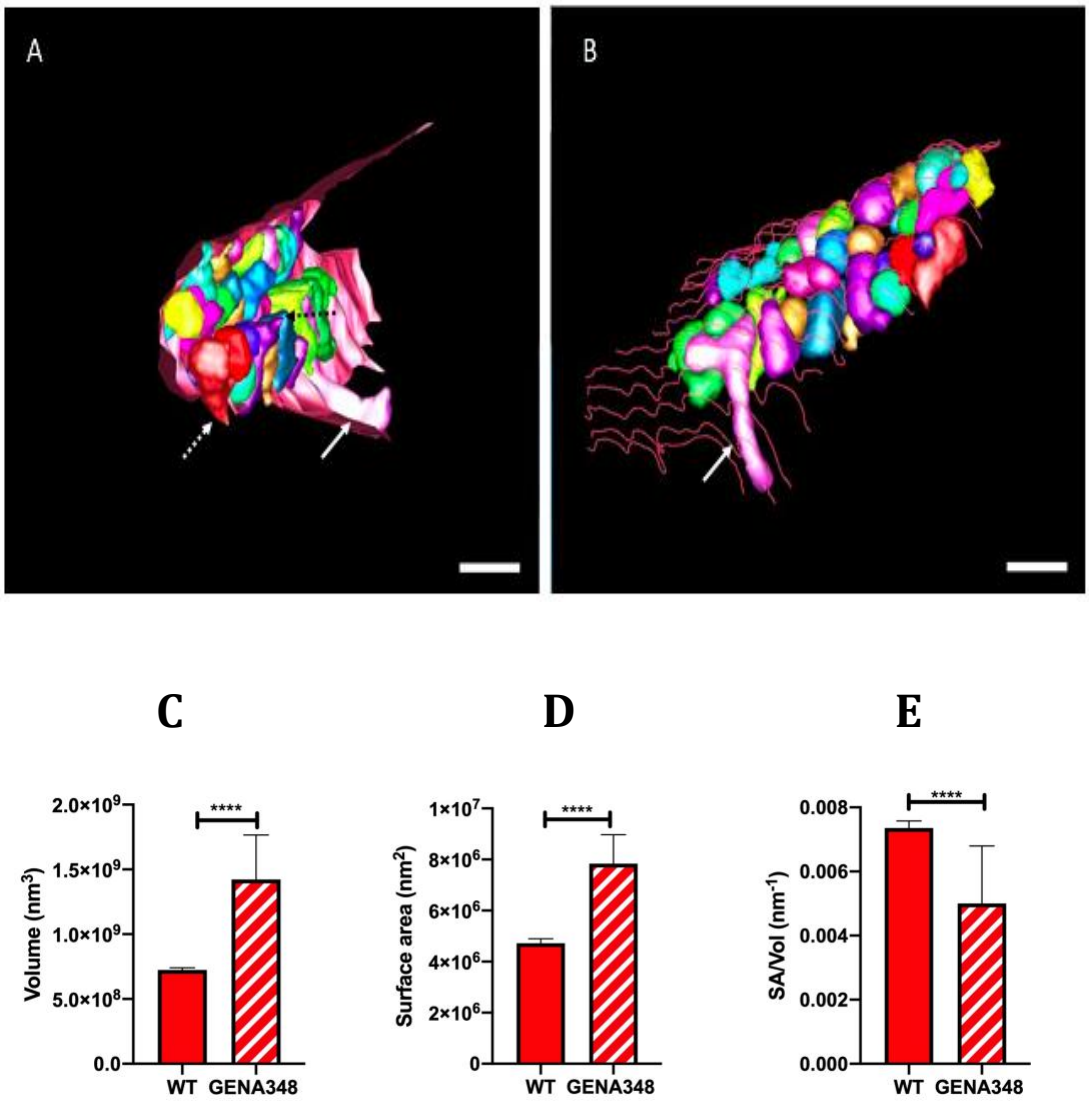

Figure 3.12 GENA348 SSM are more irregular in shape and larger than WT SSM

(A) and (B) 3-D reconstruction of a cluster of GENA348 SSM, arrows indicate tubular projections. Sarcolemma is depicted in dark pink (scale bar = 2μm). (C, D, E) A comparison of the morphometric parameters of the average values for each animal using a two-way ANOVA for multiple comparisons between rows indicated that the SSM volume and surface area are larger in the GENA348 heart with a reduction to the SA/Vol ratio. Data presented as mean ± SEM; **** $P< 0.0001$.

Due to the variability between the morphological parameters for the GENA348 datasets we employed a two-way ANOVA for the analysis. However, a student t-test (two-tailed) of the means of the surface area also showed a significant difference $P=0.0478$.

Overall comparison of the total mitochondrial networks (IFM and PNM) between control and GENA348 revealed a slight significant increase in mitochondrial volume and surface area

between control and GENA438 as shown in Figure 3.13A, B, D, E; a comparison of the mean values indicated an increase to GENA348 IFM Vol and SA as 1.34x and 1.20x respectively. Similarly, a comparison of the mean values for the PNM Vol and SA indicated the GENA348 PNM were approximately 1.26x and 1.22x larger when compared to those in WT. However, there was no difference in the overall SA/Vol ratio for both IFM and PNM subsets (Figure 3.13C and F).

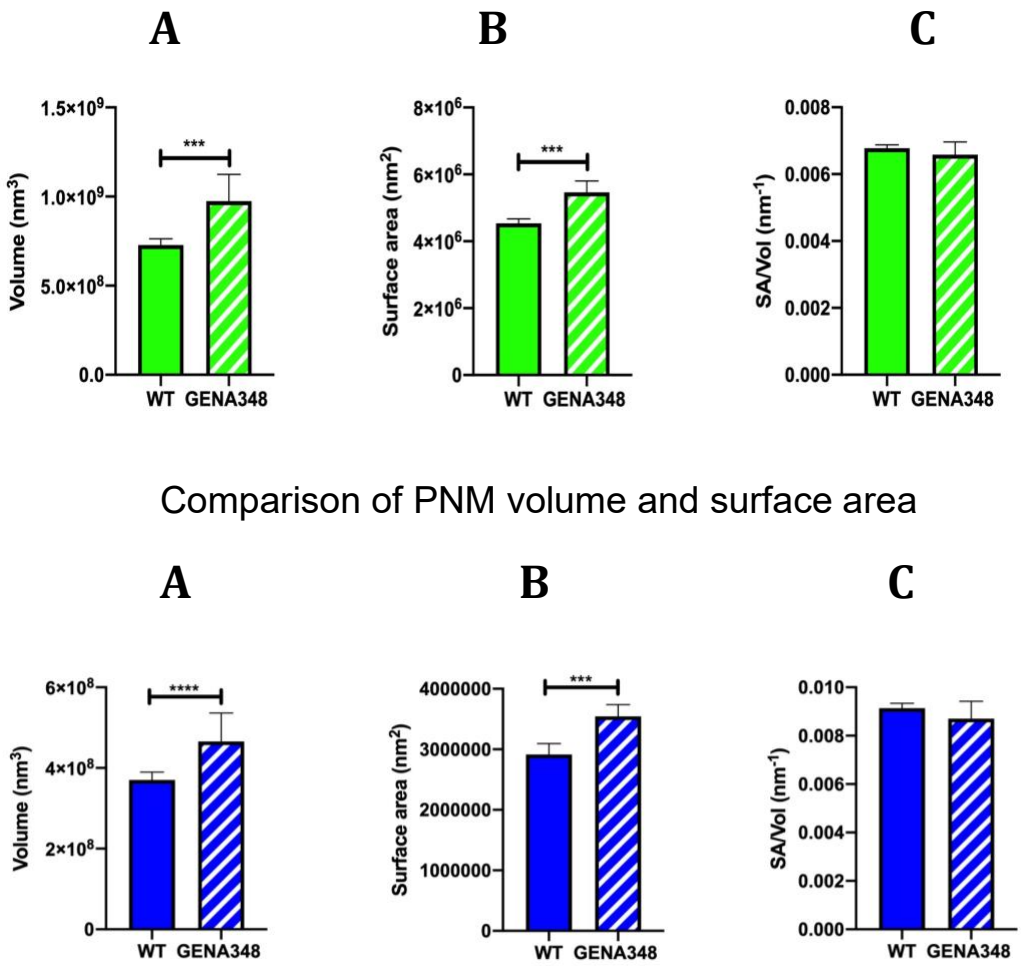

Figure 3.13 IFM and PNM volume: surface area comparison between WT and GENA348

(A, B, C) A comparison of the morphometric parameters of the average values for each animal using a two-way ANOVA for multiple comparisons between rows indicated that the IFM volume and surface area are not significantly different in the GENA348 heart regarding the SA/Vol ratio. (D, E, F) A comparison of the morphometric parameters of the average values for each animal using a two-way ANOVA for multiple comparisons between rows indicated that the PNM volume and surface area are not significantly different in the GENA348 heart regarding the SA/Vol ratio. Data presented as mean ± SEM; **** *P*< 0.0001

Interestingly, the GENA348 cardiac IFMs were often observed to have small projections/tubules extending from one end. Figure 3.14 shows a 3-D segmentation of a cluster of IFMs with the arrows highlighting projections.

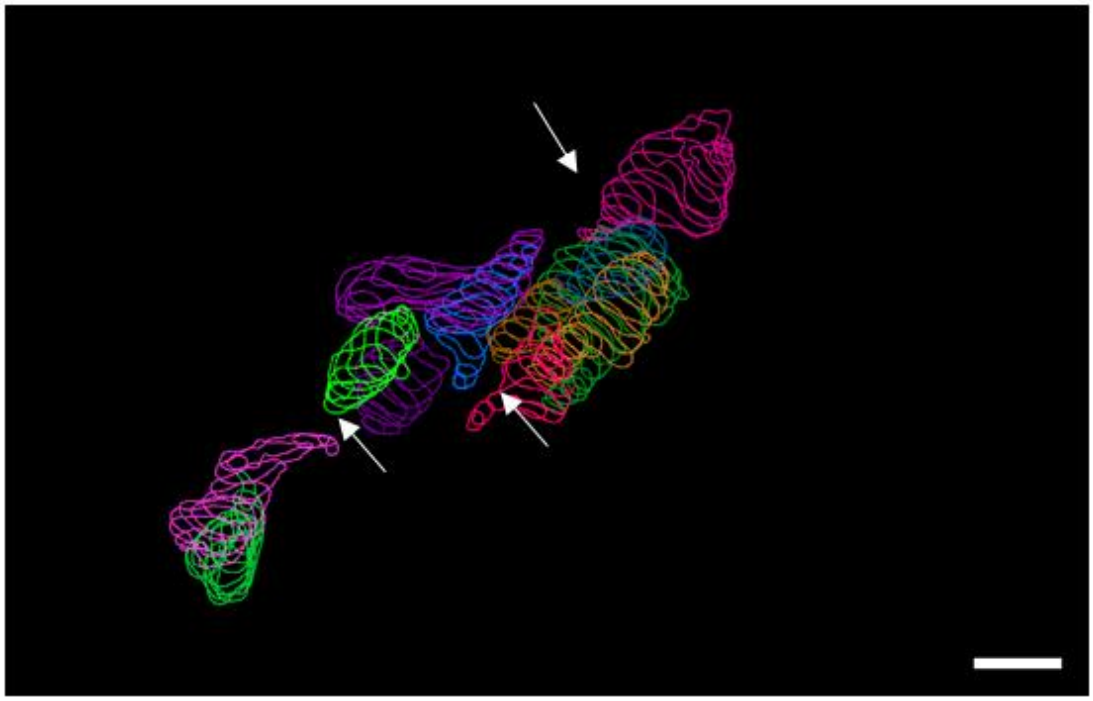

Figure 3.14 GENA348 cardiac IFM projections and tubules.

GENA348 cardiac IFMs commonly were observed to have small projections/tubules extending from one. Image shows 3-D segmentation (displayed as contours) of a cluster of IFMs with the arrows highlighting projections protruding from one end of a mitochondrion. Scale bar = 1μm

3.3.6 Mitochondrial nanotunnels

We occasionally observed mitochondrial nanotunnels within the WT mitochondrial population; however, in comparison they appeared to be much more common within PNM of the GENA348 (Figure 3.15). Mitochondrial nanotunnels are evolutionarily conserved structures identified in prokaryotic and eukaryotic cell types, thought to facilitate communication with nonadjacent mitochondrion (Huang et al., 2013). In Figure 3.15, we observe the formation of nanotunnels between PNM in the GENA348 myocardium.

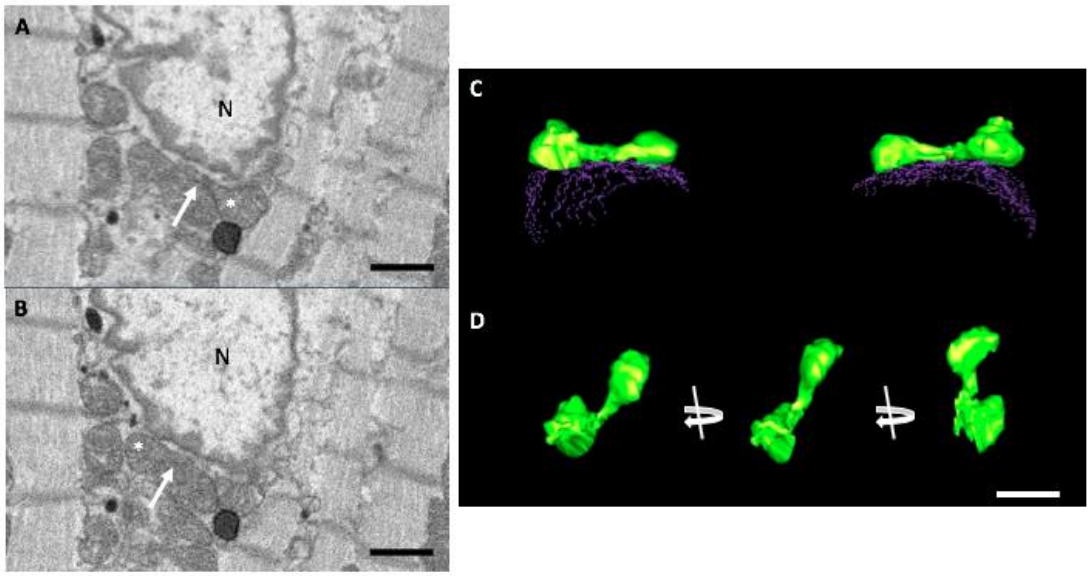

Figure 3.15 Nanotunnels form between perinuclear mitochondria in the GENA348 myocardium (A)An example image showing PNM taken from an SBF-SEM dataset. This image shows no connections between mitochondria (although it should be noted that nanotunnels were occasionally identified in WT PNM populations). B) Portion of a serial image showing a mitochondrion (indicated by asterisk) adjacent to the nucleus (N) with a small projection extending from one end (indicated by the arrow) (C) Several images further into the SBF-SEM stack shows another mitochondrion (asterisk) with a projection extending from one end (white arrow). (D) Segmentation of the two mitochondria in A and B show that the projections connect forming a tunnel between the two mitochondria forming a 'dumbbell' shape structure (green isosurface). The nuclear envelope is shown as dashed contours (purple). Portions of each mitochondria and 'nanotunnel' are in direct contact with the nucleus. (E) Three different views of the nanotunnel showing that it has a 'kinked' structure and is approximately 1 µm in length. Scale bar = 1 µm

3.4 Discussion

These studies investigated mitochondrial ultrastructure and organisation in the heart and how they are altered in the GENA348 diabetic mouse using SBF-SEM. The main findings of this chapter were that: (1) in the WT heart, SSM are a similar size to IFM but PNM are smaller than both; (2) furthermore, the SA/Vol ratio of the PNM is greater compared to either SSM or IFM; (3) despite the variability between GENA348 animals there is a common pattern with a size difference between each mitochondrial subtype, SSM>IFM>PNM; (4) as in WT cardiomyocytes, the PNM have a larger SA/vol compared to SSM and IFM. These novel findings demonstrate the mitochondrial adaptation to diabetic insult on the heart and further support the molecular alterations seen in Chapter 2, suggesting an increase in mitochondrial fusion in the GENA348 model.

We were particularly interested in comparing WT with GENA348 as an indicator of mitochondrial changes resultant of MODY2 diabetes. When comparing WT and GENA348, mitochondrial subtypes were larger in the GENA348 myocardium, with SSM exhibiting the largest increase. This supports earlier biochemical data showing an increase in fusion proteins, particularly Mfn1/2. As Mfn1/Mfn2 are fusion proteins, we postulate that this increase in protein expression was associated with an increase in mitochondrial size. It should be noted that there was inter-animal variation within the diabetic group in particular the SSM likely due to the irregular shapes.

Ultrastructural studies have been used to investigate the function of Mfn2 and the differences in mitochondrial subpopulations (Hall et al., 2016a). Hall et al. (2016b) demonstrated that Mfn1/2 deficient mouse hearts displayed small fragmented IFM. In this study, the authors ablated both cardiac-specific Mfn1/2 in mice to investigate the role of mitochondrial fusion proteins as factors that influence morphological changes. Then, mitochondrial size, respiratory function and contractile function were measured to evaluate changes in response to acute ischemia/reperfusion. Interestingly, the disrupted interactions between the mitochondria and sarcoplasmic reticulum in knockout mice reduced mitochondrial Ca^{2+} overload, attenuating oxidative stress and contributing to this cardioprotective phenotype (Hall et al., 2016b). The

inhibition of mitochondrial fission has been shown to protect the heart against acute ischemia/reperfusion (I/R) injury (Hall et al., 2016a). This is corroborated by studies that have shown similar results in Mfn2 ablated MEF cells, supporting the role of Mfn2 in mitochondrial fusion (De Brito and Scorrano, 2008). In contrast to Mfn1, Mfn2 has been shown as a multifunctional protein involved in multiple signalling pathways, beyond the regulation of mitochondrial shape (De Brito and Scorrano, 2008). Other studies have revealed the loss of Mfn2 in cardiomyocytes results in an enlarged mitochondria phenotype (Papanicolaou et al., 2011). Papanicolaou et al. (2011) showed cardiac myocyte mitochondria lacking Mfn2 exhibited some myocyte hypertrophy accompanied by mild deterioration of left ventricular function.

Another comparison to note between GENA348 and WT was an increase in mitochondrial density in the GENA348 heart, compared to WT. Previously reported increases in citrate synthase, TFAM and PGC1-α gene expression (Chapter 2) in the GENA348 myocardium support this, suggestive of increases in the mitochondrial biogenesis pathways. However, given that the functional and proteomics data in the previous Chapter indicated the presence mitochondrial dysfunction this increased number of mitochondria may also indicate that it is the result of the accumulation of damaged mitochondria, with pathways working to try and replace them.

3.4.1 Increased mitochondrial size in the GENA348 heart

In the WT myocardium the PNM are smaller than SSM and IFM but have a larger SA/Vol. This may suggest better diffusional properties that are important for mitochondria in direct contact or juxtaposed to the nuclear envelope for both efficiency of substrate uptake and ATP production. Lukyanenko et al. (2009) reported PNM to be smaller than IFM were in size and possessed a more rounded shape in cardiac cells. The differences in matrix electron density and internal membrane extension between PNM and IFM have been suggested to reflect differences in functional activity between the two types of mitochondria (Hackenbrock, 1968). In fact, this rounded shape and location are thought to favour ATP generation that drives

mitochondrial metabolism close to the nucleus. The spatial location of a given mitochondrion reflects the processes in which it supplies ATP, possibly explaining the differences in locality and volume between the types of mitochondria. The locality of the PNM may also mediate calcium handling processes, although this has yet to be tested and was beyond the scope of this thesis.

The increase in mitochondrial size of the GENA348 mitochondria is in keeping with the biochemical data, showing an increase in fusion proteins consistent with larger mitochondria. Generally, smaller fragmented mitochondria have been reported in numerous pathologies (as reviewed by Daghistani et al., 2018). Although based on a different diabetic model, (Sano et al., 2010) reported giant mitochondria in alloxan-induced diabetic rats. Alloxan accumulates in β-cells of the pancreas and breaks down DNA strands, destroying insulin-producing pancreatic cells. Using immunohistochemical analysis of prohibitin, the authors reported the presence of huge structures surrounded by a double membrane containing many irregular cristae. In general, significant increases in mitochondrial size may be attributed to growth of individual organelles or fusion of abutting mitochondria. An alternative suggestion is that extra-large mitochondria may be destroyed by autophagy, followed by the synthesis of new large mitochondria (Hoppel et al., 2009). For future studies it would be useful to measure levels of autophagy. One factor may be that many of these reports have used 2-D images rather than 3-D; depending upon the orientation of the mitochondria within the tissue and the cut angle of the section data, 2-D images may be misleading. Due to the resolution limitation of SBF-SEM (~ 10-11 nm in the X-Y plane and 50 nm in the Z-plane) it was not possible to examine the cristae structures in these samples.

Here, we show that mitochondria are enlarged in the GENA348, suggestive of a correlation with the earlier fusion data. However, the biochemical and functional data in Chapter 2 as discussed suggest that these larger mitochondria are dysfunctional and thus, raise the question as to whether targeting fusion is beneficial in disease conditions. Here we show that cardiac mitochondrial dysfunction is a characteristic of the GENA348 mouse. In the previous chapter, we determined an imbalance between fission and fusion, impaired mitophagy and

compromised motility. We also reported impaired OXPHOS in GENA348 mice suggesting defects in cardiomyocyte contractility and metabolism, with physiological assessments indicating the development of cardiac hypertrophy.

3.4.2 SSM are more enlarged than the IFM and PNM

Our data indicate that SSM are more enlarged than the IFM and PNM. SSM are in contact with the sarcolemma, possibly making them more vulnerable to oxidative stress. In a recent study, Lai et al investigated the susceptibility of heart SSM and IFM to cardiomyopathy (Lai et al., 2020). To this aim, a rat model of non-obese T2DM was used to compare heart mitochondrial energy metabolism and enzyme activities of the ETC between the two subpopulations. The study showed that SSM and IFM respiration rates were similar, with similar citrate synthase activity levels. Together this shows that the sarcolemmal location of the SSM type possibly impacts changes in mitochondrial ultrastructure in diabetes. Furthermore, it has been suggested that IFM predominantly deliver ATP for muscle contraction, whereas ATP derived from SSM is used for maintenance of basic cell function (Schwarzer et al., 2013). Heyne et al. (2020) further reported a decrease in mitochondrial respiration in IFM and an increase in SSM, postulating that this increased SSM activity may be seen as a compensatory adaptation to meet ATP demand.

Furthermore, other cardiomyopathy studies in models without insulin resistance reported dominant dysfunction of IFM, compared to SSM; of note is that the GENA348 mice are not insulin resistant. In the hamster heart, Hoppel et al. (1982) reported that the oxidative defect is confined to the IFM, whilst the SSM were normal. Similarly, Dabkowski et al. (2009) reported spatially distinct mitochondrial populations in T1DM mouse. Using Swiss-Webster mice, the authors measured ETC respiration, finding that the decrease was greater in IFM, suggesting that diabetes places a greater strain on the diabetic IFM than SMM populations. Furthermore, in skeletal muscle, Lai et al. (2017) reported that SSM are more affected than IFM in a model of insulin resistance. The decreased SA/Vol of the GENA348 SSM compared to the WT would also be consistent with compromised function (Chapter 2 – 2.3.5). A reduced surface area may lead to impaired substrate diffusion and consequently, reduced ATP production. In the

future, it may be useful to measure and compare ATP levels between the experimental models It would also be informative to fractionate the different mitochondrial subtypes and determine if functionally they are differentially affected in the GENA348 myocardium.

3.4.3 Increased mitochondrial density supports increased mitochondrial biogenesis in the GENA348 myocardium

Citrate synthase, TFAM and PGC1-α are shown to be increased in Chapter 2 in the GENA348 myocardium, suggesting an increase in mitochondrial biogenesis and content. Other studies have reported increased mitochondrial numbers in the diabetic heart, suggesting increase in mitochondrial biogenesis (Shen et al., 2004). It was suggested that this increased number compensates for impaired mitochondrial function by increasing mitochondrial number. In keeping with the biochemical data, we show here that there is a significant increase in mitochondrial density in the GENA348 myocardium. Our mitochondrial density measurements using the SBF-SEM images within the WT cardiomyocytes is in keeping with previous studies (using different approaches) estimating that mitochondria occupy between 25-30% of the cell volume (Barth et al., 1992; Schaper et al., 1985), and thus provides support for the methodology applied here as well as confidence for the increased density identified in the GENA348 heart. Studies investigating mitochondrial biogenesis have suggested that the attenuation of mitochondrial dysfunction during the development of diabetic cardiomyopathy occurs through the increase of mitochondrial turnover (Tong et al., 2019). The increased mitochondrial density in the GENA348 cardiomyocytes could be a compensatory effect for the failing functional capacity of the existing mitochondria. In skeletal muscle, the impact of a short-term HFD on mitochondrial function and dynamics was investigated (Leduc‐Gaudet et al., 2018). Using measures of fission/fusion proteins, the authors showed that short-term HFD results in an increased capacity of skeletal muscle mitochondria to oxidize fatty acids, without altering ROS production. Similarly, (Heyne et al., 2020) reported that HFD causes skeletal muscle mitochondrial dysfunction comparable to HF, building on previous findings that HFD increase mitochondrial density (Devarshi et al., 2017). Their study also showed that HFD decreased maximal mitochondrial respiration of IFM in skeletal muscle, whereas maximal

mitochondrial respiration of SSM increased, further perpetuating the differential activity of the two subpopulations.

With an increase in mitochondrial fusion, it would be expected that there would be a decrease in mitochondrial number; however, this may be offset by an upregulation in PGC-1α and TFAM transcripts, suggesting an increase in biogenesis. Although, it may also indicate that there is an accumulation of damaged mitochondria due to impaired mitophagy. Notably PINK1 and Parkin, mediators of mitophagy are down regulated in the GENA348 heart. Analysis of other markers of mitophagy such as LC3, NIX and Bnip3 (Ding and Yin, 2012) would be helpful in future studies to determine if there was a correlation between the increased numbers of mitochondria and dysregulated mitophagy

The observation of mitochondrial clustering may also be linked to the report in Chapter 2 of reduced expression of Miro1. Miro1 is an important protein that, when inhibited, perturbs mitochondrial motility, disturbs pancreatic β-cell function and interferes with insulin releases (Chen et al., 2017). In Chapter 2, both western blot data and qPCR show a decrease in Miro1 expression. Furthermore, down-regulation of Miro1 may impede the movement of mitochondria through the cardiomyocyte, contributing to disorganisation of the mitochondria within cardiomyocytes, further impairing function. Here, we observe increased mitochondrial density, which would be consistent with reduced motility leading to accumulation of mitochondria.

3.4.4 PNM nanotunnels, an adaptation to diabetic stress

While we occasionally identified PNM nanotunnels in micrographs of the WT heart samples, they appeared to be a more common occurrence in the GENA348 datasets. Mitochondrial nanotunnels are evolutionarily conserved structures identified in prokaryotic and eukaryotic cell types. In the heart, TEM and confocal microscopy have reported mitochondria extensions as able to facilitate communications with nonadjacent mitochondrion (Huang et al., 2013). The identification of small tubule like projections from the IFM and the formation of nanotunnels between PNM in the GENA348 may indicate an increased need for communicating between

the mitochondria due to the associated diabetic stress. Again, increased expression of fusion proteins data in Chapter 2 may also promote the formation of contacts between neighbouring mitochondria by the formation of nanotunnels.

Nanotunnels have also been proposed to be a result of impaired fission-fusion. Incomplete mitochondrial fission of mitochondrial tubules has been shown to generate anatomically similar structures to nanotunnels (Vincent et al., 2017). Therefore, the presence of more mitochondrial nanotunnels in the GENA348 mice hearts may also be another indication of an adaptation or remodelling in response to the diabetic stress.

3.5 Conclusion

In conclusion, this chapter demonstrates changes in mitochondrial ultrastructure and organisation in the GENA348 diabetic mouse heart using SBF-SEM with results consistent with the biochemical data in Chapter 2. Specifically, we identified SSM to be more susceptible to diabetic insult with IFM and PNM less impacted. We also noted changes to the ultrastructure through the presence of nanotunnels, increased mitochondrial density and clustering. These alterations may be in response to the increasing needs of the heart due to mitochondrial dysfunction. These findings support the previous increases in fusion protein expression, suggesting a possible adaptive mechanism in response to diabetic stimuli. However, collectively our results indicate that although increased fusion may initially be a cardioprotective mechanism in response to hyperglycaemia that in the longer-term the balance can tip towards being pathological due to the complex interplay between compensatory mechanisms and impaired mitophagy for the removal of damaged mitochondria. Further work is required to elucidate whether these changes are cardioprotective or maladaptive and so whether targeting fusion is an appropriate therapeutic strategy in the setting of hyperglycaemia in the absence of insulin resistance. The following chapter will investigate the effects of introducing a further stress, a Western high fat diet, to the GENA#48 mice that already are hyperglycaemic.

Chapter 4 The effect of a high fat diet on GENA348 cardiac phenotype

4.1 Introduction

This chapter investigated the effects of a high fat diet (HFD) upon the cardiac and mitochondrial function of the GENA348 mouse model. Obesity is widely known to significantly increase the risk of T2DM. MODY2 patients appear asymptomatic with no real impact on diet or lifestyle, and diagnosis is usually incidental, despite being hyperglycaemic (Giuffrida and Reis, 2005). However, under conditions of stress, including pregnancy or obesity, MODY2 patients require medication and monitoring. As discussed in the main introduction, the GENA348 mouse represents a viable animal model that can be manipulated to investigate the MODY2 phenotype including cardiovascular function. Thus, in this chapter, diet-induced obesity is studied to understand the effect on the heart. Although a growing global heath epidemic, the impact of obesity on MODY2 is yet to be explored in relation to cardiac and mitochondrial function. There may be additional pathogenic consequences that obesity exasperates in MODY2 patients.

4.1.1 Obesity and diabetes

Maturity onset diabetes of the young (MODY) accounts for 1-2% of diabetes diagnosis, with glucokinase (*GCK*)-MODY (MODY2) accounting for 10-60% of all MODY cases (Bishay and Greenfield, 2016). MODY2 is characterised by its high penetrance, early onset, and lifelong fasting hyperglycaemia. Although generally asymptomatic, MODY2 can result in clinical implications within pregnancy, impacting birth weight due to maternal hyperglycaemia (Hattersley et al., 1998). The identification and management of pregnancies, featuring maternal or paternal MODY has not been well evaluated, and is frequently misidentified as T2DM. There is a strong association between maternal obesity and gestational diabetes (Farren et al., 2015). Interestingly, the removal of dysfunctional mitochondria via mitophagy (Eiyama and Okamoto, 2015) has been identified as an important process that counteracts the pathogenic processes in diabetes and is an important factor to consider in research.

4.1.2 Animal Models of Obesity

Animal models are invaluable for acquiring basic knowledge about diabetes. High-fat diet (HFD) mice are regularly used as a model to study obesity and diabetes. In addition to diet-induced, chemically induced mice, genetically modified and surgical models of obesity are used to understand the pathways that lead to diabetes. In this chapter, the GENA348 (HFD) mouse will be investigated for a potentially greater, more severe cardiac phenotype compared to wild type. It is known that obesity detrimentally impacts mitochondrial function, leading to cardiomyopathies, however, the role of the glucokinase gene in this pathway yet to be investigated.

Amongst those most frequently used, genetically obese models of diabetes include *ob/ob* and *db/db* mice, whereby similarities to the human condition are reported. For example, in both *ob/ob* and *db/db* mice, severe diastolic dysfunction and cardiac failure has been reported (Semeniuk et al., 2002), similar to the profile of human diabetic patients. The *ob/ob* and *db/db* mice are deficient in leptin, a protein that regulates hunger through the control of appetite (Wang et al., 2014). Thus, obesity is induced through severe hyperphagia, eventually developing some diabetic characteristics. Leptin deficient animal models also include the Zucker fatty rat and Zucker diabetic fatty (ZDF) rat. Leptin-related rodent models display early-onset obesity, recognisable at 4 weeks of age (Della-Fera et al., 2005), suggesting a severe response to the lack of leptin. Although a useful tool, leptin administration can correct diabetic manifestation in *ob/ob* mice (Pelleymounter et al., 1995), implying a challenge for studies investigating T2DM. In humans, T2DM is linked to obesity, rather than leptin deficiency, indicating a difference in disease manifestation. Thus, data from genetically modified mouse models should be compared with clinical incidences sparingly.

For Zuker fatty rats and ZDF rats (f*a/fa*), severe obesity is recorded at 5 weeks, maintained for at least 6 months (Wang et al., 2014). The male ZDF rat (*fa/fa*) was derived from inbreeding of hyperglycaemic Zucker obese rats, characterised by a leptin receptor mutation (Schmidt et al., 2003). Zuker fatty rats present normal or mild hyperglycaemia, however, ZDF male rats are severely hyperglycaemic with normal characterisation in females (Wang et al., 2014). It is

important to note, however, that these sex differences do not exist in diabetic characteristics in humans.

In addition to the genetically induced obesity animal models mentioned above, experimentally induced obesity models such as the streptozotocin (STZ) rat. Streptozotocin is a β-cytotoxic drug that destructs the pancreatic β cells (Barragán-Bonilla et al., 2019; Portha et al., 1974). This results in a decrease in insulin circulation, increased blood glucose and the onset of diabetic symptoms. To induce severe diabetes, STZ is administered at 40–50 mg/kg body weight in adulthood, with blood glucose reflecting high levels after 3 days (Damasceno et al., 2014). This animal model is widely used due to its ease and extensive characterisation. In STZ-induced models, a number of cardiac abnormalities have been reported in literature including a diastolic and systolic dysfunction (Nemoto et al., 2006); an increase in inflammation (Becher et al., 2013); and a decrease in mitochondrial function . Furthermore, STZ-induced hyperglycaemia treated with insulin has resulted in the reversal of the diabetic cardiac phenotype (Tomita et al., 1996), suggesting the STZ rat model as a viable model for diabetes.

A number of studies have reported a failure in identifying cardiac pathologies after HFD feeding (Brainard et al., 2013a). This suggests a possibility for long-term experiments to result in compensation within the heart, possibly suggesting the change in the homeostatic properties within the heart. In this study, GENA348 mice were feeding HFD for three months. It would be interesting to compare a range of time durations, from a few weeks to a few months, in order to determine the validity of this suggestion. To assess cardiac pathologies, an echocardiography is a useful tool in research to identify morphometric hypertrophy and to provide information on cardiac function. Finally, heart failure with preserved ejection fraction (HF-PEF) is also a key aspect of consideration in diabetic heart failure (Desai and Fang, 2008).

4.1.3 Aim of study

To test this hypothesis the following aims were investigated:

1) Investigate how mitochondrial function is impacted as a result of HF feeding in both GENA348 and WT groups.

2) To investigate HFD effect upon mitochondrial protein expression, with ingenuity pathway analysis (IPA) to map the pathways that have been impacted.

3) To determine if there is evidence of inflammation under HFD condition in the wild type and GENA348 cardiac mitochondria.

4.2 Methods

GENA348 mice and aged matched WT mice were maintained on normal chow (composed of SDS) until they reached 3 months of age at which point a high fat diet was introduced (50% fat, 20% carbohydrate and 20% protein), for a further 3 months until the animals reached 6 months of age. Therefore, there were 4 experimental groups WT (chow); WT (HFD); GENA348 (chow) and GENA348 (HFD).

The methods described in Section 2.2 for biochemical analysis and mitochondrial function was carried out in the previous experimental group. However, it was not possible to directly compare the ECHO cardiac function between the GENA348 and GENA348-HFD mice as the data for the GENA348 mice was collected using different equipment.

4.3 Results

4.3.1 HFD significantly increased body weight and lung weight in both GENA348 and WT mice

A high fat diet led to increased heart weight in WT-HFD compared to controls (164.9 mg ± 3.564; *P*<0.0001; Figure. 4.1A) but in the GENA348-HFD mice, there was no change in heart weight (Figure. 4.1A). The high fat diet led to an increased body weight of WT-HFD and GENA348-HFD 47.45 g ± 1.287 (*P*<0.0001; Figure. 4.1B) and 48.98 g ± 1.225 (*P*=0.0041; Figure. 4.1B), respectively. There was no significant difference in the heart weight (HW): tibia length (TL) ratio in WT-HFD and GENA348-HFD mice compared to their control (Figure. 4.1C); a measure of cardiac hypertrophy. However, a high fat diet led to increase the lung weight in GENA348-HFD 185.3 mg ± 7.174 (*P*=0.0319; Figure. 4.1D) indicative of pulmonary congestion but with no effect on WT-HFD group. Surprisingly, high fat feeding in the WT group and GENA348-HFD did not lead to any increase in fasting blood glucose (Figure. 4.1E) but both showed a significant increase in recorded of insulin levels (4.140 ug/L ± 0.1587; *P*<0.0001; Figure. 4.1F) and (3.900 ± 0.1233 *P*<0.0001; Figure. 4.1F), respectively (Figure. 4.1F).

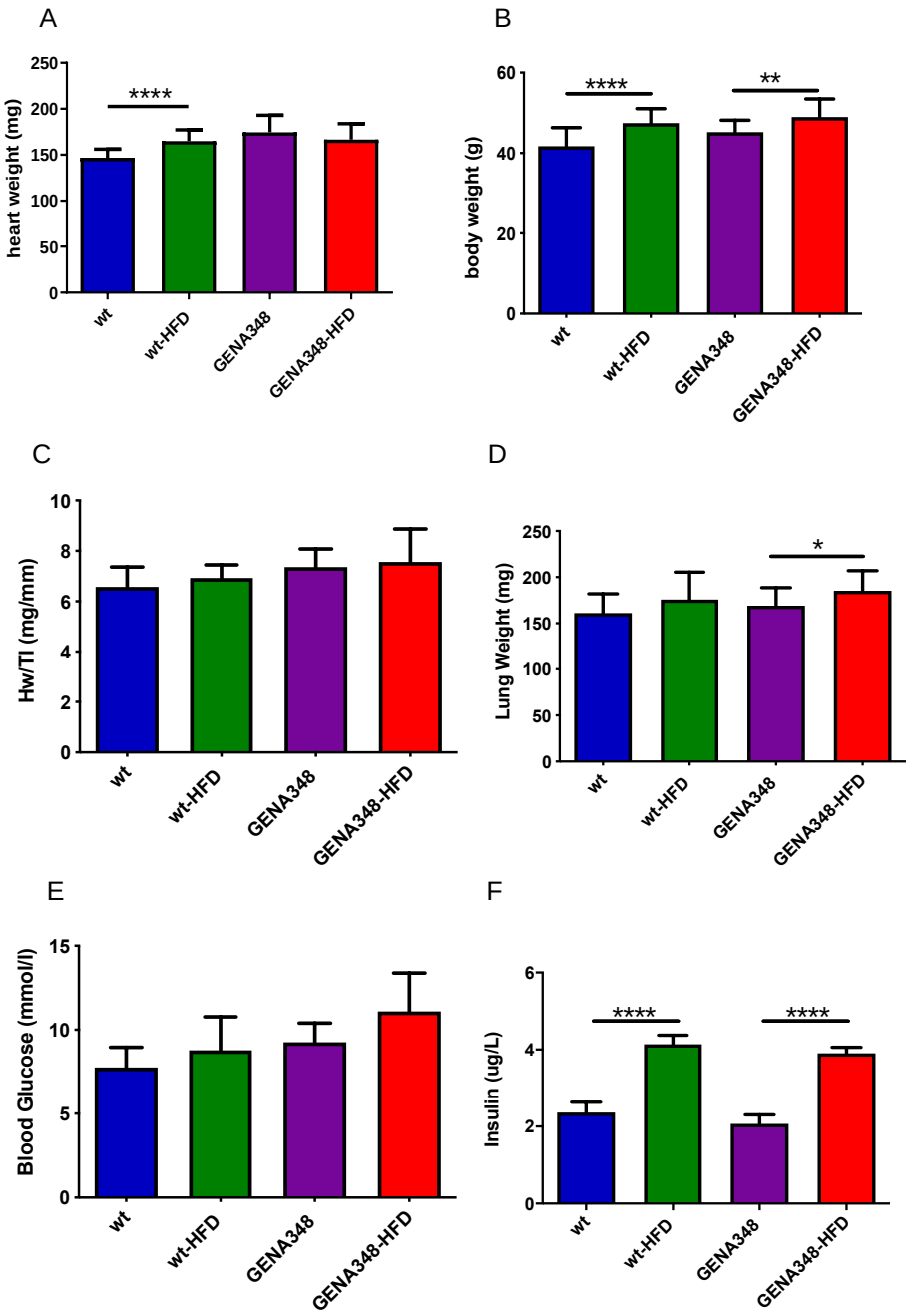

Figure 4.1 Effect of HFD on blood glucose, heart weight and body weight in WT and GENA348 mice.

(A) There was a significant increase in heart weight of WT-HFD (n=16) compared to WT (n=21) with no change in GENA348-HFD (n=15) compared to GENA348 (n=19). (B) There was a significant increase in the body weight of WT-HFD and GENA348-HFD compared to controls. (C) The ratio of HW: TL ratio showed no change in all mice group. (D) There was no change in lung weight in WT-HFD compared to control, whilst there was a significant increase in lung weight of GENA348-HFD compared to GENA348 mice. (E) There was no change in blood glucose levels of all experimental groups. (F) There was a significant increase in the insulin profile of WT-HFD (n=5) compared to WT (n=5) and an increase in GENA348-HFD (n=5) compared to GENA348 (n=6). Data is represented as the mean +/- SEM*$p \leq 0.05$ **$p \leq 0.01$ and ****$p \leq 0.0001$.

4.3.2 HFD results in increased citrate synthase activity in WT-HFD and GENA348-HFD myocardium

Citrate synthase activity in WT-HFD measured at a 1.6-fold increase compared to controls (*P*= 0.0405; Figure. 4.2). Similarly, in GENA348-HFD there was a significant 1.5-fold increase in citrate synthase activity compared to GENA348 mice (*P*= 0.0427; Figure. 4.2). Therefore, a common effect of HFD in both groups is in increased citrate synthase activity suggesting an increase in mitochondrial content.

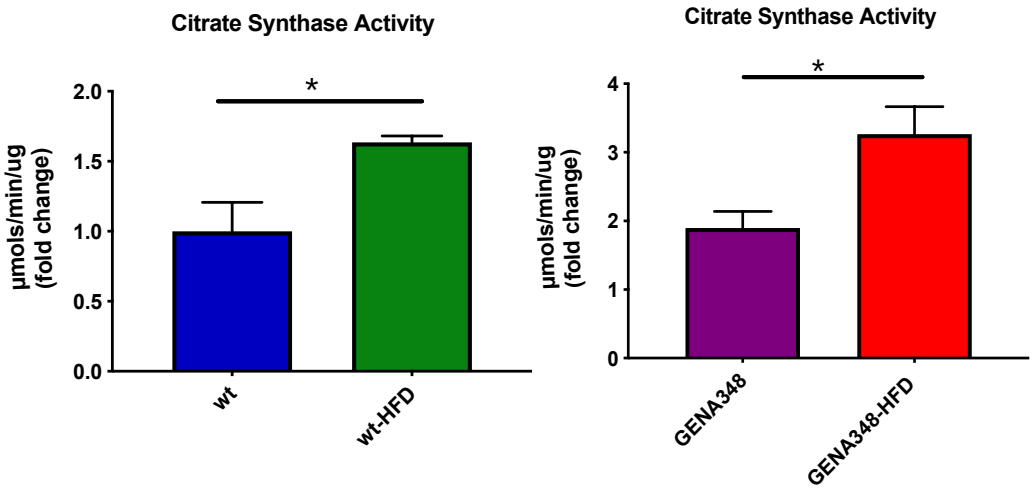

Figure 4.2 WT-HFD and GENA348-HFD myocardium exhibit an upregulation in citrate synthase activity.

Citrate synthase activity was measured as a marker of mitochondrial content revealing a significant increase in WT-HFD (n=3) compared to WT (n=3) and significant increase in GENA348-HFD (n=3) compared to GENA348 (n=3). Data is represented as mean +/- SEM *$p \leq 0.05$.

4.3.3 Increased oxygen consumption in WT-HFD and GENA348-HFD myocardium

As described in Chapter 2 we measured oxygen consumption of isolated mitochondrial fractions using a fibre optic monitoring system (Instech). We observed a linear profile in isolated mitochondria from WT-HFD mouse ventricles, taking approximately seven minutes to drop and plateau (Figure. 4.3A, green). Similarly, mitochondria from GENA348-HFD rapidly consumed O_2 and plateaued after five minutes (Figure. 4.3A, red). In order to compare oxygen consumption, the gradient between gradient between 13-9% O2 consumption was calculated in each condition. Subsequently, this value was corrected to correlate with citrate synthase levels (Spinazzi et al., 2012) to reflect the increase in mitochondrial content.

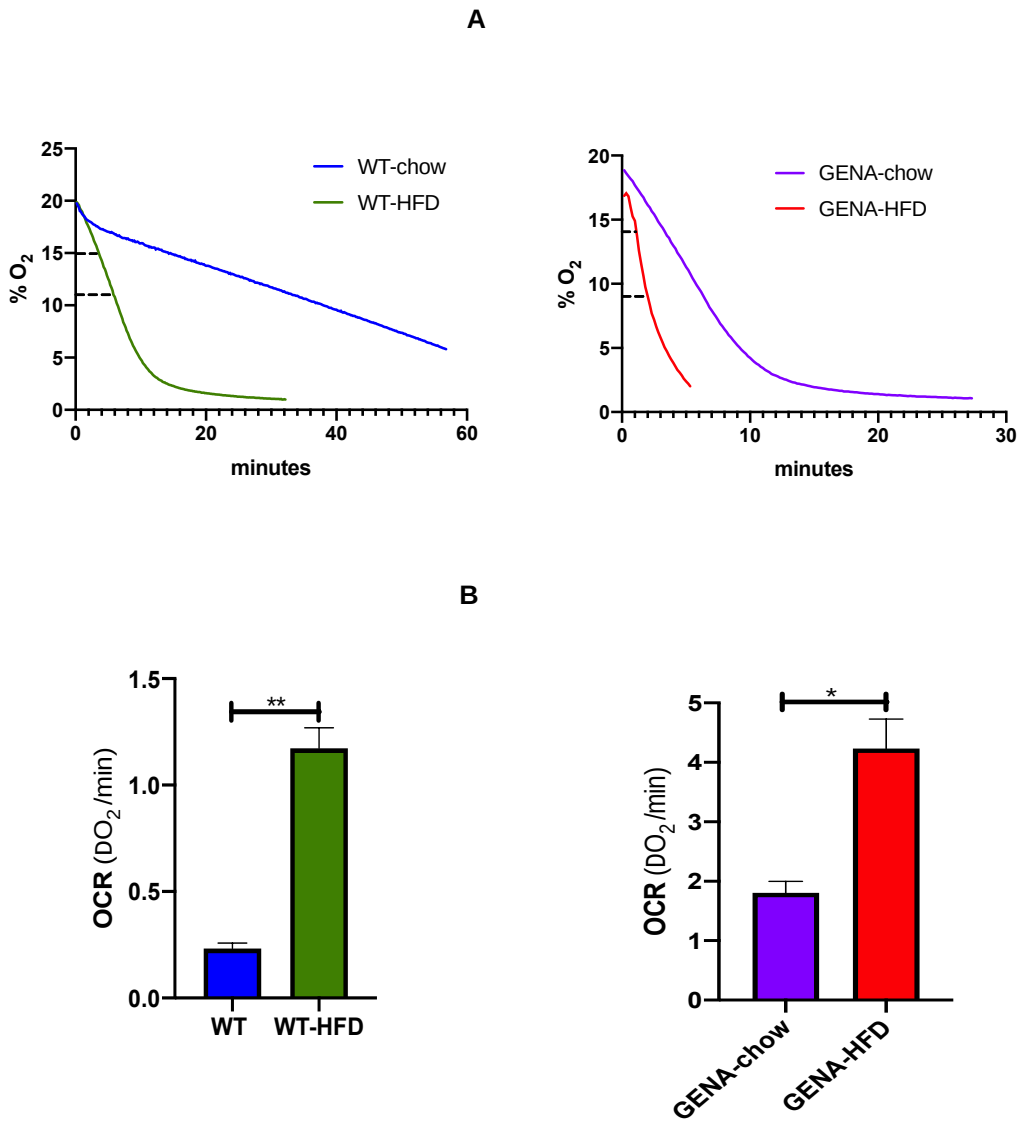

Figure 4.3 Increased oxygen consumption rate in WT-HFD and GENA348-HFD myocardium.

(A) There was a significant increase of oxygen consumption rate in WT-HFD (n=4) compared to WT (n=4). In contrast, there was a significant decrease in GENA348-HFD (n=4) compared to GENA348 (n=4) mice. (B) Representative plot showing the OCR in WT-HFD and GENA348-HFD mice after correction for citrate synthase. Data represented as mean +/- SEM ***$p \leq 0.007$and *$p \leq 0.0103$

The measured change of OCR in WT-HFD mice may be a result of increased oxygen consumption in high fat conditions, in comparison to WT-chow (Figure 4.3B). In isolated mitochondria in WT-HFD mice, OCR was 3-fold greater than controls (P=0.0002; Figure.

4.3B). A 6-fold increase in the mitochondrial oxygen consumption rate of GENA348-HFD was measured, compared to GENA348 ($P \leq 0.0001$). These results may be indicative of difunctional mitochondria in GENA348 mice and obesity. As hypothesised, this evidences the negative effects of high fat diet and diabetes on mitochondrial function.

4.3.4 Mitochondrial complex activity dysfunction in WT-HFD and GENA348-HFD

In order to further assess the activity of mitochondrial complexes, isolated mitochondria from each experimental group were investigated using an enzymatic assay. The activity of Complex I, IV and V were found to be significantly decreased; 0.6, 0.4, 0.7-fold respectively ($P<0.0001$) in WT-HFD, compared to WT (Figure. 4.4). Although not as stark, there was a significant 0.1-fold decrease of Complex II activity in WT-HFD compared to the control group ($P=0.0132$; Figure. 4.4). Similarly, Complex I, IV and V activity were significantly decreased by 0.6, 0.9, 0.6-fold espectively ($P<0.0001$) in GENA348-HFD compared to GENA348. Complex II activity was also significantly decreased 0.2-fold in WT-HFD compared to the control group ($P=0.0072$; Figure. 4.4). Mitochondrial complex results were corrected to correlate with citrate synthase data. Overall, this biochemical and functional analysis indicates that HFD causes impairment to OXPHOS and consequently ATP generation, particularly impacting Complex I, IV and V; a feature common to both the WT and GENA348 myocardium. Therefore, biochemical and functional analyses suggest that the HFD feeding results in OXPHOS impairment and consequently impacts ATP production.

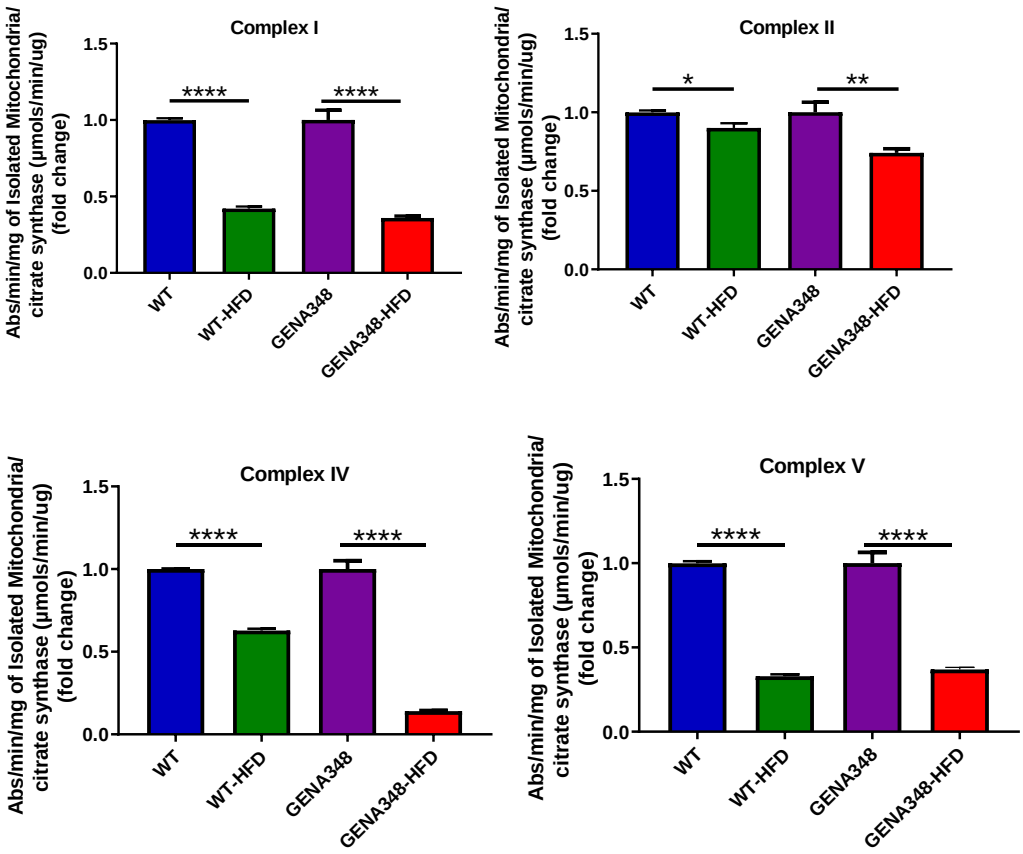

Figure 4.4 Mitochondrial dysfunction in WT-HFD and GENA348-HFD myocardium.

Function of isolated mitochondria from WT (n=5), WT-HFD (n=5), GENA348 (n=5) and GENA348-HFD (n=5) were examined using enzymatic assay. The activity of isolated mitochondria showed significant decrease in WT-HFD and GENA348 in comparison to their control group particularly Complex I, II, IV and V. Data represented as mean +/- SEM *p ≤ 0.05 and ****p ≤ 0.0001.

4.3.5 Quantitative mass spectrometry analysis of Isolated mitochondria reveals change in mitochondrial pathways

To develop a broader understanding of how mitochondria are dysregulated under the impact of a HFD, we used quantitative proteomics (Chapter 2) of isolated mitochondria in WT (n=5) and WT-HFD (n=5) mice (Methods, 2.2.11). In parallel, this comparative method was replicated in GENA348 (n=5) and GENA348-HFD (n=5) mice, further enabling the comparison of HFD on WT and GENA348 mice.

1136 proteins were identified in both WT and WT-HFD groups, with a total of 116 proteins that were up- or down-regulated in the WT-HFD mitochondria compared to WT (Figure. 4.5A). Of

the 116 proteins that were included, 60 proteins were downregulated (52%) and 56 proteins (49%) were upregulated (Figure. 4.5A). The Ingenuity Pathway Analysis (IPA) revealed an overall downregulation of proteins in WT-HFD compared to WT, suggesting widespread changes to a number of pathways regulating mitochondrial function. In correlation with the decrease in Complex activity and change to O_2 consumption rate, our proteomics revealed widespread changes to the pathways linked with mitochondrial protein degradation, apoptosis and biosynthesis. (Table 4.1) lists a number of proteins whereby a change in protein expression was identified. The majority of proteins identified were downregulated, particularly proteins with roles in motility, oxidative stress and the mitochondrial complex proteins.

Superoxide dismutase 2 (SOD2) is frequently used as a marker of oxidative stress, with the overexpression of cardiac SOD2 preventing mitochondria from undergoing oxidative stress (Kang et al., 2015). Interestingly, here, we recorded a 1.8-fold decrease in the expression of SOD in WT-HFD mice, compared to WT controls (Table 4.1), suggesting the progression of heart failure. Similarly, we recorded a 6.2-fold decrease in the protein expression of mitochondrial encoded ATP synthase membrane subunit 6 (ATP6), a Complex V-related protein (Table 4.1. ATP6 mutations are known to result in a substantially lowered capacity for ATP production (Ješina et al., 2004; Nijtmans et al., 2001). The magnitude of the downregulation of this protein in the WT-HFD suggests that mitochondrial dysfunction may result from an impact of Complex V as a result of altered ATP production capability.

Other proteins impacted by the HFD condition were proteins involved in fatty acid metabolism. Some of these proteins were upregulated, whilst others were downregulated. For example, pyruvate dehydrogenase kinase 4 (PDK4) was upregulated in WT-HFD mice by 11.3-fold, a marker of increased fatty acid oxidation (Pettersen et al., 2019). PDK4 has been suggested to be a sensitive marker of increased mitochondrial fatty acid oxidation, indicating a metabolic shift from glucose to fatty acids for energy fuel (Pettersen et al., 2019), similar to that which would be expected in a HFD. In contrast, glutathione peroxidase 4 (GPX4) was downregulated in WT-HFD mice by 1.6-fold. GPX4 is a protein known for its role in protecting cells from iron-dependent necrosis, ferroptosis (Stockwell et al., 2017). Ferroptosis has been reported as

implicated in cardiac diseases and the downregulation of GPX4 during myocardial infarction is linked to eventual heart failure (Park et al., 2019). Again, this suggests that HFD conditions result in impacted protein expression levels of key players responsible for maintaining healthy cellular processes.

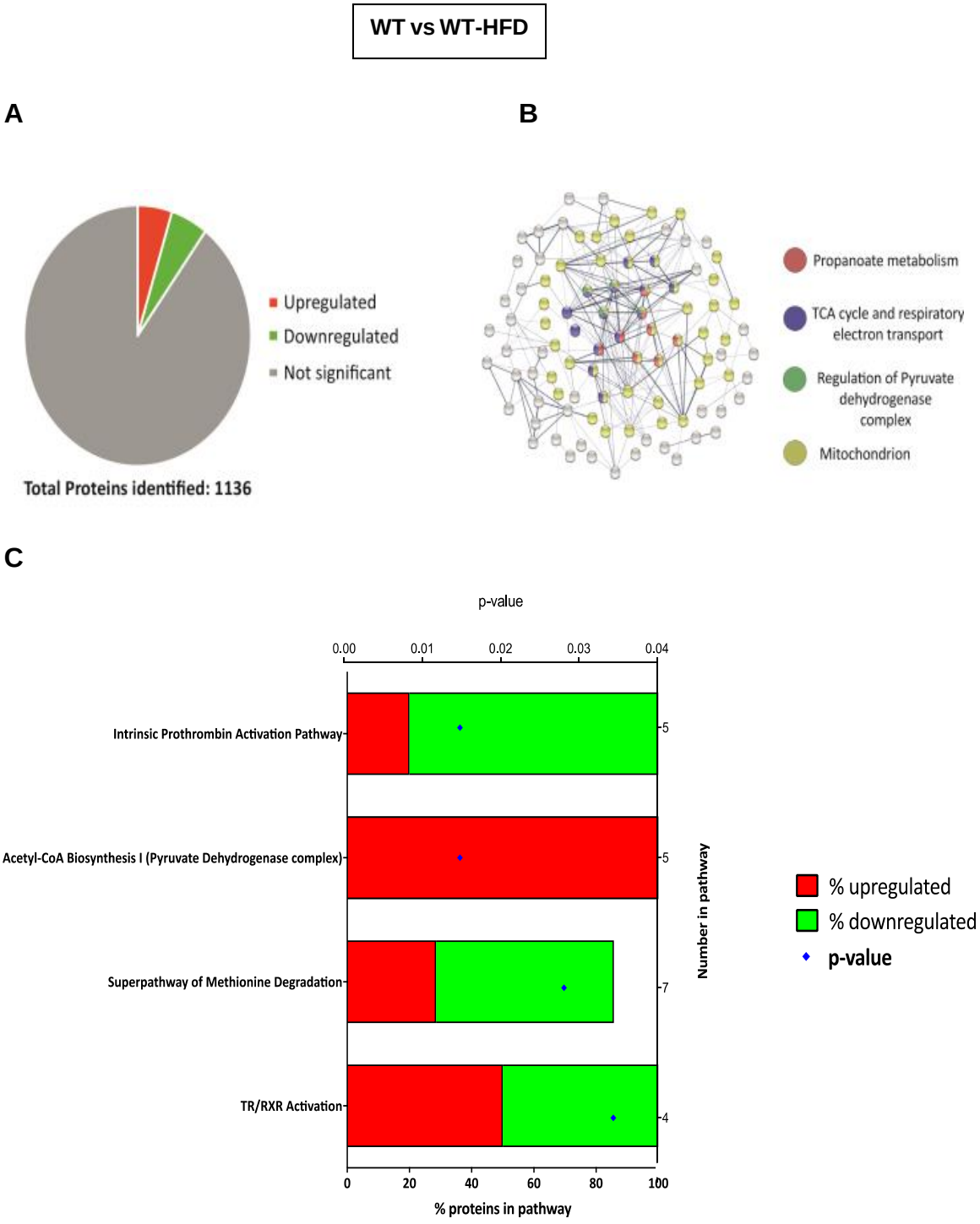

Figure 4.5 Mass spectrometry analysis of WT-HFD mice in comparison to WT.

(A) Pie chart illustrating the 1136 proteins identified, approximately 10% of the mitochondrial proteome were altered, with the majority down regulated. (B) STRING Network analysis presents significantly altered protein networks ($p<0.05$). (C) Ingenuity Pathway Analysis (IPA) revealed eight protein network pathways that are significantly altered, organised by P-value (x-axis). Each bar represents the percentage of proteins in each pathway (x-axis) that are up-regulated (red) or down-regulated (green). The total number of proteins within each pathway can be read from the right-hand Y axis.

Table 4.1 Mitochondrial dysfunction pathway protein expression changes from quantitative MS in wild type-HFD mice

Role	Protein	Accession Number	Peptide count	Unique peptide	P Value	Fold Change
Complex I	NDUFA4	NDUA4_MOUSE	9	9	0.0292	1.6
Complex II	COX15	COX15_MOUSE	6	5	0.0300	1.8
Complex V	ATP5L	ATP5L_MOUSE	7	6	0.0245	1.4
	ATP6	A0A0F6PZ10_MOUSE	3	2	0.0160	6.2
Oxidative Stress	SOD2	SODM_MOUSE	5	5	0.0008	1.8
Fatty Acid metabolism	APOE	APOE_MOUSE	6	4	0.0002	3
	CBR4	CBR4_MOUSE	6	4	0.0336	1.4
	CPT1A	CPT1A_MOUSE	15	9	0.0451	1.6
	GPX4	Q3TI34_MOUSE	6	5	0.0221	1.6
	HMGCL	HMGCL_MOUSE	4	3	0.0375	1.5
	PCCB	A0PJE6_MOUSE	7	6	0.0404	1.5
	PDK4	PDK4_MOUSE	2	2	0.0069	11.3
	UCP1	UCP1_MOUSE	7	5	0.0198	3.1
	UCP3	B2RTM2_MOUSE	4	3	0.0474	1.7
Motility	MIRO1	MIRO1_MOUSE	9	3	0.0251	1.8

Note. Fold change in red- increase, fold change in blue- decrease

In the GENA348 vs GENA348-HFD investigation, 1134 proteins were identified in each group and 203 proteins were either up or down regulated in the GENA348-HFD mitochondria compared to in the GENA348 (Figure. 4.6A). A significantly number of proteins were upregulated 177 proteins (87%), whilst 26 proteins (13%) were downregulated (Figure. 4.6A).

Ingenuity Pathway Analysis revealed an overall increase of protein expression identified in GENA348-HFD compared to GENA348, suggesting widespread changes to a number of pathways regulating mitochondrial function in HFD conditions (Table 4.2). An in-depth analysis of the proteomics revealed changes in proteins involved in oxidative stress, decreased Complex II activity and fatty acid metabolism.

The pathway with the greatest number of proteins identified was the cardiac hypertrophy signalling and phospholipase C signalling pathways (Figure 4.6C). The cardiac hypertrophy pathway has 29 proteins that were modified, of which, the majority were upregulated. Two G-protein subunits were identified as upregulated; GNAS (G-protein α-subunit) and GNB2 (G Protein Subunit B 2) were measured at 2.1-fold and 1.8-fold upregulated, respectively. The G-protein signalling pathway is involved in interacting with stimulated adrenoceptors and angiotensin II receptors that initiate intracellular signalling cascades, controlling cardiovascular pathways (Farfel et al., 1999; Frey et al., 2008). Through the identification of single-nucleotide polymorphisms, Wieneke et al. (2016) showed that the GNAS gene was associated with an increased risk of heart disease. Furthermore, a GNB2 gene mutation has been linked to sinus node dysfunction (SND) and atrioventricular block (AVB) (Stallmeyer et al., 2017). Using genome analysis mapping, the authors mapped the disease locus to the GNB2 gene, suggesting that its dysregulation is a factor for heart failure. On the other hand, our results showed apoptosis-inducing factor mitochondrion-associated 1 (AIFM1) downregulated by 2.3-fold (Table 4.2). Normally, AIFM1 is found tethered to the IMM and is involved in ATP production (Susin et al., 1999). Mutations in AIFM1 has been reported to be involved in mitochondrial diseases, thus, result in metabolic defects and severe myopathy (Wischhof et al., 2018). In one study, the targeted deletion of AIFM1 has been shown to be protective against obesity and diabetes (Pospisilik et al., 2007). The authors ablated muscle- and liver-specific AIFM1 to further investigate the link between mitochondrial OXPHOS and insulin resistance. Results showed that ablated mice had patterns of OXPHOS deficiency, increased insulin sensitivity and reduced fat mass (Pospisilik et al., 2007), evidencing the importance of AIFM1 function in the progression of heart failure.

All identified proteins related to oxidative stress were upregulated (Table 4.2), including catalase, which increased activity 3.2-fold in GENA348-HFD mice compared to GENA348 controls. Catalase is an important protein that is present in cardiac mitochondria and protects insulin-producing cells from ROS oxidative injury. It has been reported that its overexpression of catalase can protect against cell death and mitigates the impact of inflammation (Gurgul et al., 2004). As mentioned above, Complex II-related proteins were observed to have resulted in down-regulation in GENA348-HFD mice. Both succinate dehydrogenase A and C (SDHA/SDHC) proteins were downregulated in GENA348-HFD mice by 1.3-fold and 1.5-fold, respectively (Table 4.2). Inherited SDHA gene defects are a known cause of mitochondrial disease, leading to cardiomyopathy (Alston et al., 2012). Complex II is involved in both the Krebs cycle and the respiratory chain, suggesting that impaired function would result in a magnified impact on mitochondrial function.

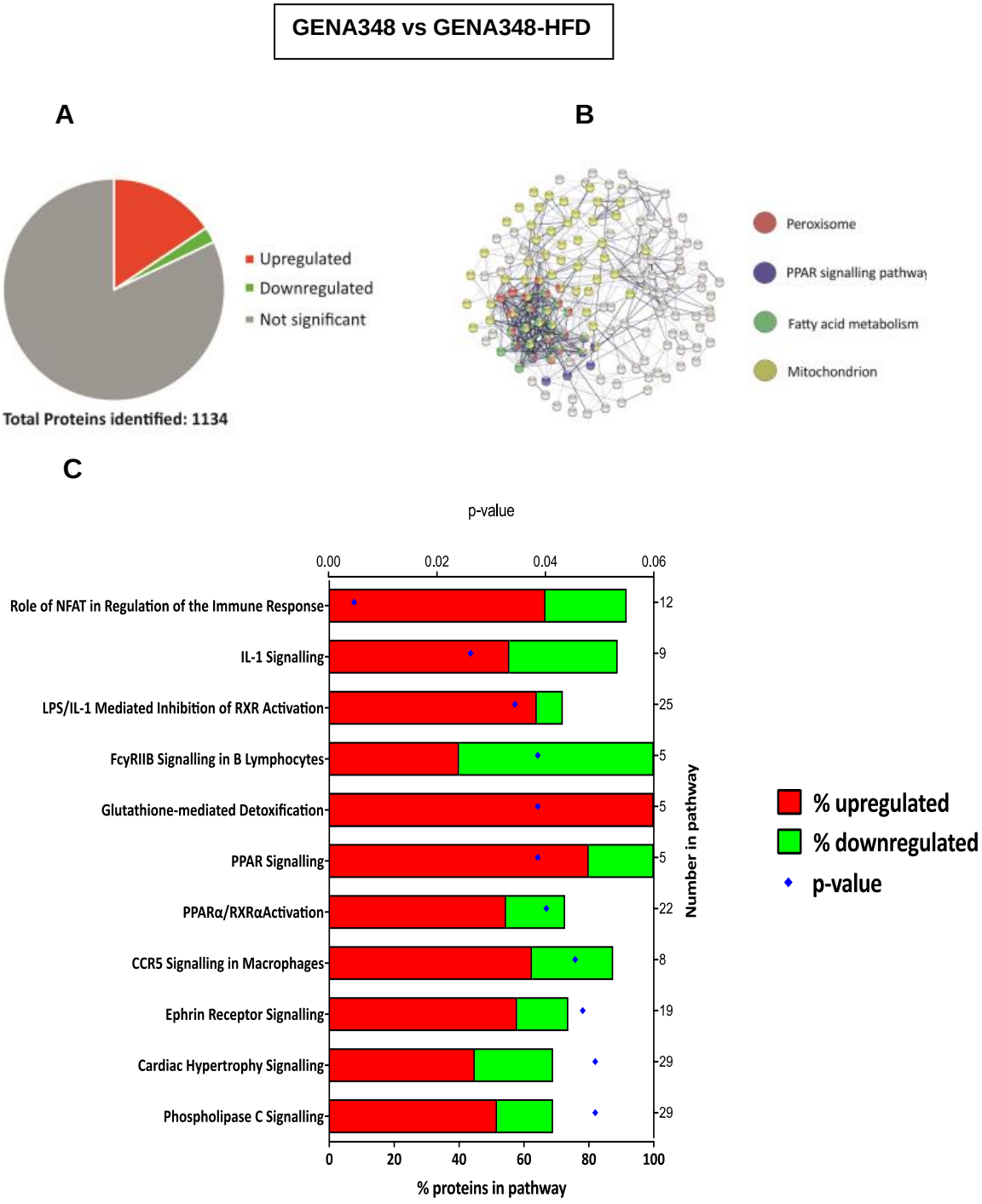

Figure 4.6 Mass spectrometry analysis of GENA348-HFD protein compared to GENA348.

(A) Chart to illustrate 1134 proteins identified. 18% of the mitochondrial proteome were altered, with the majority of proteins downregulated (87%). (B) STRING Network analysis highlights significantly altered proteins networks ($p<0.05$). (C) Ingenuity Pathway Analysis reveals 17 significantly altered protein pathways organised by P value (top x-axis). The bars detail the percentage of proteins within each pathway (bottom x-axis) that are upregulated (red) or downregulated (green), The total number of proteins within each pathway is listed on the right-hand y-axis.

Table 4.2 Mitochondrial dysfunction pathway protein expression changes from quantitative MS in GENA348 mice vs GENA348-HFD.

Role	Protein	Accession Numb	Peptide count	Unique peptide	P Value	Fold Change
Complex II	SDHA	SDHA_MOUSE	42	35	0.0386	1.3
Oxidative Stress	catalase	Q3TVZ1_MOUSE	17	6	0.0015	3.2
	ALDH5A1	SSDH_MOUSE	6	5	0.0106	1.5
	ACOX3	ACOX3_MOUSE	5	3	0.0095	2.9
	prohibitin-2	PHB2_MOUSE	17	14	0.0353	1.5
	CAT	CATB_MOUSE	4	4	0.0089	1.7
Fatty Acid Metabolism	ACAA1	SYTL4_MOUSE	6	2	0.0236	1.9
	ACAA2	TIM8A_MOUSE	3	3	0.0027	1.8
	ACSL1	ETFA_MOUSE	21	17	0.0138	1.5
	ACSL1	ACSL1_MOUSE	54	36	0.0139	1.6
	ACSL5	ACSL5_MOUSE	6	2	0.0032	3.42
	CPT2	CPT1A_MOUSE	15	9	0.0024	1.8
	CPT1A	ITPR1_MOUSE	15	4	0.0020	1.9
	CPT1B	NOMO1_MOUSE	5	4	0.0314	1.3
Cardiac Hypertrophy Signalling	GNAS	STOM_MOUSE	6	3	0.0017	2.1
	GNB2	ACADV_MOUSE	53	44	0.0199	1.8
	Calm1	MORC1_MOUSE	6	2	0.0249	1.9
	Myl10	PHB2_MOUSE	17	14	0.0353	1.5
	Aifm1	MYL9_MOUSE	8	2	0.0477	2.3

Note. Fold change in red- increase, fold change in blue- decrease

Regarding mitochondrial proteins with a role in regulating dynamics, no change was recorded to levels of Mfn1, Mfn2, Opa1 or the receptors for Drp1 Fis1 and MiD49 in both WT-HFD or GENA348-HFD conditions. As previously mentioned, Drp1 was not detected, possibly due to its solubility and the mitochondrial isolation process. Interestingly, Miro1 (Rhot1) was significantly downregulated in the WT-HFD mouse mitochondria by 1.8-fold (p=0.0251) (Table 4.1), whilst no change was recorded in GENA348-HFD mice. It appears that Miro1 is impacted in GENA348, however, this downregulation disappears in HFD feeding conditions. Further analysis of the data revealed no change to the abundance of Trak1, Trak2, Kif5b, dynein light chain 2 and Kif5A. This data indicated that the HFD impacts proteins involved in motility in WT mice, however, the diabetes GENA348 model appears to have protected Miro1 from this change.

4.3.6 HFD impacts fusion and fission proteins in WT-HFD and GENA348-HFD myocardium

To investigate changes in expression levels of fusion and fission proteins in WT-HFD and GENA348-HFD myocardium, ventricular tissue was lysed for Western blot. There was no difference in expression of Mfn1 in the GENA348-HFD compared to the GENA348 mice (Figure. 5). There were also no identified changes of Mfn1 protein expression in WT-HFD and WT-GENA348, consistent with MS data. In contrast, there was a 1.4-fold increase in Mfn2 (P=0.0364) in the WT-HFD myocardium compared to controls and no change in Mfn2 levels in GENA348-HFD compared to GENA348 (Figure. 4.7). For both the inner membrane fusion protein Opa1 and the fission protein Drp1, there was no changes to their expression when comparing HFD to WT controls (Figure. 4.7). Therefore, whilst Mfn1, Mfn2 and Opa1 proteins were elevated in the GENA348 compared to WT controls (Chapter 2, Figure. 2.10), HFD did not yield the same changes in expression of fusion-fission proteins.

As previously stated, MS results differed with Western blotting protein expression levels of Mfn2 in WT-HFD, whereas Mfn1/Opa1 results were the same and Drp1 was undetected. This data suggests that HFD has not led to other changes to expression levels of fission-fusion

proteins. In contrast, high fat feeding of the WT mice led to an increase in Mfn2 protein expression (Figure. 4.7).

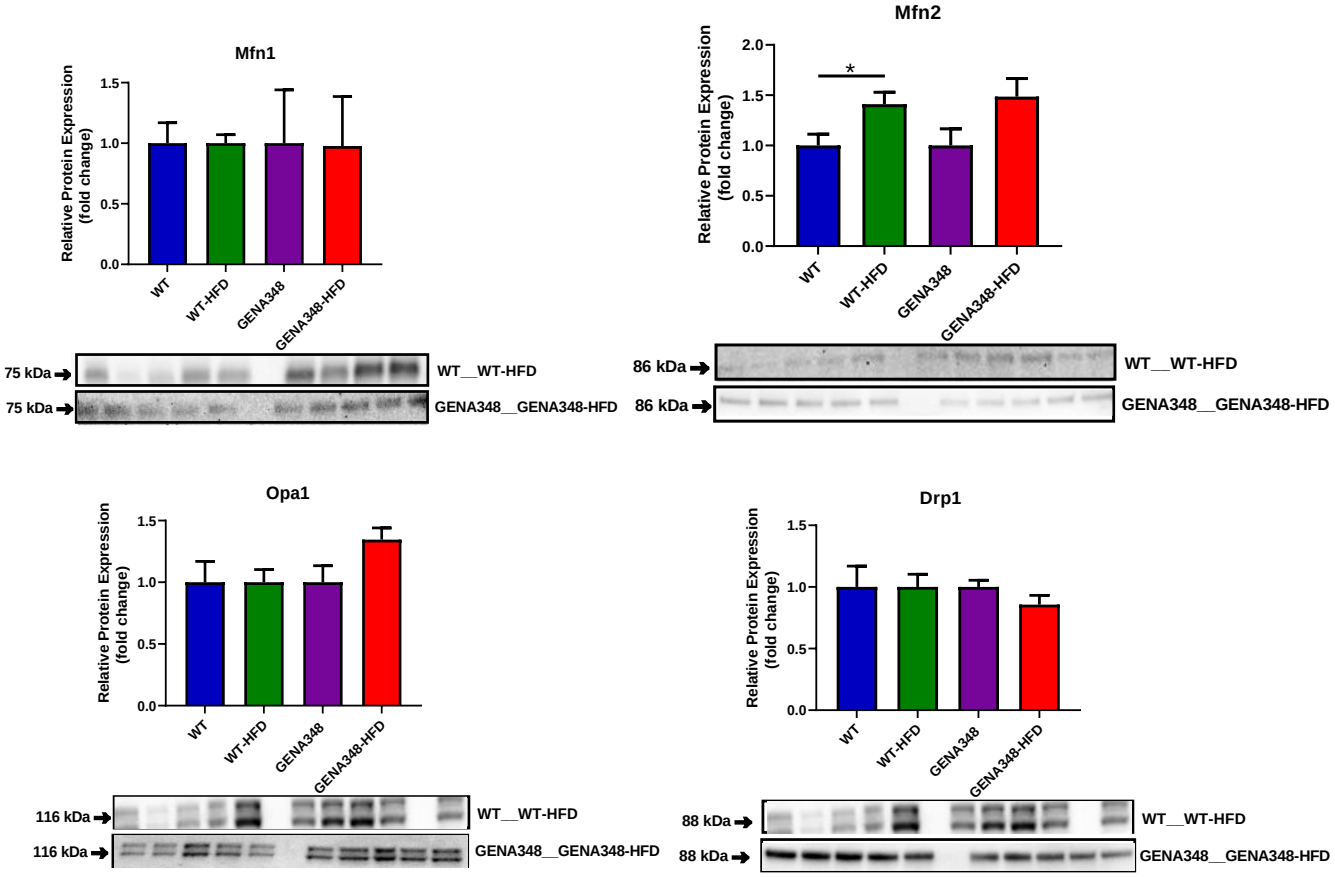

Figure 4.7 WT-HFD myocardium exhibits significant upregulation of Mfn2 protein expression.

Western blot analysis of LV from control (n=5) and WT-HFD (n=5) revealed a significant increase in WT-HFD in comparison to WT, whilst no change was recorded in protein expression of Mfn1, Opa1 or Drp1 in WT-HFD or GENA348-HFD (n=13). Data represented as mean +/- SEM *$p \leq 0.05$.

Similarly, there was no difference in Miro1 expression in GENA348-HFD compared to GENA348 mice (Figure. 4.8). In contrast, Miro1 protein expression was significant 0.4-fold downregulation in GENA348 compared to WT (Chapter 2, Figure. 2. 11) this is in agreement with MS data (Table 2.9).

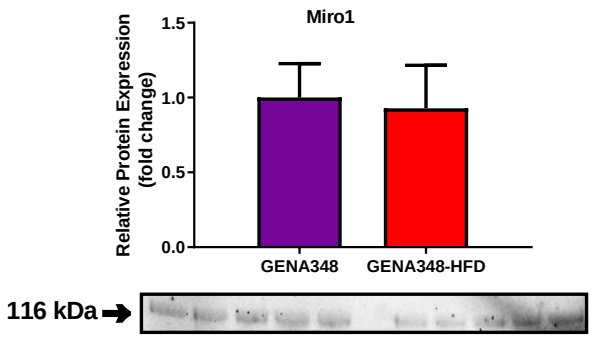

Figure 4.8 Miro1 level in GENA348-HFD myocardium.

Western blot analysis of LV revealed no change in Miro1 expression in GENA348-HFD compared to GENA348 (n=5) mice. Data represented as mean +/- SEM *$p \leq 0.05$.

Further analysis of proteins regulating mitochondrial mitophagy, namely PINK1 and Parkin, also had no change in protein expression between the WT and WT-HFD or GENA348 and GENA348-HFD (Figure. 4.9). In comparison, while there was no change to PINK1 protein expression, Parkin was significantly downregulated in GENA34 compared to WT showed (Chapter 2, Figure. 2.12). This suggests that a HFD does not exasperate mitochondrial degradation pathways, whilst it appears that in the diabetes model of GENA348, there is an impact in this pathway.

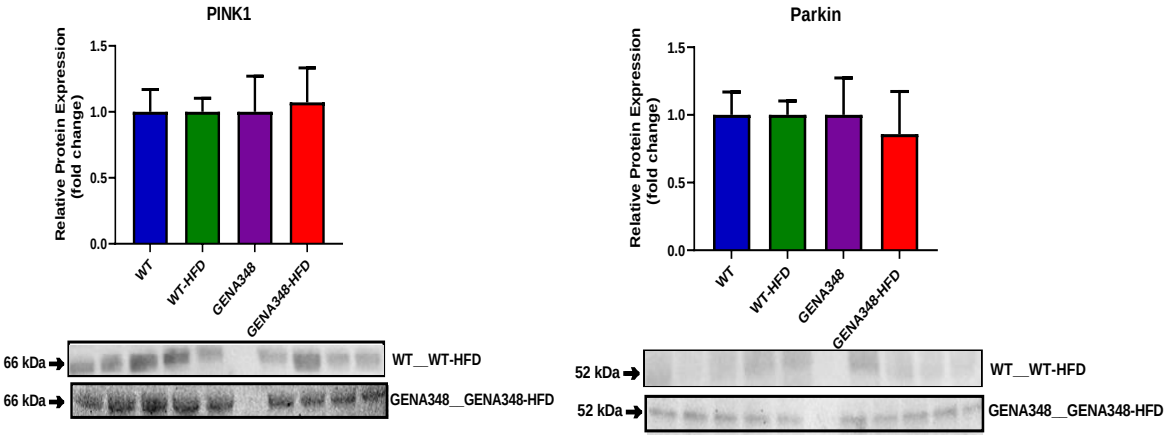

Figure 4.9 PINK1 and Parkin protein expression in WT, WT-HFD, GENA348 and GENA348-HFD myocardium.

Western blot analysis of LV revealed no change in the experimental group. Data are represented as mean +/- SEM.

4.3.7 Protein transcript levels of mitochondrial dynamics proteins in HFD myocardium

To correlate changes of protein expression of with gene transcript levels, qPCR was run. There was a 2.4-fold increase in Mfn1 expression in WT-HFD compared to WT (*P*=0.0005: Figure. 4.10). This disagrees with protein expression data and MS whereby no change in expression levels was recorded (Figure. 4.7). This could be to do with the sensitivity in the different methods used. Similarly, a 1.3-fold increase was found for Mfn2 mRNA in WT-HFD compared to WT (*p*=0.0051). This data is in agreement with protein expression (Figure. 4.7) but differs from MS results. There was also a 2.8-fold increase of Opa1 mRNA in WT-HFD compared to WT (*p*=0.0017), again differing with western blot data. Lastly, no change was previously recorded in Drp1 protein levels (Figure. 4.7), gene expression levels (Figure. 4.10), or MS results. Although there was a difference in GENA348 compared to WT controls, consistently, there was no change in gene expression of any fission-fusion protein in GENA348-HFD, compared to controls.

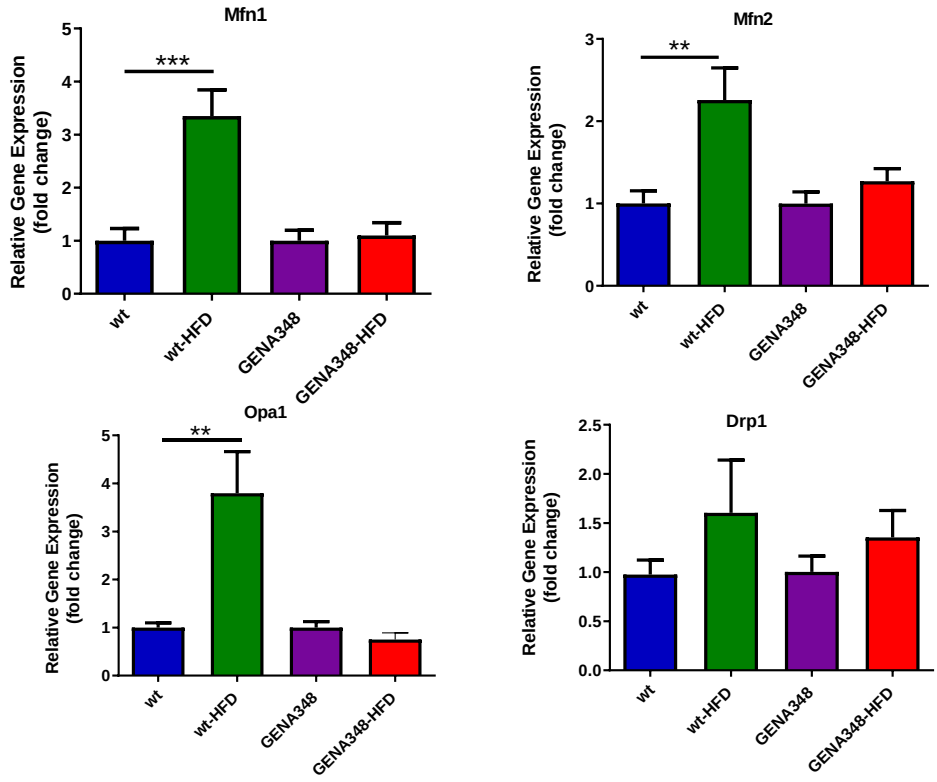

Figure 4.10 Upregulation in fusion transcript expression in WT-HFD Myocardium.

Mfn1, Mfn2 and Opa1 transcript level were assessed using qPCR and revealed a significant increase in the transcript level in WT-HFD (n=6) compared to WT (n=6) myocardium with no significant difference in transcript level of Drp1. There was no change in the fusion or fission gene expression in GENA34-HFD. Data represented as mean +/- SEM $**p \leq 0.01$ and $***p \leq 0.001$.

For both PINK1 and Parkin gene expression, there was a 0.2-fold and 0.3-fold decrease in the WT-HFD myocardium compared to the control group (P=0.0157, P=0.0054), respectively (Figure. 4.11). Furthermore, there was no change in gene expression of PINK1 or Parkin in GENA348-HFD compared to GENA348 myocardium. A reduction in PINK1/Parkin in the WT myocardium would possibly explain the increase in Mfn2, since they are involved in ubiquitinating Mfn2 for degradation.

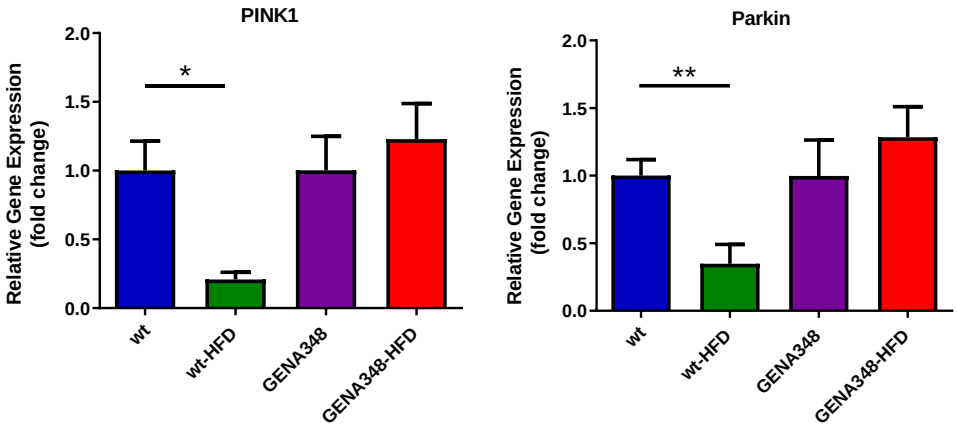

Figure 4.11 Downregulation of PINK1 and Parkin gene transcript in WT-HFD myocardium.

PINK1 and Parkin transcript level were assed using qPCR and revealed a significant decrease in WT-HFD (n=6) compared to control (n=6) with no change in PINK1 and Parkin in GENA348-HFD (n=6) compared to GENA348 (n=6). Data is represented as mean +/- SEM, *$p \leq 0.05$ and **$p \leq 0.01$.

4.3.8 Upregulation of mitochondrial biogenesis marker transcripts in the WT-HFD myocardium

High fat feeding resulted in an increase of PGC-1α and TFAM transcripts in WT-HFD compared to a control group with a 1- and 2.7-fold increase (P=0.0029 and P=0.0002), respectively. There was no effect on GENA348-HFD; it appears the increase in GENA348 and HFD removed this increase (Figure.4.13).

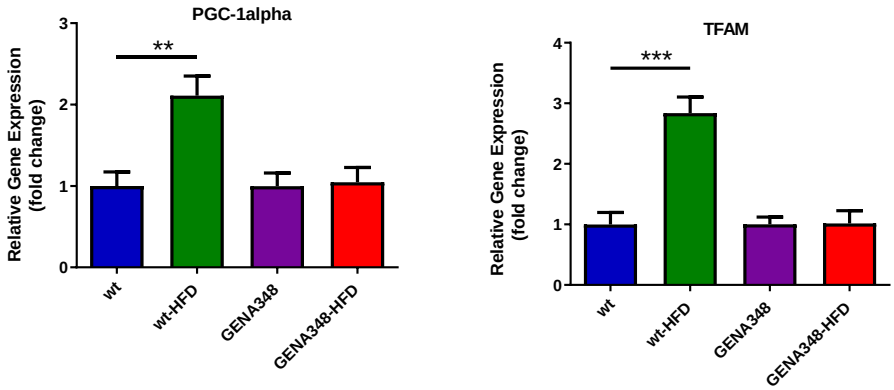

Figure 4.12 WT-HFD myocardium exhibit upregulation in the gene expression of PGC-1α and TFAM.

PGC-1α and TFAM transcript level were assed using qPCR and revealed a significant increase in WT-HFD (n=6) compared to control (n=6) with no effect on GENA348-HFD compared to GENA348. Data represented as mean +/- SEM ** $p \leq 0.01$ and *** $p \leq 0.001$.

In agreement with proteomics, there was a 0.3-fold decrease of Miro1 transcript levels in WT-HFD compared to controls (*P*=0.0255). Similarly, in agreement with MS data there was no change to mRNA levels of TRAK1, KIF5A and KIF5B in WT-HFD compared to WT mice (Figure. 4.12). There was a significant increase in the Miro1 transcript level in GENA348-HFD compared to GENA348 mice (1.7-fold, *P*= 0.0234), This result differs from MS and western blot, while there was no difference in TRAK1, TRAK2, KIF5A and KIF5B (Figure. 4.12). Transcript levels generally indicate the presence of the protein and the level that it can be expected to be found. Thus, a highly abundant protein would have a highly expressed mRNA. The differences here could be explained by the protein being controlled by its activation and not on its level of gene expression.

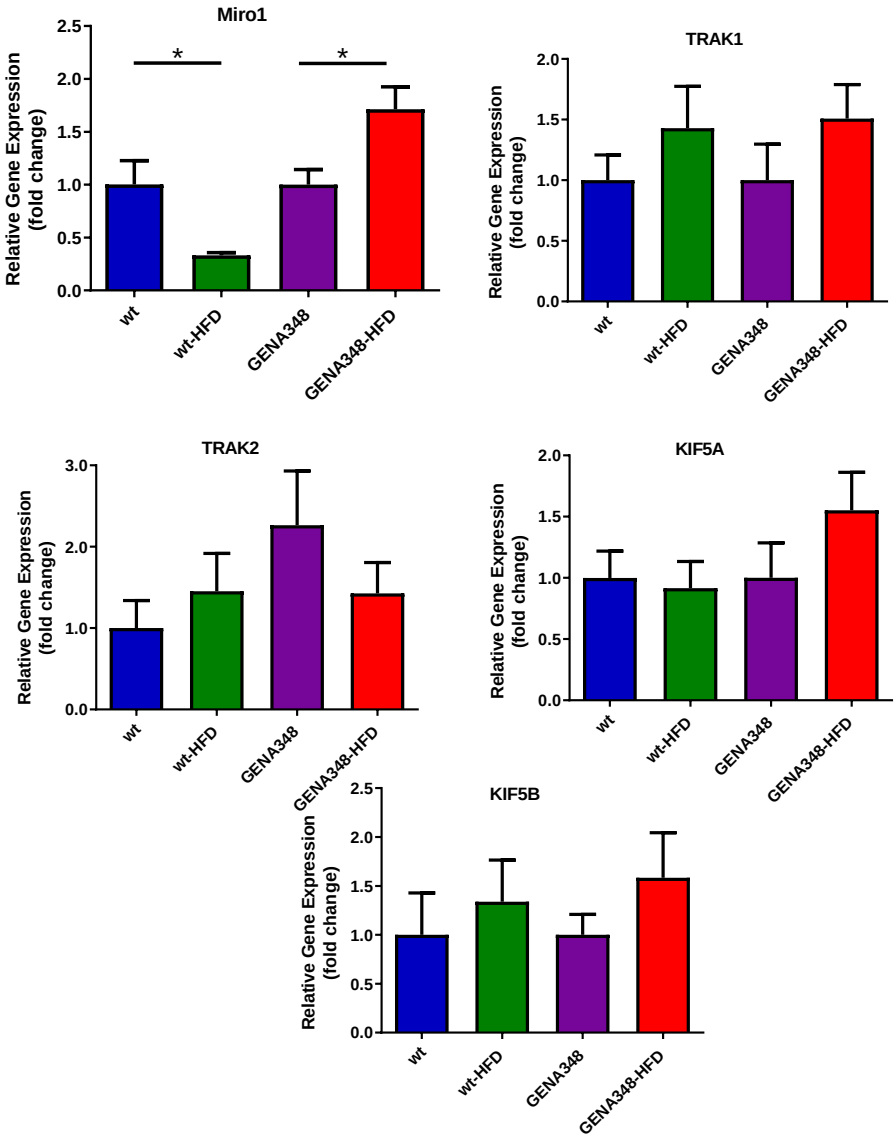

Figure 4.13 WT-HFD myocardium exhibit downregulation of Miro1 and upregulation in GENA348-HFD.

Miro1, TRAK1, TRAK2, KIF5A and KIF5B transcript level were assed using qPCR and revealed a significant decrease in Miro1 in WT-HFD (n=6) compared to control (n=6) with significant increase in GENA348-HFD (n=6) compared to GENA348 (n=6) with no significant difference in TRAK1, TRAK2, KIF5A and KIF5B in the experimental group. Data represented as mean +/- SEM *p ≤ 0.05.

4.3.9 Upregulation of inflammatory cytokines in high fat fed myocardium

To assess changes in inflammatory cytokines (IL-1β, IL-6 and TNF-α), gene expression levels of cytokines were measured in control, HFD mice, GENA348 and GENA348-HFD. Gene expression levels of IL-1β were increased by 2.3-fold in WT-HFD compared to WT, whilst no change was measured in GENA348-HFD compared to GENA348 (Figure. 4.14). High fat

feeding led to a 3.4-fold increase in IL-6 WT-HFD compared to control and a 2-fold increase in GENA348-HFD compared to GENA348 (P=0.0032; Figure 4.14 and P=0.0064; Figure. 4.14), respectively. TNF-α gene expression was increased by 3.1-fold in WT-HFD (P=0.0031), compared to WT with no change in GENA348-HFD compared to GENA348.

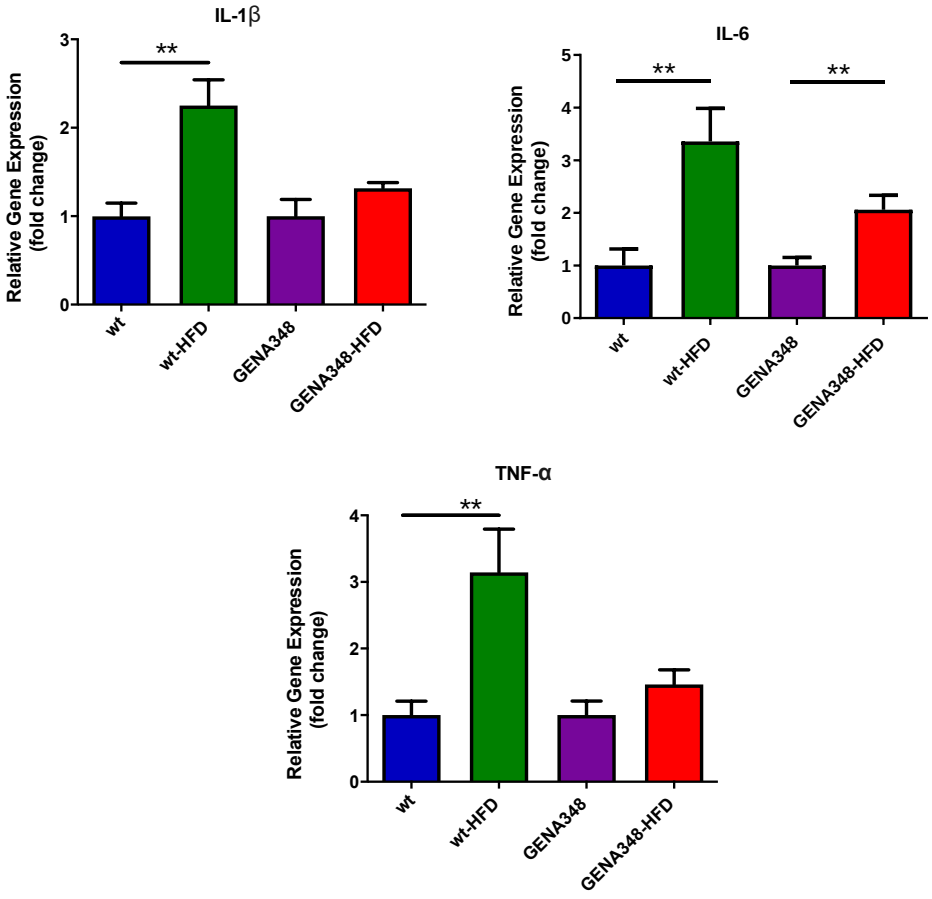

Figure 4.14 Upregulation of Inflammatory cytokines in WT-HFD myocardium.

IL-1β, IL-6 and TNF-α transcript level were assed using qPCR and revealed a significant increase in WT-HFD (n=6) compared to control (n=6) with significant increase in IL-6 in GENA348-HFD (n=6) compared to GENA348 with no change IL-1 and TNF-α. Data represented as mean +/- SEM **$p \leq 0.01$.

4.4 Discussion

We previously reported changes to mitochondrial function, protein expression of mitochondrial dynamic regulation and increased levels of inflammatory cytokines in the GENA348 myocardium, a mouse model for MODY2 diabetes (Chapter 2). A major cause for diabetes is obesity, thus, to further elucidate the impact of obesity on mitochondrial homeostasis and cardiac function, we investigated the same physiological parameters, proteomics, cellular function and levels of inflammatory markers, as that described in Chapter 2, in high fat fed mice in both the WT and GENA348.

The key findings of a HFD on the background of WT mice compared to normal chow include: (1) A significantly larger heart weight, body weight and lung weight in HFD mice compared to WT; (2) Clear evidence of increased oxygen consumption rates, although Complex activity in HFD conditions appears significantly reduced; (3) Some change in expression of proteins involved in mitochondrial fission-fusion, particularly in Mfn2 and Miro1; (4) Lastly, all inflammatory cytokines were significantly upregulated in WT-HFD. We then compared a HFD on the background of GENA348 compared to normal chow. The key findings include: (1) While the GENA348-HFD has significantly larger body weight and lung weight compared to GENA348, there was no change to heart weight or the HW:TL ratio; (2) Clear evidence of reduced OXPHOS activity and changes to oxygen consumption through diminished Complex activity in HDF conditions; (3) Lastly, only the IL-6 inflammatory cytokine was significantly upregulated in GENA348-HFD, whilst IL-1β and TNF-α remain unchanged.

4.4.1 High fat fed mice have impaired cardiac function

To study the impact of cardiac function in high-fat fed conditions, we measured a number of physiological factors (Figure. 4.1), citrate synthase activity (Figure. 4.2), oxygen consumption rate (Figure. 4.3) and run proteomics to determine changes in mitochondrial function that may lead to heart failure (Figure. 4.5). These physiological measurements were heart weight, body weight, HW:TL and lung weight. These measurements were first used to quantify cardiac hypertrophy in ageing rats (Yin et al., 1982). Tibia length is thought to stay constant after

maturity, providing an accurate measurement for changes in heart weight in relation to tibia length. Our results showed that heart weight was significant increase in WT-HFD mice compared to WT, whereas this was not mirrored in GENA348-HFD mice. Furthermore, body weight was significantly greater in both WT-HFD and GENA348-HFD compared to their respective controls. This correlates with a number of studies that show that a HFD leads to increased body weight, and leads to disease severity, such as diabetes (Droz et al., 2017). A higher body weight can also impact on heart function, leading to an increased risk of heart failure (Sardu et al., 2019). The HFD also led to an increase in lung weight in GENA348-HFD compared to controls. For the future plan, echo data will be collected for comparison, however, it was not possible during the timescale of this project due to issues with machinery.

As previously mentioned, changes to citrate synthase are associated with increased mitochondrial activity. Oxygen consumption rate measurement found that GENA348-HFD mice consumed more oxygen, compared to GENA348 mice, over time. This may suggest that mitochondria 'burn out', rapidly consuming O_2 as a result of dysfunction mitochondrial complex activity, impacting OXPHOS rates. We report a significant decrease in complex activity (I, II, IV and V) in all HFD conditions, both in WT and GENA348 (Figure. 4.4). This is corroborated by proteomics, whereby all identified complex proteins were significantly downregulated (Table 4.1 and Table 4.2). Chen et al. (2018) investigated the impact of a HFD on the respiratory chain complex in rat myocardial tissue, showing dramatically reduced complex activity and abnormal expression of genes involved in mitochondrial dynamics. The authors also compared mitochondrial morphology in HFD mice to control groups and noticed obscured striation, lower mitochondrial density and fewer cristae in the IMM (Chen et al., 2018). Although mitochondrial morphology was not completed in our study, the impaired OXPHOS rates could be a result of defected mitochondrial synthesis of fully assembled complexes, reflected by the severe change to complex activity in HFD conditions. Due to time limitations, EM data for the HFD group were not analysed, rather, pushed forward as a future plan.

In addition to HFD mice, reduced complex activity has been implicated in mouse models of obesity, whereby mitochondrial dysfunction is responsible for reduced cardiac performance.

Boudina et al. (2005) measured cardiac function, mitochondrial respiration and ATP synthesis in *ob/ob* mice. The authors reported a reduction in protein expression of complex I, III and IV, suggesting this impairment contributes towards decreased myocardial energetics and efficiency in obesity (Boudina et al., 2005). With support of our data, this shows that obesity causes impairment of the mitochondrial complexes, which are crucial to the normal functioning of the heart and impairment results in metabolic inefficiencies.

Studies have also suggested that a change in OCR in high fat-fed hearts may be explained by mitochondrial metabolism (Murray et al., 2008). It has been reported that increased protein levels of mitochondrial uncoupling proteins (UCP3) is associated with elevated free fatty acid concentrations. This suggestion is supported by our proteomics data whereby UCP3 and UCP1 were identified as proteins that were significantly upregulated in WT-HFD mice by 1.7- and 3.1-fold, respectively (Table 4.1). Furthermore, UCP3 levels in T2DM heart of rodent models are also reported to be elevated (Murray et al., 2008). As the final product of OXPHOS is ATP, it would be interesting to investigate ATP content and ATP:ADP ratio in our model to further understand the metabolic impact on mitochondria of a high fat-fed diet. OCR rates and complex dysfunction suggests the existence of multiple pathways involved.

Obesity is a chronic hypoxic condition associated with reduced nitric oxide (NO) bioavailability (Rajapakse et al., 2016). As mentioned earlier, biochemical studies showed catalase was increased 3.2-fold in the GENA438-HFD mice (Table 4.2). Increased fatty acid oxidation enhances mitochondrial H_2O_2 production, requiring an increased catalase concentration to mitigate the excessive production (Rindler et al., 2013), suggesting that catalase protects against damage against toxic ROS. It has also been reported that catalase can protect against proinflammatory cytokines (Gurgul et al., 2004). Gurgul et al. (2004) showed that overexpression of catalase was able to prevent the cytokine-induced inhibition of glucose oxidation, reducing the high rate of cell death observed without catalase. In addition, a number of cardiac hypertrophy signalling proteins were found to be upregulated in the GENA348-HFD mice in comparison to GENA348 (Table 4.2). Interestingly, calmodulin (CALM1) was identified as upregulated 1.9-fold. CALM1 is involved in the functioning of crucial calcium channels that

mediate excitation contraction coupling of the human heart (Liu et al., 2015). Liu et al. (2015) investigated 20 SNPs associated with sudden cardiac death in Chinese patients with heart failure and coronary heart disease. Of these, DNA variants located within functional regions of CALM1 were found linked to sudden cardiac death. In our data, we found that there was an increase in CALM1 expression, suggesting that the HFD resulted in similar outcomes to that of heart failure, although its exact association would require further investigation. Furthermore, myosin light chain 10 (MYL10) was also identified as upregulated 1.5-fold in GENA348-HFD data (Table 4.2). Again, MYL10 has been reported as associated with cardiomyopathy (Alcalai et al., 2008).

Oxidative stress and mitochondrial dysfunction are involved in the pathogenesis of different diseases. When the antioxidant pathways of the body become exhausted and incapable of removing the reactive oxygen species (ROS) then oxidative stress happens. ROS can damage cellular lipids, proteins and DNA, which in turn causes cellular dysfunction and organ damage. Mitochondrial dysfunction, as a secondary outcome of pathophysiology of the disease, results in increased production of ROS along with damage to cellular energy production (Stepien et al., 2017). Dysfunction of mitochondria may result in free radical-induced oxidative damage or damage by lethal metabolites which accumulate in different metabolic disorders (Orio et al., 2016). Overall, this shows that obese patients are at risk of cardiac dysfunction, irrespective of a diabetic co-morbidity.

4.4.2 Increased insulin resistance in GENA348-HFD myocardium

Insulin levels in high fat-fed mice were significantly higher, compared to controls (Figure. 4.1F). GENA348 mice are hyperglycaemic compared to WT (Chapter 2). Here, we show that HFD results in insulin resistance, known to be linked to cardiac dysfunction and progression to heart failure. In the presence of prolonged excess fatty acid oxidation, mitochondrial oxidative stress and damage leads to abnormal cardiac function (Lopaschuk et al., 2010). The role of cardiac insulin sensitivity in obesity and the impact of excess fatty acids on cardiac function has been much debated in literature. As mentioned, in humans, obesity has been traditionally associated with worsened cardiac mitochondrial function (Niemann et al., 2011), however

accumulating evidence suggests that the adaptation to fatty acid oxidation may afford the heart some protection during heart failure, preventing the worsening of cardiac function after high fat feeding (Stanley et al., 2012). Therefore, we suggest that perhaps a similar effect of HF feeding of the GENA348 mice has occurred here.

Insulin is thought to impact mitochondrial function through the repression of PDK4, an inhibitor of the pyruvate dehydrogenase complex (Kim et al., 2006). This inhibition enhances oxidative decarboxylation of pyruvate to acetyl-coenzyme A, for use in the Krebs cycle (Kim et al., 2006). Interestingly, we identified PDK4 as a protein that was highly significantly upregulated in WT-HFD mice 11.3-fold, compared to chow fed WT mice (Table 4.1). Gupte et al. (2013) investigated the impact of high-fat feeding-induced hyperinsulinemia on cardiac mitochondrial function. After feeding with a Western HFD, mice were analysed for insulin tolerance, cardiac function and mitochondrial content (Gupte et al., 2013). Their results showed that cardiac glucose uptake and mitochondrial function were enhanced in response to high-fat feeding. This study shows that hyperinsulinemia preserves mitochondrial function, presenting an alternative theory for the differences in mitochondrial function observed in HFD conditions to WT chow-fed mice. The obesity paradox also describes the discrepancy between OCR and HF prognosis (Artham et al., 2007). In some cases, patients with chronic HF and obesity show an improved survival compared to normal weight patients (Horwich et al., 2018). In fact, recently, it was shown that weight loss was unfavourable in non-obese patients without T2DM (Niedziela et al., 2019), suggesting that hyperglycaemia may afford some protection against heart failure in diabetic obese patients. This appears to be an increasingly reported finding in literature (Brainard et al., 2013b).

4.4.3 Expression of proteins involved in mitochondrial dynamics in HFD

Previously, we showed a change in fission-fusion protein expression levels (Chapter 2) in response to GENA348. In this chapter, we investigated the same proteins in HFD conditions using a number of experimental methods. The expression of genes involved in mitochondrial dynamics was measured using qPCR and Western blot. Proteomic analysis was also performed to identify the proteins affected by HFD treatment. These results could show that

the ability to reverse the changes measured in GENA348 are not feasible, or that the impact of fission-fusion proteins cannot deteriorate further. By comparing GENA348-chow to WT-HFD, we can see that the fission-fusion profile appears similar in both our obesity (WT-HFD) and diabetes (GENA348-chow) models, suggesting a common pathological development. However, it should be noted that this profile is inconsistent in the combined diabetes-obesity (GENA348-HFD) model. Further analysis of the data is discussed below.

4.4.3.1 Mfn1

In the Western blot results, Mfn1 did not differ in WT-HFD compared to WT and there was also no change in GENA348-HFD compared to GENA348 (Figure 4.7). In comparison, qPCR data showed an increase in Mfn1 in WT-HFD compared to the controls, with no change in GENA348-HFD compared to GENA348 (Figure 4.10). Western blot data was consistent with our mass spec results. This noncorrelation between transcript and protein levels could suggest tight post-translation regulation. Interestingly, in literature, Mfn1 knockout mice have demonstrated a preference for the use of lipids as the predominant energy source (Kulkarni et al., 2016). Furthermore, the authors showed that mitochondrial complex I appeared more active in these knockouts, protecting against insulin resistance. Combined with our findings, these observations suggest that mitofusins may be important for the control of mitochondria in both diabetes and obesity.

4.4.3.2 Mfn2

In our Western blot results, Mfn2 increased in WT-HFD compared to WT and there was no change in GENA348-HFD compared to GENA348 (Figure 4.7). Similarly, qPCR data showed an increase in Mfn2 in WT-HFD compared to the controls, with no change in GENA348-HFD compared to GENA348 (Figure 4.10). Here, Western blot data and qPCR were not consistent with our mass spec results. Mfn2 has been associated with mitochondrial and endoplasmic reticulum function; Mfn2 has been reported as impaired in HFD conditions (Chen et al., 2018). Chen et al. (2018) aimed to investigate the molecular mechanism behind the association of HFD and heart failure. To this aim, the authors used male rats and fed them with HFD for 28 weeks followed by measurements of genes involved in mitochondrial dynamics. Chen et al.

(2008) also measured the expression of myocardial genes involved in mitochondrial dynamics in rats fed with HFD and showed altered expression. In comparison to our data, the authors reported a significant decrease in mitochondrial fusion proteins in the HFD group, whereas a significant increase was reported in fusion proteins, such as Drp1 (Chen et al., 2018). Furthermore, in addition to abnormal mitochondrial morphology, it has been reported that Mfn2 (not Mfn1) directly interacts with perilipin 1, a lipid droplet-associated protein. In comparison to Mfn1, our observations may suggest a more important role of Mfn2 in mitochondrial dynamics and is particularly impacted in conditions of obesity or diabetes.

4.4.3.3 Opa1

In our Western blot results, Opa1 has no change in WT-HFD compared to WT and no change in GENA348-HFD compared to GENA348 (Figure 4.7). However, qPCR data showed an increase in Opa1 in WT-HFD compared to the controls, with no change in GENA348-HFD compared to GENA348 (Figure 4.10). Here, Western data was consistent with the mass spec results, but differed from qPCR data. In the literature, Opa1 has been implicated in both obesity and diabetes. Opa1 regulates lipolysis through translocating from the mitochondria to lipid droplets (Rogne et al., 2018), after which it is cleaved by the protease Oma1 (Quirós et al., 2012). This is in addition to mediating fusion of the IMM to complete fusion of the two smaller mitochondria into one. In mice, a deficiency in Oma1 has shown to cause perturbation of the mitochondrial fission-fusion pathway, a reduction of OXPHOS, enhancement of fatty acid oxidation that eventually leads to obesity (Quiros et al., 2012). Similar to that reported in this chapter, increased insulin levels have been shown to result in increased Opa1 (Parra et al., 2014). Here, the authors reported that increased insulin promoted mitochondrial fusion in cardiomyocytes, resulting in enhanced OXPHOS (Parra et al., 2014), suggesting a unique regulating pathway between mitochondrial metabolism in obesity and diabetes. Our data shows that insulin appears to affect mitochondrial dynamics in cardiomyocytes given that in the WT model there was no change to glucose levels.

As described in the main introduction Opa1 is also thought to be involved in the stabilisation of mitochondrial cristae, with the formation of Opa1-S through cleavage of Opa1-L, associated

with mitochondrial disorganisation and cristae disarray (An et al., 2013). Furthermore, neonatal cardiomyocytes cultured in high glucose concentrations were shown to reduce expression of both Opa1 and Mfn1, associated with fragmented mitochondria (Makino et al., 2011). Thus, it would be interesting to collect electron microscopy data of WT-HFD and GENA348-HFD to assess if the diet is associated with mitochondrial morphology abnormalities that may be resultant of Opa1 changes.

4.4.3.4 Drp1

In our Western blot results, Drp1 has no change in WT-HFD compared to WT and no change in GENA348-HFD compared to GENA348 (Figure 4.7). Similarly, qPCR data showed no change in Drp1 in WT-HFD compared to the controls, with no change in GENA348-HFD compared to GENA348 (Figure 4.10). Here, Western data was consistent with qPCR results. On the other hand, mass spec did not identify Drp1 in its analysis which is not surprising given that it is a soluble protein localised to the cytosol unless actively bound the mitochondrial OMM receptors Fis1, Mff, MiD49/51. These data may suggest that increased fission is not upregulated in the myocardium, as a result of obesity. In a recent study, Hu et al. (2020) investigated the role of Drp1 in mice fed HFD for signs of lipid-overload and its involvement in cardiomyocyte function. After 18 weeks of HFD, mice developed signs of obesity and T2DM. Interestingly, Drp1 appeared activated in mouse hearts as a result of HFD suggesting that Drp1 has an important role in mediating lipid overload in heart failure (Hu et al., 2020). Here, however, we did not record any differences in Drp1 in HFD-fed conditions, although it should be noted that there are some notable differences in the feeding protocols, mice strain and data maybe dependent upon the length of high fat feeding and the balance between early cardioprotective adaptations and the switch to pathological remodelling.

4.4.3.5 PINK1 & Parkin

In our Western blot results, PINK1 & Parkin had no change in WT-HFD compared to WT and no change in GENA348-HFD compared to GENA348 (Figure 4.7). qPCR data showed a decrease in both in WT-HFD compared to the controls, with no change in GENA348-HFD compared to GENA348 (Figure 4.10). Here, Western data differed to our qPCR results. As

prior mentioned, mitochondrial health is managed through PINK1-Parkin mediated mitophagy. Protein levels of both remain the same in GENA348-HFD mice, compared to GENA348 controls (Figure. 4.9 and Figure. 4.11). This may suggest an accumulation of dysfunctional mitochondria through the restriction of the PINK1-Parkin facilitated mitophagy pathway. It is known that oxidative stress, LV dysfunction, cardiac hypertrophy, and mitochondrial dysfunction all occur due to the reduction of PINK1 (Zhao et al., 2018).

4.4.3.6 Miro1

In our Western blot results, Miro1 showed no change in GENA348-HFD compared to GENA348 (Figure 4.8), however, unfortunately there is no data to compare WT-HFD with WT due to a time constraint and a lack of sufficient lysate. For those completed Westerns, results were consistent with mass spec data. qPCR reflected an increase in mRNA of miro1 in GENA348-HFD compared to GENA348 and reduction of Miro1 in WT-HFD compared to the control (Figure 4.13). Our data for Miro1 poses a number of questions.

As previously discussed, Miro1 is an important protein that acts as a switch at the centre of mitochondrial regulation. It plays a myriad of roles that coordinate cellular processes, including regulation of microtubule motor proteins within the mitochondria (Eberhardt et al., 2020). In our data, we notice a significant decrease in Miro1 associated with WT-HFD; the condition of obesity. In contrast, the GENA348-HFD condition appeared to result in the opposite, a significant increase in Miro1. These data support that obesity as a cause of mitochondrial dysfunction which may be in part due to impaired trafficking/motility of mitochondria. Notably Miro1 was down regulated in the GENA348 (chow) model; perhaps the increase in the GENA348 (HFD) is reflective of the obesity paradox with an attempt to rescue the levels of Miro1. The increase in Miro1 may be suggestive of the increased need of mitochondria to move along microtubules to attempt the regulation of mitochondrial dynamics in this condition. It is also possible that Miro1 up-regulation in the GENA348-HFD model is as a result of an aggravated inflammatory response (Figure 4.14).

4.4.3.7 PGC1-α and TFAM

The results showed an increase in both PGC1-α and TFAM mRNA in WT-HFD compared to WT, whereas no change was recorded in GENA348-HFD compared to GENA348 (Figure 4.12). There have been some studies that have investigated the link between HFD and mitochondrial biogenesis, suggesting that the attenuation of mitochondrial dysfunction during the development of diabetic cardiomyopathy occurs through the increase of mitochondrial turnover (Tong et al., 2019). To investigate mitochondrial turnover in diabetic cardiomyopathy, Tong et al. (2019) measured mitophagy markers to associate its increase or decrease with mitochondrial quality control mechanisms in the heart during HFD consumption. The authors showed that downregulation of mitophagy induces cardiac hypertrophy and dysfunction in response to HFD. Using a mitophagy-activating injection, Tong et al. (2019) measured levels of PGC1-α and TFAM; interestingly, levels of both did not change, however NRF1 (nuclear respiratory factor), another mitochondrial biogenesis marker, were significantly upregulated in response to the injection. Similarly, the activation of mitophagy in HFD-induced diabetic cardiomyopathy was reported as early as three weeks after the start of HFD in mice (Rabinovich-Nikitin et al., 2019). Here, during the early stages of diabetes, mitophagy appeared to be diminished, suggesting an alternative pathway for the removal of damaged mitochondria during T2DM.

4.4.4 Inflammatory cytokines in the GENA348-HFD myocardium

Our results show a significant increase in inflammatory marker gene expression, IL-6, IL-1β and TNF-α, in WT-HFD compared to WT. In comparison, our data shows an upregulation of only IL-6 in both HFD conditions, WT and GENA348 mice (Figure. 4.14). IL-6 is involved in lipid metabolic homeostasis, whereby it was first reported that IL-6 deficiency results in the development of mature-onset obesity (Wallenius et al., 2002). Furthermore, it has been shown that the overexpression of IL-6 in obese mice results in decreased body weight through the reduction of fat mass (Ma et al., 2015). In the heart, there is a precise balance between fatty acid uptake and β-oxidation, ensuring that the accumulation of fatty acids in the myocardium is prevented. This control is unbalanced in obesity (Goldberg et al., 2012). Excessive fatty acid

accumulation results in lipotoxicity, causing cell injury and eventual cardiac dysfunction. In this cycle, it is thought that IL-6 may be cardioprotective. IL-6 deficiency has been shown to upregulate CD36, a key carrier protein of fatty acids across the plasma membrane, thus, increasing its uptake and accumulation, aggravating lipotoxicity (Angin et al., 2012). In addition to this, IL-6 deficiency has been shown to impact mitochondrial OXPHOS, through the reduced expression of mitochondrial cytochrome c (cyto c), a key hemeprotein involved with the ETC (Bonda et al., 2016). In this study, the authors showed that a HFD reduced expression of cardiac cyto c in WT and IL-6 null mice (Bonda et al., 2016). Interestingly, this decrease was greater in IL-6 null mice, possibly suggesting that IL-6 protects cardiac cells from mitochondrial dysfunction (Bonda et al., 2016). Although not completely understood, it is thought that the IL-6 deficiency reduces PGC-1α, inhibiting mitochondrial biogenesis and decreasing OXPHOS as a result of decreased mitochondrial function. This could link and explain our earlier data whereby citrate synthase activity was altered in both HFD conditions (Figure. 4.4).

The level of inflammatory biomarker IL-6 was found to be increased in GENA348-HFD mice and thus as discussed before might suggest that the HFD to an extent has triggered rescue mechanisms rather than exacerbated the GENA348 phenotype. Interestingly TNF-α was not elevated in the GENA348-HFD compared to GENA348 (chow) but was in the WT-HFD model (Figure. 4.4). It is known that elevated levels of TNF-α are associated with T2DM. Elevated levels of TNF-α have also been linked to a HFD (Kesherwani et al., 2015). In addition, our results also showed an increase in IL-1β in WT-HFD compared to WT, but no change in GENA348-HFD compared to GENA348 (Figure 4.14). Previous studies have also shown that IL-1β expression is induced in the infarcted heart, whereby it may play a role in cardiac remodelling (Bujak et al., 2008). More recently, Geng et al. (2019) reported obesity-induced lipid overload impacts the production of ROS, leading to cardiac inflammation and oxidative stress. The authors identified fibronectin type III domain containing 5 (FNDC5), a lipolysis enhancer, as protective against such inflammation in the heart. In fact, a deficiency of FNDC5 appeared to worsen HFD-induced cardiac hypertrophy in mice (Geng et al., 2019), through the aggravation of the inflammatory pathways. Here, we also note an increase in the three

investigated inflammatory markers in WT-HFD, compared to WT alone, further supporting the detrimental role of inflammatory markers on the heart in obesity and diabetes.

4.5 Conclusion

The objective of this chapter was to investigate the effect of a high fat diet (HFD) upon the cardiac and mitochondrial function of the GENA348 mouse model, with the aim to reveal additional pathogenic consequences that obesity exasperates in MODY2 patients. Firstly, we conclude that a common pathological development is apparent in the GENA348-chow mice in comparison to WT-HFD, suggesting a similar pathophysiology in obesity and MODY2 diabetes. Secondly, although no significant difference was apparent between GENA348 and GENA348-HFD mice according to the fission-fusion proteomics, there were significant decreases in all mitochondrial complexes in all HFD mice, suggesting that obesity impacts mitochondrial function in ways yet to be understood through this work. This could be a common feature of the general pathology, initially presenting during hyperglycaemia and worsen during hyperinsulinemia. Surprisingly, there were also some indications that the ‘obesity paradox’ to an extent may be at work in the GENA348-HFD model.

Chapter 5 Inflammatory cytokines and mitochondrial function

5.1 Introduction

Increasing evidence has shown that diabetes can be classified as an inflammatory disease. In animal models, increased inflammation is a cardiac abnormality characteristic of diabetes. In diabetes Type 1 STZ-induced mice, Becher et al. (2013) reported significant impairment of cardiac function associated with an increase in cardiac CD3+ and CD8a+ immune cell invasion and fibrosis. Furthermore, in chronic HF in mice, CD4+ T-cell activation leads to disease progression (Bansal et al., 2017). Similarly, in Akita mice, an attenuation of IL-10 contributes to diabetic cardiomyopathy (Chavali et al., 2014). In Akita mice, animals develop hyperglycaemia as a result of a mutation in the Ins2 gene, causing proinsulin misfolding, aggregation and ultimately, β cell failure (Yoshioka et al., 1997). Chavali et al. (2014) investigated the localisation of TNF-α, indicating its hypertrophic cardiomyocyte localisation suggests a relationship between TNF-α and cardiac hypertrophy. In *db/db* mice (Papinska et al., 2015) and ZDF animal models (Jadhav et al., 2013), supression of inflammatory markers act as a protective mechanism against diabetic cardiomyopathy.

5.1.1 Inflammation and Mitochondrial Dysfunction

The mitochondria have a wide range of physiological roles, including inflammation, homeostasis, cell proliferation, cell death, cell signaling, metabolism, regulation of inflammatory responses, and the control of innate and adaptive immunity (Missiroli et al., 2020). The mitochondria also play a significant role in regulating pro-inflammatory signaling mediated by cytokines such as TNF-α, IL-1, IL-6, IL-12, IL-18, and IFNγ (Missiroli et al., 2020). Pro-inflammatory signaling alters the functioning of the mitochondria as they increase mitochondrial oxidative stress and promote a vicious cycle of inflammation. In particular, IL-6 has a role in neuronal reactions to injuries, while macrophages and monocytes produce IL-1 in response to infections, antibody-antigen reactions, and tissue damage. The TNF-α is involved in regulating apoptosis in different cells and is key in different signaling pathways.

Studies have shown that TNF-α impedes the oxidative phosphorylation of the mitochondria and ATP production, thereby instigating the production of reactive oxygen species (ROS) (Horssen, Schaik, and Witte, 2019). The increased accumulation of the ROS alters the dynamics of the organelles and result in mitochondrial membrane permeabilization, reduced cytoplasmic levels of NAD+ and potassium concentration, aberrant calcium mobilization, and cell death. Alterations to mitochondrial autophagy also result in the release of the mitochondrial contents into the extracellular environment and cytosol (Lopez-Armada et al., 2013: Cruz and Kang, 2018 & Sandhir, Halder and Sunkaria, 2017). This further promotes inflammation through the activation of inflammasomes such as caspase-1 that is involved in the activation of pro-inflammatory cytokines contribute to the development of inflammation and pathophysiological conditions (Horssen, Schaik and Witte, 2019: Gurung, Lukens and Kanneganti, 2015). The chronic inflammation that results from the mitochondrial dysfunction mediates the development of various chronic metabolic, neurological, cardiovascular, autoimmune, and rheumatoid diseases (Cruz and Kang, 2018). However, the inflammation induced by oxidative stress acts as a feedback mechanism for maintaining the stressful conditions that lead to chronic diseases, tissue damage, and chronic inflammation.

Besides, the damage of the mitochondria results in reduced production of ATP molecules and subsequent intracellular depletion. This leads to increased intracellular adenosine monophosphate (AMP) that binds to the γ subunit of AMPK, a key metabolic sensor whose activation initiates various multiple signaling events (Wu et al., 2014). Also, the mitochondrial biosynthetic intermediates like acetyl CoA increase, and with the free oxygen reactive radicals, signaling pathways such as hypoxic signaling are activated, and these contribute to inflammation (Eltzschig and Carmeliet, 2014: Shadel and Horvath, 2015).

5.1.2 Inflammation in the heart

Chronic inflammation that results from the mitochondrial dysfunction mediates the development of various chronic metabolic, neurological, cardiovascular, autoimmune, and rheumatoid diseases (Luscher, 2018). The dysfunction of mitochondrial cells leads to the production and activation of pro-inflammatory cytokines and inflammasomes, leading to

atherogenesis. Markedly, the accumulation of low-density lipoproteins (LDLs) in the sub-endothelial blood vessels spaces where there is abnormal permeability precedes atherosclerosis. The accumulated LDLs form bulky complexes, and the ROS and myeloperoxidases oxidize them, inducing immune-mediated phagocytosis, hence the loss of smooth muscle cells (Katsiari, Bogdanos & Sakkas, 2019). The macrophages and dendritic cells of the immune system present in the arterial intima are involved in the phagocytosis. Monocytes from the bone marrow that differentiate into macrophages infiltrate the vascular walls and uptake the modified LDLs, initiating fatty streaks (Getz & Reardon, 2015). The LDLs in these macrophages activate the TLRs-mediated pathways and inflammasomes that lead to the secretion of pro-inflammatory cytokines that promote the progression of atheromatosis and, consequently, the cardiovascular events (Katsiari, Bogdanos and Sakkas, 2019 & Stewart et al., 2010). Moreover, the macrophages, mast cells, and activated T-cells continue to accumulate in the atherosclerotic lesions when there is an injurious stimulus. Besides, the number of chemokine receptors increase in cardiac events, activating inflammatory responses and oxidative damage, further triggering cardiovascular diseases (Fioranelli et al., 2018: Steven et al., 2019). Notably, atherogenesis steps involve pro-inflammatory cytokines, and macrophages promote angiogenesis, rendering cardiomyocytes responsive to stimuli through minimal inflammation.

5.1.3 Aim of study

At the time of writing, no studies have been completed on inflammatory cytokines in MODY2 patients. The aim of this section was to test *in vitro*, the effect of cytokines upon the proteins regulating mitochondrial dynamics.

5.2 Methods

5.2.1 Cell culture – H9c2 cells

All methods employed in this component of the thesis research work are described in Chapter 2, sections X, Y, Z.

5.2.2 Testing the effects of cytokines on fission-fusion proteins and Miro1 expression

To assess mitochondrial dynamics, H9c2 cells were incubated for 24 h with IL-1β (10 nmol/l; Sigma, UK), IL-6 (10 nmol/l; Sigma, UK) and TNF-α (10 nmol/l; Sigma, UK). All experiments were performed in triplicate using passages that were between (1-20). Cells were lysed according to sections 2.2.3 and 2.2.9 for Western blotting and RT-qPCR, respectively.

5.2.3 Statistical analyses

All data are shown as the mean ± the standard error of the mean. Statistical analyses were performed using a student t-test. Results were deemed significant when $p<0.05$. All statistical analysis was performed using GraphPad Prism 8. *$p \leq 0.05$, ** $p \leq 0.01$, *** $p \leq 0.001$ and **** $p \leq 0.0001$.

5.3 Results

5.3.1 Upregulation of inflammatory cytokines in the GENA348 myocardium

Inflammatory cytokines, such as TNF-α, IL-1β and IL-6, are considered to play a role in heart failure in diabetes (Lee et al., 2017). TNF-α is an insulin resistance regulator and known to be involved in heart dysfunction in diabetes (Donato et al., 2012). TNF-α, IL-1β and IL-6 levels have been shown to be significantly elevated in diabetes, making them good molecular candidates for investigation of inflammation in the GENA348 myocardium (Kern et al., 2001; Ko et al., 2009; Liu et al., 2015). Thus, transcript levels of IL-1β, IL-6 and TNF-α were measured. Gene expression levels of IL-1β, IL-6 and TNF-α were significantly increased in GENA348, by 2.2, 2.7, and 3.1-fold (*P*=0.0101, *P*=0.0065, *P*=0.0047), respectively (Figure. 2.17).

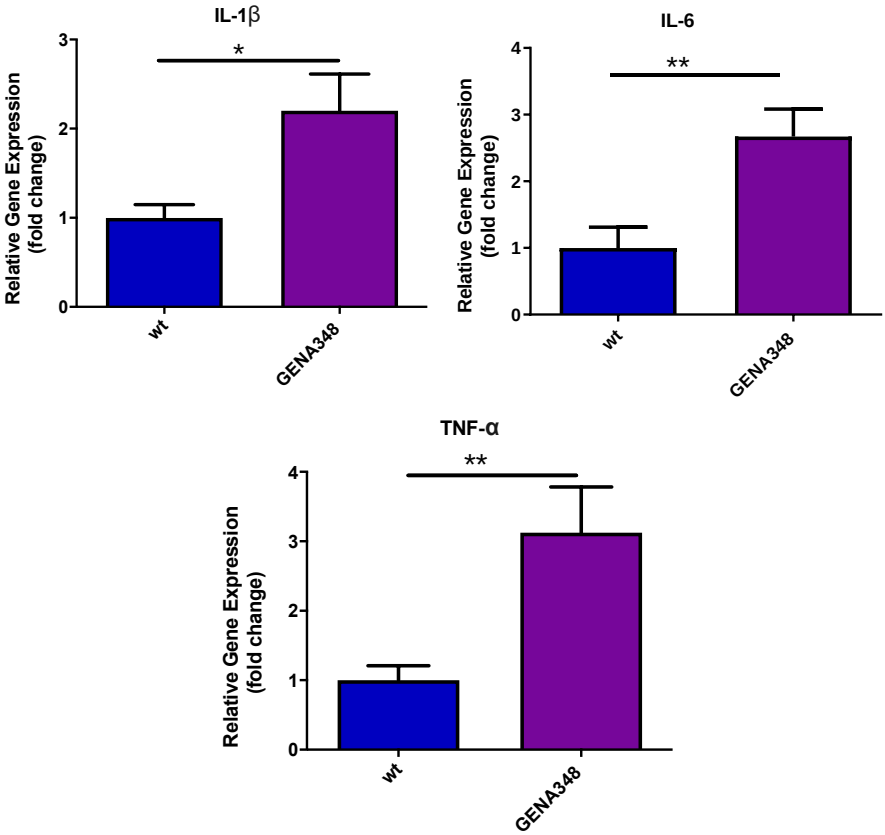

Figure 5.1 Increased inflammatory cytokines in GENA348 myocardium.

IL-1β, IL-6 and TNF-α transcript levels were assessed using qPCR and revealed a significant increase in GENA348 (n=6) compared to control (n=6). Data represented as mean +/- SEM *$p \leq 0.05$ and **$p \leq 0.01$.

5.3.2 Impact of inflammatory cytokines IL-1β, IL-6 and TNF-α on H9c2 cell mitochondria

5.3.2.1 The effects of inflammatory cytokines on H9c2 Viability

H9c2 cells were treated with IL-1β, IL-6 and TNF-α for 24 hours at 5ng/ml and 10ng/ml because 20ng/ml showed characteristics of apoptosis (Zhao et al., 2015). There was no change in cell viability upon treatment with IL-1β (5ng/ml and 10ng/ml) compared to negative control. All cells where then treated with H_2O_2 (Figure 5.). Control cells, IL-1β treated cells (5ng/ml and 10ng/ml) showed a 0.2-fold decrease in cell viability after treatment with H_2O_2 (P<0.0001; Figure 5.) showing H_2O_2 induced apoptosis.

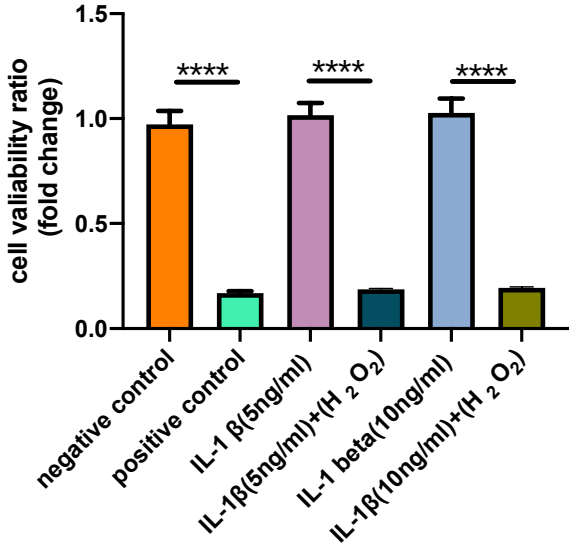

Figure 5.2 H_2O_2 treated cells exhibit a decrease in cell viability.
Cell viability assays revealed no significant difference between IL-1β (5ng/ml and 10ng/ml) treated cells and the negative control, while the H_2O_2 treatment caused a significant decrease in cell viability. Data represented as mean +/- SEM (n=3 lane from 3 different passage) ****p ≤ 0.0001.

Following treatment, the cells were lysed, qPCR and Western blot analyses were run to assess levels of Miro1 and proteins regulating mitochondrial dynamics. We first investigated the levels of Miro1 gene expression in IL-1β treated H9c2 cells However, rather than a decrease we observed a 2.1-fold increase of Miro1 in IL-1β (5ng/ml and 10ng/ml) in gene expression level (P=0.0135 and P=0.0075, respectively) (Figure 5.).

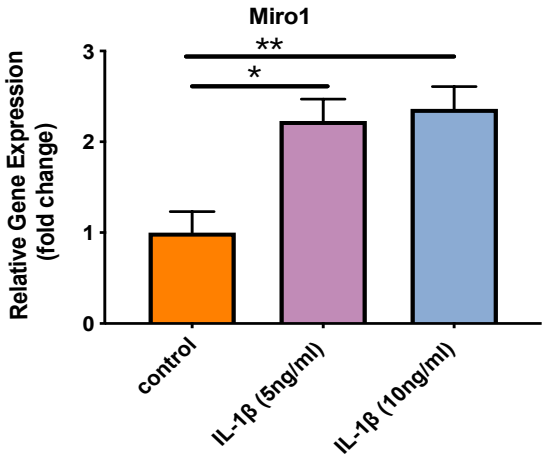

Figure 5.3 IL-1β treated cells exhibit an upregulation in Miro1 gene expression.
Miro1 transcript level were assessed using qPCR and revealed a significant increase in Miro1 in IL-1β (5ng/ml and 10ng/ml) treated cells compared to control. Data represented as mean ± SEM (n=3 lane from 3 different passage) *$p \leq 0.05$ and **$p \leq 0.01$.

In order to corroborate this result with protein expression data, we measured changes protein expression and Western blot analysis in H9c2 cells. A significant 1.8-and 2-fold increase of Miro1 in IL-1β treated cells (5ng/ml and 10ng/ml) (P=0.0358 and P=0.0135, respectively) (Figure 5.) was recorded, in comparison to control cells. This data is consistent with qPCR data.

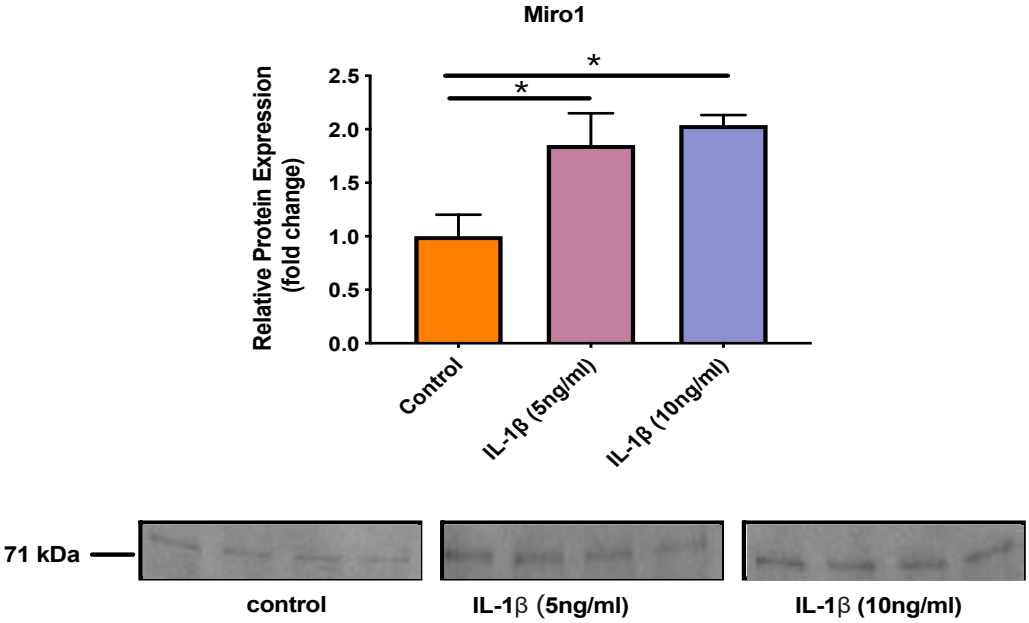

Figure 5.4 IL-1β treated cells exhibit an upregulation in Miro1 protein expression.
Western blot analysis revealed a significant increase in the Miro1 protein expression in IL-1β (5ng/ml and 10ng/ml) treated cells compared to control cells. Data represented as mean ± SEM (n=4 lane from the same page) *$p \leq 0.05$.

5.3.2.2 Mitochondrial dynamics-regulating gene expression altered in IL-1β treated H9c2 cells

At the gene level it was determined that treatment with IL-1 β (5ng/ml and 10ng/ml) led to no changes in Mfn1 and Mfn2 expression compared to controls. As shown in

Figure 5.1), a significant 0.2-fold decrease in the mRNA was identified for Opa1 in IL-1β (5ng/ml and 10ng/ml) (P=0.0323 and P<0.0290 respectively). Conversely, IL-1β treatment (5ng/ml and 10ng/ml) led to 5 and 5.5-fold increase in Drp1 (P=0.0064 and P<0.0024 respectively).

A decrease in Opa1 would indicate a loss of inner membrane (cristae) stability with increased levels of Drp1 suggesting increased fission and generation of smaller fragmented mitochondria.

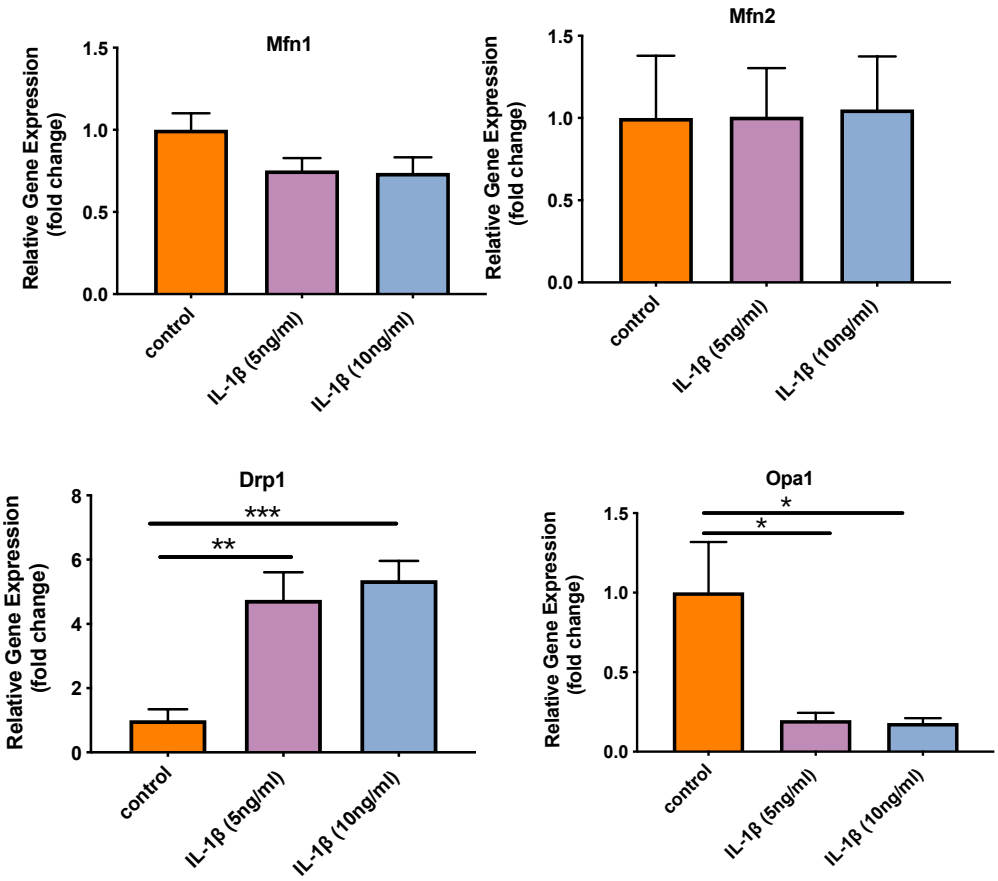

Figure 5.1 IL-1β treated cells exhibit changes in mitochondrial dynamics-regulating proteins transcript expression.
qPCR revealed a significant decrease in Opa1 and a significant increase in Drp1 in IL-1β (5ng/ml and 10ng/ml) treated cells compared to control. Data represented as mean ± SEM (n=3 lane from 3 different passage) *$p \leq 0.05$, **$p \leq 0.01$ and ***$p \leq 0.001$.

To determine if changes in Opa1 and Drp1 gene expression (Figure 5.2) correlates to increased protein levels, Western blot analysis was carried out. We observed a significant 0.7-fold decrease in the Opa1 in IL-1β (5ng/ml and 10ng/ml) treated cells (P=0.0148 and P<0.0133, respectively). This data is consistent with qPCR data.

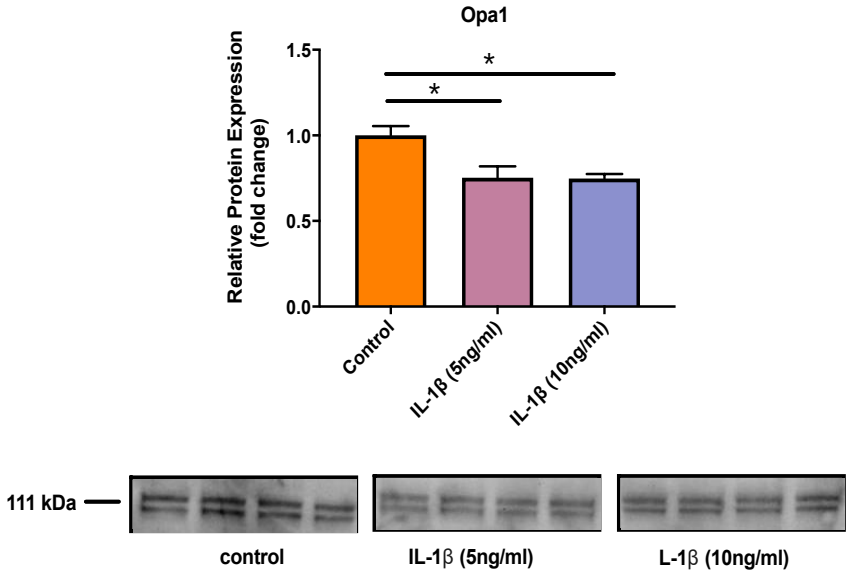

Figure 5.2 IL-1 β treated cells exhibit a downregulation in Opa1 protein expression.
Western blot analysis revealed a significant decrease in the Opa1 protein expression in IL-1β (5ng/ml and 10ng/ml) treated cells compared to control cells. Data represented as mean ± SEM (n=4 lane from same passage) *$p \leq 0.05$.

A 1.3-fold increase in Drp1 protein expression was revealed in IL-1β treated cells (5ng/ml and 10ng/ml) (*P*=0.0214 and *P*=0.0280, respectively). This data is consistent with qPCR data (Figure 5.3).

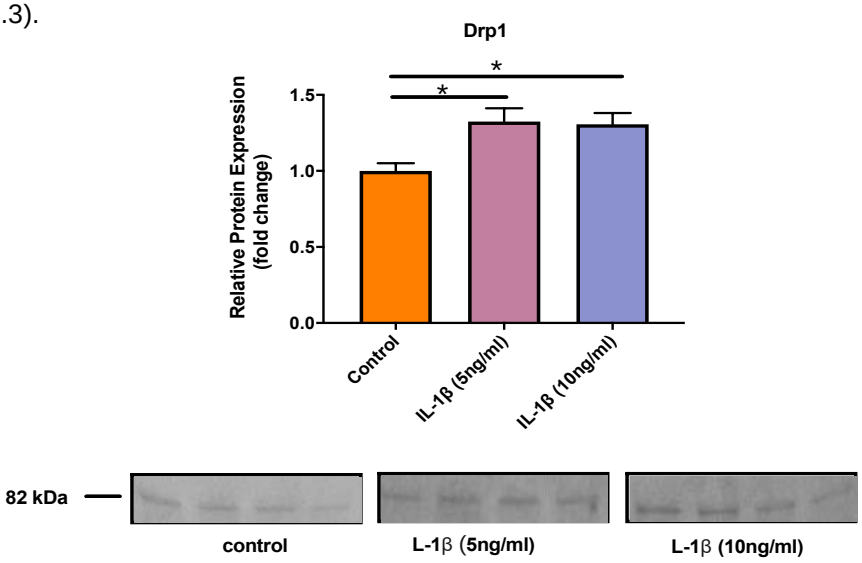

Figure 5.3 IL-1β treated cells exhibit an upregulation in Drp1 protein expression.
Western blot analysis revealed a significant increase in the Drp1 protein expression in IL-1β (5ng/ml and 10ng/ml) treated cells compared to control cells. Data represented as mean ± SEM (n=4 from same passage) *$p \leq 0.05$.

There was no significant difference in transcript levels of PINK1 and Parkin gene expression in IL-1β cells treated cells either at 5ng/ml or 10ng/ml, compared to controls (Figure 5.4).

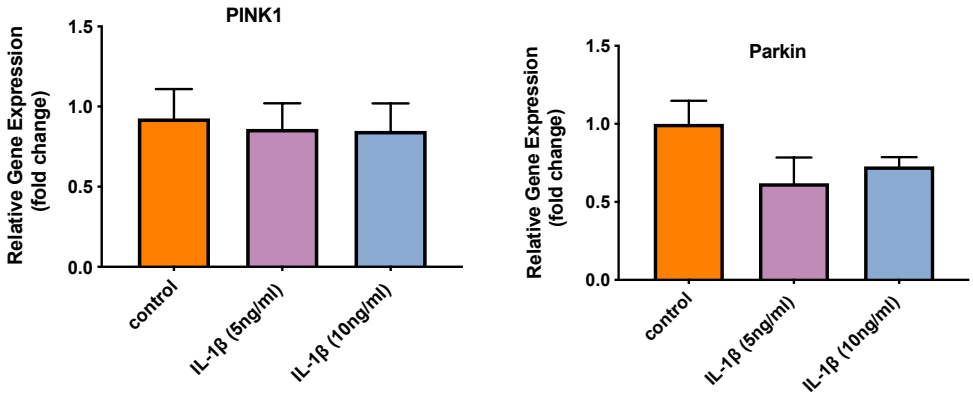

Figure 5.4 PINK1 and Parkin gene expression in IL-1β treated cells.
PINK1 and Parkin transcript level were assessed using qPCR and revealed no significant difference in IL-1β (5ng/ml and 10ng/ml) treated cells. Data represented as mean ± SEM (n=3 from 3 different passage).

Mitochondrial biogenesis markers were also measured in IL-1β (5ng/ml and 10ng/ml) treated H9c2 cells. A significant decrease was observed of levels of PGC-1α 0.4-fold and TFAM 0.2-

fold in the IL-1β treated cells, compared to controls (TFAM: *P*=0.0340, *P*=0.0442, PGC-1α: *P*=0.0195 and *P*=0.0217 5ng/ml and 10ng/ml respectively). (Figure 5.5).

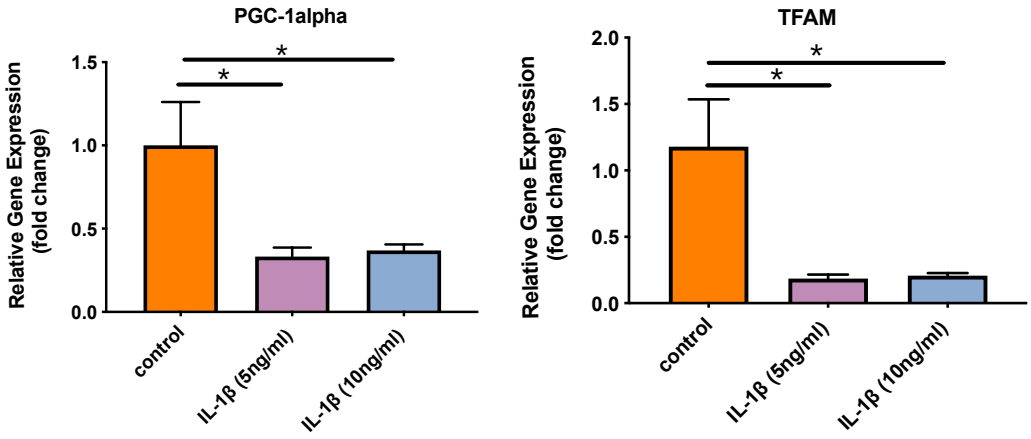

Figure 5.5 IL-1β treated H9c2 cells exhibit a downregulation in the gene expression of PGC-1α and TFAM.
PGC-1α and TFAM transcript level were assessed using qPCR and revealed a significant decrease in IL-1β (5ng/ml and 10ng/ml) treated cells. Data represented as mean ± SEM (n=3 from 3 different passage) *$p \leq 0.05$.

5.3.2.3 Treatment with IL-6 does not affect viability of H9c2 cells

Cells showed no change in viability upon treatment with IL-6 (5ng/ml and 10ng/ml) compared to negative control. All cells where treated with H_2O_2 (Figure 5.6). Both control cells and IL-6 (5ng/ml and 10ng/ml) treated cells showed a 0.2-fold decrease in cell viability after treatment with H_2O_2 (*P*<0.0001; Figure 5.6), showing H_2O_2 induce apoptosis both in the presence and absence of IL-6.

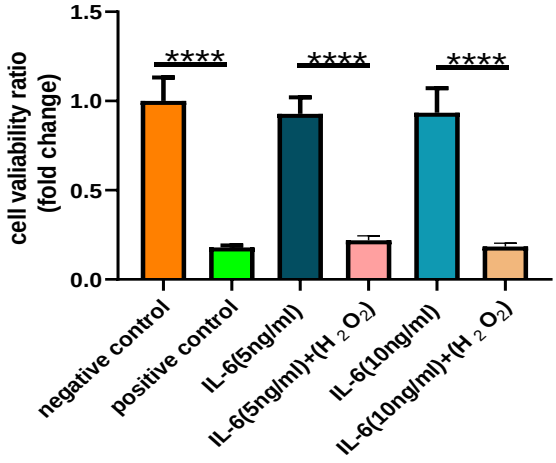

Figure 5.6 H_2O_2 treatment of H9c2 cells decreases cell viability.

Cell viability assay revealed no significant difference in positive control and IL-6 (5ng/ml and 10ng/ml) treated cells compared to negative control while the H_2O_2 treatment showed a significant decrease to both the control and IL-6 treated cells. Data represented as mean +/- SEM (n=3) ****$p \leq 0.0001$.

We next tested the effect of IL-6 upon expression of Miro1 and mitochondrial dynamic related proteins. In contrast to treatment of H9c2 cells with IL-1β, IL-6 treatment at both concentrations led to a 0.4-fold (5ng/ml) and 0.2-fold (10ng/ml) decrease in Miro1 gene expression compared to controls (P=0.0002 and P<0.0001, respectively) (Figure 5.7).

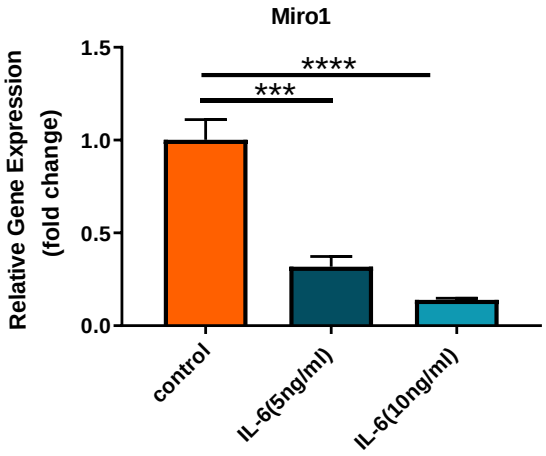

Figure 5.7 IL-6 treated cells exhibit downregulation in Miro1 gene expression.
Miro1 transcript levels were assessed using qPCR and revealed a significant decrease in Miro1 in IL-6 (5ng/ml and 10ng/ml) treated cells compared to control. Data represented as mean ± SEM (n=3 from 3 different passage) * ***$p \leq 0.001$ and ****$p \leq 0.0001$.

Western blotting similarly showed a decrease, 0.5-fold, of Miro1 in IL-6 (5ng/ml and 10ng/ml) treated cells (P=0.0110 and P=0.0146, respectively) (Figure 5.8).

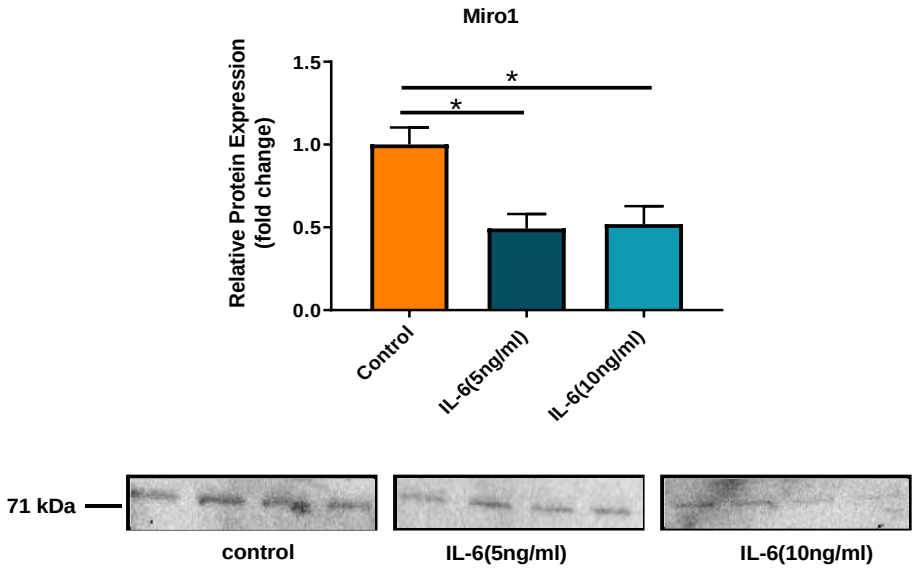

Figure 5.8 IL-6 treated cells exhibit a downregulation in Miro1 protein expression. Western blot analysis revealed a significant decrease in the Miro1 protein expression in IL-6 (5ng/ml and 10ng/ml) treated cells compared to control cells. Data represented as mean ± SEM (n=4 lane from same passage) *$p \leq 0.05$.

No significant difference was recorded in the gene expression level of Mfn1, Mfn2 and Drp1 in IL-6 (5ng/ml and 10ng/ml) treated H9c2 cells, compared to the control. Interestingly, we observed a significant 0.1-fold decrease mRNA gene expression for Opa1 in IL-6 (5ng/ml and 10ng/ml) treated cells (P=0.0029 and P<0.0026, respectively). This could suggest an interactive relationship between Opa1 and the inflammatory response (Figure 5.9).

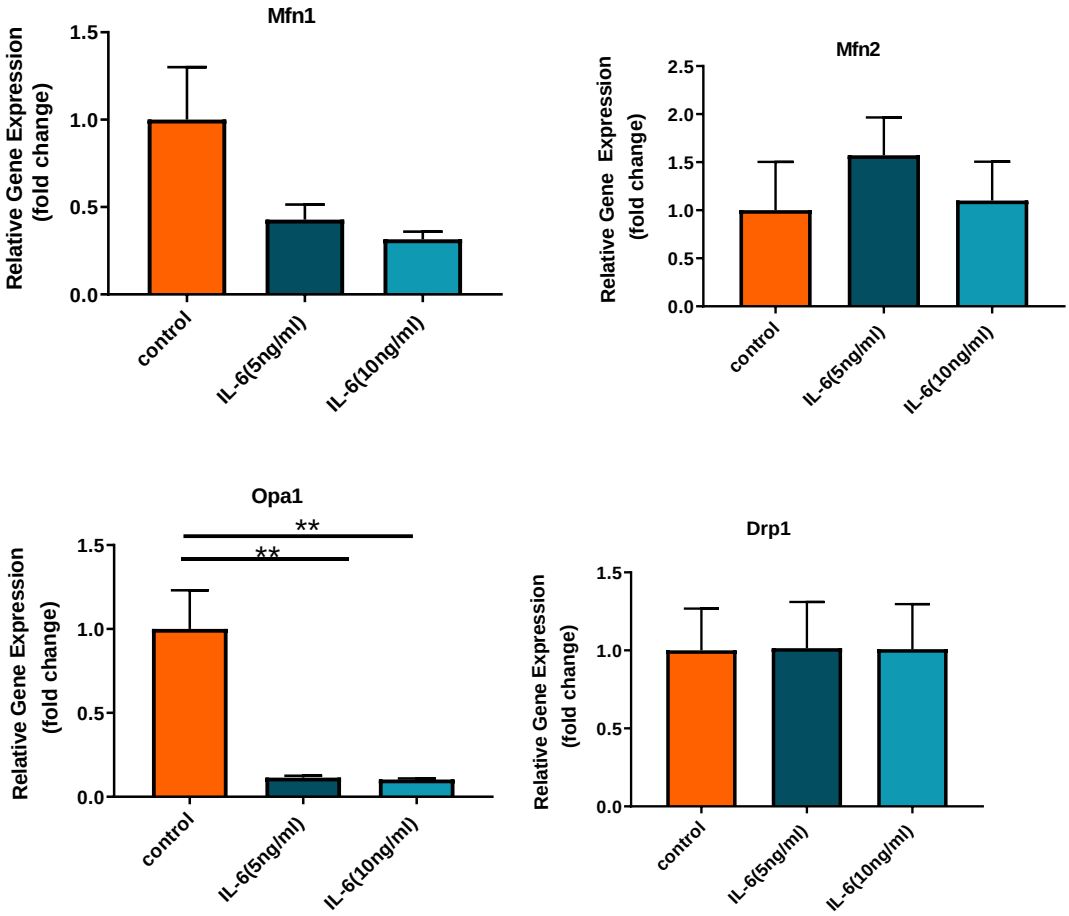

Figure 5.9 IL-6 treated cells exhibit changes in mitochondrial dynamic protein transcript expression.
Mfn1, Mfn2, Opa1 and Drp1 transcript level were assessed using qPCR and revealed a significant decrease in Opa1 only in IL-6 (5ng/ml and 10ng/ml) treated cells compared to controls. Data represented as mean ± SEM (n=3 from different passage) $^{**}p \leq 0.01$.

Western blotting identified a 0.5-fold decrease in Opa1 expression in cells after treatment with IL-6 at both 5ng/ml and 10ng/ml, (P=0.0147 and P<0.0238, respectively) compared to H9c2 control cells (Figure 5.10). This data is consistent with qPCR data.

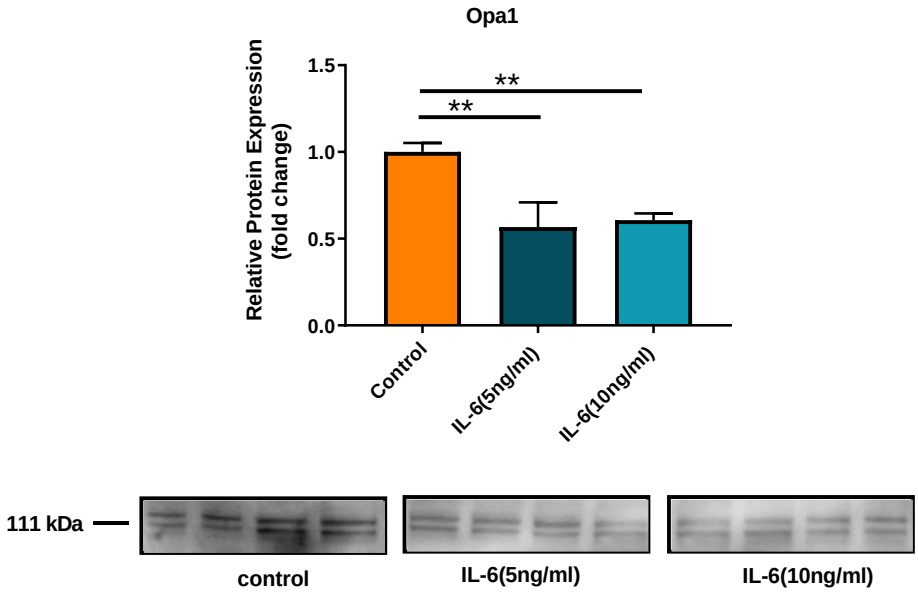

Figure 5.10 IL-6 treated cells exhibit a downregulation in Opa1 protein expression.
Western blot analysis revealed a significant decrease in the Opa1 protein expression in IL-6 (5ng/ml and 10ng/ml) treated cells compared to control cells. Data represented as mean ± SEM (n=4 lane from same passage) $^{**}p \leq 0.01$.

We further investigated PINK1 and Parkin gene expression and found no significant difference in transcript levels in IL-6 (5ng/ml and 10ng/ml) treated cells, compared to controls (Figure 5.11).

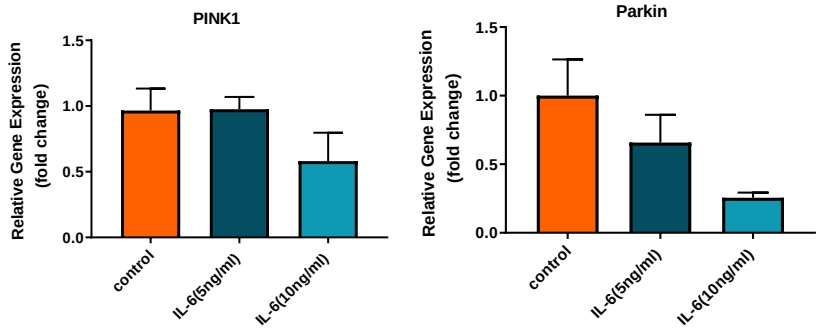

Figure 5.11 PINK1 and Parkin gene expression in IL-6 treated cells.
PINK1 and Parkin transcript level were assessed using qPCR and revealed no significant difference in IL-6 (5ng/ml and 10ng/ml) treatment. Data represented as mean ± SEM (n=3 lane from 3 different passage).

5.3.2.4 Mitochondrial biogenesis markers are significantly downregulated in IL-6 treated H9c2 cells

There was a significant decrease in levels of PGC-1α and TFAM transcripts in the IL-6 (5ng/ml and 10ng/ml) treated cells compared to control with a 0.1-fold (PGC-1α) and 0.3-fold (TFAM) decrease (PGC-1α: *P*=0.0015, *P*=0.0014, TFAM: *P*=0.0162 and *P*=0.0172 respectively), indicating a non-equilibrium state in the biogenesis of mitochondria in IL-6 (5ng/ml and 10ng/ml) treated H9c2 cells (Figure 5.12).

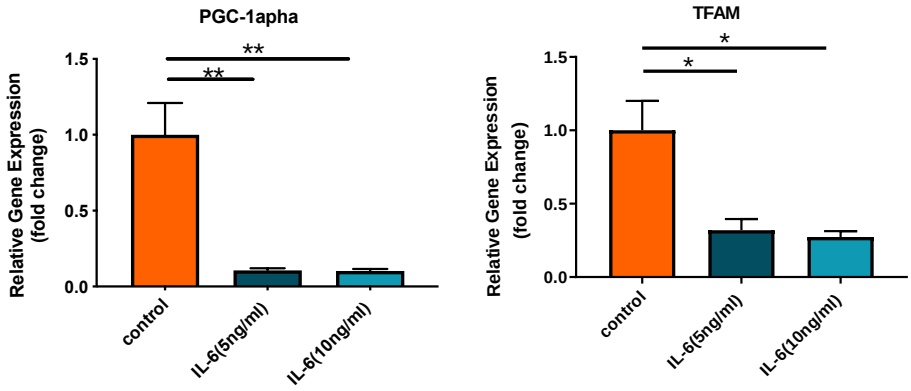

Figure 5.12 IL-6 treated H9c2 cells exhibit downregulation in the gene expression of PGC-1α and TFAM.
PGC-1α and TFAM transcript level were assessed using qPCR and revealed a significant decrease in IL-6 (5ng/ml and 10ng/ml) treated cells compared to control. Data represented as mean ± SEM (n=3 lane from 3 different passage) *$p \leq 0.05$ and **$p \leq 0.01$.

5.3.2.5 Cell viability not affected in TNF-α (5ng/ml and 10ng/ml) treated H9c2 cells

Cells showed no change in viability after treatment with TNF-α (5ng/ml and 10ng/ml) compared to negative control. All cells were then treated with H_2O_2 (Figure 5.13). Control cells and TNF-α (5ng/ml and 10ng/ml) treated cells showed 0.1-fold decrease in cell viability after treatment with H_2O_2 (*P*<0.0001; Figure 5.13) showing treatment with TNF-α does not affect normal cellular H_2O_2 induced apoptosis.

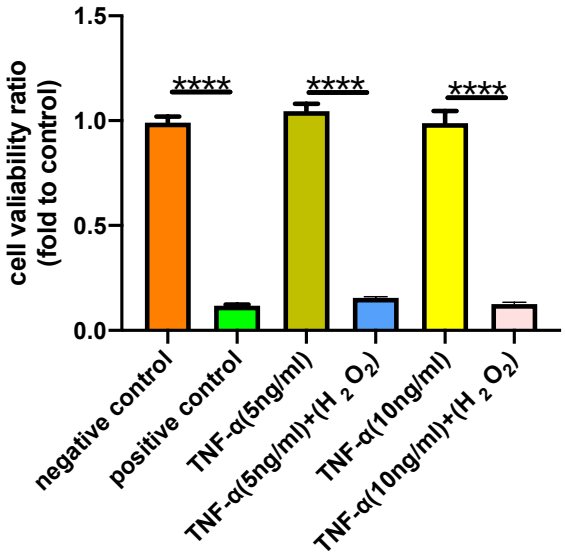

Figure 5.13 H_2O_2 treatment of H9c2 cells decreases cell viability.
Cell viability assay revealed no significant difference in TNF-α (5ng/ml and 10ng/ml) treated cells compared to negative control while the H_2O_2 treatment caused a significant decrease in cell viability. Data represented as mean +/- SEM (n=3 lane from 3 different passage) ****$p \leq 0.0001$.

Interestingly, TNF-α led to an increase in Miro 1 at the gene expression level as shown in (Figure 5.14). A significant 3.4- and 4.5-fold increase was recorded in Miro1 gene expression levels in TNF-α treated cells (5ng/ml and 10ng/ml) compared to the control (P=0.0128 and P=0.0004, respectively).

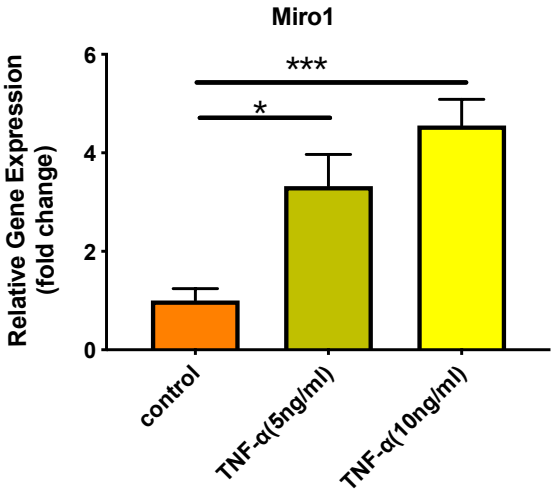

Figure 5.14 TNF-α treated cells exhibit an upregulation in Miro1 gene expression.
Miro1 transcript level were assessed using qPCR and revealed a significant increase in Miro1 in TNF-α (5ng/ml and 10ng/ml) treated cells compared to control. Data represented as mean ± SEM (n=3 lane from 3 different passage) *$p \leq 0.05$ and ***$p \leq 0.001$.

Western blotting revealed a significant 5- and 8-fold increase in Miro1 after TNF-α treatment (5ng/ml and 10ng/ml) (*P*=0.0489 and *P*=0.0005, respectively) compared to control H9c2 cells (Figure 5.15). This data is consistent with qPCR data.

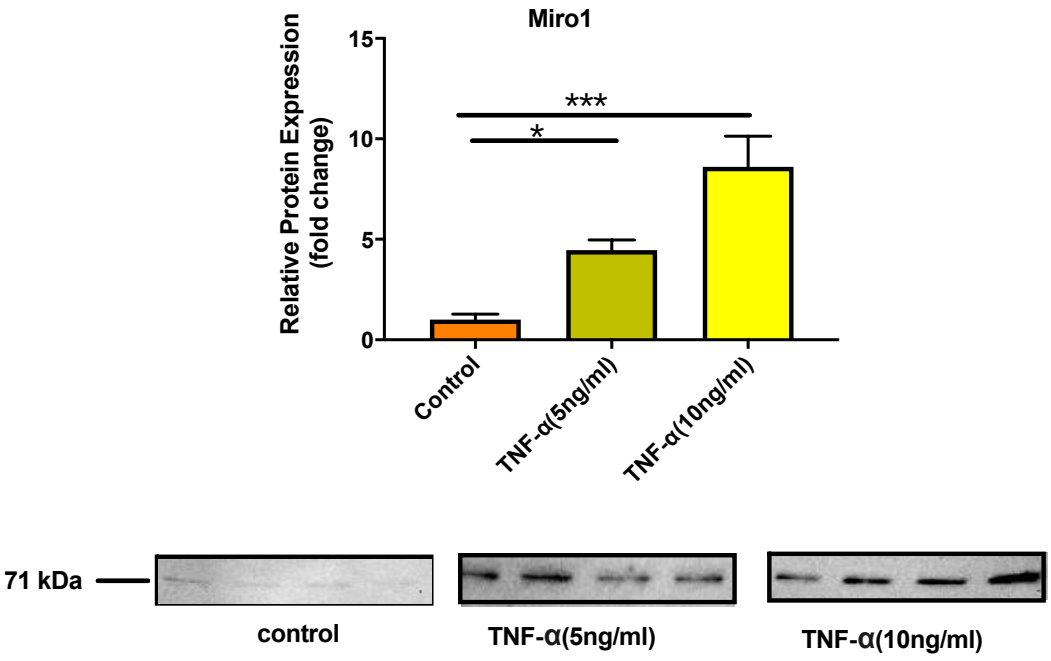

Figure 5.15 TNF-α treated cells exhibit an upregulation in Miro1 protein expression. Western blot analysis revealed a significant increase in the Miro1 protein expression in TNF-α (5ng/ml and 10ng/ml) treated cells compared to control cells. Data represented as mean ± SEM (n=4 lane from same passage) *$p \leq 0.05$ and ***$p \leq 0.001$.

Treatment of H9c2 cells with TNF-α did not affect gene expression levels of Mfn1, Mfn2 or Opa1, compared to the control. However, there was a significant 4- and 8-fold increase in the mRNA of Drp1 in TNF-α treated cells (5ng/ml and 10ng/ml) (*P*=0.0006 and *P*<0.0001, respectively) (Figure 5.16).

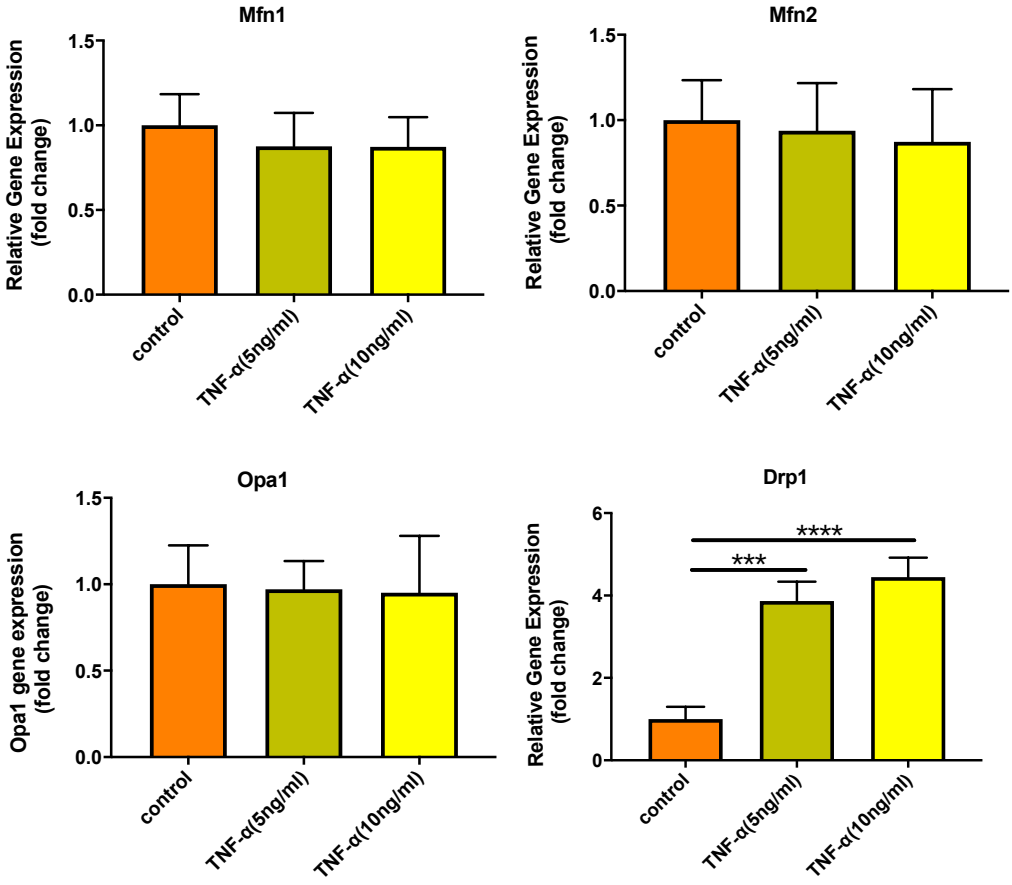

Figure 5.16 TNF-α treated cells exhibit an increase in fission protein Drp1 transcript expression.
Mfn1, Mfn2, Opa1 and Drp1 transcript level were assessed using qPCR and revealed a significant increase in Drp1 transcript in TNF-α (5ng/ml and 10ng/ml) treated cells compared to control. Data represented as mean ± SEM (n=3 lane from 3 different passage) ****p* ≤ 0.001 and ****p ≤ 0.0001.

Western blotting showed a 3- and 5-fold increase in Drp1 in cells when treated with TNF-α (5ng/ml and 10ng/ml) (*P*=0.0167 and *P*<0.0004, respectively). This data is consistent with qPCR results (Figure 5.17).

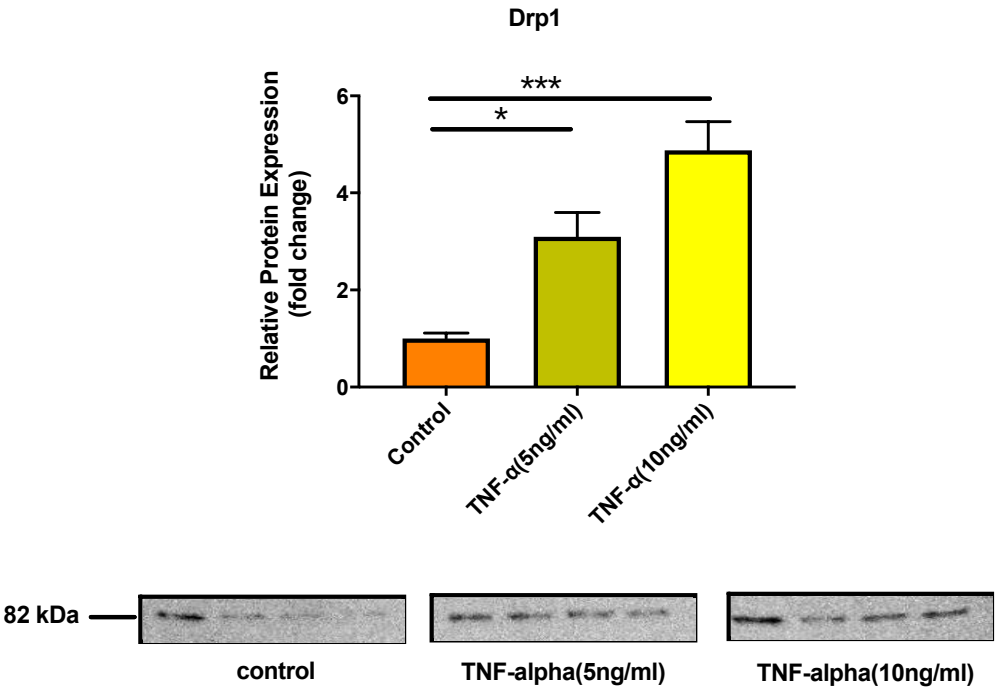

Figure 5.17 TNF-α treated cells exhibit an upregulation in Drp1 protein expression.
Western blot analysis revealed a significant increase in the Drp1 protein expression in TNF-α (5ng/ml and 10ng/ml) treated cells compared to control cells. Data represented as mean ± SEM (n=4 lane from same passage) *$p \leq 0.05$ and ***$p \leq 0.00$.

There was no significant difference in the gene expression of PINK1 and Parkin in cells when treated with TNF-α (5ng/ml and 10ng/ml), compared with controls (Figure 5.18).

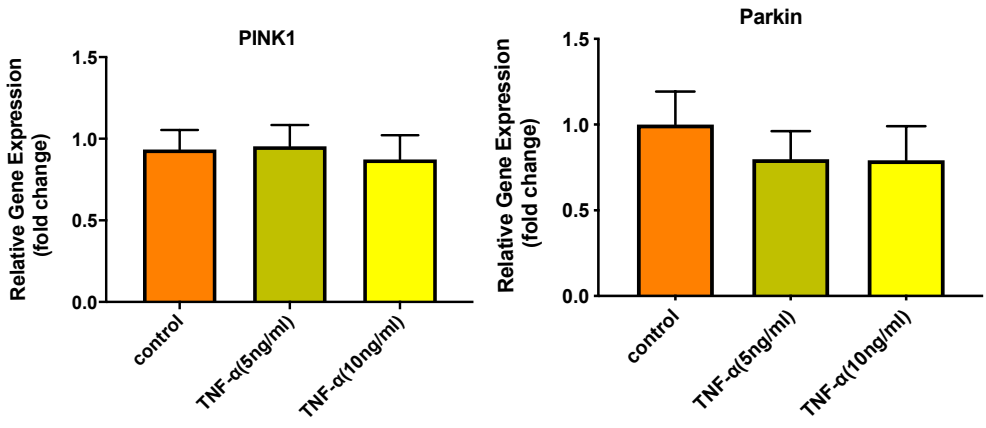

Figure 5.18 PINK1 and Parkin gene expression in TNF-α.
PINK1 and Parkin transcript levels were assessed in H9c2 cells using qPCR and revealed no significant difference after TNF-α (5ng/ml and 10ng/ml) treatment. Data represented as mean ± SEM (n=3 lane from 3 different passage).

5.3.2.6 No change in mitochondrial biogenesis marker transcript levels in the in TNF-α treated H9c2 cells

Next, the regulation of mitochondrial biogenesis marker transcripts was investigated in TNF-α (5ng/ml and 10ng/ml) treated H9c2 cells. There was no change in levels of PGC-1α and TFAM transcripts in the TNF-α (5ng/ml and 10ng/ml) compared to controls (Figure 5.19).

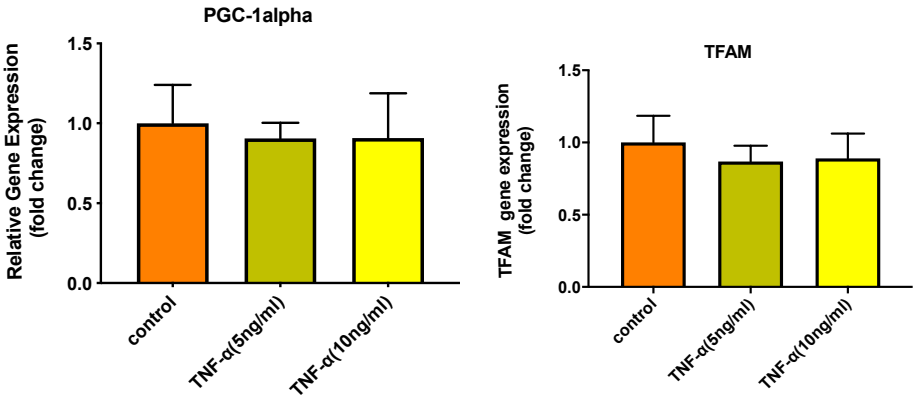

Figure 5.19 TNF-α treated H9c2 cells exhibit no change in the gene expression of PGC-1α and TFAM.
PGC-1α and TFAM transcript levels were assessed using qPCR and revealed no significant difference in TNF-α (5ng/ml and 10ng/ml) treated cells compared to control. Data represented as mean ± SEM (n=3 lane from 3 different passage).

5.3.2.7 Reduced citrate synthase activity in IL-1β, IL-6 and TNF-α H9c2 cells

As previously mentioned, citrate synthase can be measured to determine mitochondrial content. This data can help distinguish if a change could be attributed to an alteration of the mitochondrial structure. We observed a significant 0.6-, 0.5-, 0.7-fold decrease in citrate synthase activity in IL-1β, IL-6 and TNF-α treated cells, compared to controls ($p<0.0001$, Figure 5.20). This is indicative of a possible role for the cytokines in changing the mitochondrial structure and content, thus leading to a modification in citrate synthase activity.

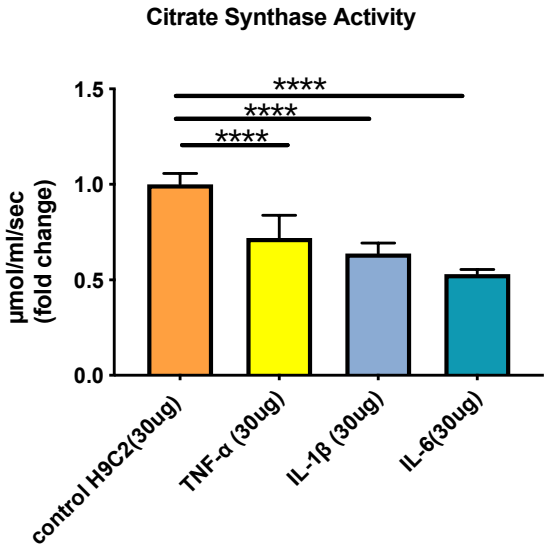

Figure 5.20 IL-1β, IL-6 and TNF-α treatment exhibit downregulation in citrate synthase activity.
There was a significant decrease in citrate synthase activity in IL-1 β, IL-6 and TNF-α treated cells compared to control H9c2 cells. Data represented as mean ± SEM (n=3 lane from 3 different passage) ****$p \leq 0.0001$.

5.3.2.8 Oxygen consumption in IL-1β, IL-6 and TNF- α H9c2 cells

As described earlier O_2 consumption rate was measured in isolated mitochondria from control and IL-1β cells, IL-6 cells and TNF-α treated cells. Isolated mitochondria from cells took five minutes to plateau. The gradient for (20-140) seconds was calculated for each group (Figure 5.21A). There was a significant increase in oxygen consumption rate in IL-1β and IL-6 with 1.7-fold change. The oxygen percentage rate of TNF-α was found to be the same compared to control (Figure 5.21B).

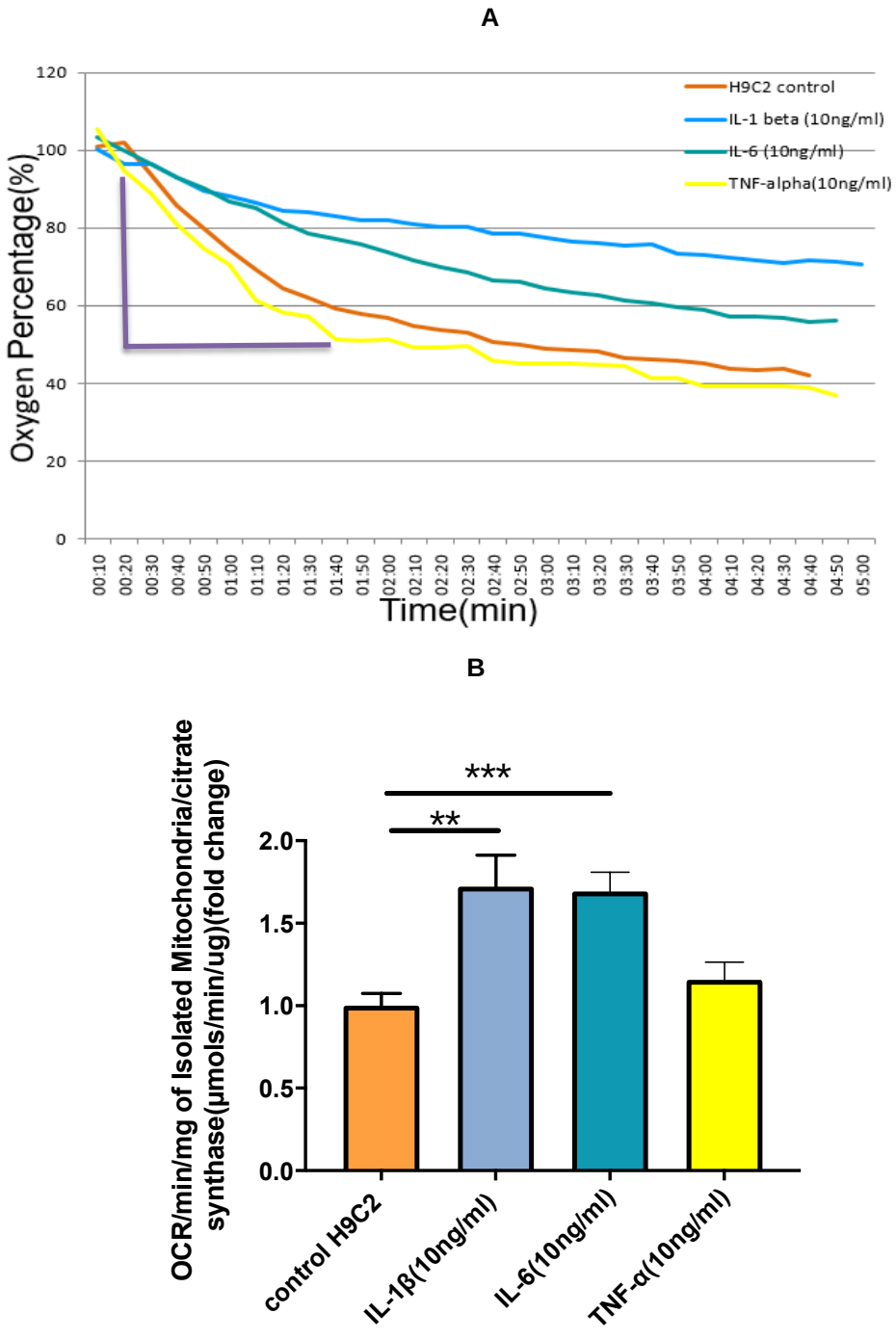

Figure 5.21 Oxygen consumption rate in IL-1β, IL-6 and TNF-α treated cells.
(A) There was a significant increase in IL-1β and IL-6 (10ng/ml) while no change in oxygen consumption rate in TNF-α compared to control H9c2 cells. (B) Representative plot indicating oxygen percentage varying with time in IL-1β, IL-6 and TNF-α treated cells. Data represented as mean +/- SEM (n=3 lane from 3 different passage) $^{**}p \leq 0.01$ and $^{***}p \leq 0.001$.

5.4 Discussion

Thus, the main objective of this chapter was to investigate Miro1's function in mitochondrial dynamics and function. The main findings were: (1) Cytokines differentially affected Miro1 expression with IL-1 β treated cells leading to increased Miro1 expression, whereas IL-6 and TNF-α led to a decrease in Miro1 expression. (2) Treatment of H9c2 cells with IL-1 β, IL-6 and TNF-α also impacted proteins regulating fission and fusion. IL-1β and IL-6 treated H9c2 cells resulted in decrease in Opa1 transcript expression. Whereas there was an increase in Drp1 expression after application of IL-1 β and TNF-α. (3) IL-1 β and IL-6 treatment resulted in an increased rate of mitochondrial oxygen consumption with TNF-α treated cells showing no change compared to controls. (4) there is evidence of increased levels of inflammatory cytokines within the GENA348 myocardium, compared to controls.

Zhong et al. (2017) have linked diabetes with cardiac dysfunction as a result of inflammation. Increasing evidence has shown that diabetes can be classified as an in inflammatory disease as a result of the auto-immune destruction of pancreatic B-cells (Zhong et al., 2017) (Marques-Vidal et al., 2012). To our knowledge, there have been no published studies of inflammation and MODY2. Therefore, another aim to this study was to investigate cytokine levels in GENA348 mice. This data will advance understanding of the characteristics of GENA348 and effect of glucokinase malfunction with potential translational value for MODY2 patients. Here, we found inflammatory cytokine levels, IL-1β, IL-6 and TNF-α, as significantly increased in GENA348 mice. As discussed, earlier, different cytokines are associated with either deleterious or cardioprotective roles in the heart, with a general lack of consensus.

5.4.1 Inflammatory cytokines (IL-1β/ IL-6/ TNF-α) impact upon mitochondrial dynamics, biogenesis, citrate synthase and OCR

Here, we have dissected out the putative effects of these cytokines on proteins regulating mitochondrial dynamics. The table below (Table 5.3) details the summary of results for the impact on inflammatory cytokines IL-1β, IL-6 and TNF-α.

Table 5.1 Summary of inflammatory cytokine results (up arrow – upregulation; down arrow – downregulation; dash – no change)

	IL-1β	IL-6	TNF-α
OCR	↑	↑	-------
Citrate synthase	↓	↓	↓
Biogenesis	↓	↓	-------
Mitochondrial dynamics	* Opa1 ↓ *Drp1 ↑	↓	* Drp1 ↑
Miro1	↑	↓	↑

IL-1 increases in patients with heart failure, relating to impaired systolic function (Szekely and Arbel, 2018). More specifically, IL-Iβ increases NOS in cardiac myocytes, reducing energy production through mitochondrial dysfunction (Tatsumi et al., 2000). Blockade of IL-1 has been investigated as a therapeutic avenue, with the aim to disrupt its detrimental effect on left ventricular function and progression of heart failure (Szekely and Arbel, 2018). As discussed, blockade of IL-1 represents a putative therapeutic approach for treating several cardiovascular conditions. Interestingly, here we determined that IL-1β leads to down regulation of Opa1 and upregulation of Drp1, which has the potential to promote fission. The biogenesis markers, PGC-1α and TFAM, were down regulated in agreement with citrate synthase activity. Respiration rates were increased, suggesting a greater need for ATP in mitochondrial biogenesis. In future work, it would be useful to measure levels of ATP production. Therefore, the data suggest that IL-1β has altered the fission-fusion axis towards destabilised smaller mitochondria, reduced mitochondrial content and impaired OXPHOS. However, surprisingly,

Miro1 levels were upregulated. This could be a compensatory mechanism to modulate mitochondrial availability as a result of destabilised mitochondria.

Depending on the cardiovascular condition, IL-6 can be cardioprotective or pathological and is elevated in response to injury, activating immune cells. Although in the long-term, IL-6 elevation is pathogenic, studies have shown that short-term IL-6 signalling can be protective for the heart (Fontes et al., 2015). In the heart, elevated IL-6 is associated with cardiac injury and depressed function (Yang et al., 2004), whilst acute cardio protection occurs through the induction of an anti-apoptotic programme in myocytes (Yamauchi-Takihara and Kishimoto, 2000). In humans, IL-6 has been studied as a therapeutic option in DCM patients (Podewski et al., 2003). Here, the authors investigated the intricate balance between cardiomyocyte hypertrophy and apoptosis, related to the JAK-STAT signalling pathway. In this pathway, JAK-STAT activation mediates IL-6 signalling via a shared gp130 receptor, controlled in a negative feedback loop by suppressors of cytokine signalling (SOCS1, SOCS3); together this pathway has been implicated in a critical myocyte survival pathway (Podewski et al., 2003). Yasukawa et al. (2001) reported a decrease in myocardium SOCS3 protein (non-limiting IL-6 family signalling), resulted in continuous IL-6 signalling and was a characteristic found in the left ventricle of DCM patients. This is mirrored in cultured cardiac myocytes whereby the overexpression of SOCS3 supressed the anti-apoptotic abilities of IL-6. Here, we determined that IL-6 leads to down regulation of Opa1 and no change in Drp1. The biogenesis markers were down regulated in agreement with reduced citrate synthase activity. In future work, it would be useful to measure levels of ATP production. Therefore, the data suggest that, like IL-1β, IL-6 has altered the fission-fusion axis towards destabilised smaller mitochondria, reduced mitochondrial content and impaired OXPHOS. In contrast to IL-1β, Miro1 levels were down-regulated by IL-6 treatment.

TNF-α is another cytokine found elevated in heart failure, contributing towards cardiac dysfunction through its association with IL-6 (Schumacher et al., 2018). TNF-α responds to injury through an acute pro-inflammatory stage, followed by an anti-inflammatory response, prolonged as a result of cardiac stress. This can progress to chronic inflammation, resulting in

the generation of proinflammatory cytokines through cardiac tissue infiltration of macrophages (Schumacher et al., 2018). Due to this pathophysiology, TNF-α is a good candidate for a marker of heart failure (Hartupee and Mann, 2013). It has been shown that the downstream cellular effects of TNF-α are mediated by two receptors, TNF receptor 1 or 2 (TNFR1 or TNFR2) (Cabal-Hierro and Lazo, 2012). It is thought that TNFR1 activation is deleterious (mediating cell death), whilst TNFR2 activation is beneficial (promoting cell activation, migration and proliferation) (Al-Lamki, 2005), adding to the complexity of the signalling pathways in cardiac pathophysiology. In order to utilise TNF-α as a potential therapeutic target, it is important to understand the differential roles of signal events initiated by both receptors. Here, our results were surprising. We determined that TNF-α leads to the up regulation of Drp1, with no change in other fission-fusion proteins or biogenesis markers. Like IL-1β, Miro-1 expression was up regulated.

It was determined that there is a significant increase in the transcript level of inflammatory biomarkers TNF-α, IL-1β, and IL-6 in GENA348 mice myocardium. Evidence suggests that IL-1β is able to depress cardiac function through nitrogen oxide pathways (Bujak and Frangogiannis, 2009; Schulz et al., 1995). IL-1β induces cardiomyocyte apoptosis alone, or in combination with TNF-α (Ing et al., 1999), further evidencing its importance in contractile function and cardiac repair. Similarly, in a study of 88 heart failure patients for inflammatory activation and disease progression, increased IL-6 expression was been described to cause left ventricular dysfunction in heart failure with reduced ejection fraction (Ptaszynska-Kopczynska et al., 2017). Anti-inflammatory drugs have also been investigated as a potential treatment for diabetic sufferers (Pollack et al., 2016).

IL-1 has also been identified as a feature of diabetes (Gabay et al., 2010). IL-1 triggers a series of signalling events through the binding of IL-1α/IL-1β to cell surface receptors. This activates the signal transduction cascade, causing inflammation and β-cell damage, leading to T2DM (Banerjee and Saxena, 2012). This signal cascade involves a protein known as mitogen activated protein kinase (MAPK), that when increases, transmits stress and apoptotic signalling (Miyauchi et al., 2009). Cytokines such as IL-1 act through the upregulation of genes

including Fas and inducible nitric oxide synthase (iNOS). IL-1 expression has been linked to the progression of diabetes. Using an IL-1 receptor mice knockout, Thomas et al. (2004) reported slow diabetes progression in IL-1 receptor deficient animals. However, authors report that 75% of IL-1 deficient mice still developed spontaneous diabetes, suggesting IL-1 may not be essential for disease progression (Thomas et al. (2004), and the presence of redudancy with TNF may explain this unchanged diabetes frequency. There have been some of studies that have investigated the cardiac role of IL-1 in a diabetic model, establishing IL-1 as an inflammatory connection between metabolic dysfunction and heart failure. In an streptozotocin (STZ) model of diabetic mice, Monnerat et al. (2016) reported that IL-1β causes a prolongation of the action potential duration and calcium spikes in cardiomyocytes, resultant of arrhythmia. STZ damages pancreatic β cells, resulting in hypoinsulinemia and hyperglycemia (Graham et al., 2011). Interestingly, this was treated with the use of an IL-1 receptor antagonist. Inflammation is central to the development of diabetic cardiomyopathy (Sarkar et al., 2018). Sakar et al. (2018) have shown that inflammation increases leukeocyte invasion in the myocardium, releasing inflammatory serine proteases (ISPs) that trigger cardiac dysfunction.

IL-6 has a pleiotropic role, acting on various tissues and organs. IL-6 has been implicated in diabetes and cardiovasular complications (Qu et al., 2014). Elevation of IL-6, similar has been chacterised as a marker of metabolic disorder and cardiovascular disease (Scheller et al., 2011), however, a casual association is yet to be elucidated. In IL-6 diabetic knockout mice, cardiac function improved, suggesting a protective effect against diabetic cardiomyopathy and (Zhang et al., 2016). In this study, wildtype (WT) diabetic mice were induced by STZ and investigated 12-weeks after diabetes induction (Zhang et al., 2016). In relation to the present study, this suggests that an elevation of IL-6 in the GENA348 worsens cardiac function. Future work could include investigating if there is migration of e.g. macrophages into the GENA348 myocardium to act as a source of the inflammatory cytokines, although cell types such as fibroblasts can secrete cytokines. Generally, it can be said that chronic inflammation and diabetes depend on each other and play a common role (Feng et al., 2018). A possible future diagnostic application of inflammatory markers may be to refine diabetes risk prediction to target individuals for patient-centred lifestyle interventions.

5.5 Conclusion

Inflammatory markers in the myocardium were measured to determine molecular changes in the GENA348 myocardium. In summary, our study shows evidence of increased levels of inflammatory cytokines within the GENA348 myocardium, compared to controls. An intriguing finding was that Miro1 expression is differentially regulated by the three cytokines investigated here; the next step would be to investigate the mechanism involved to advance current understanding of how inflammation may be a driver of mitochondrial dysfunction.

Chapter 6 General Discussion

Maturity Onset of Diabetes in the Young (MODY2) is a genetic form of diabetes with a mutation in the Gck gene (Carmody et al., 2016). It is thought that MODY affects 1-2% of people diagnosed with diabetes mellitus (Kleinberger and Pollin, 2015), with the majority of MODY2 cases undiagnosed due to the absence of diabetes-like clinical symptoms. Heart failure is a well-known feature of patients with T1DM and T2DM diabetes. However, cardiovascular complications experienced by MODY2 patients are less clear, despite also presenting with marked hyperglycaemia and diabetic complications similar to those exhibited in T2DM (Velho et al., 1997). Diabetes suffers are at a higher risk of developing cardiovascular dysfunction. Treatment, particularly for MODY2 patients, is limited as the molecular mechanisms leading to dysfunction are complex and poorly understood. Due to its high energetic demands, the heart requires mitochondria to constantly supply energy (Bugger and Abel, 2010) and impaired mitochondrial function is known to lead to cardiac cell death and eventual heart failure (Bugger and Abel, 2010). To understand mitochondrial structural and molecular remodelling that leads to diabetic cardiomyopathy was studied using a genetic T2DM mouse model, GENA348 as it represents a mild phenotype. As discussed earlier the GENA348 mouse contains an A to T transversion mutation in the glucokinase gene (Toye et al., 2004). and has been shown to be analogous and clinically relevant to the MODY2 (Fabiano et al., 2016). Obesity is a key risk factor for the development of T2DM, and so, the second aspect of this project investigated cardiovascular function as a result of a high fat diet. Identifying changes in the early stages of disease, as a result of obesity, can be important to prevent disease progression. To this aim, 3D electron microscopy imaging was combined with biochemistry, mitochondrial bioenergetic profiling, physiological analyses echocardiography. and cell and molecular biology techniques.

This thesis demonstrates that the GENA348 mice develop mitochondrial dysfunction, as early as 6 months of age and equivalent to 30 human years. More specifically, a mitochondrial proteomic screen identified an imbalance in a number of fission-fusion proteins, resulting in larger mitochondria, impaired mitophagy and compromised motility. We also recorded impaired OXPHOS in GENA348 mice, further suggesting defects in cardiomyocyte

contractility. A clear link between proteins regulating mitochondrial fission and fusion and mitochondrial ultrastructure has been demonstrated with image analysis of tissue taken from the GENA348 myocardium revealing enlargement of the mitochondria compared with controls. The impact of obesity on MODY2 is yet to be explored in relation to cardiac impairment. Thus, the second aim was to study the cardiac phenotype of GENA348 mice fed normal chow or HFD and to investigate how high-fat feeding impacts mitochondrial function in our mouse model. Here, we noted a common pathological development in the GENA348-chow mice compared to WT-HFD, suggesting a similar pathophysiology in obesity and MODY2 diabetes, particularly with respect to the development of impaired mitochondrial function. Through the initial studies, we noted a marked decrease in Miro1 expression in the GENA348 mouse model (and also in the WT high fat fed mouse), a regulator of mitochondrial transport and homeostasis (López-Doménech et al., 2018). Through Miro1 knockdown *in-vitro* investigations employing a cardiomyocyte cell line, we found evidence that Miro1 expression is linked to the balance between fission and fusion proteins and mitophagy, through an increase of protein expression of mitochondrial dynamic-regulating factors, such as Opa1 and PINK1.

One hallmark of diabetes/obesity is chronic inflammation and a link between the mitochondrial proteins and inflammatory signalling pathways have been indicated in skeletal muscle. However, molecular and cellular mechanisms are yet to be fully defined within the heart. Therefore, the final part of this project investigated the impact of specific inflammatory triggers upon mitochondrial function and morphology with an emphasis upon fission and fusion, since these processes influence both mitochondria morphology and mitochondrial bioenergetics. Our data show a complex interplay between three different cytokines

6.1 Main Findings

6.1.1 The GENA348 mouse develops mitochondrial dysfunction

This thesis builds upon a previous student reporting that at 6 months of age the GENA348 mice develop early LV dysfunction (Gibbon ,2011) now demonstrates that the GENA348 mice also exhibit mitochondrial dysfunction at 6 months. These results are coherent with that reported in patients with T2DM, whereby diastolic dysfunction marked the inability to maintain and increase left ventricular filling volumes (Wilson et al., 2017). More specifically, biochemistry methods coupled with a mitochondrial proteomic screen identified an imbalance in several fission-fusion proteins, proteins associated with mitophagy and motility. We also recorded impaired OXPHOS in GENA348 mice, which may be one contributing factor to defects in cardiomyocyte contractility.

As discussed in Chapter 3, typically small fragmented mitochondria have been reported in various models of heart disease, including diabetes with down-regulation of Mfn2 reported (Hall et al., 2016). However, the GENA348 mouse model differs from many other models in that the mice are not insulin resistant, Although, work by a previous student in our group, Lucy Murfitt, also reported elevated levels of Mfn2 in an STZ rat model of T1DM (Lucy Murfitt Thesis, 2016). Like our results, there were defects in ETC Complex activities, and the PNM were enlarged. The upregulation of fusion proteins could in part be explained by the downregulation in PINK1/Parkin in the GENA348 myocardium. PINK1/Parkin regulate levels of Mfn1 and Mfn2 ubiquitination, marking mitochondria for mitophagy (Sarraf et al., 2013).

Here, we also showed that the mitochondria, primarily the SSM were enlarged in the GENA348 myocardium and there was an increase in mitochondrial density; the data is consistent with the biochemical data such as an increase in fusion proteins and increased citrate synthase activity. Furthermore, the data showed an upregulation of Opa1 in GENA348 mice, a protein required for the fusion of the IMM the necessary next step after fusion of the OMM, and for stabilisation of the cristae (Olichon et al., 2007). This increased expression is consistent with the overexpression of Mfn1 and Mfn2, and the formation of new mitochondria. As discussed

above there are a range of conflicting data in the literature possibly since different animal models (species and strains) at different ages with different methods of disease induction, type of diabetes and stage of disease have been studied. Taken together, this shows that an increase in Mfn1/Mfn2 in response to diabetic insult, is associated with mitochondrial dysfunction and altered morphology.

Table 6.1 Comparison between the level of mitochondrial dynamic protein in the GENA348 myocardium compared to reports from studies of T2DM:

	GENA348	T2DM	Reference
Mfn1	↑	↓	(Park, Wiederkehr & Wollheim, 2012)
OPA1	↑	↓	(Patten et al., 2020)
DRP1	--------	↑	(Josifova et al., 2008)
PINK1	↓	↑	(Xiagn et al., 2020)
PARKIN	↓	↑	(Xiagn et al., 2020)
PGC1ALPHA	↑	↑	(Haijiang et al., 2016)
TFAM	↑	↑	(Koh et al., 2019)

OCR measurements, whilst important, alone are insufficient for the accurate quantification of energy metabolism due to variability in oxidation and phosphorylation rates (Salin et al., 2015). Variability can arise as a result of environmental changes, including growth rate; thus, both ATP generation and OCR require measurement in synchrony for a more accurate

representation of the overall consumption rate. The OCR data would suggest that initially the mitochondria are able to generate more ATP compared to WT mitochondria but are then unable to sustain that level of output. Taking both the OCR and molecular data, it would suggest that increased fusion (as indicated by increased levels of Mfn2) is not necessarily beneficial for function. Therefore, future work should include measuring the rate of ATP production and membrane potential. In humans, cardiac metabolism measurements present challenges, particularly with obtaining cardiac tissue and low sensitivity techniques such as magnetic resonance. The use of chemical exchange saturation transfer (CrCEST) has been used in a mouse model studying myocardial mitochondrial function, through measuring the conversion of phosphocreatine to creatine by creatine kinase as an indication of ATP production (Haris et al., 2014). This could be a useful technique applied for future work, though currently we do not have a small animal MRI machine. One can also simply measure ATP using tissue extracts and Glo reagent, which is a luminescence-based assay that measures proteasome activity (Strucksberg et al., 2010).

Proteomics identified that a myriad of mitochondrial signalling pathways was impaired in the GENA348 heart including fatty acid metabolism, oxidative stress and metabolism. An example of this was a significant decrease in the carnitine palmitoyl transferase protein subunit (CPT1B) included in the mitochondrial l-carnitine shuttle pathway transport of fatty acids into the lumen for energy production via β-oxidation. Another such protein, prohibitin-2, was identified as significantly decreased in the GENA348 mouse. Prohibitin is a protein implicated in mitochondrial protein folding alongside various cellular functions. Its downregulation has been reported as relevant in various diseases, thought to attenuate oxidative stress conditions (Zhou et al., 2013). Thus, this method provided an insight into such proteins that are impacted in MODY2 diabetes. Further analyses also indicated that a feature of the GENA348 heart included elevated levels of inflammatory cytokines within the GENA348 myocardium. An early characteristic of cardiac complication associated with diabetes is recognised by an increase in inflammatory markers (Becher et al., 2013), In agreement with this, we found a significant increase in the transcript level of inflammatory biomarkers TNF-α, IL-1β, and IL-6 in GENA348 mice myocardium. These data could suggest that inflammatory markers could be used

diagnostically and be indicative of a possible therapy using anti-inflammatory drugs for MODY2 sufferers (Pollack et al., 2016) and for intervention of diabetic cardiomyopathy.

In conclusion, we have shown that at 6 months of age the GENA348 mice have developed cardiac complications and at the cellular and molecular level exhibit impaired mitochondrial dysfunction. Therefore, from a translational perspective these data suggest that MODY2 patients require increased monitoring and are at risk of developing cardiac failure.

6.1.2 Obesity exacerbates mitochondrial dysfunction in the GENA348 mice

Obesity significantly increases the risk of T2DM and, although asymptomatic; however, to our knowledge there have been no in-depth studies of how obesity impacts MODY2 patients. Using the GENA348 model, diet-induced obesity was investigated for its impact on mitochondrial cardiac function. Here, mice at 3 months of age were fed a high-fat diet for three months. In literature, studies have investigated the impact of obesity and diabetes using other genetic models of diabetes, such as *db/db* or the ZDF rat, with chemically induced obesity using streptozotocin to destroy pancreatic β cells. Some studies have reported the failure in identifying cardiac pathologies after HFD feeding (Brainard et al., 2013), which could be representative of the variability in the different models for inducing obesity and diabetes, the length and the type of high fat diet.

Unsurprisingly, a HFD led to an increased body weight, a risk factor for developing T2DM. In addition, HFD led to increased lung weight, suggestive of pulmonary congestion. The mice were now also insulin resistant. However, a comparison of the expression levels of proteins associated with mitochondrial fission-fusion, mitophagy and motility showed no change in the GENA348 myocardium after high fat feeding; with the exception of Miro1 that was upregulated. Given that the high fat fed mice are now insulin resistant these data may suggest that insulin resistance/signalling does not influence mitochondrial dynamics. Similarly, there was no change to TFAM and PGC1-α, regulators of mitochondrial biogenesis, which is perhaps incongruent with the increase in citrate synthase levels indicative of increased mitochondrial content. Changes to mitochondrial biogenesis markers have been linked to HFD. In an

investigation of mitochondrial turnover by Tong et al. (2019) revealed no change in levels of PGC1-α and TFAM during HFD consumption. Although these proteins did not change in expression in the GENA348 heart due to HFD, there are other mitochondrial biogenesis markers, such as NRF1, that could be investigated for changes the GENA348 mouse. Interestingly, there was an increase in Miro1 levels which would suggest that the organisation of the mitochondria may be altered as a result of a high fat diet. Future work could collect SBF-SEM datasets of the GENA348-HFD myocardium to compare with the data in Chapter 3.

While there were no changes to the principal proteins regulating mitochondrial a proteomic screen of isolated mitochondria was carried out. We found a significant upregulation of 117 proteins that show an obvious widespread change to pathways involved in mitochondrial function regulation as a result of obesity. These included proteins involved in oxidative stress management, mitochondrial complex activity and fatty acid metabolism. Interestingly, the pathway with the greatest modification of protein expression was that involved in cardiac hypertrophy signalling, such as the G-protein signalling pathway. In the diabetic state, excess fatty acids are present inside the cell leading to excessive mitochondrial FAO. Increased oxidative stress is common in models of diabetic cardiomyopathy. Studies have shown that oxidative stress correlates with excess lipid delivery and elevated mitochondrial FAO rates, suggesting that mitochondria are a crucial source of free radicals in the diabetic heart (Van De Weijer et al., 2011). It is also a possibility that dysfunctional ROS scavenging mechanisms cause increased oxidative stress in the diabetic heart. We identified a significant 1.8-fold decrease in both SOD1 and SOD2 in the GENA348 compared to WT controls and a significant 1.8-fold decrease in SOD2 in WT-HFD mice, compared to WT controls. As previously mentioned, SOD2 is a marker of oxidative stress, with the overexpression of cardiac SOD2 preventing mitochondria from undergoing oxidative stress (Kang et al., 2015). Thus, such protein changes are strongly suggestive of heart failure progression.

The proteomics data also likely explain that there were also a significant decrease to the activity of the mitochondrial complexes in all HFD mice; which would also explain the decrease in OCR in the GENA348-HFD cardiac mitochondria. Again, these data are in agreement with

studies showing a dramatic reduction in complex activity in response to high fat fed animal models e.g. (Chen et al., 2018).

Interestingly, expression of proteins involved in mitochondrial dynamics presented a similar profile when comparing GENA348-chow and WT-HFD, suggesting a comparative fission-fusion profile. A previous study showed that Mfn1 liver-specific deletion knockout mice demonstrated a preference for the use of lipids as the predominant energy source (Kulkarni et al., 2016). Based on this, it may have been expected to observe an increase of Mfn1 in the GENA348-HFD heart. It should be noted that Kulkarni et al. (2016) was testing the effect of reduced mitochondial fusion on a hepatic model; however, in our model, no change was measured in Mfn1 in all HFD conditions. Interestingly, an increase in Mfn2 was recorded in WT-HFD compared to the WT controls with many of the changes mirroring those observed between WT and GENA348-chow mice. Mfn2 has been reported as impaired in HFD conditions (Chen et al., 2018). Why there is no change or further increase to Mfn2 expression in the GENA348 mouse after high fat feeding may suggest that it is mechanisms around the development of hyperglycaemia and not insulin resistance that drive changes to Mfn2 expression. Additionally, the increase in Mfn2 may be a cardioprotective or adaptive mechanism with the cardiomyocytes having a limited capacity for adaptation. It should also be noted that Chen et al. (2018) investigated HFD conditions with rats fed HFD for 28-weeks. This is a 2.3-fold increase in terms of duration of high-fat feeding compared to the three months in this study and may suggest that longer durations of high-fat feeding cause worsening of the cardiac dysfunction.

Overall, this data suggests that obesity impacts mitochondrial dynamics in both WT and the GENA348. However, the study comparing the GENA348-chow and GENA348-HFD highlights that while there may be no change to proteins governing fission-fusion, mitophagy or biogenesis there is evidence of worsen mitochondrial function through a myriad of pathways including oxidative stress. Interestingly, while there was no change to the levels of IL1β or TNF-α, IL-6 was elevated after high fat feeding in the GENA348 mice, indicative of a change to the inflammatory profile. Inflammatory events triggered at the start of diabetes causes the

release of pro-inflammatory cytokines including TNF-α, IL-1β, and IL-6 (Medzhitov and Janeway, 2000), which gradually increase as the disease progresses. A number of studies have shown that elevated levels of IL-6 are associated with T2DM (Meigs et al., 2004; Pradhan et al., 2001), supporting a role of elevated IL-6 as a potential marker for predicting the development of T2DM. It is thought that pro-inflammatory cytokines downregulate the major anabolic cascades involved in insulin signalling to impair glucose homeostasis, particularly in obesity-related diabetes (Hotamisligil et al., 1995; Bastard et al., 2006). In response to pro-inflammatory mediators, the endothelial lining of the microvasculature increases expression of intracellular adhesion molecule 1 (ICAM-1) and/or vascular cell adhesion molecule (VCAM-1), to interact with leukocyte-expressed integrins, enabling their capture and migration to the injured area (Henderson et al., 2001). In fact, adipose tissue acts as motor for obesity-induced inflammation, through the recruitment of macrophages leading to the activation of IL-6 cytokine secretion (Vachharajani and Granger, 2009).

Further work could expand on characterising cytokine levels in each of the animal models here using method such as ELISA broad screen or measuring plasma levels, such as IL-18. In a study of obese and T2DM patients, Zilverschoon et al. (2008) investigated the concentration of IL-18 for its role in improving insulin resistance. The study showed that patients with T2DM and obesity exhibited increased circulating concentrations of IL-18, suggestive of IL-18 resistance that is associated with a mechanism that may be due to defective signalling. An investigation into such plasma concentrations could further explain the results of this study.

6.1.3 Miro1 impacts mitochondrial homeostasis and inflammation in rat ventricular H9c2 cells

Building upon the findings that several cytokines were elevated in the GENA348 myocardium, we undertook studies to investigate if there is a link between increased TNF-α and IL-6 and mitochondrial dynamics focussing on Miro1, due to its upregulation in GENA348-HFD. This result suggests an impact of mitochondrial transport in our MODY2 model which worsened with obesity. Saotome et al. (2008), showed that knockdown of Miro1 H9c2 cells resulted in mitochondrial morphological defects and dysfunction of mitochondrial movement through the

cardiomyocyte. The PINK1/Parkin pathway targets Miro1 for phosphorylation and degradation, leading to the arrest of mitochondrial movement (Wang et al., 2011); although these were down-regulated in the GENA348-chow, no further change was observed after high fat feeding. We showed that knockdown of Miro1 did not directly affect Mfn1, Mfn2 or Drp1 levels but there was data showed a significant increase in Opa1 gene expression. Further, this was accompanied by a decrease in mitochondrial volume and surface area (although it should be noted that for SBF-SEM, there was a low n-number of 1). Thus, repeats are necessary to corroborate and validate findings. It is known that Opa1 protects the mitochondria through stabilising the cristae morphology (Frezza et al., 2006), suggesting that the increase in Opa1 reflects the need for mitigating mitochondrial stress. The data also showed no change in Parkin and an increase in PINK1. Since the PINK1/Parkin works in synchrony for mitochondrial quality control, it could be indicative that this pathway is damaged but then it might be expected to see changes to Mfn1/2 protein levels which was not the case. However, PINK1 works upstream to Parkin, so disruption in this pathway would impact PINK1 initially. These results may indicate a more complex pathway is involved for regulating MIro1 and also Mfn1/2.

Miro1 knockdown also resulted in a differentially altered expression of mitochondrial biogenesis markers PGC1-α and TFAM. Knockdown of Miro1 in H9c2 cells led to a decrease in PGC-1α whilst TFAM expression was significantly increased. The increase in TFAM expression could indicate that mitochondria are damaged or under stress, requiring the formation of new mitochondria. However, this doesn't appear true for PGC1-α, which would be expected to also have increased expression due to the same reason. The rate of oxygen consumption and citrate synthase activity were unchanged in Miro1 knockdown, again, suggesting that there was no change in mitochondrial content. These results contradict our data and what is known about PGC-1α and how it regulates mitochondrial respiration through altering mitochondrial density (Austin and St-Pierre, 2012). As discussed above other measure of metabolic function and levels of ROS levels could form the basis of future work to assess more detailed effects of MIro1 loss. For the first time, our data used 3D electron microscopy to investigate changes in mitochondrial morphology in Miro1 knock down H9c2 cells. The results showed a decrease in mitochondrial volume and surface area as a result of Miro1

knockdown. Although this change is prominent, it does not indicate change to internal mitochondrial structure. Given more time, a greater sample size would have been employed coupled with imaging using TEM at higher resolutions to visualise the cristae organisation.

A further novel finding from this research was the link between inflammatory cytokines and mitochondrial dynamics and motility at the cellular level. Our data suggests that IL-1β alters the fission-fusion axis towards destabilised smaller mitochondria, reduced mitochondrial content and impaired OXPHOS. However, surprisingly, Miro1 levels were upregulated, reflecting a possible compensatory mechanism to modulate mitochondrial availability as a result of destabilised mitochondria. In contrast to IL-1β, Miro1 levels were down-regulated in IL-6 conditions, possibly due to differing roles of each cytokine and the cardioprotective abilities of IL-6. Lastly, we investigated the involvement of TNF-α as another cytokine elevated in heart failure and associated with IL-6. Here, we found upregulated Miro1, similar to IL-1β results. To compare, in our animal studies, it was determined that there is a significant increase in the transcript level of inflammatory biomarkers TNF-α, IL-1β and IL-6 in GENA348 mice myocardium. There was also a significant increase in inflammatory marker gene expression, IL-6, IL-1β and TNF-α in WT-HFD compared to WT, whilst only IL-6 was upregulated in GENA348-HFD mice. This, it appears that Miro1 expression is differentially regulated by all three cytokines investigated in this study. Further study could investigate this mechanism to advance current understanding of how inflammation may be a driver of mitochondrial dysfunction.

6.2 Methodical Considerations

6.2.1 Clinical relevance of animal models

Animal models are commonly used for research into cardiac pathology and disease, providing a reliable alternative to the use of human participants or tissue samples. In this study investigating MODY2 diabetes and obesity, the GENA348 mouse model enabled reliable investigation into disease development. This model is easy to generate and displays excellent characteristics that replicate the human phenotype. Previous studies have demonstrated that

the GENA348 mouse is clinically relevant as a MODY2 model (Fabiano et al., 2016), making it a strong candidate model for use in this study. Despite this, there have been a lack of studies about MODY2 and inflammation or MODY2 and cardiac function associated with the mitochondria. Unfortunately, it was not possible to carry out echo data for GENA348 and to compare with GENA348-HFD, due to the use of differing echo machines.

6.2.2 Clinical relevance of cell models

For the investigation in Miro1, cell culture studies were used, focusing on the immortal H9c2 cell line, derived from rat neonatal cardiac myoblasts. Cell culture studies enable tighter control into the culture environment and provide greater detail into molecular disease development, particularly in the pathogenesis of T2DM. Using H9c2 cells provides a strong advantage in that an endless supply of cells are available, negating the need for ethical considerations, such as that for studies with mouse models. For cardiac studies, it can be difficult to isolate primary cardiomyocytes for each stage of the study. AS discussed in the previous Chapter compared to primary rat neonatal cardiomyocytes, H9c2 cells showed an almost identical response to hypertrophic factors angiotensin II and endothelin-1 (Watkins et al., 2011). Primary cell lines can also be hard to isolate in a pure population, are more sensitive and require frequent media changes. Furthermore, primary cardiomyocytes are well known to become flattened and rounded after 48h in culture (Mitcheson et al., 1998), making molecular manipulation using transfection techniques difficult. However, it is important to note that extensive passage of cell lines such as H9c2 can result in the divergence of primary cell phenotypes and was considered during the undertaking of this work.

To overcome this, new cell line stocks were used after every 15 passage repeats. Neonatal rat cardiomyocytes (NRCM) have a disadvantage when studying mitochondrial function as the substrate occurs through glycolysis rather than in mature cardiomyocytes whereby fatty acid oxidation takes place. Overall, neither cell model provides a complete solution and choice of either option comes with its advantages and disadvantages. As a method of validation, future work could test if the results in this thesis can be replicated in primary adult cardiomyocytes.

6.2.3 Limitations of SBF-SEM

SBF-SEM is a novel technique whereby high-contrast images are obtained from fixed tissue. Here, SBF-SEM was used to investigate putative remodelling of the GENA348 cardiac mitochondria and to determine volume and surface area of individual mitochondria. This enabled an improved understanding of why molecular level proteins mediating mitochondrial dynamics and biogenesis were perturbed along which changes OXPHOS and linking this to ultrastructural mitochondrial changes. However, there are several limitations of the method. The rate-limiting step is that features such as mitochondria need to be manually segmented so although sample preparation and data collection took approximately two weeks, data analysis required at least three months. The resolution of SBF-SEM is also limited such that the internal features of the mitochondria are not resolved. Other similar techniques such as focussed ion-beam scanning (FIB)-SEM work on a similar principle to SBF-SEM but can yield higher resolution images in the X:Y:Z planes but captures a much smaller field of view (Xu et al., 2017). There was a greater variability in mitochondrial morphological parameters in the GENA348 mitochondria a contributory factor may be the low n-number and/or a reflection of the remodelling. However, we and others have previously shown that for this technique than n=3 per experimental group yields reliable data even for acute conditions such as myocardial infarction where variability due to differences in infarct size may play a role (Pinali et al., 2017).

6.3 Directions for Further Research

6.3.1 Investigate the direct effects of fission-fusion proteins using cell culture

One of the main findings of this thesis was a significant upregulation in molecular levels of Mfn1, Mfn2 and Opa1, whilst Drp1 was downregulated, associated with changes to mitochondrial morphology in the GENA348 mouse. Through our data, we showed that the GENA348 mouse exhibits altered mitochondrial dynamics. To further investigate these pathways, expression of these proteins could be modified through cell culture techniques in combination with the manipulation of PINK1/Parkin. This data would provide an insight into

understanding the mitochondrial molecular pathways involved in the pathogenesis of diabetes, as seen in the EM images. Additionally, studies could also extend to older GENA348 mice e.g. 1 year of age as unpublished data from the Cartwright group have shown that LV dysfunction worsens; although maintaining animals for long periods of time is very costly.

6.3.2 Investigate increased inflammatory markers as a diabetes risk predictor

Our data showed an elevation of IL-6 in the GENA348, suggestive of a worsening in cardiac function. IL-6 has been implicated in diabetes and cardiovascular complications (Qu et al., 2014) and is a characteristic marker of metabolic disorder and cardiovascular disease (Qu et al., 2014). It would, therefore, be interesting to knockout IL-6 in GENA348 mice and investigate cardiac function. Elevation of IL-6, similar has been characterised as a marker of metabolic disorder and cardiovascular disease (Scheller et al., 2011). In line with other studies, it would be expected that this knockout would provide protection against diabetic cardiomyopathy (Zhang et al., 2016). In this study of IL-6 diabetic knockout mice, cardiac function improved, suggesting a protective effect against diabetic cardiomyopathy (Zhang et al., 2016). Here, wildtype diabetic mice were induced by STZ and investigated 12-weeks after diabetes induction (Zhang et al., 2016). In relation to the present study, this suggests that an elevation of IL-6 in the GENA348 worsens cardiac function. Thus, this could provide valuable data as a therapeutic marker and suggesting future risk probability. Future work could investigate the migration of macrophages into the GENA348 myocardium as a source of inflammatory cytokines, although cell types such as fibroblasts can secrete cytokines. Generally, it can be said that chronic inflammation and diabetes depend on each other and play a common role (Feng et al., 2018) and the novel work from this thesis has shown that it is also a feature of the GENA348 mouse. Again, this would provide an insight into how inflammation characterises in cardiac abnormality.

6.4 Conclusion

Through the combination of a wide range of experimental techniques, this PhD research investigated mitochondrial dysfunction linked to the pathogenesis of cardiovascular

complications identified in T1DM and T2DM, using a mouse model (GENA348) with a mutation in the glucose kinase gene. Our data reveals that the GENA348 mice develop cardiovascular complications, with an imbalance in mitochondrial dynamics. However, it is unclear whether increased fusion is a cardioprotective response. The role of fission-fusion proteins that regulate mitochondrial dynamics and morphological changes determined by these proteins will provide invaluable information that can be used for therapeutic intervention in the treatment of cardiac mitochondrial dysfunction in MODY2 diabetes. Further our data indicate that monitoring of cardiac function in MODY2 patients may be important since our mouse model incorporating the *Gck* mutation appears to develop diastolic dysfunction.

Bibliography

Aigner, B., Rathkolb, B., Herbach, N., de Angelis, M. H., Wanke, R. & Wolf, E. (2008). 'Diabetes models by screen for hyperglycemia in phenotype-driven ENU mouse mutagenesis projects', *American Journal of Physiology-Endocrinology and Metabolism*, 294(2), pp. E232-E240.

Al-Lamki, R. (2005). 'Wang J, Vandenabeele P, Bradley JA, Thiru S, Luo D, Min W, Pober JS, Bradley JR', TNFR1-and TNFR2-mediated signaling pathways in human kidney are cell type-specific and differentially contribute to renal injury. *FASEB* J, 19, pp. 1637-1645.

Al-Awar, A., Kupai, K., Veszelka, M., Szűcs, G., Attieh, Z., Murlasits, Z., Török, S., Pósa, A., & Varga, C. (2016). Experimental Diabetes Mellitus in Different Animal Models. *Journal of diabetes research*, 9051426.

Alcalai, R., Seidman, J. G. & Seidman, C. E. (2008). 'Genetic basis of hypertrophic cardiomyopathy: from bench to the clinics', *Journal Of Cardiovascular Electrophysiology*, 19(1), pp. 104-110.

Alhindi, Y., Vaanholt, L. M., Al-Tarrah, M., Gray, S., Speakman, J. R., Hambly, C., Al-Anazi, B. S., Gabriel, B. M., Lionikas, A. & Ratkevicius, A. (2019). 'Corrigendum to “Low Citrate Synthase Activity Is Associated with Glucose Intolerance and Lipotoxicity”', *Journal of Nutrition and Metabolism*, 2019.

Alston, C. L., Davison, J. E., Meloni, F., van der Westhuizen, F. H., He, L., Hornig-Do, H.-T., Peet, A. C., Gissen, P., Goffrini, P. & Ferrero, I. (2012). 'Recessive germline SDHA and SDHB mutations causing leukodystrophy and isolated mitochondrial complex II deficiency', *Journal of Medical Genetics,* 49(9), pp. 569-577.

An, H.-J., Cho, G., Lee, J.-O., Paik, S.-G., Kim, Y. S. & Lee, H. (2013). 'Higd-1a interacts with Opa1 and is required for the morphological and functional integrity of mitochondria', *Proceedings of the National Academy of Sciences,* 110(32), pp. 13014-13019.

Ande, S. R., Xu, Y. X. Z. & Mishra, S. (2017). 'Prohibitin: a potential therapeutic target in tyrosine kinase signaling', *Signal Transduction and Targeted Therapy*, 2(1), pp. 1-8.

Angin, Y., Steinbusch, L. K., Simons, P. J., Greulich, S., Hoebers, N. T., Douma, K., van Zandvoort, M. A., Coumans, W. A., Wijnen, W. & Diamant, M. (2012). 'CD36 inhibition prevents lipid accumulation and contractile dysfunction in rat cardiomyocytes', *Biochemical Journal*, 448(1), pp. 43-53.

Anık, A., Çatlı, G., Abacı, A. & Böber, E. (2015). 'Maturity-onset diabetes of the young (MODY): an update', *Journal of Pediatric Endocrinology And Metabolism*, 28(3-4), pp. 251-263.

Artham, S. M., Lavie, C. J., Milani, R. V. & Ventura, H. O. (2007). 'The obesity paradox and discrepancy between peak oxygen consumption and heart failure prognosis—it's all in the fat', *Congestive Heart Failure*, 13(3), pp. 177-180.

Asghar, O., Al-Sunni, A., Khavandi, K., Khavandi, A., Withers, S., Greenstein, A., Heagerty, A. M. & Malik, R. A. (2009). 'Diabetic cardiomyopathy', Clinical science, 116(10), pp. 741-760.

Ashrafi, G. & Schwarz, T. (2013). 'The pathways of mitophagy for quality control and clearance of mitochondria', *Cell Death & Differentiation*, 20(1), pp. 31-42.

Association, A. D. (2014). 'Diagnosis and classification of diabetes mellitus', *Diabetes Care*, 37(Supplement 1), pp. S81-S90.

Atkinson, M. A., Eisenbarth, G. S. & Michels, A. W. (2014). 'Type 1 diabetes', *The Lancet*, 383(9911), pp. 69-82.

Austin, S. & St-Pierre, J. (2012). 'PGC1α and mitochondrial metabolism–emerging concepts and relevance in ageing and neurodegenerative disorders', *J Cell Sci*, 125(21), pp. 4963-4971.

Bach, D., Naon, D., Pich, S., Soriano, F. X., Vega, N., Rieusset, J., Laville, M., Guillet, C., Boirie, Y. & Wallberg-Henriksson, H. (2005). 'Expression of Mfn2, the Charcot-Marie-Tooth neuropathy type 2A gene, in human skeletal muscle: effects of type 2 diabetes, obesity, weight loss, and the regulatory role of tumor necrosis factor α and interleukin-6', *Diabetes*, 54(9), pp. 2685-2693.

Bach, D., Pich, S., Soriano, F. X., Vega, N., Baumgartner, B., Oriola, J., Daugaard, J. R., Lloberas, J., Camps, M. & Zierath, J. R. (2003). 'Mitofusin-2 determines mitochondrial network architecture and mitochondrial metabolism A novel regulatory mechanism altered in obesity', *Journal of Biological Chemistry*, 278(19), pp. 17190-17197.

Banerjee, M. & Saxena, M. (2012). 'Interleukin-1 (IL-1) family of cytokines: role in type 2 diabetes', *Clinica Chimica Acta*, 413(15-16), pp. 1163-1170.

Bansal, S. S., Ismahil, M. A., Goel, M., Patel, B., Hamid, T., Rokosh, G. & Prabhu, S. D. (2017). 'Activated T lymphocytes are essential drivers of pathological remodeling in ischemic heart failure', *Circulation: Heart Failure*, 10(3), p. e003688.

Barker, J. M. (2006). 'Type 1 diabetes-associated autoimmunity: natural history, genetic associations, and screening', *The Journal of Clinical Endocrinology & Metabolism*, 91(4), pp. 1210-1217.

Barragán-Bonilla, M. I., Mendoza-Bello, J. M., Aguilera, P., Parra-Rojas, I., Illades-Aguiar, B., Ramírez, M. & Espinoza-Rojo, M. (2019). 'Combined Administration of Streptozotocin and Sucrose Accelerates the Appearance of Type 2 Diabetes Symptoms in Rats', *Journal of Diabetes Research*.198374556

Barth, E., Stammler, G., Speiser, B. & Schaper, J. Ultrastructural quantitation of mitochondria and myofilaments in cardiac muscle from 10 different animal species including man. *J. Mol. Cell. Cardiol.* 24, 669–681 (1992).

Bastard JP, Maachi M, Lagathu C, et al. Recent advances in the relationship between obesity, inflammation, and insulin resistance. *Eur Cytokine Netw*. 2006;17(1):4-12.

Becher, P., Lindner, D., Fröhlich, M., Savvatis, K., Westermann, D. & Tschöpe, C. (2013). 'Assessment of cardiac inflammation and remodeling during the development of streptozotocin-induced diabetic cardiomyopathy in vivo: a time course analysis', *International Journal of Molecular Medicine*, 32(1), pp. 158-164.

Bell, D. S. (2003). 'Heart failure: the frequent, forgotten, and often fatal complication of diabetes', *Diabetes Care*, 26(8), pp. 2433-2441.

Birsa, N., Norkett, R., Wauer, T., Mevissen, T. E., Wu, H.-C., Foltynie, T., Bhatia, K., Hirst, W. D., Komander, D. & Plun-Favreau, H. (2014). 'Lysine 27 ubiquitination of the mitochondrial transport protein Miro is dependent on serine 65 of the Parkin ubiquitin ligase', *Journal of Biological Chemistry*, 289(21), pp. 14569-14582.

Bishay, R. H. & Greenfield, J. R. (2016). 'A review of maturity onset diabetes of the young (MODY) and challenges in the management of glucokinase-MODY', *Medical Journal of Australia*, 205(10), pp. 480-485.

Blander, G. & Guarente, L. (2004). 'The Sir2 family of protein deacetylases', *Annual Review of Biochemistry*, 73(1), pp. 417-435.

Bonda, T. A., Szynaka, B., Sokołowska, M., Dziemidowicz, M., Waszkiewicz, E., Winnicka, M. M., Bernaczyk, P., Wawrusiewicz-Kurylonek, N. & Kamiński, K. A. (2016). 'Interleukin 6 modulates PPARα and PGC-1α and is involved in high-fat diet induced cardiac lipotoxicity in mouse', *International Journal of Cardiology*, 219, pp. 1-8.

Boudina, S., Sena, S., O'Neill, B., Tathireddy, P., Young, M. & Abel, E. (2005). 'Reduced 472 mitochondrial oxidative capacity and increased mitochondrial uncoupling impair myocardial 473 energetics in obesity', *Circulation*, 112(2686-2695), p. 434.

Boureux, A., Vignal, E., Faure, S. & Fort, P. (2007). 'Evolution of the Rho family of ras-like GTPases in eukaryotes', *Molecular Biology and Evolution*, 24(1), pp. 203-216.

Boutant, M., Kulkarni, S. S., Joffraud, M., Ratajczak, J., Valera-Alberni, M., Combe, R., Zorzano, A. & Cantó, C. (2017). 'Mfn2 is critical for brown adipose tissue thermogenic function', *The EMBO Journal*, 36(11), pp. 1543-1558.

Bowman, P., Flanagan, S., Edghill, E., Damhuis, A., Shepherd, M., Paisey, R., Hattersley, A. T. & Ellard, S. (2012). 'Heterozygous ABCC8 mutations are a cause of MODY', *Diabetologia*, 55(1), pp. 123-127.

Brainard, R. E., Watson, L. J., DeMartino, A. M., Brittian, K. R., Readnower, R. D., Boakye, A. A., Zhang, D., Hoetker, J. D., Bhatnagar, A. & Baba, S. P. (2013a). 'High fat feeding in mice is insufficient to induce cardiac dysfunction and does not exacerbate heart failure', *PLoS One*, 8(12).

Bratic, A. & Larsson, N.-G. (2013). 'The role of mitochondria in aging', *The Journal of Clinical Investigation*, 123(3), pp. 951-957.

Brocheriou, V., Hagège, A. A., Oubenaïssa, A., Lambert, M., Mallet, V. O., Duriez, M., Wassef, M., Kahn, A., Menasché, P. & Gilgenkrantz, H. (2000). 'Cardiac functional improvement by a human Bcl-2 transgene in a mouse model of ischemia/reperfusion injury', *The Journal of Gene Medicine*, 2(5), pp. 326-333.

Buchanan, J., Mazumder, P. K., Hu, P., Chakrabarti, G., Roberts, M. W., Yun, U. J., Cooksey, R. C., Litwin, S. E. & Abel, E. D. (2005). 'Reduced cardiac efficiency and altered substrate metabolism precedes the onset of hyperglycemia and contractile dysfunction in two mouse models of insulin resistance and obesity', *Endocrinology*, 146(12), pp. 5341-5349.

Bugger, H. & Abel, E. D. (2010). 'Mitochondria in the diabetic heart', *Cardiovascular Research*, p. cvq239.

Bujak, M. & Frangogiannis, N. G. (2009). 'The role of IL-1 in the pathogenesis of heart disease', *Archivum Immunologiae Et Therapiae Experimentalis*, 57(3), pp. 165-176.

Bujak, M., Dobaczewski, M., Chatila, K., Mendoza, L. H., Li, N., Reddy, A. & Frangogiannis, N. G. (2008). 'Interleukin-1 receptor type I signaling critically regulates infarct healing and cardiac remodeling', *The American Journal of Pathology*, 173(1), pp. 57-67.

Byrne, M. M., Sturis, J., Clement, K., Vionnet, N., Pueyo, M. E., Stoffel, M., Takeda, J., Passa, P., Cohen, D. & Bell, G. I. (1994). 'Insulin secretory abnormalities in subjects with hyperglycemia due to glucokinase mutations', *The Journal of Clinical Investigation*, 93(3), pp. 1120-1130.

Cabal-Hierro, L. & Lazo, P. S. (2012). 'Signal transduction by tumor necrosis factor receptors', *Cellular Signalling*, 24(6), pp. 1297-1305.

Cao, Y., Xu, C., Ye, J., He, Q., Zhang, X., Jia, S., Qiao, X., Zhang, C., Liu, R. & Weng, L. (2019). 'Miro2 regulates inter-mitochondrial communication in the heart and protects against TAC-induced cardiac dysfunction', *Circulation Research*, 125(8), pp. 728-743.

Carafa, V., Rotili, D., Forgione, M., Cuomo, F., Serretiello, E., Hailu, G. S., Jarho, E., Lahtela-Kakkonen, M., Mai, A. & Altucci, L. (2016). 'Sirtuin functions and modulation: from chemistry to the clinic', *Clinical Epigenetics*, 8(1), p. 61.

Carmody, D., Naylor, R. N., Bell, C. D., Berry, S., Montgomery, J. T., Tadie, E. C., Hwang, J. L., Greeley, S. A. W. & Philipson, L. H. (2016). 'GCK-MODY in the US National Monogenic Diabetes Registry: frequently misdiagnosed and unnecessarily treated', *Acta Diabetologica*, 53(5), pp. 703-708.

Cartoni, R., Léger, B., Hock, M. B., Praz, M., Crettenand, A., Pich, S., Ziltener, J. L., Luthi, F., Dériaz, O. & Zorzano, A. (2005). 'Mitofusins 1/2 and ERRα expression are increased in human skeletal muscle after physical exercise', *The Journal of Physiology*, 567(1), pp. 349-358.

Chan, D. C. (2012). 'Fusion and fission: interlinked processes critical for mitochondrial health', A*nnual Review of Genetics*, 46, pp. 265-287.

Chang, C. R. & Blackstone, C. (2007). 'Drp1 phosphorylation and mitochondrial regulation', *EMBO Reports*, 8(12), pp. 1088-1089.

Chavali, V., Tyagi, S. C. & Mishra, P. K. (2014). 'Differential expression of dicer, miRNAs, and inflammatory markers in diabetic Ins2+/− Akita hearts', *Cell Biochemistry and Biophysics*, 68(1), pp. 25-35.

Chazin, W. J. (2011). 'Relating form and function of EF-hand calcium binding proteins', *Accounts of Chemical Research*, 44(3), pp. 171-179.

Chen, D., Li, X., Zhang, L., Zhu, M. & Gao, L. (2018). 'A high-fat diet impairs mitochondrial biogenesis, mitochondrial dynamics, and the respiratory chain complex in rat myocardial tissues', *Journal of Cellular Biochemistry*, 119(11), pp. 9602-9602.

Chen, H. & Chan, D. C. (2005). 'Emerging functions of mammalian mitochondrial fusion and fission', *Human Molecular Genetics*, 14(suppl_2), pp. R283-R289.

Chen, L., Liu, C., Gao, J., Xie, Z., Chan, L. W., Keating, D. J., Yang, Y., Sun, J., Zhou, F. & Wei, Y. (2017). 'Inhibition of Miro1 disturbs mitophagy and pancreatic β-cell function interfering insulin release via IRS-Akt-Foxo1 in diabetes', *Oncotarget*, 8(53), p. 90693.

Chen, Y. & Dorn, G. W. (2013). 'PINK1-phosphorylated mitofusin 2 is a Parkin receptor for culling damaged mitochondria', *Science*, 340(6131), pp. 471-475.

Chen, Y., Liu, Y. & Dorn, G. W. (2011). 'Mitochondrial fusion is essential for organelle function and cardiac homeostasis', *Circulation Research*, 109(12), pp. 1327-1331.

Cheng, Z., & Ristow, M. (2013). Mitochondria and metabolic homeostasis. *Antioxidants & redox signaling*, *19*(3), 240–242.

Choi, J., Ravipati, A., Nimmagadda, V., Schubert, M., Castellani, R. J. & Russell, J. W. (2014). 'Potential roles of PINK1 for increased PGC-1α-mediated mitochondrial fatty acid oxidation and their associations with Alzheimer disease and diabetes', *Mitochondrion*, 18, pp. 41-48.

Cipolat, S., de Brito, O. M., Dal Zilio, B. & Scorrano, L. (2004). 'OPA1 requires mitofusin 1 to promote mitochondrial fusion', Proceedings of the National Academy of Sciences, 101(45), pp. 15927-15932.

Claude, A. & Fullam, E. F. (1945). 'An electron microscope study of isolated mitochondria: method and preliminary results', *The Journal of Experimental Medicine*, 81(1), p. 51.

Cogliati, S., Frezza, C., Soriano, M. E., Varanita, T., Quintana-Cabrera, R., Corrado, M., Cipolat, S., Costa, V., Casarin, A. & Gomes, L. C. (2013). 'Mitochondrial cristae shape determines respiratory chain supercomplexes assembly and respiratory efficiency', *Cell*, 155(1), pp. 160-171.

Colca, J. R., McDonald, W. G., Waldon, D. J., Leone, J. W., Lull, J. M., Bannow, C. A., Lund, E. T. & Mathews, W. R. (2004). 'Identification of a novel mitochondrial protein ("mitoNEET") cross-linked specifically by a thiazolidinedione photoprobe', *American Journal of Physiology-Endocrinology and Metabolism*, 286(2), pp. E252-E260.

Cong, W., Ruan, D., Xuan, Y., Niu, C., Tao, Y., Wang, Y., Zhan, K., Cai, L., Jin, L. & Tan, Y. (2015). 'Cardiac-specific overexpression of catalase prevents diabetes-induced pathological changes by inhibiting NF-κB signaling activation in the heart', *Journal of Molecular and Cellular Cardiology*, 89, pp. 314-325.

Crunkhorn, S., Dearie, F., Mantzoros, C., Gami, H., Da Silva, W. S., Espinoza, D., Faucette, R., Barry, K., Bianco, A. C. & Patti, M. E. (2007). 'Peroxisome proliferator activator receptor γ coactivator-1 expression is reduced in obesity potential pathogenic role of saturated fatty acids and p38 mitogen-activated protein kinase activation', *Journal of Biological Chemistry*, 282(21), pp. 15439-15450.

Cruz C, Kang MJ. 2018. Mitochondrial dysfunction and damage associated molecular patterns (DAMPs) in chronic inflammatory diseases. *Mitochondrion,* 41: 37-44.

Dabkowski, E. R., Baseler, W. A., Williamson, C. L., Powell, M., Razunguzwa, T. T., Frisbee, J. C. & Hollander, J. M. (2010). 'Mitochondrial dysfunction in the type 2 diabetic heart is associated with alterations in spatially distinct mitochondrial proteomes', *American Journal of Physiology-Heart and Circulatory Physiology*, 299(2), pp. H529-H540.

Dabkowski, E. R., Williamson, C. L., Bukowski, V. C., Chapman, R. S., Leonard, S. S., Peer, C. J., Callery, P. S. & Hollander, J. M. (2009). 'Diabetic cardiomyopathy-associated dysfunction in spatially distinct mitochondrial subpopulations', *American Journal of Physiology-Heart and Circulatory Physiology,* 296(2), pp. H359-H369.

Daghistani, H. M., Rajab, B. S. & Kitmitto, A. (2019). 'Three-dimensional electron microscopy techniques for unravelling mitochondrial dysfunction in heart failure and identification of new pharmacological targets', *British Journal Of Pharmacology*, 176(22), pp. 4340-4359.

Damasceno, D. C., Netto, A. O., Iessi, I. L., Gallego, F. Q., Corvino, S. B., Dallaqua, B., Sinzato, Y. K., Bueno, A., Calderon, I. M., & Rudge, M. V. (2014). 'Streptozotocin-induced diabetes models: pathophysiological mechanisms and fetal outcomes'. *BioMed research international*, *2014*, 819065.

De Brito, O. M. & Scorrano, L. (2008). 'Mitofusin 2: a mitochondria-shaping protein with signaling roles beyond fusion', *Antioxidants & Redox Signaling*, 10(3), pp. 621-634.

Della-Fera, M. A., Choi, Y. H., Hartzell, D. L., Duan, J., Hamrick, M. & Baile, C. A. (2005). 'Sensitivity of ob/ob mice to leptin-induced adipose tissue apoptosis', *Obesity Research*, 13(9), pp. 1540-1547.

Delvecchio, M., Mozzillo, E., Salzano, G., Iafusco, D., Frontino, G., Patera, P. I., Rabbone, I., Cherubini, V., Grasso, V. & Tinto, N. (2017). 'Monogenic diabetes accounts for 6.3% of cases referred to 15 Italian pediatric diabetes centers during 2007 to 2012', *The Journal of Clinical Endocrinology & Metabolism*, 102(6), pp. 1826-1834.

Denk, W. & Horstmann, H. (2004). 'Serial block-face scanning electron microscopy to reconstruct three-dimensional tissue nanostructure', *PLoS Biology*, 2(11). e329

Desai, A. & Fang, J. C. (2008). 'Heart failure with preserved ejection fraction: hypertension, diabetes, obesity/sleep apnea, and hypertrophic and infiltrative cardiomyopathy', *Heart Failure Clinics*, 4(1), pp. 87-97.

Devarshi, P. P., McNabney, S. M. & Henagan, T. M. (2017). 'Skeletal muscle nucleo-mitochondrial crosstalk in obesity and type 2 diabetes', International journal of molecular sciences, 18(4), p. 831.

Ding WX, Yin XM. Mitophagy: mechanisms, pathophysiological roles, and analysis. *Biol Chem*, 393(7):547-564

Donato, A. J., Henson, G. D., Morgan, R. G., Enz, R. A., Walker, A. E. & Lesniewski, L. A. (2012). 'TNF-α impairs endothelial function in adipose tissue resistance arteries of mice with diet-induced obesity', *American Journal of Physiology-Heart and Circulatory Physiology*, 303(6), pp. H672-H679.

Droz, B. A., Sneed, B. L., Jackson, C. V., Zimmerman, K. M., Michael, M. D., Emmerson, P. J., Coskun, T. & Peterson, R. G. (2017). 'Correlation of disease severity with body weight and high fat diet in the FATZO/Pco mouse', *PloS ONE*, 12(6). e0179808.

Dutta, S. & Sengupta, P. (2016). 'Men and mice: relating their ages', *Life Sciences*, 152, Pp. 244-248.

Eberhardt, E. L., Ludlam, A. V., Tan, Z. & Cianfrocco, M. A. (2020). 'Miro: A molecular switch at the center of mitochondrial regulation', *Protein Science*. 29(6):1269-1284.

Ehtisham, S., Hattersley, A., Dunger, D. & Barrett, T. (2004). 'First UK survey of paediatric type 2 diabetes and MODY', *Archives of Disease in Childhood*, 89(6), pp. 526-529.

Eigentler, A., Fontana-Ayoub, M., Fasching, M., Lassnig, B., Stadlmann, S., Rieger, G., Haffner, B., Lemieux, H. & Gnaiger, E. (2012). 'Selected media and chemicals for respirometry with mitochondria and permeabilized cells', *Mitochondrial Physiology Network*, 3(9), pp. 1-9.

Eiyama, A. & Okamoto, K. (2015). 'PINK1/Parkin-mediated mitophagy in mammalian cells', *Current Opinion in Cell Biology*, 33, pp. 95-101.

Eltzschig H, Carmeliet P. 2014. Hypoxia and inflammation. *New England journal of medicine,* 364(7): 656-665.

Fabiano, M. C., Verrienti, A., Carbone, A., Sponziello, M., Bellitti, P. & Bruno, R. (2016). 'Genotype-Phenotype Correlation in a MODY 2 Family: An Under-Diagnosed Disease', *Journal of Diabetes Mellitus*, 6(4), pp. 263-268.

Facundo, H. d. T. F., Brainard, R. E., de Lemos Caldas, F. R. & Lucas, A. M. B. (2017). 'Mitochondria and cardiac hypertrophy', Mitochondrial Dynamics in Cardiovascular Medicine: Springerpp. 203-226.

Farfel, Z., Bourne, H. R. & Iiri, T. (1999). 'The expanding spectrum of G protein diseases', *New England Journal of Medicine*, 340(13), pp. 1012-1020.

Farren, M., Daly, N., O'Higgins, A. C., McKeating, A., Maguire, P. J. & Turner, M. J. (2015). 'The interplay between maternal obesity and gestational diabetes mellitus', *Journal of Perinatal Medicine*, 43(3), pp. 311-317.

Fawcett, D. W. & McNutt, N. S. (1969). 'The ultrastructure of the cat myocardium: I. Ventricular papillary muscle', *The Journal of Cell Biology*, 42(1), pp. 1-45.

Fendler, W., Borowiec, M., Baranowska-Jazwiecka, A., Szadkowska, A., Skala-Zamorowska, E., Deja, G., Jarosz-Chobot, P., Techmanska, I., Bautembach-Minkowska, J. & Mysliwiec, M. (2012). 'Prevalence of monogenic diabetes amongst Polish children after a nationwide genetic screening campaign', *Diabetologia*, 55(10), pp. 2631-2635.

Feng, M., Wang, L., Chang, S. & Yuan, P. (2018). 'Penehyclidine hydrochloride regulates mitochondrial dynamics and apoptosis through p38MAPK and JNK signal pathways and

provides cardioprotection in rats with myocardial ischemia–reperfusion injury', *European Journal of Pharmaceutical Sciences*, 121, pp. 243-250.

Fex, M., Nicholas, L. M., Vishnu, N., Medina, A., Sharoyko, V. V., Nicholls, D. G., Spégel, P. & Mulder, H. (2018). 'The pathogenetic role of β-cell mitochondria in type 2 diabetes', *Journal of Endocrinology*, 236(3), pp. R145-R159.

Fontes, J. A., Rose, N. R. & Čiháková, D. (2015). 'The varying faces of IL-6: From cardiac protection to cardiac failure', *Cytokine*, 74(1), pp. 62-68.

Frank, S., Gaume, B., Bergmann-Leitner, E. S., Leitner, W. W., Robert, E. G., Catez, F., Smith, C. L. & Youle, R. J. (2001). 'The role of dynamin-related protein 1, a mediator of mitochondrial fission, in apoptosis', *Developmental Cell*, 1(4), pp. 515-525.

Fransson, Å., Ruusala, A. & Aspenström, P. (2003). 'Atypical Rho GTPases have roles in mitochondrial homeostasis and apoptosis', *Journal of Biological Chemistry*, 278(8), pp. 6495-6502.

Fransson, Å., Ruusala, A. & Aspenström, P. (2006). 'The atypical Rho GTPases Miro-1 and Miro-2 have essential roles in mitochondrial trafficking', *Biochemical and Biophysical Research Communications*, 344(2), pp. 500-510.

Franz, M. J., Boucher, J. L., Rutten-Ramos, S., & VanWormer, J. J. (2015). Lifestyle weight-loss intervention outcomes in overweight and obese adults with type 2 diabetes: a systematic review and meta-analysis of randomized clinical trials. *Journal of the Academy of Nutrition and Dietetics*, *115*(9), 1447–1463.

Frederick, R. L., McCaffery, J. M., Cunningham, K. W., Okamoto, K. & Shaw, J. M. (2004). 'Yeast Miro GTPase, Gem1p, regulates mitochondrial morphology via a novel pathway', *The Journal of Cell Biology*, 167(1), pp. 87-98.

Frey, T. G. & Mannella, C. A. (2000). 'The internal structure of mitochondria', *Trends in Biochemical Sciences*, 25(7), pp. 319-324.

Frey, U. H., Lieb, W., Erdmann, J., Savidou, D., Heusch, G., Leineweber, K., Jakob, H., Hense, H.-W., Löwel, H. & Brockmeyer, N. H. (2008). 'Characterization of the GNAQ promoter and association of increased Gq expression with cardiac hypertrophy in humans', *European Heart Journal*, 29(7), pp. 888-897.

Frezza, C., Cipolat, S., De Brito, O. M., Micaroni, M., Beznoussenko, G. V., Rudka, T., Bartoli, D., Polishuck, R. S., Danial, N. N. & De Strooper, B. (2006). 'OPA1 controls apoptotic cristae remodeling independently from mitochondrial fusion', *Cell*, 126(1), pp. 177-189.

Frustaci, A., Kajstura, J., Chimenti, C., Jakoniuk, I., Leri, A., Maseri, A., Nadal-Ginard, B. & Anversa, P. (2000). 'Myocardial cell death in human diabetes', *Circulation Research*, 87(12), pp. 1123-1132.

Fioranelli M, Bottaccioli A, Bottaccioli F, bianchi M, Rovesti M, Roccia M. 2018. Stress and inflammation in coronary artery disease: A review psychoneuroendocrineimmunology-based. *Frontiers in immunology,* 9: 2031.

Fu, J., Wang, T., Liu, J., Wang, X., Zhang, Q., Li, M. & Xiao, X. (2019). 'Using Clinical Indices to Distinguish MODY2 (GCK Mutation) and MODY3 (HNF1A Mutation) from Type 1 Diabetes in a Young Chinese Population', *Diabetes Therapy*, 10(4), pp. 1381-1390.

Gabay, C., Lamacchia, C. & Palmer, G. (2010). 'IL-1 pathways in inflammation and human diseases', *Nature Reviews Rheumatology*, 6(4), p. 232.

Gao Q, Wang X, Ye H, et al. 2012. Changes in the expression of cardiac mitofusin-2 in different stages of diabetes in rats. *Molecular medicine reports,* 6(4): 811-814.

Geng, Z., Fan, W.-Y., Zhou, B., Ye, C., Tong, Y., Zhou, Y.-B. & Xiong, X.-Q. (2019). 'FNDC5 attenuates obesity-induced cardiac hypertrophy by inactivating JAK2/STAT3-associated inflammation and oxidative stress', *Journal of Translational Medicine*, 17(1), p. 107.

Getz G, reardon C. 2015. Atherogenic lipids and macrophage subsets. *Current opinion lipidol,* 26: 357-361.

Gibbon, s. (2011). A thesis submitted to the University of Manchester for the degree of PhD in the Faculty of Medical and Human Sciences. Insights into a novel mouse model of Type 2 Diabetes

Gibbons, S., Hegab, Z., Zi, M., Prehar, S., Mohammed, T., Cox, R., Cartwright, E., Neyses, L. & Mamas, M. (2011). '67 Spontaneous cardiac hypertrophy and adverse LV remodelling in a novel human relevant mouse model of diabetes; a mechanistic insight', *Heart*, 97(Suppl 1), pp. A41-A41.

Giuffrida, F. M. & Reis, A. F. (2005). 'Genetic and clinical characteristics of maturity-onset diabetes of the young', *Diabetes, Obesity and Metabolism*, 7(4), pp. 318-326.

Gurung P, Lukens J, Kanneganti T. 2015. Mitochondrial: Diversity in the regulation of the NLRP3 inflammasome. *Trends in molecular biology,* 21(3): 193-201.

Glater, E. E., Megeath, L. J., Stowers, R. S. & Schwarz, T. L. (2006). 'Axonal transport of mitochondria requires milton to recruit kinesin heavy chain and is light chain independent', *The Journal of Cell Biology,* 173(4), pp. 545-557.

Glotov, O. S., Serebryakova, E. A., Turkunova, M. E., Efimova, O. A., Glotov, A. S., Barbitoff, Y. A., Nasykhova, Y. A., Predeus, A. V., Polev, D. E. & Fedyakov, M. A. (2019). 'Whole-exome sequencing in Russian children with non-type 1 diabetes mellitus reveals a wide spectrum of genetic variants in MODY-related and unrelated genes', *Molecular Medicine Reports*, 20(6), pp. 4905-4914.

Goldberg, I. J., Trent, C. M. & Schulze, P. C. (2012). 'Lipid metabolism and toxicity in the heart', *Cell Metabolism*, 15(6), pp. 805-812.

Gorman, T., Hope, D., Brownlie, R., Yu, A., Gill, D., Löfvenmark, J., Wedin, M., Mayers, R., Snaith, M. & Smith, D. (2008). 'Effect of high-fat diet on glucose homeostasis and gene expression in glucokinase knockout mice', *Diabetes, Obesity and Metabolism*, 10(10), pp. 885-897.

Graham, M. L., Janecek, J. L., Kittredge, J. A., Hering, B. J. & Schuurman, H.-J. (2011). 'The streptozotocin-induced diabetic nude mouse model: differences between animals from different sources', *Comparative Medicine*, 61(4), pp. 356-360.

Greene, N. P., Brown, J. L., Rosa-Caldwell, M. E., Lee, D. E., Blackwell, T. A. & Washington, T. A. (2018). 'Skeletal muscle insulin resistance as a precursor to Diabetes: Beyond glucoregulation', *Current Diabetes Reviews*, 14(2), pp. 113-128.

Guo, X., Macleod, G. T., Wellington, A., Hu, F., Panchumarthi, S., Schoenfield, M., Marin, L., Charlton, M. P., Atwood, H. L. & Zinsmaier, K. E. (2005). 'The GTPase dMiro is required for axonal transport of mitochondria to Drosophila synapses', *Neuron*, 47(3), pp. 379-393.

Gupte, A. A., Minze, L. J., Reyes, M., Ren, Y., Wang, X., Brunner, G., Ghosn, M., Cordero-Reyes, A. M., Ding, K. & Pratico, D. (2013). 'High-fat feeding-induced hyperinsulinemia increases cardiac glucose uptake and mitochondrial function despite peripheral insulin resistance', *Endocrinology*, 154(8), pp. 2650-2662.

Gurgul, E., Lortz, S., Tiedge, M., Jörns, A. & Lenzen, S. (2004). 'Mitochondrial catalase overexpression protects insulin-producing cells against toxicity of reactive oxygen species and proinflammatory cytokines', *Diabetes*, 53(9), pp. 2271-2280.

Guthrie, R. A. & Guthrie, D. W. (2004). 'Pathophysiology of diabetes mellitus', *Critical Care Nursing Quarterly,* 27(2), pp. 113-125.

Hackenbrock, C. R. (1968). 'Ultrastructural bases for metabolically linked mechanical activity in mitochondria II. Electron transport-linked ultrastructural transformations in mitochondria', *Journal of Cell Biology*, 37(2), pp. 345-369.

Hall, A., Burke, N., Dongworth, R., Kalkhoran, S., Dyson, A., Vicencio, J., Dorn, G., Yellon, D. & Hausenloy, D. (2016). 'Hearts deficient in both Mfn1 and Mfn2 are protected against acute myocardial infarction', *Cell Death & Disease*, 7(5), pp. e2238-e2238.

Haris, M., Singh, A., Cai, K., Kogan, F., McGarvey, J., DeBrosse, C., Zsido, G. A., Witschey, W. R., Koomalsingh, K. & Pilla, J. J. (2014). 'A technique for in vivo mapping of myocardial creatine kinase metabolism', *Nature Medicine*, 20(2), pp. 209-214.

Hartupee, J. & Mann, D. L. (2013). 'Positioning of inflammatory biomarkers in the heart failure landscape', *Journal of Cardiovascular Translational Research*, 6(4), pp. 485-492.

Hattersley, A. T. & Patel, K. A. (2017). 'Precision diabetes: learning from monogenic diabetes', *Diabetologia*, 60(5), pp. 769-777.

Hattersley, A. T., Beards, F., Ballantyne, E., Appleton, M., Harvey, R. & Ellard, S. (1998). 'Mutations in the glucokinase gene of the fetus result in reduced birth weight', *Nature Genetics*, 19(3), p. 268.

Hattersley, A., Turner, R., Patel, P., O'Rahilly, S., Wainscoat, J., Permutt, M., Tanazawa, Y., Chin, K. & Watkins, P. (1992). 'Linkage of type 2 diabetes to the glucokinase gene', *The Lancet*, 339(8805), pp. 1307-1310.

Heck, A. J. & van den Heuvel, R. H. (2004). 'Investigation of intact protein complexes by mass spectrometry', *Mass Spectrometry Reviews*, 23(5), pp. 368-389.

Henderson, R. B., Lim, L. H., Tessier, P. A., Gavins, F. N., Mathies, M., Perretti, M., & Hogg, N. (2001). The use of lymphocyte function-associated antigen (LFA)-1-deficient mice to determine the role of LFA-1, Mac-1, and alpha4 integrin in the inflammatory response of neutrophils. *The Journal of experimental medicine*, *194*(2), 219–226.

Hendgen-Cotta, U. B., Esfeld, S., Jastrow, H., Totzeck, M., Altschmied, J., Goy, C., Haendeler, J., Winterhager, E. & Rassaf, T. (2018). 'Mouse cardiac mitochondria do not separate in subsarcolemmal and interfibrillar subpopulations', *Mitochondrion*, 38, pp. 1-5.

Heyne, E., Schrepper, A., Doenst, T., Schenkl, C., Kreuzer, K. & Schwarzer, M. (2020). 'High-fat diet affects skeletal muscle mitochondria comparable to pressure overload-induced heart failure', *Journal of Cellular and Molecular Medicine*.

Hoppel, C. L., Tandler, B., Fujioka, H. & Riva, A. (2009). 'Dynamic organization of mitochondria in human heart and in myocardial disease', *The International Journal of Biochemistry & Cell Biology*, 41(10), pp. 1949-1956.

Hoppel, C. L., Tandler, B., Parland, W., Turkaly, J. & Albers, L. (1982). 'Hamster cardiomyopathy. A defect in oxidative phosphorylation in the cardiac interfibrillar mitochondria', *Journal of Biological Chemistry*, 257(3), pp. 1540-1548.

Hoppins, S. & Nunnari, J. (2009). 'The molecular mechanism of mitochondrial fusion', *Biochimica et Biophysica Acta (BBA)-Molecular Cell Research*, 1793(1), pp. 20-26.

Horwich, T. B., Fonarow, G. C. & Clark, A. L. (2018). 'Obesity and the obesity paradox in heart failure', *Progress in Cardiovascular Diseases*, 61(2), pp. 151-156.

Hotamisligil GS, Arner P, Caro JF, Atkinson RL, Spiegelman BM (1995). Increased adipose tissue expression of tumor necrosis factor-alpha in human obesity and insulin resistance. *J Clin Invest*. 95(5):2409-2415.

Hsieh, C.-H., Shaltouki, A., Gonzalez, A. E., da Cruz, A. B., Burbulla, L. F., Lawrence, E. S., Schüle, B., Krainc, D., Palmer, T. D. & Wang, X. (2016). 'Functional impairment in miro degradation and mitophagy is a shared feature in familial and sporadic Parkinson's disease', *Cell Stem Cell*, 19(6), pp. 709-724.

Hu, Q., Zhang, H., Gutierrez Cortes, N., Wu, D., Wang, P., Zhang, J., Mattison, J. A., Smith, E., Bettcher, L. F. & Wang, M. (2020). 'Increased Drp1 Acetylation by Lipid Overload Induces Cardiomyocyte Death and Heart Dysfunction', *Circulation Research*.

Huang, X., Sun, L., Ji, S., Zhao, T., Zhang, W., Xu, J., Zhang, J., Wang, Y., Wang, X. & Franzini-Armstrong, C. (2013). 'Kissing and nanotunneling mediate intermitochondrial communication in the heart', *Proceedings of the National Academy of Sciences*, 110(8), pp. 2846-2851.

Hussain, A., Ghosh, S., Kalkhoran, S. B., Hausenloy, D. J., Hanssen, E. & Rajagopal, V. (2018). 'An automated workflow for segmenting single adult cardiac cells from large-volume serial block-face scanning electron microscopy data', *Journal of Structural Biology*, 202(3), pp. 275-285.

Hussain, S., Richardson, E., Ma, Y., Holton, C., De Backer, I., Buckley, N., Dhillo, W., Bewick, G., Zhang, S. & Carling, D. (2015). 'Glucokinase activity in the arcuate nucleus regulates glucose intake', *The Journal of Clinical Investigation*, 125(1), pp. 337-349.

Hwang, J. S., Shin, C. H., Yang, S. W., young Jung, S. & Huh, N. (2006). 'Genetic and clinical characteristics of Korean maturity-onset diabetes of the young (MODY) patients', *Diabetes Research and Clinical Practice*, 74(1), pp. 75-81.

Haijiang W, Deng X, Shi Y, Su Y, Wei J, Duan H. 2016. PGC-1α, glucose metabolism and type 2 diabetes mellitus. *Journal of endocrinology,* 229(3): 99-115.

Horssen J, Schaik P, Witte M. (2019). Inflammation and mitochondrial dysfunction: A Vicious cycle in neurodegenerative disorders. *Neuroscience letters,* 25.

Ide, T., Tsutsui, H., Hayashidani, S., Kang, D., Suematsu, N., Nakamura, K.-i., Utsumi, H., Hamasaki, N. & Takeshita, A. (2001). 'Mitochondrial DNA damage and dysfunction associated with oxidative stress in failing hearts after myocardial infarction', *Circulation Research*, 88(5), pp. 529-535.

Ing, D. J., Zang, J., Dzau, V. J., Webster, K. A. & Bishopric, N. H. (1999). 'Modulation of cytokine-induced cardiac myocyte apoptosis by nitric oxide, Bak, and Bcl-x', *Circulation Research*, 84(1), pp. 21-33.

Jaap, A., Hammersley, M., Shore, A. & Tooke, J. (1994). 'Reduced microvascular hyperaemia in subjects at risk of developing type 2 (non-insulin-dependent) diabetes mellitus', *Diabetologia*, 37(2), p. 214.

Jadhav, A., Tiwari, S., Lee, P. & Ndisang, J. F. (2013). 'The heme oxygenase system selectively enhances the anti-inflammatory macrophage-M2 phenotype, reduces pericardial adiposity, and ameliorated cardiac injury in diabetic cardiomyopathy in Zucker diabetic fatty rats', *Journal of Pharmacology and Experimental Therapeutics*, 345(2), pp. 239-249.

Jang, K.-M. (2020). 'Maturity-onset diabetes of the young: update and perspectives on diagnosis and treatment', *Yeungnam University Journal of Medicine*.

Ješina, P., Tesařová, M., Fornůsková, D., Vojtíšková, A., Pecina, P., Kaplanova, V., Hansíková, H., Zeman, J. & Houštěk, J. (2004). 'Diminished synthesis of subunit a (ATP6) and altered function of ATP synthase and cytochrome c oxidase due to the mtDNA 2 bp microdeletion of TA at positions 9205 and 9206', *Biochemical Journal*, 383(3), pp. 561-571.

Jin, L., Zhou, Y., Han, L. & Piao, J. (2019). 'MicroRNA302-367-PI3K-PTEN-AKT-mTORC1 pathway promotes the development of cardiac hypertrophy through controlling autophagy', *In Vitro Cellular & Developmental Biology-Animal*, pp. 1-8.

Jofuku, A., Ishihara, N. & Mihara, K. (2005). 'Analysis of functional domains of rat mitochondrial Fis1, the mitochondrial fission-stimulating protein'*, Biochemical and Biophysical Research Communications*, 333(2), pp. 650-659.

Joseph, A.-M., Joanisse, D. R., Baillot, R. G. & Hood, D. A. (2011). 'Mitochondrial dysregulation in the pathogenesis of diabetes: potential for mitochondrial biogenesis-mediated interventions', *Experimental Diabetes Research.*

Josifova T, Schneider U, Henrich P, Schrader W. 2008. Eye disorders in diabetes: potential drug targets. *Infectious disorders drug targets,* 8(2): 70-75.

Katsiari C, Bogdanos D, Sakkas L. 2019. Inflammation and cardiovascular disease. *World journal of translational medicine,* 8(1): 1-8.

Koh, J., Johnson M, Dasari S, et al. 2019. TFAM enhances fat oxidation and attenuates high-fat diet-induced insulin resistance in skeletal muscle. *Diabetes,* 68(8): 1552-1564.

Kang, P. T., Chen, C.-L., Ohanyan, V., Luther, D. J., Meszaros, J. G., Chilian, W. M. & Chen, Y.-R. (2015). 'Overexpressing superoxide dismutase 2 induces a supernormal cardiac function by enhancing redox-dependent mitochondrial function and metabolic dilation', *Journal of Molecular and Cellular Cardiology*, 88, pp. 14-28.

Kay, L., Pienaar, I. S., Cooray, R., Black, G. & Soundararajan, M. (2018). 'Understanding miro GTPases: implications in the treatment of neurodegenerative disorders', *Molecular Neurobiology*, 55(9), pp. 7352-7365.

Kelley, D. E., He, J., Menshikova, E. V. & Ritov, V. B. (2002). 'Dysfunction of mitochondria in human skeletal muscle in type 2 diabetes', *Diabetes*, 51(10), pp. 2944-2950.

Kern, P. A., Ranganathan, S., Li, C., Wood, L. & Ranganathan, G. (2001). 'Adipose tissue tumor necrosis factor and interleukin-6 expression in human obesity and insulin resistance', *American Journal of Physiology-Endocrinology and Metabolism*, 280(5), pp. E745-E751.

Kesherwani, V., Chavali, V., Hackfort, B. T., Tyagi, S. C. & Mishra, P. K. (2015). 'Exercise ameliorates high fat diet induced cardiac dysfunction by increasing interleukin 10', *Frontiers in Physiology*, 6, p. 124.

Khelifa, S. B., Martinez, R., Dandana, A., Khochtali, I., Ferchichi, S. & Castaño, L. (2018). 'Maturity Onset Diabetes of the Young (MODY) in Tunisia: Low frequencies of GCK and HNF1A mutations', *Gene*, 651, pp. 44-48.

Kim, Y. I., Lee, F. N., Choi, W. S., Lee, S. & Youn, J. H. (2006). 'Insulin regulation of skeletal muscle PDK4 mRNA expression is impaired in acute insulin-resistant states', *Diabetes*, 55(8), pp. 2311-2317.

Kiriyama, Y. & Nochi, H. (2018). 'Intra-and intercellular quality control mechanisms of mitochondria', *Cells*, 7(1), p. 1.

Kittler, J. (2015). 'Regulation of mitochondrial trafficking, function and quality control by the mitochondrial GTPases Miro1 and Miro2', *SpringerPlus*, 4(1), p. L33.

Kleinberger, J. W. & Pollin, T. I. (2015). 'Undiagnosed MODY: time for action', *Current Diabetes Reports*, 15(12), p. 110.

Klupa, T., Solecka, I., Nowak, N., Szopa, M., Kiec-Wilk, B., Skupien, J., Trybul, I., Matejko, B., Mlynarski, W. & Malecki, M. (2011). 'The influence of dietary carbohydrate content on glycaemia in patients with glucokinase maturity-onset diabetes of the young', *Journal of International Medical Research*, 39(6), pp. 2296-2301.

Ko, H. J., Zhang, Z., Jung, D. Y., Jun, J. Y., Ma, Z., Jones, K. E., Chan, S. Y. & Kim, J. K. (2009). 'Nutrient stress activates inflammation and reduces glucose metabolism by suppressing AMP-activated protein kinase in the heart', *Diabetes*, 58(11), pp. 2536-2546.

Koshiba, T., Detmer, S. A., Kaiser, J. T., Chen, H., McCaffery, J. M. & Chan, D. C. (2004). 'Structural basis of mitochondrial tethering by mitofusin complexes', *Science*, 305(5685), pp. 858-862.

Kremer JR, Mastronarde D N, McIntosh JR (19 96). Computer visualization of three-dimensional image data using IMOD. *J StructBiol* 116: 71–76

Kulkarni, S. S., Joffraud, M., Boutant, M., Ratajczak, J., Gao, A. W., Maclachlan, C., Hernandez-Alvarez, M. I., Raymond, F., Metairon, S. & Descombes, P. (2016). 'Mfn1 deficiency in the liver protects against diet-induced insulin resistance and enhances the hypoglycemic effect of metformin', *Diabetes*, 65(12), pp. 3552-3560.

Kuznetsov AV, Javadov S, Sickinger S, Frotschnig S, Grimm M (2015). H9c2 and HL-1 cells demonstrate distinct features of energy metabolism, mitochondrial function and sensitivity to hypoxia-reoxygenation. *Biochim Biophys Acta*. 1853(2):276-284.

Kuznetsov, A. V., Hermann, M., Saks, V., Hengster, P. & Margreiter, R. (2009). 'The cell-type specificity of mitochondrial dynamics', *The International Journal of Biochemistry & Cell Biology*, 41(10), pp. 1928-1939.

Kuznetsov, A. V., Javadov, S., Sickinger, S., Frotschnig, S. & Grimm, M. (2015). 'H9c2 and HL-1 cells demonstrate distinct features of energy metabolism, mitochondrial function and

sensitivity to hypoxia-reoxygenation', *Biochimica et Biophysica Acta (BBA)-Molecular Cell Research*, 1853(2), pp. 276-284.

Lopez-Armada M, Riveiro-Naveira R, Vaamonde -Garcia C, Valcarcel-Ares M. 2013. Mitochondrial dysfunction and the inflammatory response. *Mitochondrion,* 13(2): 106-118.

Luscher T. 2018. Inflammation: The new cardiovascular risk factor. *European heart journal,* 39(38): 3483-3487.

Missiroli S, Genovese I, Perrone M, Vazzani B, Vitto V, Giorgi C. 2020. The role of mitochondria in inflammation: from cancer to neurodegenerative disorders. *Journal of clinical medicine,* 9, 740.

Lai, N., Kummitha, C., Loy, F., Isola, R. & Hoppel, C. (2020). 'Bioenergetic functions in subpopulations of heart mitochondria are preserved in a non-obese type 2 diabetes rat model (Goto-Kakizaki)', *Scientific Reports,* 10(1), pp. 1-11.

Lalande, S., Hofman, P. & Baldi, J. (2010). 'Effect of reduced total blood volume on left ventricular volumes and kinetics in type 2 diabetes', *Acta Physiologica*, 199(1), pp. 23-30.

Landry A. P., Cheng Z., and Ding H. (2015) Reduction of mitochondrial protein mitoNEET [2Fe-2S] clusters by human glutathione reductase. *Free Radic. Biol. Med.* 81, 119–127

Larsen, S., Nielsen, J., Hansen, C. N., Nielsen, L. B., Wibrand, F., Stride, N., Schroder, H. D., Boushel, R., Helge, J. W. & Dela, F. (2012). 'Biomarkers of mitochondrial content in skeletal muscle of healthy young human subjects', *The Journal of Physiology*, 590(14), pp. 3349-3360.

Laybutt, D., Preston, A., Åkerfeldt, M., Kench, J., Busch, A., Biankin, A. & Biden, T. (2007). 'Endoplasmic reticulum stress contributes to beta cell apoptosis in type 2 diabetes', *Diabetologia*, 50(4), pp. 752-763.

Ledermann, H. (1995). 'Is maturity onset diabetes at young age (MODY) more common in Europe than previously assumed?', *The Lancet*, 345(8950), p. 648.

Leduc-Gaudet, J. P., Reynaud, O., Chabot, F., Mercier, J., Andrich, D. E., St-Pierre, D. H. & Gouspillou, G. (2018). 'The impact of a short-term high-fat diet on mitochondrial respiration, reactive oxygen species production, and dynamics in oxidative and glycolytic skeletal muscles of young rats', *Physiological Reports*, 6(4), p. e13548.

Lee, B., Appleton, M., Shore, A., Tooke, J. & Hattersley, A. (1999). 'Impaired maximum microvascular hyperaemia in patients with MODY 3 (hepatocyte nuclear factor-1α gene mutations)', *Diabetic Medicine*, 16(9), pp. 731-735.

Lee, J., Lee, S., Zhang, H., Hill, M. A., Zhang, C. & Park, Y. (2017). 'Interaction of IL-6 and TNF-α contributes to endothelial dysfunction in type 2 diabetic mouse hearts', *PLoS One*, 12(11).

Lee, M. M. Y., McMurray, J. J., Lorenzo-Almorós, A., Kristensen, S. L., Sattar, N., Jhund, P. S. & Petrie, M. C. (2019). 'Diabetic cardiomyopathy', *Heart*, 105(4), pp. 337-345.

Lee, Y.-j., Jeong, S.-Y., Karbowski, M., Smith, C. L. & Youle, R. J. (2004). 'Roles of the mammalian mitochondrial fission and fusion mediators Fis1, Drp1, and Opa1 in apoptosis', *Molecular Biology of The Cell*, 15(11), pp. 5001-5011.

LeRoith, D., Olefsky, J. M. & Taylor, S. I. (2015). Diabetes Mellitus: a Fundamental and Clinical Text. Philadelphia: LWW (PE).

Li, Z. & Graham, B. H. (2012). 'Measurement of mitochondrial oxygen consumption using a Clark electrode', *Mitochondrial Disorders: Springer*. pp. 63-72.

Liesa, M., Palacín, M. & Zorzano, A. (2009). 'Mitochondrial dynamics in mammalian health and disease', *Physiological Reviews*, 89(3), pp. 799-845.

Linscheid, N., Logantha, S. J. R., Poulsen, P. C., Zhang, S., Schrölkamp, M., Egerod, K. L., Thompson, J. J., Kitmitto, A., Galli, G. & Humphries, M. J. (2019). 'Quantitative proteomics and single-nucleus transcriptomics of the sinus node elucidates the foundation of cardiac pacemaking', *Nature Communications*, 10(1), pp. 1-19.

Liu, L., Liu, Y., Ge, X., Liu, X., Chen, C., Wang, Y., Li, M., Yin, J., Zhang, J. & Chen, Y. (2018). 'Insights into pathogenesis of five novel GCK mutations identified in Chinese MODY patients', *Metabolism*, 89, pp. 8-17.

Liu, S., Sawada, T., Lee, S., Yu, W., Silverio, G., Alapatt, P., Millan, I., Shen, A., Saxton, W. & Kanao, T. (2012). 'Parkinson's disease–associated kinase PINK1 regulates Miro protein level and axonal transport of mitochondria', *PLoS Genetics*, 8(3), p. e1002537.

Liu, Z., Liu, X., Yu, H., Pei, J., Zhang, Y., Gong, J. & Pu, J. (2015). 'Common variants in TRDN and CALM1 are associated with risk of sudden cardiac death in chronic heart failure patients in Chinese Han population', *PloS ONE*, 10(7).

Liu, Z., Zhao, N., Zhu, H., Zhu, S., Pan, S., Xu, J., Zhang, X., Zhang, Y. & Wang, J. (2015). 'Circulating interleukin-1β promotes endoplasmic reticulum stress-induced myocytes apoptosis in diabetic cardiomyopathy via interleukin-1 receptor-associated kinase-2', *Cardiovascular Diabetology*, 14(1), p. 125.

Lonn, E., Bosch, J., Yusuf, S., Sheridan, P., Pogue, J., Arnold, J., Ross, C., Arnold, A., Sleight, P. & Probstfield, J. (2005). 'Effects of long-term vitamin E supplementation on cardiovascular events and cancer: a randomized controlled trial', *Jama*, 293(11), pp. 1338-1347.

Lopaschuk, G. D., Ussher, J. R., Folmes, C. D., Jaswal, J. S. & Stanley, W. C. (2010). 'Myocardial fatty acid metabolism in health and disease', *Physiological Reviews*, 90(1), pp. 207-258.

López-Doménech, G., Covill-Cooke, C., Ivankovic, D., Halff, E. F., Sheehan, D. F., Norkett, R., Birsa, N. & Kittler, J. T. (2018). 'Miro proteins coordinate microtubule-and actin-dependent mitochondrial transport and distribution', *The EMBO Journal*, 37(3), pp. 321-336.

Lorenzo-Almoros, A., Tunon, J., Orejas, M., Cortés, M., Egido, J. & Lorenzo, O. (2017). 'Diagnostic approaches for diabetic cardiomyopathy', *Cardiovascular Diabetology*, 16(1), p. 28.

Lucy Murfitt Thesis (2016) – Available https://www.escholar.manchester.ac.uk/item/?pid=uk-ac-man-scw:307250

Lukyanenko, V., Chikando, A. & Lederer, W. (2009). 'Mitochondria in cardiomyocyte Ca2+ signaling', *The International Journal of Biochemistry & Cell Biology*, 41(10), pp. 1957-1971.

Luptak, I., Sverdlov, A. L., Panagia, M., Qin, F., Pimentel, D. R., Croteau, D., Siwik, D. A., Ingwall, J. S., Bachschmid, M. M. & Balschi, J. A. (2018). 'Decreased ATP production and myocardial contractile reserve in metabolic heart disease', *Journal of Molecular and Cellular Cardiology*, 116, pp. 106-114.

Ma, Y., Gao, M., Sun, H. & Liu, D. (2015). 'Interleukin-6 gene transfer reverses body weight gain and fatty liver in obese mice', *Biochimica et Biophysica Acta (BBA)-Molecular Basis of Disease*, 1852(5), pp. 1001-1011.

MacAskill, A. F., Brickley, K., Stephenson, F. A. & Kittler, J. T. (2009a). 'GTPase dependent recruitment of Grif-1 by Miro1 regulates mitochondrial trafficking in hippocampal neurons', *Molecular and Cellular Neuroscience*, 40(3), pp. 301-312.

MacAskill, A. F., Rinholm, J. E., Twelvetrees, A. E., Arancibia-Carcamo, I. L., Muir, J., Fransson, A., Aspenstrom, P., Attwell, D. & Kittler, J. T. (2009). 'Miro1 is a calcium sensor for glutamate receptor-dependent localization of mitochondria at synapses', *Neuron*, 61(4), pp. 541-555.

Mackenzie, R. W. & Elliott, B. T. (2014). 'Akt/PKB activation and insulin signaling: a novel insulin signaling pathway in the treatment of type 2 diabetes', *Diabetes, Metabolic Syndrome and Obesity: Targets and Therapy*, 7, p. 55.

Maisch, B., Alter, P. & Pankuweit, S. (2011). 'Diabetic cardiomyopathy—fact or fiction?', *Herz*, 36(2), pp. 102-115.

Makino, A., Suarez, J., Gawlowski, T., Han, W., Wang, H., Scott, B. T. & Dillmann, W. H. (2011). 'Regulation of mitochondrial morphology and function by O-GlcNAcylation in neonatal cardiac myocytes', *American Journal of Physiology-Regulatory, Integrative and Comparative Physiology*, 300(6), pp. R1296-R1302.

Mamas, M., Gibbons, S., Zi, M., Prehar, S., Oceandy, D., Cartwright, E., Cox, R. & Neyses, L. (2009). GENA348, a novel human relevant mouse model of diabetes displays spontaneous cardiac hypertrophy. *BMJ Publishing Group Ltd and British Cardiovascular Society.*

Marin, T. L., Gongol, B., Zhang, F., Martin, M., Johnson, D. A., Xiao, H., Wang, Y., Subramaniam, S., Chien, S. & Shyy, J. Y.-J. (2017). 'AMPK promotes mitochondrial biogenesis and function by phosphorylating the epigenetic factors DNMT1, RBBP7, and HAT1', *Sci. Signal.*, 10(464).

Marques-Vidal, P., Schmid, R., Bochud, M., Bastardot, F., Von Känel, R., Paccaud, F., Glaus, J., Preisig, M., Waeber, G. & Vollenweider, P. (2012). 'Adipocytokines, hepatic and inflammatory biomarkers and incidence of type 2 diabetes. The CoLaus study', *PloS ONE*, 7(12).

Martin, D., Bellanné-Chantelot, C., Deschamps, I., Froguel, P., Robert, J.-J. & Velho, G. (2008). 'Long-term follow-up of oral glucose tolerance test–derived glucose tolerance and insulin secretion and insulin sensitivity indexes in subjects with glucokinase mutations (MODY2)', *Diabetes Care*, 31(7), pp. 1321-1323.

Martin, O. J., Lai, L., Soundarapandian, M. M., Leone, T. C., Zorzano, A., Keller, M. P., Attie, A. D., Muoio, D. M. & Kelly, D. P. (2014). 'A role for peroxisome proliferator-activated receptor γ coactivator-1 in the control of mitochondrial dynamics during postnatal cardiac growth', *Circulation Research*, 114(4), pp. 626-636.

McDonald, T. J. & Ellard, S. (2013). 'Maturity onset diabetes of the young: identification and diagnosis', *Annals of Clinical Biochemistry*, 50(5), pp. 403-415.

McDonald, T. J., Shields, B. M., Lawry, J., Owen, K. R., Gloyn, A. L., Ellard, S. & Hattersley, A. T. (2011). 'High-sensitivity CRP discriminates HNF1A-MODY from other subtypes of diabetes', *Diabetes Care*, 34(8), pp. 1860-1862.

Medzhitov R, Janeway C Jr (2000). Innate immunity. *N Engl J Med*. 343(5):338-344.

Meeusen, S., McCaffery, J. M. & Nunnari, J. (2004). 'Mitochondrial fusion intermediates revealed in vitro', *Science*, 305(5691), pp. 1747-1752.

Meigs JB, Hu FB, Rifai N, Manson JE. Biomarkers of endothelial dysfunction and risk of type 2 diabetes mellitus. *JAMA*. 2004;291(16):1978-1986.

Miglioranza, M. H., Picano, E., Badano, L. P., Sant'Anna, R., Rover, M., Zaffaroni, F., Sicari, R., Kalil, R. K., Leiria, T. L. & Gargani, L. (2017). 'Pulmonary congestion evaluated by lung ultrasound predicts decompensation in heart failure outpatients', *International Journal of Cardiology*, 240, pp. 271-278.

Miller, S. P., Anand, G. R., Karschnia, E. J., Bell, G. I., LaPorte, D. C. & Lange, A. J. (1999). 'Characterization of glucokinase mutations associated with maturity-onset diabetes of the young type 2 (MODY-2): different glucokinase defects lead to a common phenotype', *Diabetes*, 48(8), pp. 1645-51.

Mishra, P. & Chan, D. C. (2014). 'Mitochondrial dynamics and inheritance during cell division, development and disease', *Nature Reviews Molecular Cell Biology*, 15(10), pp. 634-646.

Misko, A., Jiang, S., Wegorzewska, I., Milbrandt, J. & Baloh, R. H. (2010). 'Mitofusin 2 is necessary for transport of axonal mitochondria and interacts with the Miro/Milton complex', *Journal of Neuroscience*, 30(12), pp. 4232-4240.

Mitcheson JS, Hancox JC, Levi AJ. Cultured adult cardiac myocytes: future applications, culture methods, morphological and electrophysiological properties. *Cardiovasc Res*. 1998;39(2):280-300.

Miyauchi, K., Takiyama, Y., Honjyo, J., Tateno, M. & Haneda, M. (2009). 'Upregulated IL-18 expression in type 2 diabetic subjects with nephropathy: TGF-β1 enhanced IL-18 expression in human renal proximal tubular epithelial cells', *Diabetes Research and Clinical Practice*, 83(2), pp. 190-199.

Mojarrab, M., Jamshidi, M., Ahmadi, F., Alizadeh, E. & Hosseinzadeh, L. (2013). 'Extracts of Artemisia ciniformis protect cytotoxicity induced by hydrogen peroxide in H9c2 cardiac muscle cells through the inhibition of reactive oxygen species', *Advances in Pharmacological Sciences*.

Mokdad, A. H., Ford, E. S., Bowman, B. A., Dietz, W. H., Vinicor, F., Bales, V. S. & Marks, J. S. (2003). 'Prevalence of obesity, diabetes, and obesity-related health risk factors, *Jama*, 289(1), pp. 76-79.

Monnerat, G., Alarcón, M. L., Vasconcellos, L. R., Hochman-Mendez, C., Brasil, G., Bassani, R. A., Casis, O., Malan, D., Travassos, L. H. & Sepúlveda, M. (2016). 'Macrophage-dependent IL-1β production induces cardiac arrhythmias in diabetic mice', *Nature Communications*, 7(1), pp. 1-15.

Morino, K., Petersen, K. F., Dufour, S., Befroy, D., Frattini, J., Shatzkes, N., Neschen, S., White, M. F., Bilz, S. & Sono, S. (2005). 'Reduced mitochondrial density and increased IRS-1 serine phosphorylation in muscle of insulin-resistant offspring of type 2 diabetic parents', *The Journal of Clinical Investigation*, 115(12), pp. 3587-3593.

Morlino, G., Barreiro, O., Baixauli, F., Robles-Valero, J., González-Granado, J. M., Villa-Bellosta, R., Cuenca, J., Sánchez-Sorzano, C. O., Veiga, E. & Martín-Cófreces, N. B. (2014). 'Miro-1 links mitochondria and microtubule Dynein motors to control lymphocyte migration and polarity', *Molecular and Cellular Biology*, 34(8), pp. 1412-1426.

Murray, A. J., Cole, M. A., Lygate, C. A., Carr, C. A., Stuckey, D. J., Little, S. E., Neubauer, S. & Clarke, K. (2008). 'Increased mitochondrial uncoupling proteins, respiratory uncoupling and decreased efficiency in the chronically infarcted rat heart', *Journal of Molecular and Cellular Cardiology*, 44(4), pp. 694-700.

Nanayakkara, S., Patel, H. C. & Kaye, D. M. (2018). 'Hospitalisation in patients with heart failure with preserved ejection fraction', Clinical Medicine Insights: *Cardiology*, 12, p. 1179546817751609.

Narendra, D. P., Jin, S. M., Tanaka, A., Suen, D.-F., Gautier, C. A., Shen, J., Cookson, M. R. & Youle, R. J. (2010). 'PINK1 is selectively stabilized on impaired mitochondria to activate Parkin', *PLOS Biology*, 8(1).

Narendra, D., Tanaka, A., Suen, D.-F. & Youle, R. J. (2008). 'Parkin is recruited selectively to impaired mitochondria and promotes their autophagy', *The Journal of Cell Biology*, 183(5), pp. 795-803.

Nemani, N., Carvalho, E., Tomar, D., Dong, Z., Ketschek, A., Breves, S. L., Jaña, F., Worth, A. M., Heffler, J. & Palaniappan, P. (2018). 'MIRO-1 determines mitochondrial shape transition upon GPCR activation and Ca2+ stress', *Cell Reports*, 23(4), pp. 1005-1019.

Nemoto, O., Kawaguchi, M., Yaoita, H., Miyake, K., Maehara, K. & Maruyama, Y. (2006). 'Left ventricular dysfunction and remodeling in streptozotocin-induced diabetic rats', *Circulation Journal*, 70(3), pp. 327-334.

Nguyen, T. T., Oh, S. S., Weaver, D., Lewandowska, A., Maxfield, D., Schuler, M.-H., Smith, N. K., Macfarlane, J., Saunders, G. & Palmer, C. A. (2014). 'Loss of Miro1-directed mitochondrial movement results in a novel murine model for neuron disease', *Proceedings of the National Academy of Sciences*, 111(35), pp. E3631-E3640.

Niedziela, J. T., Hudzik, B., Strojek, K., Poloński, L., Gąsior, M. & Rozentryt, P. (2019). 'Weight loss in heart failure is associated with increased mortality only in non-obese patients without diabetes', *Journal of Cachexia, Sarcopenia and Muscle*, 10(6), pp. 1307-1315.

Niemann, B., Chen, Y., Teschner, M., Li, L., Silber, R.-E. & Rohrbach, S. (2011). 'Obesity induces signs of premature cardiac aging in younger patients: the role of mitochondria', *Journal of the American College of Cardiology*, 57(5), pp. 577-585.

Nijtmans, L. G., Henderson, N. S., Attardi, G. & Holt, I. J. (2001). 'Impaired ATP synthase assembly associated with a mutation in the human ATP synthase subunit 6 gene', *Journal of Biological Chemistry*, 276(9), pp. 6755-6762.

Olichon, A., Elachouri, G., Baricault, L., Delettre, C., Belenguer, P. & Lenaers, G. (2007). 'OPA1 alternate splicing uncouples an evolutionary conserved function in mitochondrial fusion from a vertebrate restricted function in apoptosis', *Cell Death & Differentiation*, 14(4), pp. 682-692.

Ong, S.-B., Hall, A. R. & Hausenloy, D. J. (2013). 'Mitochondrial dynamics in cardiovascular health and disease', *Antioxidants & Redox Signaling*, 19(4), pp. 400-414.

Ong, S.-B., Subrayan, S., Lim, S. Y., Yellon, D. M., Davidson, S. M. & Hausenloy, D. J. (2010). 'Inhibiting mitochondrial fission protects the heart against ischemia/reperfusion injury', *Circulation*, 121(18), p. 2012.

Orio, F., Muscogiuri, G., Nese, C., Palomba, S., Savastano, S., Tafuri, D., Colarieti, G., La Sala, G., Colao, A. & Yildiz, B. O. (2016). 'Obesity, type 2 diabetes mellitus and cardiovascular

disease risk: an uptodate in the management of polycystic ovary syndrome', *European Journal of Obstetrics & Gynecology and Reproductive Biology*, 207, pp. 214-219.

Osbak, K. K., Colclough, K., Saint-Martin, C., Beer, N. L., Bellanné-Chantelot, C., Ellard, S. & Gloyn, A. L. (2009). 'Update on mutations in glucokinase (GCK), which cause maturity-onset diabetes of the young, permanent neonatal diabetes, and hyperinsulinemic hypoglycemia', *Human Mutation*, 30(11), pp. 1512-1526.

Owen, K. R., Thanabalasingham, G., James, T. J., Karpe, F., Farmer, A. J., McCarthy, M. I. & Gloyn, A. L. (2010). 'Assessment of high-sensitivity C-reactive protein levels as diagnostic discriminator of maturity-onset diabetes of the young due to HNF1A mutations', *Diabetes Care*, 33(9), pp. 1919-1924.

Park K, Wiederkehr A, Wollheim C, 2012. Defective mitochondrial function and motility due to Mitofusion1 overexpression in insulin secreting cells. *Korean journal of physiology and pharmacology,* 16(1): 71-77.

Patten D, Harper M, Boardman N. 2020. Harnessing the protective role of OPA1 in diabetic cardiomyopathy. *Acta physiologica,* 229(1).

Page, R., Levy, J., Barrow, B., Turner, R., Patel, P., Hattersley, A., Lo, D., Wainscoat, J., Permutt, M. & Bell, G. (1995). 'Clinical characteristics of subjects with a missense mutation in glucokinase', *Diabetic Medicine*, 12(3), pp. 209-217.

Palade, G. E. (1952). 'The fine structure of mitochondria', *The Anatomical Record*, 114(3), pp. 427-451.

Palmer, C. S., Osellame, L. D., Laine, D., Koutsopoulos, O. S., Frazier, A. E. & Ryan, M. T. (2011). 'MiD49 and MiD51, new components of the mitochondrial fission machinery', *EMBO Reports*, 12(6), pp. 565-573.

Palmer, J. W., Tandler, B. & Hoppel, C. L. (1977). 'Biochemical properties of subsarcolemmal and interfibrillar mitochondria isolated from rat cardiac muscle', *Journal of Biological Chemistry*, 252(23), pp. 8731-8739.

Palmer, J. W., Tandler, B. & Hoppel, C. L. (1986). 'Heterogeneous response of subsarcolemmal heart mitochondria to calcium', *American Journal of Physiology-Heart and Circulatory Physiology*, 250(5), pp. H741-H748.

Papanicolaou, K. N., Khairallah, R. J., Ngoh, G. A., Chikando, A., Luptak, I., O'Shea, K. M., Riley, D. D., Lugus, J. J., Colucci, W. S. & Lederer, W. J. (2011). 'Mitofusin-2 maintains mitochondrial structure and contributes to stress-induced permeability transition in cardiac myocytes'*, Molecular and Cellular Biology*, 31(6), pp. 1309-1328.

Papinska, A., Mordwinkin, N., Meeks, C., Jadhav, S. & Rodgers, K. (2015). 'Angiotensin-(1–7) administration benefits cardiac, renal and progenitor cell function in db/db mice', *British Journal of Pharmacology,* 172(18), pp. 4443-4453.

Park, T.-J., Park, J. H., Lee, G. S., Lee, J.-Y., Shin, J. H., Kim, M. W., Kim, Y. S., Kim, J.-Y., Oh, K.-J. & Han, B.-S. (2019). 'Quantitative proteomic analyses reveal that GPX4 downregulation during myocardial infarction contributes to ferroptosis in cardiomyocytes', *Cell Death & Disease*, 10(11), pp. 1-15.

Parra, V., Verdejo, H. E., Iglewski, M., Del Campo, A., Troncoso, R., Jones, D., Zhu, Y., Kuzmicic, J., Pennanen, C. & Lopez-Crisosto, C. (2014). 'Insulin stimulates mitochondrial fusion and function in cardiomyocytes via the Akt-mTOR-NFκB-Opa-1 signaling pathway', *Diabetes*, 63(1), pp. 75-88.

Pavić, T., Juszczak, A., Pape Medvidović, E., Burrows, C., Šekerija, M., Bennett, A. J., Ćuća Knežević, J., Gloyn, A. L., Lauc, G. & McCarthy, M. I. (2018). 'Maturity onset diabetes of the young due to HNF1A variants in Croatia', *Biochemia medica: Biochemia medica*, 28(2), pp. 285-295.

Pawlikowska, P., Gajkowska, B. & Orzechowski, A. (2007). 'Mitofusin 2 (Mfn2): a key player in insulin-dependent myogenesis in vitro', *Cell and Tissue Research*, 327(3), pp. 571-581.

Pelleymounter, M. A., Cullen, M. J., Baker, M. B., Hecht, R., Winters, D., Boone, T. & Collins, F. (1995). 'Effects of the obese gene product on body weight regulation in ob/ob mice', *Science*, 269(5223), pp. 540-543.

Peng, K., Xiao, J., Yang, L., Ye, F., Cao, J. & Sai, Y. (2019). 'Mutual Antagonism of PINK1/Parkin and PGC-1α Contributes to Maintenance of Mitochondrial Homeostasis in Rotenone-Induced Neurotoxicity', *Neurotoxicity Research*, 35(2), pp. 331-343.

Peters, D. T., Kay, L., Eswaran, J., Lakey, J. H. & Soundararajan, M. (2018). 'Human Miro Proteins Act as NTP Hydrolases through a Novel, Non-Canonical Catalytic Mechanism', *International Journal of Molecular Sciences*, 19(12), p. 3839.

Petersen, K. F., Dufour, S., Befroy, D., Garcia, R. & Shulman, G. I. (2004). 'Impaired mitochondrial activity in the insulin-resistant offspring of patients with type 2 diabetes', *New England Journal of Medicine*, 350(7), pp. 664-671.

Pettersen, I. K. N., Tusubira, D., Ashrafi, H., Dyrstad, S. E., Hansen, L., Liu, X.-Z., Nilsson, L. I. H., Løvsletten, N. G., Berge, K. & Wergedahl, H. (2019). 'Upregulated PDK4 expression is a sensitive marker of increased fatty acid oxidation', *Mitochondrion*, 49, pp. 97-110.

Pickrell, A. M. & Youle, R. J. (2015). 'The roles of PINK1, parkin, and mitochondrial fidelity in Parkinson's disease', *Neuron*, 85(2), pp. 257-273.

Pinali, C., Malik, N., Davenport, J. B., Allan, L. J., Murfitt, L., Iqbal, M. M., Boyett, M. R., Wright, E. J., Walker, R., Zhang, Y., Dobryznski, H., Holt, C. M., & Kitmitto, A. (2017). Post-Myocardial Infarction T-tubules Form Enlarged Branched Structures With Dysregulation of Junctophilin-2 and Bridging Integrator 1 (BIN-1). *Journal of the American Heart Association*, *6*(5)

Pinali, C. & Kitmitto, A. (2014). 'Serial block face scanning electron microscopy for the study of cardiac muscle ultrastructure at nanoscale resolutions', *Journal of Molecular and Cellular Cardiology*, 76, pp. 1-11.

Pinali, C., Bennett, H. J., Davenport, J. B., Caldwell, J. L., Starborg, T., Trafford, A. W. & Kitmitto, A. (2015). 'Three-dimensional structure of the intercalated disc reveals plicate domain and gap junction remodeling in heart failure', *Biophysical Journal*, 108(3), pp. 498-507.

Piñero-Piloña, A. & Raskin, P. (2001). 'Idiopathic type 1 diabetes', *Journal of Diabetes and Its Complications,* 15(6), pp. 328-335.

Podewski, E. K., Hilfiker-Kleiner, D., Hilfiker, A., Morawietz, H., Lichtenberg, A., Wollert, K. C. & Drexler, H. (2003). 'Alterations in Janus kinase (JAK)-signal transducers and activators of transcription (STAT) signaling in patients with end-stage dilated cardiomyopathy', *Circulation*, 107(6), pp. 798-802.

Pollack, R. M., Donath, M. Y., LeRoith, D. & Leibowitz, G. (2016). 'Anti-inflammatory agents in the treatment of diabetes and its vascular complications', *Diabetes Care*, 39(Supplement 2), pp. S244-S252.

Popkov, V., Plotnikov, E., Lyamzaev, K., Silachev, D., Zorova, L., Pevzner, I., Jankauskas, S., Zorov, S., Babenko, V. & Zorov, D. (2015). 'Mitodiversity', *Biochemistry* (Moscow), 80(5), pp. 532-541.

Portha, B., Levacher, C., Picon, L. & Rosselin, G. (1974). 'Diabetogenic effect of streptozotocin in the rat during the perinatal period', *Diabetes*, 23(11), pp. 889-895.

Pospisilik, J. A., Knauf, C., Joza, N., Benit, P., Orthofer, M., Cani, P. D., Ebersberger, I., Nakashima, T., Sarao, R. & Neely, G. (2007). 'Targeted deletion of AIF decreases mitochondrial oxidative phosphorylation and protects from obesity and diabetes', *Cell*, 131(3), pp. 476-491.

Postic, C., Shiota, M. & Magnuson, M. (2001). 'Cell-specific roles of glucokinase in glucose homeostasis', *Recent Progress in Hormone Research*, 56, pp. 195-218.

Postic, C., Shiota, M., Niswender, K. D., Jetton, T. L., Chen, Y., Moates, J. M., Shelton, K. D., Lindner, J., Cherrington, A. D. & Magnuson, M. A. (1999). 'Dual roles for glucokinase in glucose homeostasis as determined by liver and pancreatic β cell-specific gene knock-outs using Cre recombinase', *Journal of Biological Chemistry*, 274(1), pp. 305-315.

Pradhan AD, Manson JE, Rifai N, Buring JE, Ridker PM. C-reactive protein, interleukin 6, and risk of developing type 2 diabetes mellitus. *JAMA*. 2001;286(3):327-334.

Prudente, S., Jungtrakoon, P., Marucci, A., Ludovico, O., Buranasupkajorn, P., Mazza, T., Hastings, T., Milano, T., Morini, E. & Mercuri, L. (2015). *'Loss-of-function mutations in the APPL1 gene in familial diabetes mellitus*'.

Pruhova, S., Dusatkova, P., Kraml, P. J., Kulich, M., Prochazkova, Z., Broz, J., Zikmund, J., Cinek, O., Andel, M. & Pedersen, O. (2013). 'Chronic mild hyperglycemia in GCK-MODY patients does not increase carotid intima-media thickness', International journal of endocrinology.

Ptaszynska-Kopczynska, K., Szpakowicz, A., Marcinkiewicz-Siemion, M., Lisowska, A., Waszkiewicz, E., Witkowski, M., Jakim, P., Galar, B., Musial, W. J. & Kamiński, K. A. (2017). 'Interleukin-6 signaling in patients with chronic heart failure treated with cardiac resynchronization therapy', *Archives of Medical Science: AMS*, 13(5), p. 1069.

Qu, D., Liu, J., Lau, C. W. & Huang, Y. (2014). 'IL-6 in diabetes and cardiovascular complications', *British Journal of Pharmacology*, 171(15), pp. 3595-3603.

Quirós, P. M., Ramsay, A. J., Sala, D., Fernández-Vizarra, E., Rodríguez, F., Peinado, J. R., Fernández-García, M. S., Vega, J. A., Enríquez, J. A. & Zorzano, A. (2012). 'Loss of mitochondrial protease OMA1 alters processing of the GTPase OPA1 and causes obesity and defective thermogenesis in mice', *The EMBO Journal*, 31(9), pp. 2117-2133.

Rabinovich-Nikitin, I., Dhingra, R. & Kirshenbaum, L. A. (2019). Activation of Mitophagy in High-Fat Diet–Induced Diabetic Cardiomyopathy. *Am Heart Assoc*.

Rajapakse, N. W., Head, G. A. & Kaye, D. M. (2016). 'Say NO to obesity-related hypertension: role of the L-arginine–nitric oxide pathway', *Hypertension*, 67(5), pp. 813-819.

Randall, T. S., Moores, C. & Stephenson, F. A. (2013). 'Delineation of the TRAK binding regions of the kinesin-1 motor proteins', *FEBS Letters*, 587(23), pp. 3763-3769.

Reis, K., Fransson, Å. & Aspenström, P. (2009). 'The Miro GTPases: at the heart of the mitochondrial transport machinery', *FEBS Letters*, 583(9), pp. 1391-1398.

Rindler, P. M., Plafker, S. M., Szweda, L. I. & Kinter, M. (2013). 'High dietary fat selectively increases catalase expression within cardiac mitochondria', *Journal of Biological Chemistry*, 288(3), pp. 1979-1990.

Ritov, V. B., Menshikova, E. V., He, J., Ferrell, R. E., Goodpaster, B. H. & Kelley, D. E. (2005). 'Deficiency of subsarcolemmal mitochondria in obesity and type 2 diabetes', *Diabetes*, 54(1), pp. 8-14.

Riva, A., Tandler, B., Loffredo, F., Vazquez, E. & Hoppel, C. (2005). 'Structural differences in two biochemically defined populations of cardiac mitochondria', *American Journal of Physiology-Heart and Circulatory Physiology*, 289(2), pp. H868-H872.

Rizzuto, R., De Stefani, D., Raffaello, A. & Mammucari, C. (2012). 'Mitochondria as sensors and regulators of calcium signalling', *Nature Reviews Molecular Cell Biology*, 13(9), pp. 566-578.

Roberts N, Cruz-Orive LM, Reid NM, Brodie DA, Bourne M, Edwards RH Rogne, M., Chu, D.-T., Küntziger, T. M., Mylonakou, M.-N., Collas, P. & Tasken, K. (2018). 'OPA1-anchored PKA phosphorylates perilipin 1 on S522 and S497 in adipocytes differentiated from human adipose stem cells', *Molecular Biology of the Cell*, 29(12), pp. 1487-1501.

Rosca, M. G. & Hoppel, C. L. (2010). 'Mitochondria in heart failure', *Cardiovascular Research*, 88(1), pp. 40-50.

Rubler, S., Dlugash, J., Yuceoglu, Y. Z., Kumral, T., Branwood, A. W. & Grishman, A. (1972). 'New type of cardiomyopathy associated with diabetic glomerulosclerosis', *The American Journal of Cardiology*, 30(6), pp. 595-602.

Ruiz-Meana, M., Fernandez-Sanz, C. & Garcia-Dorado, D. (2010). 'The SR–mitochondria interaction: a new player in cardiac pathophysiology', *Cardiovascular Research*, 88(1), pp. 30-39.

Russo, G. J., Louie, K., Wellington, A., Macleod, G. T., Hu, F., Panchumarthi, S. & Zinsmaier, K. E. (2009). 'Drosophila Miro is required for both anterograde and retrograde axonal mitochondrial transport', *Journal of Neuroscience*, 29(17), pp. 5443-5455.

Shadel G, Horvath T. 2015. Mitochondrial ROS signaling in organismal homeostasis. *Cell,* 163(3): 560-569.

Steven S, Frenis K, Oelze M, et al. 2019. Vascular inflammation and oxidative stress: Major triggers for cardiovascular disease. *Oxidative medicine and cellular longevity*.

Stewart C, Stuart L, Wilkinson K, et al. 2010. CD36 ligands promote sterile inflammation through assembly of a TLR 4 and 6 heterodimer. *Nature immunology,* 11(2): 155-161.

Salin, K., Auer, S. K., Rey, B., Selman, C. & Metcalfe, N. B. (2015). 'Variation in the link between oxygen consumption and ATP production, and its relevance for animal performance', Proceedings of the Royal Society B: *Biological Sciences*, 282(1812), p. 20151028.

Sano, T., Ozaki, K., Matsuura, T. & Narama, I. (2010). 'Giant mitochondria in pancreatic acinar cells of alloxan-induced diabetic rats', *Toxicologic Pathology*, 38(4), pp. 658-665.

Santel, A., Frank, S., Gaume, B., Herrler, M., Youle, R. J. & Fuller, M. T. (2003). 'Mitofusin-1 protein is a generally expressed mediator of mitochondrial fusion in mammalian cells', *Journal of Cell Science*, 116(13), pp. 2763-2774.

Saotome, M., Safiulina, D., Szabadkai, G., Das, S., Fransson, Å., Aspenstrom, P., Rizzuto, R. & Hajnóczky, G. (2008). 'Bidirectional Ca2+-dependent control of mitochondrial dynamics by the Miro GTPase', *Proceedings of the National Academy of Sciences*, 105(52), pp. 20728-20733.

Sardu, C., De Lucia, C., Wallner, M. & Santulli, G. (2019). 'Diabetes mellitus and its cardiovascular complications: new insights into an old disease', *Journal of Diabetes Research*.

Sarkar, A., Shukla, S. K., Alqatawni, A., Kumar, A., Addya, S., Tsygankov, A. Y. & Rafiq, K. (2018). 'The role of allograft inflammatory factor-1 in the effects of experimental diabetes on B cell functions in the heart', *Frontiers in Cardiovascular Medicine*, 5, p. 126.

Sarparanta, J., Garcia-Macia, M. & Singh, R. (2017). 'Autophagy and mitochondria in obesity and type 2 diabetes', *Current Diabetes Reviews*, 13(4), pp. 352-369.

Sarraf, S. A., Raman, M., Guarani-Pereira, V., Sowa, M. E., Huttlin, E. L., Gygi, S. P. & Harper, J. W. (2013). 'Landscape of the PARKIN-dependent ubiquitylome in response to mitochondrial depolarization', *Nature*, 496(7445), pp. 372-376.

Schaper, J., Meiser, E. & Stammler, G. Ultrastructural morphometric analysis of myocardium from dogs, rats, hamsters, mice, and from human hearts. *Circ. Res.* **56**, 377–391 (1985).

Scheller, J., Chalaris, A., Schmidt-Arras, D. & Rose-John, S. (2011). 'The pro-and anti-inflammatory properties of the cytokine interleukin-6', *Biochimica et Biophysica Acta (BBA)-Molecular Cell Research*, 1813(5), pp. 878-888.

Scheubel, R. J., Tostlebe, M., Simm, A., Rohrbach, S., Prondzinsky, R., Gellerich, F. N., Silber, R.-E. & Holtz, J. (2002). 'Dysfunction of mitochondrial respiratory chain complex I in human failing myocardium is not due to disturbed mitochondrial gene expression', *Journal of the American College of Cardiology*, 40(12), pp. 2174-2181.

Schilling, J. D. (2015). 'The mitochondria in diabetic heart failure: from pathogenesis to therapeutic promise', *Antioxidants & Redox Signaling*, 22(17), pp. 1515-1526.

Schmidt, R. E., Dorsey, D. A., Beaudet, L. N. & Peterson, R. G. (2003). 'Analysis of the Zucker Diabetic Fatty (ZDF) type 2 diabetic rat model suggests a neurotrophic role for insulin/IGF-I in diabetic autonomic neuropathy', *The American Journal of Pathology*, 163(1), pp. 21-28.

Schnabel, R. & Blankenberg, S. (2007). Oxidative stress in cardiovascular disease: successful translation from bench to bedside

Schuler, M.-H., Lewandowska, A., Caprio, G. D., Skillern, W., Upadhyayula, S., Kirchhausen, T., Shaw, J. M. & Cunniff, B. (2017). 'Miro1-mediated mitochondrial positioning shapes intracellular energy gradients required for cell migration', *Molecular Biology of the Cell*, 28(16), pp. 2159-2169.

Schulz, R., Panas, D. L., Catena, R., Moncada, S., Olley, P. M. & Lopaschuk, G. D. (1995). 'The role of nitric oxide in cardiac depression induced by interleukin-1β and tumour necrosis factor-α', *British Journal of Pharmacology*, 114(1), pp. 27-34.

Schwarz, T. L. (2013). 'Mitochondrial trafficking in neurons', *Cold Spring Harbor Perspectives in Biology*, 5(6), p. a011304.

Schwarzer, M., Schrepper, A., Amorim, P. A., Osterholt, M. & Doenst, T. (2013). 'Pressure overload differentially affects respiratory capacity in interfibrillar and subsarcolemmal mitochondria', *American Journal of Physiology-Heart and Circulatory Physiology*, 304(4), pp. H529-H537.

Semeniuk, L. M., Kryski, A. J. & Severson, D. L. (2002). 'Echocardiographic assessment of cardiac function in diabetic db/db and transgenic db/db-hGLUT4 mice', *American Journal of Physiology-Heart and Circulatory Physiology*, 283(3), pp. H976-H982.

Shen, X., Zheng, S., Thongboonkerd, V., Xu, M., Pierce, W. M., Jr., Klein, J. B. & Epstein, P. N. (2004). 'Cardiac mitochondrial damage and biogenesis in a chronic model of type 1 diabetes', *Am J Physiol Endocrinol Metab*, 287(5), pp. E896-905.

Sheng, Z.-H. (2014). 'Mitochondrial trafficking and anchoring in neurons: new insight and implications', *J Cell Biol*, 204(7), pp. 1087-1098.

Sheridan, C. & Martin, S. J. (2010). 'Mitochondrial fission/fusion dynamics and apoptosis', *Mitochondrion*, 10(6), pp. 640-648.

Shimada, T., Horita, K., Murakami, M. & Ogura, R. (1984). 'Morphological studies of different mitochondrial populations in monkey myocardial cells', *Cell and Tissue Research*, 238(3), pp. 577-582.

Shin, J.-H., Ko, H. S., Kang, H., Lee, Y., Lee, Y.-I., Pletinkova, O., Troconso, J. C., Dawson, V. L. & Dawson, T. M. (2011). 'PARIS (ZNF746) repression of PGC-1α contributes to neurodegeneration in Parkinson's disease', *Cell*, 144(5), pp. 689-702.

Siasos, G., Tsigkou, V., Kosmopoulos, M., Theodosiadis, D., Simantiris, S., Tagkou, N. M., Tsimpiktsioglou, A., Stampouloglou, P. K., Oikonomou, E. & Mourouzis, K. (2018). 'Mitochondria and cardiovascular diseases—from pathophysiology to treatment', *Annals of Translational Medicine*, 6(12).

Signes, A. & Fernandez-Vizarra, E. (2018). 'Assembly of mammalian oxidative phosphorylation complexes I–V and supercomplexes', *Essays in Biochemistry*, 62(3), pp. 255-270.

Sivitz, W. I. & Yorek, M. A. (2010). 'Mitochondrial dysfunction in diabetes: from molecular mechanisms to functional significance and therapeutic opportunities', *Antioxidants & Redox Signaling*, 12(4), pp. 537-577.

Skyler, J. S., Fonseca, V. A., Segal, K. R. & Rosenstock, J. J. D. C. (2015). 'Allogeneic mesenchymal precursor cells in type 2 diabetes: a randomized, placebo-controlled, dose-escalation safety and tolerability pilot study', 38(9), pp. 1742-1749.

Smirnova, E., Shurland, D.-L., Ryazantsev, S. N. & van der Bliek, A. M. (1998). 'A human dynamin-related protein controls the distribution of mitochondria', *The Journal of Cell Biology*, 143(2), pp. 351-358.

Song, M., Mihara, K., Chen, Y., Scorrano, L. & Dorn II, G. W. (2015). 'Mitochondrial fission and fusion factors reciprocally orchestrate mitophagic culling in mouse hearts and cultured fibroblasts', *Cell Metabolism*, 21(2), pp. 273-286.

Song, Z., Chen, H., Fiket, M., Alexander, C. & Chan, D. C. (2007). 'OPA1 processing controls mitochondrial fusion and is regulated by mRNA splicing, membrane potential, and Yme1L', *The Journal of Cell Biology*, 178(5), pp. 749-755.

Spinazzi, M., Casarin, A., Pertegato, V., Salviati, L. & Angelini, C. (2012). 'Assessment of mitochondrial respiratory chain enzymatic activities on tissues and cultured cells', *Nature Protocols*, 7(6), p. 1235.

Stallmeyer, B., Kuß, J., Kotthoff, S., Zumhagen, S., Vowinkel, K., Rinné, S., Matschke, L. A., Friedrich, C., Schulze-Bahr, E. & Rust, S. (2017). 'A mutation in the G-protein gene GNB2 causes familial sinus node and atrioventricular conduction dysfunction', *Circulation Research*, 120(10), pp. e33-e44.

Stanley, W. C., Dabkowski, E. R., Ribeiro Jr, R. F. & O'Connell, K. A. (2012). 'Dietary fat and heart failure: moving from lipotoxicity to lipoprotection', *Circulation Research*, 110(5), pp. 764-776.

Steele, A. M., Shields, B. M., Wensley, K. J., Colclough, K., Ellard, S. & Hattersley, A. T. (2014). 'Prevalence of vascular complications among patients with glucokinase mutations and prolonged, mild hyperglycemia', *Jama*, 311(3), pp. 279-286.

Stepien, K. M., Heaton, R., Rankin, S., Murphy, A., Bentley, J., Sexton, D. & Hargreaves, I. P. J. J. o. c. m. (2017). 'Evidence of oxidative stress and secondary mitochondrial dysfunction in metabolic and non-metabolic disorders', 6(7), p. 71.

Sternisha, S. M. & Miller, B. G. (2019). 'Molecular and cellular regulation of human glucokinase', *Archives of Biochemistry And Biophysics*, 663, pp. 199-213.

Stockwell, B. R., Angeli, J. P. F., Bayir, H., Bush, A. I., Conrad, M., Dixon, S. J., Fulda, S., Gascón, S., Hatzios, S. K. & Kagan, V. E. (2017). 'Ferroptosis: a regulated cell death nexus linking metabolism, redox biology, and disease', *Cell*, 171(2), pp. 273-285.

Strucksberg, K. H., Tangavelou, K., Schröder, R., & Clemen, C. S. (2010). Proteasomal activity in skeletal muscle: a matter of assay design, muscle type, and age. *Analytical biochemistry*, *399*(2), 225–229. https://doi.org/10.1016/j.ab.2009.12.026

Supale, S., Thorel, F., Merkwirth, C., Gjinovci, A., Herrera, P. L., Scorrano, L., Meda, P., Langer, T. & Maechler, P. (2013). 'Loss of prohibitin induces mitochondrial damages altering β-cell function and survival and is responsible for gradual diabetes development', *Diabetes*, 62(10), pp. 3488-3499.

Susin, S. A., Lorenzo, H. K., Zamzami, N., Marzo, I., Snow, B. E., Brothers, G. M., Mangion, J., Jacotot, E., Costantini, P. & Loeffler, M. (1999). 'Molecular characterization of mitochondrial apoptosis-inducing factor', *Nature*, 397(6718), pp. 441-446.

Suzuki, M., Danilchanka, O. & Mekalanos, J. J. (2014). 'Vibrio cholerae T3SS effector VopE modulates mitochondrial dynamics and innate immune signaling by targeting Miro GTPases', *Cell Host & Microbe*, 16(5), pp. 581-591.

Szekely, Y. & Arbel, Y. (2018). 'A review of Interleukin-1 in heart disease: where do we stand today?', *Cardiology and Therapy*, 7(1), pp. 25-44.

Szopa, M., Osmenda, G., Wilk, G., Matejko, B., Skupien, J., Zapala, B., Mlynarski, W., Guzik, T. & Malecki, M. T. (2015). 'Intima-media thickness and endothelial dysfunction in GCK and HNF1A-MODY patients', *Eur J Endocrinol*, 172(3), pp. 277-283.

Tang, B. (2018). 'Miro—Working beyond Mitochondria and Microtubules', *Cells*, 7(3), p. 18.

Tang, B. L. (2016). 'MIRO GTPases in mitochondrial transport, homeostasis and pathology', *Cells*, 5(1), p. 1.

Tatsumi, T., Matoba, S., Kawahara, A., Keira, N., Shiraishi, J., Akashi, K., Kobara, M., Tanaka, T., Katamura, M. & Nakagawa, C. (2000). 'Cytokine-induced nitric oxide production inhibits mitochondrial energy production and impairs contractile function in rat cardiac myocytes', *Journal of the American College of Cardiology*, 35(5), pp. 1338-1346.

Thanabalasingham, G. & Owen, K. R. (2011). 'Diagnosis and management of maturity onset diabetes of the young (MODY)', *BMJ*, 343, p. d6044.

Thomas, H. E., Irawaty, W., Darwiche, R., Brodnicki, T. C., Santamaria, P., Allison, J. & Kay, T. W. (2004). 'IL-1 receptor deficiency slows progression to diabetes in the NOD mouse', *Diabetes*, 53(1), pp. 113-121.

Tomita, M., Mukae, S., Geshi, E., Umetsu, K., Nakatani, M. & Katagiri, T. (1996). 'Mitochondrial respiratory impairment in streptozotocin-induced diabetic rat heart', *Japanese Circulation Journal*, 60(9), pp. 673-682.

Tong, M., Saito, T., Zhai, P., Oka, S.-i., Mizushima, W., Nakamura, M., Ikeda, S., Shirakabe, A. & Sadoshima, J. (2019). 'Mitophagy is essential for maintaining cardiac function during high fat diet-induced diabetic cardiomyopathy', *Circulation Research*, 124(9), pp. 1360-1371.

Toye, A. A., Moir, L., Hugill, A., Bentley, L., Quarterman, J., Mijat, V., Hough, T., Goldsworthy, M., Haynes, A. & Hunter, A. J. (2004). 'A new mouse model of type 2 diabetes, produced by N-ethyl-nitrosourea mutagenesis, is the result of a missense mutation in the glucokinase gene', *Diabetes*, 53(6), pp. 1577-1583.

Turrens, J. F. (2003). 'Mitochondrial formation of reactive oxygen species', *The Journal of Physiology*, 552(2), pp. 335-344.

Twig, G. & Shirihai, O. S. (2011). 'The interplay between mitochondrial dynamics and mitophagy', *Antioxidants & Redox Signaling*, 14(10), pp. 1939-1951.

Roberts, N., Cruz-Orive, L. M., Reid, N. M., Brodie, D. A., Bourne, M., & Edwards, R. H. (1993). Unbiased estimation of human body composition by the Cavalieri method using magnetic resonance imaging. *Journal of microscopy*, *171*(Pt 3), 239–253.

Urbanova, J., Brunerova, L. & Brož, J. (2018). 'Hidden MODY–Looking for a needle in a haystack', *Frontiers in Endocrinology*, 9, p. 355.

Vachharajani, V. & Granger, D. N. (2009). 'Adipose tissue: a motor for the inflammation associated with obesity', *IUBMB Life*, 61(4), pp. 424-430.

van de Weijer, T., Schrauwen-Hinderling, V. B. & Schrauwen, P. (2011). 'Lipotoxicity in type 2 diabetic cardiomyopathy', *Cardiovascular Research*, 92(1), pp. 10-18.

Varadi, A., Cirulli, V. & Rutter, G. A. (2004). 'Mitochondrial localization as a determinant of capacitative Ca2+ entry in HeLa cells', *Cell Calcium*, 36(6), pp. 499-508.

Velho, G. & Robert, J.-J. (2002). 'Maturity-onset diabetes of the young (MODY): genetic and clinical characteristics', *Hormone Research In Paediatrics*, 57(Suppl. 1), pp. 29-33.

Velho, G., Blanche, H., Vaxillaire, M., Bellanne-Chantelot, C., Pardini, V., Timsit, J., Passa, P., Deschamps, I., Robert, J.-J. & Weber, I. (1997). 'Identification of 14 new glucokinase mutations and description of the clinical profile of 42 MODY-2 families', *Diabetologia*, 40(2), pp. 217-224.

Velho, G., Vaxillaire, M., Boccio, V., Charpentier, G. & Froguel, P. (1996). 'Diabetes complications in NIDDM kindreds linked to the MODY3 locus on chromosome 12q', *Diabetes Care,* 19(9), pp. 915-919.

Vernay, A., Marchetti, A., Sabra, A., Jauslin, T. N., Rosselin, M., Scherer, P. E., Demaurex, N., Orci, L. & Cosson, P. (2017). 'MitoNEET-dependent formation of intermitochondrial junctions', *Proceedings of the National Academy of Sciences*, 114(31), pp. 8277-8282.

Vincent AE, Turnbull DM, Eisner V, Hajnóczky G, Picard M. Mitochondrial Nanotunnels. *Trends Cell Biol*. 2017;27(11):787-799

Vionnet, N., Stoffel, M., Takeda, J., Yasuda, K., Bell, G., Zouali, H., Lesage, S., Velho, G., Iris, F. & Passa, P. (1992). 'Nonsense mutation in the glucokinase gene causes early-onset non-insulin-dependent diabetes mellitus', *Nature*, 356(6371), p. 721.

Voulgari, C., Papadogiannis, D. & Tentolouris, N. (2010). 'Diabetic cardiomyopathy: from the pathophysiology of the cardiac myocytes to current diagnosis and management strategies', *Vascular Health and Risk Management*, 6, p. 883.

Wada, J. & Nakatsuka, A. (2016). 'Mitochondrial dynamics and mitochondrial dysfunction in diabetes', *Acta Medica Okayama*, 70(3), pp. 151-158.

Wallenius, V., Wallenius, K., Ahrén, B., Rudling, M., Carlsten, H., Dickson, S. L., Ohlsson, C. & Jansson, J.-O. (2002). 'Interleukin-6-deficient mice develop mature-onset obesity', *Nature Medicine*, 8(1), pp. 75-79.

Wang, B., Charukeshi Chandrasekera, P. & J Pippin, J. (2014). 'Leptin-and leptin receptor-deficient rodent models: relevance for human type 2 diabetes', *Current Diabetes Reviews*, 10(2), pp. 131-145.

Wang, X. & Schwarz, T. L. (2009). 'The mechanism of Ca2+-dependent regulation of kinesin-mediated mitochondrial motility', *Cell*, 136(1), pp. 163-174.

Wang, X., Winter, D., Ashrafi, G., Schlehe, J., Wong, Y. L., Selkoe, D., Rice, S., Steen, J., LaVoie, M. J. & Schwarz, T. L. (2011). 'PINK1 and Parkin target Miro for phosphorylation and degradation to arrest mitochondrial motility', *Cell*, 147(4), pp. 893-906.

Watkins, S. J., Borthwick, G. M. & Arthur, H. M. (2011). 'The H9C2 cell line and primary neonatal cardiomyocyte cells show similar hypertrophic responses in vitro', *In Vitro Cellular & Developmental Biology-Animal,* 47(2), pp. 125-131.

Weihofen, A., Thomas, K. J., Ostaszewski, B. L., Cookson, M. R. & Selkoe, D. J. (2009). 'Pink1 forms a multiprotein complex with Miro and Milton, linking Pink1 function to mitochondrial trafficking', *Biochemistry*, 48(9), pp. 2045-2052.

Weng, H., Ma, Y., Chen, L., Cai, G., Chen, Z., Zhang, S. & Ye, Q. (2020). 'Sirtuins and the mitochondrial unfolded protein response', *Curr Neuropharmacol 18(7).*

Whelihan, M. F., Zachary, V., Orfeo, T. & Mann, K. G. (2012). 'Prothrombin activation in blood coagulation: the erythrocyte contribution to thrombin generation', Blood, *The Journal of the American Society of Hematology*, 120(18), pp. 3837-3845.

WHO (2016).Diabetes. Available at: http://www.who.int/mediacentre/factsheets/fs312/en/ (Accessed: 20 September).

Wieneke, H., Svendsen, J. H., Lande, J., Spencker, S., Martinez, J. G., Strohmer, B., Toivonen, L., Le Marec, H., Garcia-Fernandez, F. J. & Corrado, D. (2016). 'Polymorphisms in the GNAS gene as predictors of ventricular tachyarrhythmias and sudden cardiac death: results from the DISCOVERY Trial and Oregon Sudden Unexpected Death Study', *Journal of the American Heart Association*, 5(12), p. e003905.

Wiley SE, Murphy AN, Ross SA, van der Geer P, Dixon JE (2007). MitoNEET is an iron-containing outer mitochondrial membrane protein that regulates oxidative capacity. *Proc Natl Acad Sci USA* 104:5318–5323

Wilson, G. A., Wilkins, G. T., Cotter, J. D., Lamberts, R. R., Lal, S. & Baldi, J. C. (2017). 'Impaired ventricular filling limits cardiac reserve during submaximal exercise in people with type 2 diabetes', *Cardiovascular Diabetology*, 16(1), p. 160.

Wischhof, L., Gioran, A., Sonntag-Bensch, D., Piazzesi, A., Stork, M., Nicotera, P. & Bano, D. (2018). 'A disease-associated Aifm1 variant induces severe myopathy in knockin mice', Molecular Metabolism, 13, pp. 10-23.

Witek, P., Korga, A., Burdan, F., Ostrowska, M., Nosowska, B., Iwan, M. & Dudka, J. (2016). 'The effect of a number of H9C2 rat cardiomyocytes passage on repeatability of cytotoxicity study results', *Cytotechnology*, 68(6), pp. 2407-2415.

Wittenberg, J. B. & Wittenberg, B. A. (2007). 'Myoglobin-enhanced oxygen delivery to isolated cardiac mitochondria', *Journal of Experimental Biology*, 210(12), pp. 2082-2090.

Wittig, I. & Schägger, H. (2008). 'Structural organization of mitochondrial ATP synthase', *Biochimica et Biophysica Acta (BBA)-Bioenergetics*, 1777(7-8), pp. 592-598.

Wyatt, E., Wu, R., Rabeh, W., Park, H.-W., Ghanefar, M. & Ardehali, H. (2010). 'Regulation and cytoprotective role of hexokinase III', *PloS one*, 5(11).

Wu S, Wu Y, Wu T, Wei Y. 2014. Role of AMPK-mediated adaptive responses in human cells with mitochondrial dysfunction to oxidative stress. *Biochim biophy acta,* 1840(4): 1331-1344.

Xiang R, Huang Y, Zhang Y, et al. 2020. Type-2 diabetes-induced hyposalivation of the submandibular gland through PINK1/Parkin-mediated mitophagy. *Journal of cellular physiology,* 235(1): 232-244.

Xu, C. S., Hayworth, K. J., Lu, Z., Grob, P., Hassan, A. M., García-Cerdán, J. G., Niyogi, K. K., Nogales, E., Weinberg, R. J., & Hess, H. F. (2017). Enhanced FIB-SEM systems for large-volume 3D imaging. *eLife*, *6*, e25916.

Xu, A., Lin, Y., Sheng, H., Cheng, J., Mei, H., Ting, T. H., Zeng, C., Liang, C., Zhang, W., Li, C., Li, X. & Liu, L. (2020). 'Molecular Diagnosis of Maturity-Onset Diabetes of the Young in a Cohort of Chinese Children', *Pediatr Diabetes*. 21(3):431-440.

Xu, J. Y., Dan, Q. H., Chan, V., Wat, N. M., Tam, S., Tiu, S. C., Lee, K. F., Siu, S. C., Tsang, M. W. & Fung, L. M. (2005). 'Genetic and clinical characteristics of maturity-onset diabetes of the young in Chinese patients', *European Journal of Human Genetics*, 13(4), pp. 422-427.

Yamauchi-Takihara, K. & Kishimoto, T. (2000). 'Cytokines and their receptors in cardiovascular diseases—role of gp130 signalling pathway in cardiac myocyte growth and maintenance', *International Journal of Experimental Pathology*, 81(1), p. 1.

Yang F, Liu X, Zhao Y, et al. Investigation of Three-Dimensional Microstructure of Tricalcium Silicate (C_3S) by Electron Microscopy. *Materials (Basel)*. 2018;11(7):1110.

Yang, S., Zheng, R., Hu, S., Ma, Y., Choudhry, M. A., Messina, J. L., Rue III, L. W., Bland, K. I. & Chaudry, I. H. (2004). 'Mechanism of cardiac depression after trauma-hemorrhage: increased cardiomyocyte IL-6 and effect of sex steroids on IL-6 regulation and cardiac function', *American Journal of Physiology-Heart and Circulatory Physiology*, 287(5), pp. H2183-H2191.

Yasukawa, H., Hoshijima, M., Gu, Y., Nakamura, T., Pradervand, S., Hanada, T., Hanakawa, Y., Yoshimura, A., Ross, J. & Chien, K. R. (2001). 'Suppressor of cytokine signaling-3 is a biomechanical stress–inducible gene that suppresses gp130-mediated cardiac myocyte hypertrophy and survival pathways', *The Journal of Clinical Investigation*, 108(10), pp. 1459-1467.

Yi, M., Weaver, D. & Hajnóczky, G. r. (2004). 'Control of mitochondrial motility and distribution by the calcium signal: a homeostatic circuit', *The Journal of Cell Biology*, 167(4), pp. 661-672.

Yin, F., Spurgeon, H. A., Rakusan, K., Weisfeldt, M. L. & Lakatta, E. G. (1982). 'Use of tibial length to quantify cardiac hypertrophy: application in the aging rat', *American Journal of Physiology-Heart and Circulatory Physiology*, 243(6), pp. H941-H947.

Yoshioka, M., Kayo, T., Ikeda, T. & Koizuni, A. (1997). 'A novel locus, Mody4, distal to D7Mit189 on chromosome 7 determines early-onset NIDDM in nonobese C57BL/6 (Akita) mutant mice', *Diabetes*, 46(5), pp. 887-894.

Zaccardi, F., Webb, D. R., Yates, T. & Davies, M. J. (2016). 'Pathophysiology of type 1 and type 2 diabetes mellitus: a 90-year perspective', *Postgraduate Medical Journal*, 92(1084), pp. 63-69.

Zhang, Y., Wang, J.-H., Zhang, Y.-Y., Wang, Y.-Z., Wang, J., Zhao, Y., Jin, X.-X., Xue, G.-L., Li, P.-H. & Sun, Y.-L. (2016). 'Deletion of interleukin-6 alleviated interstitial fibrosis in streptozotocin-induced diabetic cardiomyopathy of mice through affecting TGFβ1 and miR-29 pathways', *Scientific Reports*, 6(1), pp. 1-11.

Zhang, Z., Liu, L., Wu, S. & Xing, D. (2016). 'Drp1, Mff, Fis1, and MiD51 are coordinated to mediate mitochondrial fission during UV irradiation–induced apoptosis', *The FASEB Journal*, 30(1), pp. 466-476.

Zhao, D., Sun, Y., Tan, Y., Zhang, Z., Hou, Z., Gao, C., Feng, P., Zhang, X., Yi, W., Gao, F. J. O. m. & longevity, c. (2018). 'Short-duration swimming exercise after myocardial infarction attenuates cardiac dysfunction and regulates mitochondrial quality control in aged mice', (3):1-16.

Zhao, M., Yang, Y., Bi, X., Yu, X., Jia, H., Fang, H. & Zang, W. (2015). 'Acetylcholine attenuated TNF-α-induced apoptosis in H9c2 cells: role of calpain and the p38-MAPK pathway'*, Cellular Physiology and Biochemistry*, 36(5), pp. 1877-1889.

Zhong, J., Gong, Q. & Mima, A. (2017). 'Inflammatory regulation in diabetes and metabolic dysfunction', *Journal of diabetes research*.1-2.

Zhou, L. & O'Rourke, B. (2012). 'Cardiac mitochondrial network excitability: insights from computational analysis', *American Journal of Physiology-Heart and Circulatory Physiology*, 302(11), pp. H2178-H2189.

Zilverschoon GR, Tack CJ, Joosten LA, Kullberg BJ, van der Meer JW, Netea MG (2008). Interleukin-18 resistance in patients with obesity and type 2 diabetes mellitus. *Int J Obes (Lond*). 32(9):1407-1414.

Zorova, L. D., Popkov, V. A., Plotnikov, E. Y., Silachev, D. N., Pevzner, I. B., Jankauskas, S. S., Babenko, V. A., Zorov, S. D., Balakireva, A. V. & Juhaszova, M. (2018). 'Mitochondrial membrane potential', *Analytical Biochemistry*, 552, pp. 50-59.